Physics Area - Ph.D. course in Astroparticle Physics

SISSA, Trieste

The chime of cosmic bells: Nonlinear effects and new physics in the black hole ringdown

SUPERVISOR:
Enrico Barausse

CANDIDATE:
Lodovico Capuano

ACADEMIC YEAR 2024/2025

"Die nahen Kleinigkeiten und die ferne Ewigkeit haben einen Zusammenhang, und wir wissen nicht, welchen."

"There is a tie between the nearby little things and the faraway eternity, and we do not know what it is"

— Joseph Roth, Der blinder Spiegel

Declaration

I hereby declare that, except where specific reference is made to the work of others, the contents of this thesis are original and have not been submitted in whole or in part for consideration for any other degree or qualification in this, or any other university.

The discussion is based on the following works:

- L. Capuano, L. Santoni, E. Barausse, "Black hole hairs in scalar-tensor gravity and the lack thereof", *Phys.Rev.D* 108 (2023) 6, 6 – Published 29 September, 2023, ArXiv: 2304.12759 [gr-qc]
- L. Capuano, L. Santoni, E. Barausse, "Perturbation of the Vaidya metric in the frequency domain: quasinormal modes and tidal response", *Phys.Rev.D* 110 (2024) 8, 084081 – Published 30 October, 2024, ArXiv: 2407.06009 [gr-qc]
- P. Cano, L. Capuano, N. Franchini, S. Maenaut, S. H. Völkel, "Parametrized quasi-normal mode framework for modified Teukolsky equations", *Phys.Rev.D* 110 (2024) 10, 104007 – Published 5 November, 2024, ArXiv: 2407.15947 [gr-qc]
- L. Capuano, M. Vaglio, R. Chandramouli, C. Pitte, A. B. Kuntz, E. Barausse, "Systematic bias in LISA ringdown analysis due to waveform inaccuracy", ArXiv: 2506.21181 [gr-qc]

During the Ph.D, I also co-authored the following works, that are not included in the thesis:

- A. Östreicher, L. Capuano, S. Matarrese, L. Heisenberg, M. Bartelmann,"Kinetic field theory: generic effects of alternative gravity theories on non-linear cosmic density-fluctuations", *JCAP* 07(2023)029 – Published Jul 13, 2023, ArXiv: 2210.16014 [astro-ph.CO]
- P. Cano, L. Capuano, N. Franchini, S. Maenaut, S. H. Völkel, "Higher-derivative corrections to the Kerr quasinormal mode spectrum", *Phys.Rev.D* 110 (2024) 12, 124057 – Published Dec 15, 2024, ArXiv: 2409.04517 [gr-qc]
- C. Smarra, L. Capuano, A. B. Kuntz, "Probing supermassive black hole scalarization with Pulsar Timing Arrays", ArXiv: 2505.20402 [gr-qc]

Abstract

Gravitational waves offer a powerful tool to test the nature of gravity in the strong-field regime, where deviations from Einstein's General Relativity may emerge. Black hole mergers, in particular, are ideal laboratories for such tests, as their dynamics and emitted radiation encode detailed information about the underlying gravitational theory.

This thesis explores two complementary avenues for probing gravity with black hole binaries. The first part focuses on black hole solutions in scalar–tensor theories, which extend General Relativity by adding an extra scalar field. In this context, "no-hair" theorems usually forbid black holes from carrying scalar charge, but existing results cover only special cases. We generalize these theorems, proving that in the most general shift-symmetric scalar-tensor theory, stationary black holes cannot possess scalar charge — even in higher-dimensional spacetimes. We also identify situations where this result can be circumvented, such as when the scalar field evolves linearly in time or couples to specific curvature invariants. These exceptions are phenomenologically relevant, as they can lead to distinctive gravitational wave signatures like dipolar radiation, potentially detectable by current and future detectors.

The second part of the thesis employs the black hole perturbation theory framework to study how subtle changes in BH properties affect their quasinormal mode spectrum—the characteristic "ringing" observed in the post-merger gravitational wave signal. We analyze scenarios where the black hole mass changes over time, such as the nonlinear self-absorption of gravitational radiation, finding shifts in quasinormal frequencies, possible instabilities, and non-zero tidal responses. We also develop a parametrized framework to describe generic small deviations from GR in the Teukolsky equation. We demonstrate how this approach can be applied to a broad range of physical scenarios.

We finally assess the impact of incomplete ringdown modeling on parameter estimation for the space-based detector LISA, by incorporating multiple fundamental, overtone, and quadratic modes.

In summary, the work refines theoretical constraints on black hole properties, highlights specific scenarios and conditions where deviations from GR could be observable, and outlines approaches that may help connect theoretical predictions with future GW measurements.

Acknowledgements

Acronyms

- ADM: Arnowitt-Deser-Misner;
- BH: black hole;
- BHPT: black hole perturbation theory;
- CDM: cold dark matter;
- CH: cosmological horizon;
- DHOST: degenerate-higher-order-scalar-tensor;
- EH: event horizon;
- EFT: effective field theory;
- FIM: Fisher information matrix;
- FJBD: Fierz-Jordan-Brans-Dicke;
- GB: Gauss-Bonnet;
- GR: General Relativity;
- GW: gravitational wave;
- HDG: Higher-Derivative Gravity;
- LISA: Laser Interferometer Space Antenna
- IR: infrared;
- PTA: pulsar timing arrays;
- PSD: power-spectral density;
- QNM: quasinormal mode;
- SET: stress-energy tensor;
- SMBH: supermassive black hole;
- SMBHB: supermassive black hole binary;
- SNR: signal-to-noise ratio;

- TDI: time domain interferometry;
- TT: transverse-traceless;
- UV: ultraviolet;
- WKB: Wentzel-Kramers-Brillouin;

Notation and conventions

In the first part of this thesis, i.e. Chapter 1 and 2 (and Appendix A), we will work in natural units $c = \hbar = 1$, while in the remaining chapters we will adopt geometric units $c = G = 1$. Moreover, in the whole thesis, we will adopt the mostly plus signature of the metric, $(-,+,+,\dots)$. We will use Greek indices $\mu, \nu, \alpha, \dots$ for the tensor components on d dimensional spacetime, lowercase Latin indices $i, j, k, \dots$ (from the middle of the alphabet) for the $d-1$ components corresponding to spatial coordinates only, and lowercase Latin indices $a, b, c, \dots$ (from the beginning of the alphabet) to label the components associated to angular coordinates. Notice that we will always consider a four-dimensional spacetime, with the exception of Chapter 2 and Appendix A. We will also use Latin indices $i, j, k, \dots$ for components of multi-valued quantities that are not spacetime tensors, such as coefficients in the recurrence relations in Chapter 4 and 5, or parameters of astrophysical sources in Chapter 6. A slightly different convention for indices is adopted though in Appendix A.1. We will finally also employ the boldface for indicating abstract vectors in Chapter 6 .

Contents

List of Figures

Part I

Black hole uniqueness and its breakdown

Chapter 1

Gravitation, black holes and gravitational waves

1.1 General Relativity and black holes

Among the fundamental interactions in nature, gravity remains the most elusive. The uniqueness of gravity is two-fold. On the one hand, unlike other elementary forces, it is universal, meaning that it is sourced by energy itself, rather than a specific charge. On the other hand, gravity is unique for its extreme weakness, set by the Planck scale, which renders it exceptionally hard to probe its nature in a quantum regime. The universality of gravity is well captured by the geometrical description introduced in 1915 by Einstein with the theory of General Relativity (GR) [1], in which the spacetime and its energy content are dynamically intertwined. In this picture, gravity emerges as the *curvature* of spacetime. This concept can be quantified from the definition of a metric tensor $g_{\mu\nu}$. The curvature is then encoded in the Riemann tensor, defined as [2, 3]

$$R^{\rho}{}_{\sigma\mu\nu} = \partial_\mu \Gamma^\rho_{\nu\sigma} - \partial_\nu \Gamma^\rho_{\mu\sigma} + \Gamma^\rho_{\mu\lambda}\Gamma^\lambda_{\nu\sigma} - \Gamma^\rho_{\nu\lambda}\Gamma^\lambda_{\mu\sigma} \tag{1.1}$$

where we introduced the Levi-Civita connection

$$\Gamma^\rho_{\mu\nu} = \frac{1}{2} g^{\rho\lambda} \left(\partial_\mu g_{\nu\lambda} + \partial_\nu g_{\mu\lambda} - \partial_\lambda g_{\mu\nu} \right) . \tag{1.2}$$

In a classical field theory perspective, the dynamics of gravity is described by an action for the metric tensor $S\left[g_{\mu\nu}\right]$ [4]. The simplest local and diffeomorphism-invariant kinetic term that can be constructed from the metric and its derivatives is the Ricci scalar, $R = g^{\mu\nu} R_{\mu\nu}$, where $R_{\mu\nu} = R^\rho{}_{\mu\rho\nu}$ is the Ricci tensor [5]. The action takes the form [2, 3]

$$S_{\rm EH} = \frac{M_{\rm Pl}^2}{2} \int \mathrm{d}^4x \, \sqrt{-g} \left(R - 2\Lambda_c \right) , \tag{1.3}$$

where we introduced the Planck mass $M_{\rm Pl} = (8\pi G)^{-1/2}$. The object Λ_c is called cosmological constant. As we will see in the following section, this term can be related with the large-scale dynamics of the universe.

Eq. (1.3) is known as Einstein-Hilbert action, and turns out to be also the only possible local and diffeomorphism-invariant action in four spacetime dimensions, if one requires that the metric tensor be the only dynamical field and that the equations of motion be second-order. This result is an implication of the more general Lovelock's theorem in arbitrary spacetime dimension [5].

The matter content of spacetime can be included in this picture with a separate contribution, encoded in an action $S_{\text{matter}}\left[g_{\mu\nu}, \Psi_m\right]$, where Ψ_m is a generic matter field. Thus, the total action has the form [2, 3]

$$S_{\text{tot}} = S_{\text{EH}}\left[g_{\mu\nu}\right] + S_{\text{matter}}\left[g_{\mu\nu}, \psi\right] \,, \tag{1.4}$$

The equation of motion, or *Einstein Equation*, obtained from the variation of Eq. (1.4), reads

$$G_{\mu\nu} + \Lambda_c g_{\mu\nu} = \frac{T_{\mu\nu}}{M_{\text{Pl}}^2} \,, \tag{1.5}$$

where we introduced the Einstein tensor $G_{\mu\nu} = R_{\mu\nu} - R\, g_{\mu\nu}/2$, and the *stress-energy tensor* (SET)

$$T_{\mu\nu} = \frac{2}{\sqrt{-g}} \frac{\delta S_{\text{matter}}}{\delta g^{\mu\nu}} \,. \tag{1.6}$$

The Bianchi identity, holding for the left-hand side of the Einstein Equation, implies

$$\nabla_\mu T^{\mu\nu} = 0 \,. \tag{1.7}$$

Notice that, on a flat background described by the Minkowski metric $\eta_{\mu\nu}$, this definition of SET, for a matter field ψ described by the Lagrangian density $\mathcal{L}(\psi, \partial_\mu\psi)$, reduces to the canonical field theory definition [1] [7].

$$T^\mu{}_\nu = \frac{\partial \mathcal{L}}{\partial(\partial_\mu \psi)} \partial_\nu \psi - \delta^\mu_\nu \mathcal{L} \,. \tag{1.8}$$

The predictions of GR in the weak field regime, where its effect can be expressed in the form of perturbative corrections to Newtonian gravity, have been widely confirmed by experimental tests performed in the solar system [8], such as Shapiro time delay [9], the anomalous perihelion precession of Mercury [10], or light deflection [11, 12]. However, the most crucial implications of GR manifest in the strong-field regime, around so called *compact objects*. While the physics of extremely compact stars, such as neutron stars, is dramatically affected by the strong-field behavior of the gravitational interaction [13, 14], the most intriguing consequence of GR regards the existence of ultra-compact *vacuum solutions* of Einstein Equation, namely black holes (BHs) [15–17]. Although these solutions describe vacuum spacetimes, it is still possible to associate a well-defined notion of total mass to them, for example via the Arnowitt-Deser-Misner (ADM) mass definition [18], which captures the gravitational energy content as measured by an observer at spatial infinity.

BHs are mainly characterized by the presence of an *event horizon* (EH), a null hypersurface that delineates the boundary of causal influence, beyond which events cannot affect an outside observer [19–21]. Moreover, Hawking showed in 1974 that the BH EH produces thermal radiation at an equilibrium temperature related to the BH mass [22, 23]. The emission of radiation by the EH is responsible for a process known as evaporation, which causes the progressive shrinking of BHs on extremely large time scales.

In GR, BHs are also typically characterized by the presence of curvature singularities, i.e. points of spacetime in which the solution is not defined [19, 24, 25]. The presence

[1] Notice that this holds if the Lagrangian density only depends on the field and on its first derivatives. Moreover, unlike the covariant definition of Eq. (1.6), this SET is not automatically symmetric. It can, however, be symmetrized with the Belifante-Rosenfeld procedure [6], i.e. with the redefinition $T^\mu{}_\nu \to T^\mu{}_\nu + \partial_\lambda S^{\lambda\mu}{}_\nu$. The tensor $S^{\lambda\mu}{}_\nu$ is symmetric in the indices $\lambda\mu$, so that the redefined tensor satisfies $\partial_\mu T^\mu{}_\nu = 0$.

of singularities is interpreted as a theoretical limit of GR, which should in principle be completed in the ultraviolet (UV) regime by a more general theory that is able to resolve the small-scale structure of BH interior [26–28].

The simplest BH realization in GR is given by the Schwarzschild solution, which is also the only nontrivial vacuum static solution to Einstein equation. The line element can be expressed in spherical polar coordinates (t, r, θ, ϕ) as

$$\mathrm{d}s^2 = -\left(1 - \frac{r_s}{r}\right)\mathrm{d}t^2 + \left(1 - \frac{r_s}{r}\right)^{-1}\mathrm{d}r^2 + r^2\left(\mathrm{d}\theta^2 + \sin\theta^2\mathrm{d}\phi^2\right) . \tag{1.9}$$

In more detail, the radial coordinate r is called the areal radius, and it is defined in such a way that a spherical surface with $r = \text{const}$ has area $A(r) = 4\pi r^2$. The characteristic scale r_s is the so-called Schwarzschild radius, representing the location of the EH, and can be expressed in terms of the ADM mass M of the BH as $r_s = 2GM$. The point at $r = 0$ is the aforementioned curvature singularity. This can be seen, by looking at the curvature invariant $R^{\mu\nu\rho\sigma}R_{\mu\nu\rho\sigma} = 12r_s^2/r^6$, which is divergent at $r \to 0$, indicating a genuine singularity of the spacetime.

On the other hand, the most general BH solution in GR represents a stationary rotating object, with dimensionless angular momentum a, and carrying an electric charge Q. This solution is known as Kerr-Newmann BH [29], and is described, in Boyer-Lindquist coordinates, by the line element

$$\begin{aligned}\mathrm{d}s^2 = &-\left(1 - \frac{r_s r}{\Sigma}\right)\mathrm{d}t^2 - \frac{2a\left(r_s r - Q^2\right)\sin^2\theta}{\Sigma}\mathrm{d}t\,\mathrm{d}\phi + \Sigma\left(\frac{\mathrm{d}r^2}{\Delta} + \mathrm{d}\theta^2\right) \\ &+ \frac{\left((r^2+a^2)^2 - a^2\Delta\sin^2\theta\right)\sin^2\theta}{\Sigma}\mathrm{d}\phi^2 ,\end{aligned} \tag{1.10}$$

with

$$\begin{aligned}\rho^2 &= r^2 + a^2\cos^2\theta, \\ \Delta &= r^2 - r_s r + a^2 + Q^2 .\end{aligned} \tag{1.11}$$

In this case, the BH has two different horizons, given by the roots of the function Δ, while the singularity is not a point anymore, but rather a ring of points, given by $r = 0$, $\theta = \pi/2$. The form of Eq (3.114) highlights a key feature of BHs in GR: they are completely characterized by a maximal set of three parameters: mass, spin, and electric charge. This statement is also known as *no-hair conjecture* [30–33], and we are going to discuss it in more detail in the next chapter.

The existence of BHs in our universe has been largely demonstrated in different astrophysical scenarios, and with various astrophysical techniques [34–40], as we will discuss in more detail in the last section of this chapter. In particular, we know that they can emerge in the astrophysical context as the final evolutionary stage of massive stars, after a process of gravitational collapse [41–43]. Furthermore, we know that *supermassive* BHs (SMBHs), with millions or even billions of solar masses, exist at the center of galaxies, although their formation and evolution is still not fully understood [44, 45]. In astrophysical contexts, BHs are expected to be essentially uncharged, since any significant net electric charge would be rapidly neutralized by the surrounding plasma and interstellar medium through accretion of oppositely charged particles [46]. On the other hand, astrophysical BHs are generally (highly) spinning [47, 48]. Hence, it is believed that astrophysical BHs are described by the Kerr metric, obtained from Eq. (3.114), with $Q = 0$. This conjecture is also known as "Kerr hypothesis" [30–33].

1.2 Going beyond: effective field theories and new degrees of freedom

As already discussed, GR provides a successful description of the gravitational interaction in the universe [8]. However, it suffers of some limitations that is worth addressing here. First of all, the aforementioned curvature singularities signal the incompleteness of the theory in the UV [19, 25, 49]. This is also connected to the problem of reconciling GR with quantum mechanics. Indeed, if one tries to deal with the metric tensor as a quantum field, for instance expanding it perturbatively around a flat background, one finds that the quantum fluctuations possess nonlinear interactions that lead to UV divergences that cannot be cured with the inclusion of a finite amount of counterterms in the action [50–52]. In other words, gravity is not renormalizable. This should be contrasted with the case of the Standard Model of particle physics, which describes the other three fundamental interactions in nature, which is a renormalizable theory [2] [59]. Different unified theories have been proposed as UV-completions of GR, such as string theory [60], asymptotically safe quantum gravity [61], loop quantum gravity [62], or Hořava-Lifshitz gravity [63]. Another well-known theoretical problem plaguing GR is the so-called information loss paradox [64, 65]. In the process of evaporation of a BH through the Hawking mechanism, the emitted radiation is thermal and carries no information. When the BH eventually disappears, the whole amount of information that entered the EH during the BH history disappears with it. This is in conflict with the unitary evolution required by quantum mechanics, that should preserve the initial information.

In addition to the issues related to the UV side, GR also appears to be partially incomplete in the infrared (IR), namely at very large scales. In fact, the dynamics of large gravitating systems such as galaxies, galaxy clusters, or even the universe in its entirety appear to require additional theoretical ingredients to be explained. The main observational anomalies in the universe, such as the behavior of galaxy rotation curves [66, 67], the growth of cosmic structures [68, 69], the spectrum of the cosmic microwave background [70, 71], and the late-time accelerated expansion of the universe [72, 73] are addressed in the standard model of cosmology with the inclusion of non-relativistic or "cold" dark matter (CDM), and dark energy in the form of a cosmological constant Λ_c [71, 74]. This picture is usually called ΛCDM, for intuitive reasons. However, the ΛCDM model is also affected by some theoretical issues, in particular the so-called cosmological constant problem [75–77]. The experimentally measured value of the energy density of the cosmological constant is $\rho_\Lambda \simeq 10^{-122} M_{\rm Pl}^4$. On the other hand, if one wants to interpret the cosmological constant as energy of the vacuum, it is possible to estimate its value by summing the contribution of all modes with momentum k and mass m_i up to a high energy cutoff scale $\Lambda_{\rm UV} \gg m_i$ [77]. Namely

$$\rho_{\rm vac} = \int \frac{{\rm d}^3 k}{(2\pi)^3} \frac{1}{2} \sqrt{k^2 + m_i^2} \simeq \frac{\Lambda_{\rm UV}^4}{16\pi^2} \,. \tag{1.12}$$

It is not hard to notice that natural choices for the cutoff $\Lambda_{\rm UV}$, coming from known high-energy physics, produce an enormous discrepancy between the theoretical prediction and the observed value of the cosmological constant. In particular, setting the cutoff at the Planck scale results in a discrepancy of about 120 orders of magnitude. Even choosing lower energy scales associated with the Standard Model, such as the electroweak symmetry breaking scale, still leads to an extremely large mismatch. Such inconsistency represents one of

[2] Notice that renormalizability does not guarantee, in principle, that the theory is the ultimate description of nature. In fact, there are still theoretical puzzles related to the Standard Model of particle physics, such as the neutrino masses [53–55] or the hierarchy problem [56–58].

the most striking fine-tuning problems in modern physics. Reconciling the theoretical vacuum energy with the measured value would require an extreme and unnatural cancellation between different contributions in the action, rendering the result highly unstable under quantum corrections.

In addition to this theoretical tension, recent observational results reported by the DESI collaboration [78], suggest possible deviations from the cosmic expansion predicted by the ΛCDM model.

All these problems in the standard model of cosmology suggest that something important is missing in our description of the universe dynamics and the nature of gravity at very large scales.

In summary, although GR provides a good description of gravitating systems at intermediate scales, there are several theoretical and observational reasons to explore possible generalizations. This can be practically done relaxing the assumptions of the four-dimensional Lovelock's theorem [5], i.e. considering a higher spacetime dimensionality, breaking some symmetries (such as local Lorentz invariance) or locality, including other fundamental fields, or allowing for higher-order equations of motion. Let us focus for a moment on this last possibility.

Adopting the picture of GR as the low-energy limit of some unknown UV-complete theory of gravitation, one can complement the Einstein-Hilbert action with additional terms, which are higher-order in the curvature. In other words, one can construct an Effective Field Theory (EFT) of gravity [79]. The top-down construction of an EFT describing the dynamics of some light degree of freedom $\varphi_{\rm L}$ is generally performed integrating out UV physics mediated by some heavy field $\varphi_{\rm H}$. This procedure can be schematically expressed in the path-integral formulation as follows [79]

$$e^{iS_{\rm EFT}[\varphi_L]} \equiv \int \mathcal{D}\varphi_{\rm H}\, e^{iS_{\rm UV}[\varphi_{\rm L},\varphi_{\rm H}]}\,. \tag{1.13}$$

The resulting action has the general structure

$$S_{\rm EFT}\left[\varphi_{\rm L}\right] = \int {\rm d}x^4 \sum_i c_i \frac{\mathcal{O}_i\left[\varphi_{\rm L}\right]}{\Lambda_{\rm UV}^{d_i-4}}\,, \tag{1.14}$$

where $\Lambda_{\rm UV}$ is a typical cutoff energy scale, and $d_i > 4$ is the energy dimension of the local operator $\mathcal{O}_i$, and c_i are constant coefficients that depend on the UV physics.

However, since the high-energy completion of GR is unknown, we practically want to proceed the other way round, i.e. following a bottom-up construction. This means writing down the most general IR action, given a set of basic assumptions. The coefficients of the EFT operators, in this scheme, are not known a priori, while they can in principle be determined from experiments. The main ingredients to construct the EFT of gravity in this way are relevant degrees of freedom, the symmetries of the IR theory, and the expansion and power-counting scheme.

In particular, if one requires that the EFT of gravity is diffeomorphism-invariant, and describes no dynamical degree of freedom but the metric tensor, one obtains the following action [80, 81]

$$S_{\rm EFT} = \frac{M_{\rm Pl}^2}{2}\int {\rm d}^4x\,\sqrt{-g}\left(R + \frac{\mathcal{L}^{(6)}}{\Lambda_{\rm UV}^4} + \frac{\mathcal{L}^{(8)}}{\Lambda_{\rm UV}^6} + \dots\right)\,, \tag{1.15}$$

where $\mathcal{L}^{(i)}$ include terms with i derivatives. Notice that some terms, among the different possible operators at a given order in the derivative expansion, do not affect the vacuum

GR solutions and can then be omitted in the EFT. In particular, at four-derivative order, the possible curvature invariants are [80, 81]

$$\mathcal{L}^{(4)} = \alpha_1 \mathcal{G} + \alpha_2 R^{\mu\nu\rho\sigma} \tilde{R}_{\mu\nu\rho\sigma} + \alpha_3 R^{\mu\nu} R_{\mu\nu} + \alpha_4 R^2 \,, \tag{1.16}$$

where we defined the Gauss-Bonnet (GB) invariant

$$\mathcal{G} = R^{\mu\nu\rho\sigma} R_{\mu\nu\rho\sigma} - 4 R^{\mu\nu} R_{\mu\nu} + R^2 \,, \tag{1.17}$$

and the dual Riemann tensor

$$\tilde{R}_{\mu\nu\rho\sigma} = \frac{1}{4} \varepsilon_{\mu\nu}{}^{\alpha\beta} \, \varepsilon_{\rho\sigma}{}^{\gamma\delta} \, R_{\alpha\beta\gamma\delta} \,, \tag{1.18}$$

with $\varepsilon_{\mu\nu}{}^{\alpha\beta}$ being the Levi-Civita tensor.

The first two invariants, multiplying the coefficients α_1 and α_2, are topological terms, meaning that their contribution to the equation of motion is trivial [3, 5]. The remaining terms, vanish on a Ricci-flat background, and hence do not provide any perturbative correction to GR BH solutions [80, 81]. For this reason, the higher-derivative corrections to GR that we are considering start from the sixth order in derivatives. Moreover, the number of independent operators at a given order can be further reduced using different kind of tensor identities. In practice, in the end, one is only left with pure-Riemann terms. At sixth order in the derivative expansion one only has the two independent terms [80, 81]

$$\mathcal{L}^{(6)} = \lambda_{\rm ev} \, R^{\rho\sigma}{}_{\mu\nu} \, R^{\delta\gamma}{}_{\rho\sigma} \, R^{\mu\nu}{}_{\delta\gamma} + \lambda_{\rm odd} \, R^{\rho\sigma}{}_{\mu\nu} \, R^{\delta\gamma}{}_{\rho\sigma} \, \tilde{R}^{\mu\nu}{}_{\delta\gamma} \,, \tag{1.19}$$

where $\lambda_{\rm odd}$ and $\lambda_{\rm even}$ are dimensionless couplings. The second term is clearly parity-violating.

Moving to the successive order, we have

$$\mathcal{L}^{(8)} = \epsilon_1 \mathcal{C}^2 + \epsilon_2 \tilde{\mathcal{C}}^2 + \epsilon_3 \mathcal{C}\mathcal{C} \,, \tag{1.20}$$

where we defined the invariants

$$\mathcal{C} = R_{\mu\nu\rho\sigma} R^{\mu\nu\rho\sigma} \,, \qquad \tilde{\mathcal{C}} = R_{\mu\nu\rho\sigma} \tilde{R}^{\mu\nu\rho\sigma} \,. \tag{1.21}$$

The term multiplying the coefficient ϵ_3 is parity-violating, while the other two are parity preserving. Notice that the dimensionless coupling $\lambda_{\rm odd,even}$ and $\epsilon_{1,2,3}$ can in principle be constrained requiring causality and unitarity [82–84].

The equation of motion for the metric tensor in this EFT are clearly higher than second order. As it is widely known, this kind of theory is generally affected by the presence of unstable modes, the so-called ghosts [85, 86]. This also happens when we introduce the higher-derivative corrections described above, but such unstable modes only appear at energy scales which are outside the range of validity of the EFT [80].

On the other hand, these higher-derivative operators provide corrections to the GR BH solutions [81], that can in principle become relevant at the horizon scale, and consequently produce interesting phenomenological consequences, particularly in the context of BH perturbations [87, 88]. We will return to this in Chapter II and 5.

In the model described so far, that we will call Higher-Derivative Gravity (HDG) from now on, the only dynamical degree of freedom, within the regime of validity of the EFT, is the metric tensor [80, 81]. However, in the low-energy limit of some UV completions of GR like string theory, other fields are generally present [60]. These fields are typically scalars or pseudo-scalars. This motivates the study of more general extensions of GR in

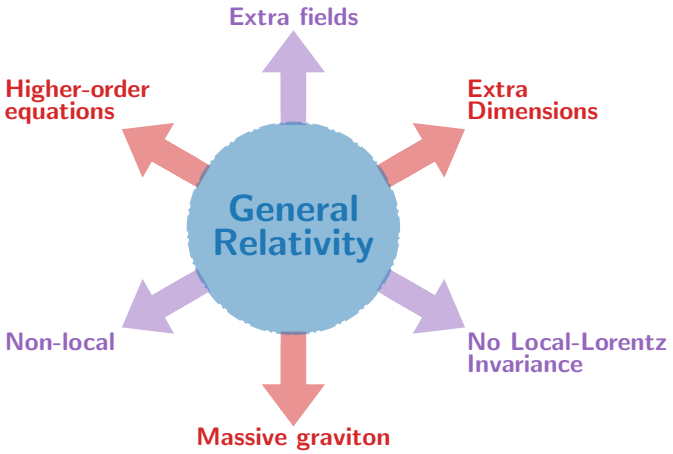

Figure 1.1: Different directions in which GR can be extended. Every direction corresponds to relaxing one of the hypothesis of the four-dimensional Lovelock's theorem.

which at least one scalar degree of freedom is included. Furthermore, *scalar-tensor* (ST) theories of gravity have had a huge historical relevance in cosmology for they allow for self-accelarating solutions and can then provide a dynamical explanation for dark energy, in contrast with the cosmological constant approach [89–91]. For all the reasons above, ST theories are probably the most popular and most widely investigated class of modified gravity.

In the next chapter, we are going to expand on ST theories and the possibility of having detectable deviations from GR in BH solutions.

To conclude this section, we mention that several other ways exist, to construct a theory of gravity beyond GR. Other kind of degrees of freedom can be included in the gravitational sector, still preserving the symmetries of GR (Proca theory [92], bimetric gravity [93]). On the other hand, other examples of theories, in which different underlying assumptions are relaxed, are Lorentz-violating theories (Hořava-Lifshitz [63] and Einstein-Aether gravity [94]), massive gravity (where the graviton acquires a mass term) [95], non-local theories [96], or theories including extra spacetime dimensions [97–100]. All these possibilities are synthesized in the cartoon of Fig. 1.1.

In the next section, which is going to conclude the first chapter, we are going to provide an overview of the most relevant observational channel for testing BH physics, and in a wider perspective, gravity: gravitational waves (GWs).

1.3 Gravitational waves

As already discussed, BHs, in addition to being intriguing mathematical solutions and theoretical puzzles, are also astrophysical objects that populate our universe [101]. Today we are able to probe them with a variety of accurate observational techniques [8, 102]. Among these, the most powerful and informative channel is arguably given by GWs [40, 103]. When two compact objects find themselves in a binary system, the gravitational binding energy is progressively radiated away in the form of propagating ripples of spacetime curvature. This process leads to the final coalescence of the two bodies. The corresponding signal can be roughly divided in three stages: inspiral, merger and ringdown (Fig. 1.2) [104]. The last stage, corresponding to the post-merger emission of gravitational radiation, will be the main focus of this thesis, and we are going to dedicate the whole Chapter II to its

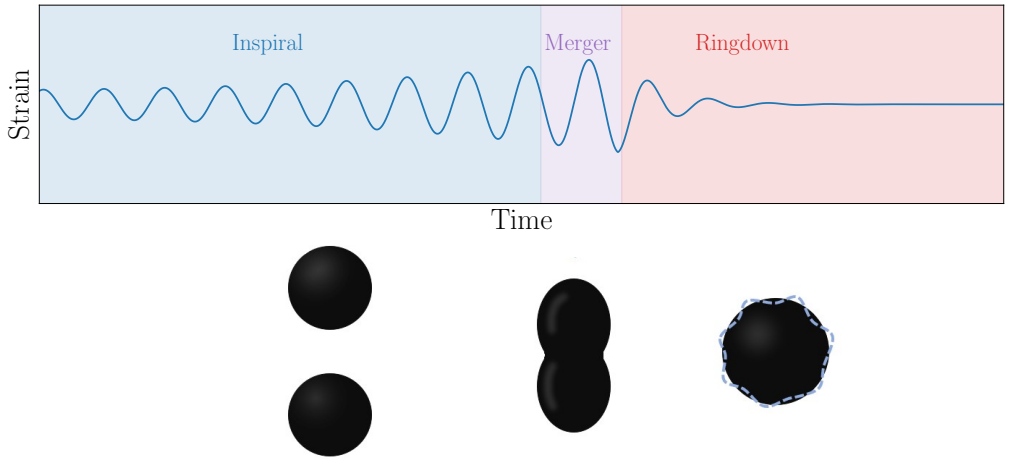

Figure 1.2: Three stages of a typical GW signal.

mathematical description. On the other hand, we provide here an euristic overview of the fundamental concepts in GW physics, in order to frame the discussion in the upcoming chapters within a broader perspective.

The spacetime of a propagating GW can be described as some perturbation on top of a background [105–110]. For simplicity, let us consider the background to be given by the flat Minkowsky metric: i.e. $g_{\mu\nu} = \eta_{\mu\nu} + \epsilon\, h_{\mu\nu} + \mathcal{O}\left(\epsilon^2\right)$, with $\epsilon \ll 1$. At linear order in ϵ, the Einstein Equation can be cast into the form of a wave equation for $h_{\mu\nu}$, with propagation speed equal to the speed of light. The propagation speed could, in principle, be different in an alternative theory of gravity.

Due to the diffeomorphism invariance of GR, the metric perturbation can be redefined with the gauge transformation [7, 107]

$$h_{\mu\nu} \to h_{\mu\nu} - \left(\partial_\mu \xi_\nu + \partial_\nu \xi_\mu\right) . \tag{1.22}$$

where ξ_μ is an infinitesimal vector field.

The most appropriate choice, for a plane GW propagating in vacuum, in GR, is the so called transverse-traceless (TT) gauge. Choosing as propagation direction the z axis of the cartesian coordinate system (t, x, y, z), one can express the metric perturbation as

$$h^{\mathrm{TT}}_{\mu\nu}(t,z) = \begin{pmatrix} 0 & 0 & 0 & 0 \\ 0 & h_+(t-z) & h_\times(t-z) & 0 \\ 0 & h_\times(t-z) & -h_+(t-z) & 0 \\ 0 & 0 & 0 & 0 \end{pmatrix} , \tag{1.23}$$

where the dependence on t, z is of the form $\exp(-2\pi i f(t-z))$, for a given oscillation frequency f. The two degrees of freedom h_+ and $h_\times$ represent the physical polarization states of the massless graviton. Beyond Einstein's gravity, in the most general theoretical setup, up to four additional polarization states can appear, i.e. two scalar ("breathing" and longitudinal), and two vector modes [111].

On the other hand, the amplitude of the GW is set by the properties of the source [112–115]. During the inspiral of a binary system of compact objects with comparable masses m_1 and m_2, observed at distance d, this reads

$$h_{\mu\nu} \propto \frac{\mu v^2}{d}(1 + \dots) , \tag{1.24}$$

where $\mu = m_1 m_2/(m_1 + m_2)$ is the reduced mass of the system and v is the orbital velocity in units of the speed of light. The dots represent higher-order *Post-Newtonian* corrections [115], i.e. contribution from higher powers of v.

The observable effect of a GW is described by the strain, defined as the fractional change in proper distance between freely falling test masses [116]. As a GW passes through a detector, it stretches and compresses space, causing variations in the separation between suspended mirrors [117, 118]. The specific pattern of stretching and squeezing depends on the polarization of the wave; in GR these amount to the aforementioned plus and cross modes. In practice, detectors are affected by various sources of contamination, and any real measurement is a combination of signal and noise [118]. The detector's noise amplitude as a function of frequency is called *sensitivity curve* of the instrument, and it indicates how sensitive it is across its operational bandwidth [119]. We refer the reader to Chapter 6 for more quantitative definitions of signal, noise and detector sensitivity curve.

Due to the intrinsic non-linearity of GR, not only do GW represent the dynamical geometric response of a spacetime to an evolving energy content. They also constitute a source of energy themselves, that can back-react on the spacetime background [106–110]. One might expect that the energy of a GW can be quantified through the definition of a SET, in the same fashion as that of any other dynamical field. However, the application of this concept to gravitational radiation is rather subtle. In an euristic way, one can derive a SET starting from the Einstein-Hilbert action, expanded around flat spacetime up to quadratic order in ϵ. In the TT gauge, this reads

$$S = -\frac{M_{\rm Pl}^2 \epsilon^2}{8} \int d^4x \, \partial_\alpha h^{\rm TT}_{\mu\nu} \, \eta^{\alpha\beta} \, \partial_\beta h^{\rm TT} \mu\nu \, + \mathcal{O}\left(\epsilon^3\right) . \tag{1.25}$$

We will from now on omit the book-keeping parameter ϵ.

Using the canonical definition of Eq. (1.8), one gets

$$T^{\rm GW,flat}_{\alpha\beta} \sim \frac{M_{\rm Pl}^2}{4} \, \partial_\alpha h^{\rm TT}_{\mu\nu} \, \partial_\beta h^{{\rm TT},\mu\nu} \, . \tag{1.26}$$

This definition, while being nice and simple, cannot be rigorously applied to a curved spacetime. In fact, in GR, the effects of the gravitational field can always be made to vanish locally by an appropriate choice of coordinates, and so, an actual SET for the gravitational field cannot be strictly defined. This is because, if a quantity is a tensor and non-vanishing in one frame, it must remain non-vanishing in all other coordinate systems related by a regular diffeomorfism. This issue can be overcome, with the definition of a *non-local*, effective SET for GWs. It turns out [109, 110] that this object is given by

$$T^{\rm GW}_{\alpha\beta} = \frac{M_{\rm Pl}^2}{4} \left\langle \partial_\alpha h^{\rm TT}_{\mu\nu} \, \partial_\beta h^{{\rm TT},\mu\nu} \right\rangle , \tag{1.27}$$

where the bracket $\langle \cdot \rangle$ has to be conceived as an averaging over spacetime scales that are much larger than the GW wavelenght f^{-1} and much smaller than the global spacetime curvature radius. Notice that, modulo this averaging operation, Eq. (1.27) appears the same as Eq. (1.26). This definition of SET allows to practically compute fluxes of GWs, and, in particular, the radiated power $\dot{E}_{\rm GW}$. In the case of two inspiraling compact objects introduced above, one has [112, 120]

$$\dot{E}_{\rm GW} = \frac{32}{5} \left(\frac{G^2 m_1 m_2}{d^2} \right)^2 v^2 + \dots , \tag{1.28}$$

At leading order, the energy loss due to gravitational radiation is balanced by the decay of the orbital energy, i.e., $\dot{E}_{\rm orb} = -\dot{E}_{\rm GW}$. This allows one to relate the time evolution of the GW frequency to the emitted power, providing an expression for $\dot{f}(f)$. The presence of other radiation channels in modified theories of gravity, would obviously lead to a different frequency evolution law. For instance, in a ST theory of gravity, in which compact objects possess in general *scalar charges*, scalar radiation is also emitted during the inspiral. In contrast with GWs, the leading multipole order in scalar radiation is the dipole, which would dominate over the quadrupole, especially at early stages [3] [8, 121]. The power emitted through this channel reads

$$\dot{E}_{\rm dip} = \frac{G}{3}\left(\frac{G_{\rm eff} m_1 m_2}{d^2}\right)^2 \left(q_s^{(1)} - q_s^{(2)}\right)^2 , \tag{1.29}$$

where we introduced the dimensionless scalar charges $q_s^{(1,2)}$, and the effective gravitational constant $G_{\rm eff} = G\left(1 + q_s^{(1)} q_s^{(2)}\right)$. Another effect of this kind occurs in models including extra spacetime dimensions, such as brane-world scenarios, where GWs can leak into the bulk [122, 123]. All these kinds of effect modify the binary's orbital decay rate, resulting in a potentially observable imprint in the GW phase evolution.

The first indirect evidence of GWs came through the observation of a very peculiar class of astrophysical objects: pulsars. A pulsar is a rapidly rotating neutron star that emits narrow beams of electromagnetic radiation, acting as an extremely precise cosmic clock due to the regularity of its pulses [124, 125]. The study of the Hulse-Taylor pulsar, discovered in 1975 [126], showed that the evolution of its orbital period matches the predictions from GR due to the emission of GWs [127, 128]. In particular, the matching to the GR prediction leaves little room for additional channels of energy loss, such as dipolar gravitational radiation that could arise if neutron stars carried an effective scalar charge. The absence of any measurable excess in the Hulse–Taylor data has therefore been used to set stringent upper limits on possible scalar charges of neutron stars, and more generally on any new gravitational degrees of freedom that could be radiated in binary systems [129]. Observations of other relativistic binaries, such as PSR J1738+0333, PSR J0737–3039A/B, and PSR J0348+0432, further tightened these constraints, showing that any deviation from the GR prediction for the orbital decay rate must be smaller than a few parts in a thousand [130–133].

In 2015, a GW signal, GW150914, was directly detected for the first time, and ushered in the era of GW astronomy [40]. Since this first detection, the number of observed GW events has grown considerably [134–136]. At the present time, a large catalog of binary BH mergers, as well as binary neutron star and BH–neutron star mergers has been collected. So far, all GW detections have been performed by the LIGO and Virgo collaborations, using three ground-based interferometers located in Livingston and Hanford (USA), and Cascina (Italy). The network, also including KAGRA [137, 138], the Japanese underground detector in Kamioka, is currently performing the fourth observing run. Data from these detectors have already placed tight constraints on several classes of modified gravity theories. For instance, the near-simultaneous detection of GW170817 and its electromagnetic counterpart ruled out a wide range of models predicting anomalous GW propagation speeds [139]. Furthermore, tests based on the absence of dipole radiation, consistency of the waveform phase, and polarization content have so far found no significant deviations

[3] The dipole term depends on the squared difference of the scalar charges, so the regime in which it dominates over the quadrupole depends on the specific system. In a mass-symmetric system this effect is absent.

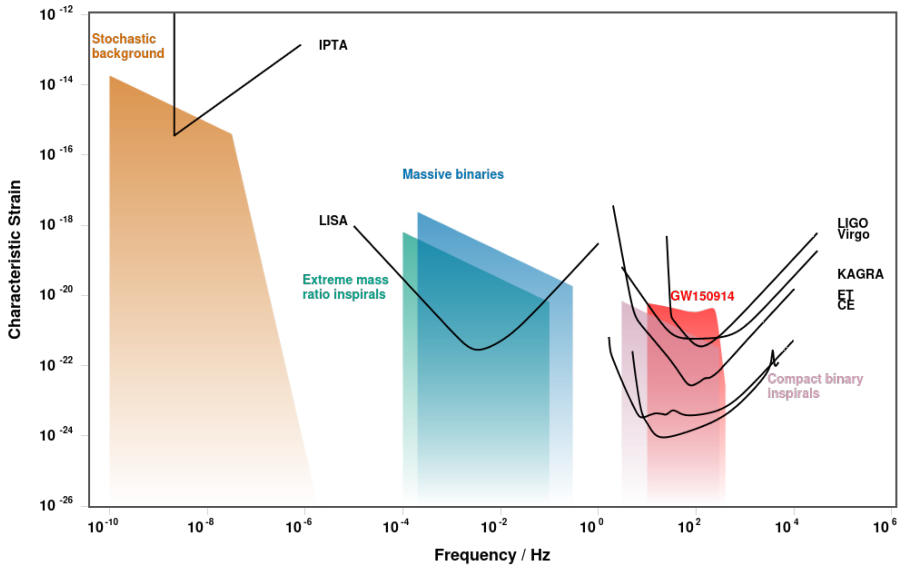

Figure 1.3: Sensitivity curves of the main GW detectors as a function of frequency. Image taken from [144].

from GR [140, 141]. Nonetheless, there still remains room for exploring beyond-GR signatures, particularly in the non-linear and strong-field regime. As detectors improve and the catalog of events grows, increasingly stringent and model-independent tests of gravity will become possible. Moreover, these future GW detection are going to be crucial not only in the fundamental physics perspective, but also for astrophysical purposes, such as understanding BH populations, their formation channels, and the evolution of compact binaries.

Looking ahead, third-generation ground-based detectors – such as the Einstein Telescope [142] and Cosmic Explorer [143] – are under development, aiming to achieve sensitivities approximately 100 times greater than those of the current facilities. All the aforementioned current and upcoming detectors are sensitive in the $1 - 10^4$ Hz frequency band, corresponding to GW signals emitted by coalescing stellar-mass BHs and neutron stars.

To explore the physics of massive and SMBHs, a new class of GW detectors is under development: space-based interferometers. Unlike ground-based observatories, these detectors will operate in space, allowing them to access lower frequency bands —ranging from 10^{-5} Hz to 10^{-1} Hz— which are ideal for observing the inspiral and merger of SMBH binaries (SMBHB), and extreme mass-ratio inspirals. Among the most prominent missions, the Laser Interferometer Space Antenna (LISA) [145] —a joint ESA-NASA project— is planned for launch in the mid-2030s and will consist of three spacecrafts in heliocentric orbit, forming a triangular constellation with arm lengths of 2.5 million kilometers. Thanks to its unprecedented sensitivity, LISA will be the optimal target for detailed analyses of the ringdown signal. We will dedicate Chapter 6 to this discussion. Other proposed missions include TianQin [146] and Taiji [147], led by China and scheduled for launch in the early 2030s, which will use a similar triangular configuration in Earth orbit, and DECIGO [148], a Japanese mission concept designed to bridge the frequency gap between LISA and ground-based detectors, targeting the decihertz range.

At the IR end of the GW frequency spectrum, Pulsar Timing Arrays (PTAs) are designed to probe nanohertz GWs, which are produced by extremely massive and slowly evolving systems such as SMBH binaries (with masses up to $10^9\,M_\odot$) [149–151]. PTAs do

not rely on laser interferometry; instead, they monitor millisecond pulsars—highly stable astrophysical clocks—spread across the sky. GWs travelling through the galaxy induce correlated fluctuations in the times of arrival of pulses from these objects. By precisely measuring these timing residuals across a large array of pulsars over many years, PTAs are sensitive to long-wavelength GW signals. Several international collaborations are currently active in this domain, including NANOGrav (North America) [152], EPTA (Europe) [153], PPTA (Parkes, Australia) [154], and the Indian PTA [155], now joined under the International Pulsar Timing Array (IPTA) [156]. In 2023, multiple PTAs reported compelling evidence of a stochastic background consistent with GWs emitted by a large population of SMBHBs [4] [161–166].The sensitivity curve of some representative detectors among the ones mentioned above, are represented in Fig. 1.3, together with the signal of different astrophysical sources on different mass scales.

We finally briefly mention that, at the opposite end of the spectrum, high-frequency GWs, typically in the MHz to GHz range, are hypothesized to originate from exotic high-energy physics phenomena. Their detection would require novel experimental approaches such as microwave cavity detectors and superconducting circuits [167, 168].

This overview of various GW detectors concludes the introductory chapter of the thesis. In the next chapter, we will explore ST theories of gravity in greater detail and discuss the possibility of BH solutions endowed with scalar charges. As mentioned previously, this scenario has fundamental implications for GW tests of gravity. Subsequently, beginning with Chapter II, we will delve into the physics of BH ringdown.

[4] Other possible explanations, involving more exotic scenarios related to early universe physics have been proposed. See for instance [157–160].

Chapter 2

No-hair theorems and their circumvention

2.1 Introduction

Scalar-tensor theories of gravity are the simplest and oldest extension of GR. In their basic form, they date back to the pioneering work by Fierz [169], Jordan [170], Brans and Dicke [171], who suggested supplementing the tensor gravitons of GR with a scalar degree of freedom conformally coupled to matter. This Fierz-Jordan-Brans-Dicke (FJBD) theory, and generalizations of it in which the conformal coupling to matter is expanded to nonlinear orders [121, 172], have been for decades the paradigmatic extensions of GR when performing experimental tests in the Solar System [102] and binary pulsars [173]. This has resulted in very tight bounds on these theories [8].

The observational evidence for a dark sector in cosmology [71, 72, 74, 174] and the direct detection of GWs by LIGO and Virgo [40] have spurred a resurgence of interest in scalar-tensor theories. It was realized that FJBD-like theories are not the most general ghost-free theories allowing for a scalar degree of freedom in addition to the tensor ones. Indeed, FJBD-like theories are just a special case of more general EFTs, where all possible scalar-tensor operators are organized in a derivative expansion. Higher derivative operators typically provide subleading corrections on a given solution at low energies, however there are cases where they can be as important as the ones with fewer derivatives, within the domain of validity of the low energy expansion. This property can be made robust by the presence of exact or approximate symmetries, which determine different sets of power-counting rules for the coupling constants in the effective Lagrangian, even in the absence of an explicit UV completion [175–177]. The simplest realization of these effective theories belongs to the Horndeski class [178], described by the following action[1]

$$\begin{aligned} S = \frac{M_{\rm Pl}^2}{2}\int \mathrm{d}^4x\sqrt{-g}\Big\{ & K(\psi,X) - G_3(\psi,X)\Box\psi + G_4(\psi,X)R \\ & + G_{4X}(\psi,X)\left[(\Box\psi)^2 - \left(\nabla_\mu\nabla_\nu\psi\right)^2\right] + G_5(\psi,X)G_{\mu\nu}\nabla^\mu\nabla^\nu\psi \\ & - \tfrac{G_{5X}(\psi,X)}{6}\left[(\Box\psi)^3 - 3\,(\Box\psi)\left(\nabla_\mu\nabla_\nu\psi\right)^2 + 2\left(\nabla_\mu\nabla_\nu\psi\right)^3\right]\Big\} + S_{\rm matter}[g_{\mu\nu},\Psi_m] \end{aligned} \tag{2.1}$$

where g, ∇, R and $G_{\mu\nu}$ and $M_{\rm Pl}$ are the metric determinant, Levi-Civita connection, Ricci scalar, Einstein tensor and reduced Planck mass; K, G_3, G_4, and G_5 are arbitrary

[1] In Eq. (2.1) we are not explicit about the energy scales associated with the derivative operators, which are absorbed in the definitions of K and G_i; we will restore them later on when needed.

functions of $X \equiv -\nabla_\mu\psi\nabla^\mu\psi/2$ and the scalar field ψ; $G_{iX} \equiv \partial G_i/\partial X$, $\Box \equiv \nabla^\mu\nabla_\mu$, $\left(\nabla_\mu\nabla_\nu\psi\right)^2 \equiv \nabla_\mu\nabla^\nu\psi\nabla_\nu\nabla^\mu\psi$ and $\left(\nabla_\mu\nabla_\nu\psi\right)^3 \equiv \nabla_\mu\nabla^\rho\psi\nabla_\rho\nabla^\nu\psi\nabla_\nu\nabla^\mu\psi$; and Ψ_m are the matter fields. The class of theories given by Eq. (2.1) can be further generalized to the beyond Horndeski [179, 180] and degenerate-higher-order-scalar-tensor (DHOST) theories [181–186] (see [187] for a review). The latter is defined as the most general class of scalar-tensor theories with no propagating ghost degrees of freedom, although only a subset of those can be considered as "robust" EFTs [176, 177, 188].

The coincident detection of GWs and gamma rays from the neutron star merger GW170817 [189], as well as the requirement that GWs do not decay into dark energy [190, 191] and that the scalar mode be nonlinearly stable [192], have already placed very strong constraints on DHOST, under the assumption that the theory provides a dark energy like phenomenology on cosmological scales. With this assumption, the only theories still viable are described by the action [193]

$$S = \int \mathrm{d}^4x\sqrt{-g}\left[\frac{M_{\rm Pl}^2}{2}\Phi\, R + K(\psi, X) + \frac{3\,\Phi_X^2}{2\,\Phi}\nabla^\mu\psi\nabla_{\mu\rho}\psi\nabla^{\rho\nu}\psi\nabla_\nu\psi\right] + S_{\rm matter}[g_{\mu\nu}, \Psi_m]\,, \tag{2.2}$$

where Φ and K are functions of ψ and X (with $\Phi_X \equiv \partial\Phi/\partial X$). With a conformal transformation from the "Jordan frame" to the "Einstein frame", i.e. $g_{\mu\nu} \to \Phi^{-1}\, g_{\mu\nu}$, the action can be rewritten (redefining the function K) as the "K-essence" action

$$S = \int \mathrm{d}^4x\sqrt{-g}\left[\frac{M_{\rm Pl}^2}{2}R + K(\psi, X)\right] + S_{\rm matter}\left[\frac{g_{\mu\nu}}{\Phi(\psi, X)}, \Psi_m\right]. \tag{2.3}$$

The conformal coupling to matter $\Phi(\psi, X)$ can potentially be tested with observations of neutron stars (in isolation [172] or in binaries [194, 195]). The kinetic function $K(\psi, X)$ also has important consequences for the dynamics of matter systems. For instance, specific kinetic functions can give rise to self-accelerated solutions in cosmology [196], or to nonlinear screening mechanisms that "hide" the deviations from GR on local scales (at least in quasistatic situations [197–200]). However, the cleanest probes of the kinetic term $K(\psi, X)$ are provided by vacuum systems (e.g. BHs), since for those the effect of the conformal coupling function $\Phi(\psi, X)$ vanishes. This is particularly interesting in light of the several BH binary systems detected by LIGO and Virgo [136].

The deviations of the GW signal (and more generally of the geometry) of BHs in scalar-tensor theories from their GR counterparts is parametrized in terms of scalar hairs (also referred to as sensitivities [201, 202] or scalar charges [121, 172]). These parameters model the effective coupling between BHs and the scalar graviton in these theories, and are therefore absent in GR. In fact, these charges can also be thought of as quantifying violations of the no-hair theorem [16, 32, 203, 204] and of the strong equivalence principle [102], which are satisfied in GR but not necessarily in more general gravitational theories.

A more quantitative definition of scalar charge can be derived in a point-particle (or worldline) EFT [205–207] perspective. As discussed in Chapter 1, an EFT is typically constructed by integrating out UV degrees of freedom, thereby capturing the relevant long-distance physics. In our astrophysical context, the key idea is that, at sufficiently large distances, the detailed internal structure of a compact object can be integrated out, allowing it to be modeled as an effective point particle of mass $m_{\rm pp}$ traveling along a worldline. In the following, we will only consider the case of a non-spinning compact object. The inclusion of spin in this picture can be found in [208, 209].

The point-particle action, at lowest order, can be expressed as the Nambu-Goto action [210, 211]

$$S_{\rm pp} = -m_{\rm pp} \int d\tau \sqrt{-g_{\mu\nu} \frac{dx^\mu}{d\tau} \frac{dx^\nu}{d\tau}} \,, \tag{2.4}$$

where τ is an affine parameter along the particle's worldline, and $x^\mu(\tau)$ denotes the spacetime position of the particle as a function of τ. The variation of the point-particle action with respect to $x(\tau)$, yields the well-known geodesic equation

$$\frac{dx^\rho}{d\tau} \nabla_\rho \left(\frac{dx^\mu}{d\tau} \right) = 0 \,. \tag{2.5}$$

As a simple instance, which should better clarify this approach, we sketch how the Schwarzschild metric can be reconstructed in this framework. We will consider in the following that no matter field is present, i.e. we will forget about the action $S_{\rm matter}$. By expanding the spacetime metric around flat spacetime in the usual way, and solving the Einstein Equation perturbatively, at linear order and in the point-particle's rest frame, one has

$$G_{\mu\nu} \left[h^{(1)}_{\mu\nu} \right] = -8\pi G \, m_{\rm pp} \, \delta^t_\mu \delta^t_\nu \delta^{(3)}_D(\vec{x}) \,. \tag{2.6}$$

Choosing the harmonic gauge $\partial^\rho \partial^\sigma h_{\rho\sigma} = \frac{1}{2} \Box h^\alpha_\alpha$, and considering the static limit, i.e. $\Box \simeq \nabla^2$, one has

$$\nabla^2 h^{(1)}_{\mu\nu} = -4\pi G \, m_{\rm pp} \left(2\delta^t_\mu \delta^t_\nu + \eta_{\mu\nu} \right) \delta^{(3)}_D(\vec{x}) \,, \tag{2.7}$$

which is solved by

$$h^{(1)}_{\mu\nu} = \frac{2G m_{\rm pp}}{\tilde{r}} \delta_{\mu\nu} \,, \tag{2.8}$$

where $\tilde{r}$ indicates a harmonic radial coordinate. The full metric $g_{\mu\nu} = \eta_{\mu\nu} + \epsilon h^{(1)}_{\mu\nu} + \mathcal{O}(\epsilon^2)$ can be matched to the Schwarzschild one in harmonic coordinates, given more in general by the condition $\partial_\mu \left(\sqrt{-\tilde{g}} \, \tilde{g}^{\mu\nu} \right) = 0$. In the limit $r_s \ll \tilde{r}$, one has

$$g^{\rm (Sch)}_{\mu\nu} = \eta_{\mu\nu} + \frac{r_s}{\tilde{r}} \delta_{\mu\nu} + \mathcal{O}\left(\frac{r_s}{\tilde{r}} \right)^2 \,. \tag{2.9}$$

This can clearly be matched to the point-particle result with the identification $M = m_{\rm pp}$.

In a ST theory, the mass of a compact object can in general depend on the scalar field, so one has to replace $m_{\rm pp} \to m_{\rm pp}(\psi)$. Hence, the total action has the general form

$$S_{\rm tot} = I - \int {\rm d}\tau \sqrt{-g_{\mu\nu} \frac{dx^\mu}{d\tau} \frac{dx^\nu}{d\tau}} m_{\rm pp}(\psi) \,, \tag{2.10}$$

where I represents the action of a ST theory in the bulk. Varying $S_{\rm tot}$ with respect to the metric tensor and the scalar field, one obtains a system of coupled equations of motion that can be solved perturbatively around flat spacetime and constant background scalar field ψ_∞. In the rest frame of the compact object and in harmonic coordinates, on gets

$$\begin{aligned} \tilde{g}_{\mu\nu} &= \eta_{\mu\nu} + \frac{2G m_{\rm pp}(\psi_\infty)}{\tilde{r}} \delta_{\mu\nu} + \mathcal{O}\left(\tilde{r}^{-2} \right) \,, \\ \psi &= \psi_\infty - \frac{G m'_{\rm pp}(\psi_\infty)}{\tilde{r}} + \mathcal{O}\left(\tilde{r}^{-2} \right) \,. \end{aligned} \tag{2.11}$$

These expressions can be matched with the large-distance behavior of a stationary solution, representing a compact object in a ST theory of gravity. Using the same system of harmonic coordinates, one has, at leading order,

$$\begin{aligned} \tilde{g}_{\mu\nu} &= \eta_{\mu\nu} + \frac{2GM}{\tilde{r}}\delta_{\mu\nu} + \mathcal{O}\left(\tilde{r}^{-2}\right) , \\ \psi &= \psi_\infty + \frac{Q_S}{\tilde{r}} + \mathcal{O}\left(\tilde{r}^{-2}\right) , \end{aligned} \tag{2.12}$$

where M is the ADM mass of the compact object, and Q_S is the scalar charge, related to the dimensionless one introduced in the previous chapter as $Q_S = Mq_s$. The matching between the two results leads to the identification

$$\begin{aligned} m_{\rm pp}(\psi_\infty) &= M , \\ m'_{\rm pp}(\psi_\infty) &= -Q_S . \end{aligned} \tag{2.13}$$

Thus the scalar charge of a compact object, appears as a measure of the dependence of its gravitational mass on the background scalar field. Notice that this definition of scalar charge holds in the Einstein frame. In the presence of matter, such as in the case of neutron stars, it is generally useful to introduce a Jordan-frame counterpart of the scalar charge, called sensitivity "s", defined as

$$s = \frac{\partial \ln M_J}{\partial \ln \Phi} , \tag{2.14}$$

where M_J is the Jordan-frame mass of the object. Since we are interested in vacuum solutions, from now on we are going to employ the definition of scalar charge Q_S.

The appearance of scalar hairs, quantified by a non-vanishing Q_S, is, however, not a general feature of ST theories of gravity. In FJBD-like theories, with or without a scalar field mass, no-hair theorems exist and dictate that BH solutions must match the GR ones if one assumes asymptotically flat boundary conditions [212].[2] This theorem also applies to BHs in K-essence, under the same asymptotically flat boundary conditions and provided that the kinetic function satisfies suitable "stability" conditions [214].

BH hairs, however, generically appear, even in K-essence and FJBD-like theories, if the scalar field grows with time far from the BH [215–218], as would be expected if one were to match to a cosmological solution on large scales. Moreover, if one does not require the scalar field to provide an effective dark energy phenomenology, the aforementioned bounds on the DHOST class (coming from gravitational-wave propagation, the decay of GWs into the scalar mode, and the nonlinear stability of the latter) are no more applicable. No-hair theorems exist for subsets of the DHOST class in spherical symmetry [219], but they rely on shift symmetry and on the assumption that the free functions appearing in the DHOST action are analytic. Therefore, not only are scalar charges generically expected for DHOST theories that break shift symmetry in vacuum, but these theorems also do not apply to actions including interactions between the scalar field and the GB invariant [220, 221] (which corresponds to a nonanalytic $G_5 \propto \ln|X|$ [222, 223]). These couplings are known to produce BH charges that can be even nonperturbatively large (BH scalarization) in both the spherical [224, 225] and rotating [226, 227] case.

In this chapter, we generalize existing no-hair theorems in the context of scalar-tensor gravity and review the situations where these theorems can be violated. In more detail, in Sec. 2.2, we provide the proof of a no-hair theorem for stationary asymptotically flat BHs, holding for any shift-symmetric scalar-tensor theory (including Horndeski and DHOST). In Sec. 2.3, we show that this result can be generalized to an arbitrary number d of spacetime

[2] Note that introducing a matter content, one can derive also no-hair theorems for stars [213].

dimensions, under suitable assumptions on the topology of the horizon. In Sec. 2.4, we provide examples which violate the no-hair theorems, explaining which assumptions of our proof are violated. We also compute the scalar charge associated with a linear time dependence of the scalar field, under suitable regularity conditions at the EH. Finally, in Sec. 2.5, we further comment on possible extensions of the existing theorems dropping the shift-symmetry assumption.

2.2 No-hair theorem for rotating BHs

In this section, we prove a no-hair theorem for rotating BHs in four spacetime dimensions, which we generalize to arbitrary spacetime dimensions in Sec. 2.3. In particular, we show that asymptotically flat, axisymmetric and stationary BHs in shift-symmetric scalar-tensor theories cannot develop a term $\propto 1/r$ in the scalar profile at large distances. This is equivalent to saying that BHs cannot have a scalar charge [121, 172].

The fundamental assumptions that we make are the following:

(i) the metric is circular; i.e. it has two commuting Killing vectors associated respectively to the invariance under shifts in the time coordinate t (stationarity) and in the azimuthal angle ϕ (axisymmetry), and it is invariant under the reflection isometry $\{t \to -t,\, \phi \to -\phi\}$;

(ii) the spacetime is asymptotically flat, reducing at large radii to the Minkowski metric $\eta_{\mu\nu}$, plus subleading corrections $h_{\mu\nu} \sim \mathcal{O}(1/r)$;

(iii) The action and the field equations for the scalar field ψ are invariant under shifts $\psi \to \psi + c$, with c a constant;

(iv) if a nontrivial solution for the scalar field exists, it has the same symmetries as the spacetime, i.e., it does not depend on the coordinates associated with the Killing vectors of the metric;

(v) the squared norm $J^\mu J_\mu$ of the conserved Noether current J_μ associated with the shift symmetry $\psi \to \psi + c$ is regular at the horizon;

(vi) the current J_μ reduces asymptotically to that of a free massless scalar field, i.e. $J_\mu = -\partial_\mu \psi$ at large distances.

Note that the latter condition is expected to hold in any standard effective theory for a scalar coupled to gravity, where derivative interactions computed on the background are more suppressed by powers of $1/r$ at large distances.[3] To be concrete, we will sometimes

[3] In particular, it holds for the Horndeski Lagrangian (2.1) and more in general for the DHOST class [181–186].

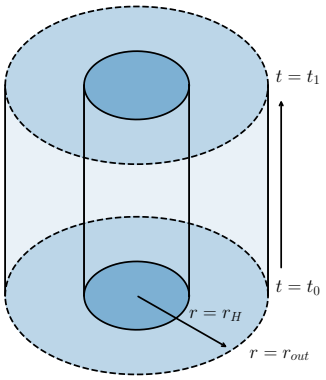

Figure 2.1: Schematic representation of the boundary $\partial\mathcal{M}$ appearing in Eq. (2.17).

refer below to the explicit Horndeski action in Eq. (2.1), with shift current J_μ given by

$$\begin{aligned} J_\mu = &- \nabla_\mu\psi \Big\{ K_X - G_{3X}\Box\psi + G_{4X}R + G_{4XX}\left[(\Box\psi)^2 - (\nabla_\alpha\nabla_\beta\psi)^2\right] \\ &+ G_{5X}G^{\alpha\beta}\nabla_\alpha\nabla_\beta\psi - G_{5XX}\left[(\Box\psi)^3 - 3\Box\psi\,(\nabla_\alpha\nabla_\beta\psi)^2 + 2(\nabla_\alpha\nabla_\beta\psi)^3\right]\Big\} \\ &- \partial^\nu X \Big\{ - g_{\mu\nu}\,G_{3X} + 2G_{4XX}(\Box\psi\, g_{\mu\nu} - \nabla_\mu\nabla_\nu\psi) + G_{5X}G_{\mu\nu} \\ &- \frac{1}{2}G_{5XX}\left[g_{\mu\nu}(\Box\psi)^2 - g_{\mu\nu}(\nabla_\alpha\nabla_\beta\psi)^2 - 2\Box\psi\,\nabla_\mu\nabla_\nu\psi\right. \\ &\left. + 2\nabla_\mu\nabla_\sigma\psi\nabla^\sigma\nabla_\nu\psi\right]\Big\} + 2G_{4X}R_{\mu\sigma}\nabla^\sigma\psi \\ &+ G_{5X}(-\Box\psi\,R_{\mu\sigma}\nabla^\sigma\psi + R^\alpha{}_\nu{}^\beta{}_\mu\nabla_\alpha\nabla_\beta\psi\nabla^\nu\psi + R_\alpha{}^\beta\nabla^\alpha\psi\nabla_\mu\nabla_\beta\psi)\,. \end{aligned} \tag{2.15}$$

However, our result is more general, as it relies only on assumptions (i)-(vi), and does not depend on the explicit form of the (shift-symmetric) scalar action. We will discuss in Sec. 2.4.1 the possibility of relaxing some of the assumptions above.

Let us start by noting that, thanks to the shift symmetry, the scalar's equations of motion can be expressed, in absence of matter, in the form of a (covariant) conservation law,

$$\nabla^\mu J_\mu = 0\,, \tag{2.16}$$

where ∇_μ is the covariant derivative. Integrating Eq. (2.16) over the spacetime outside the horizon and using Stokes' theorem, one gets

$$\oint_{\partial\mathcal{M}} \mathrm{d}\Sigma_\mu\, g^{\mu\nu}\, J_\nu = 0\,, \tag{2.17}$$

where $\partial\mathcal{M}$ is the three-dimensional boundary of the BH exterior region and $\mathrm{d}\Sigma_\mu$ is the element of the hypersurface $\partial\mathcal{M}$. Introducing a radial coordinate r constant on the horizon ($r = r_{\rm H}$) - which can be done without loss of generality if we assume that the horizon has the topology of a sphere [228] - and a time coordinate t, the boundary $\partial\mathcal{M}$ includes four contributions: two with fixed radius ($r = r_{\rm H}$ or $r = r_{\rm out} \to \infty$) and variable $t \in [t_0, t_1]$ (with t_0 and t_1 two constants), and two with $t = t_0$ or $t = t_1$ and $r \in [r_{\rm H}, r_{\rm out}]$. See Fig. 2.1 for a sketch of the domain of integration.

Let us focus first on the horizon contribution to the boundary integral in Eq. (2.17). The Cotton-Darboux theorem [229, 230] ensures that it is always possible to recast the

metric of a three-manifold into diagonal form via a local coordinate transformation. In particular, in $d = 4$ dimensions, under the assumptions of stationarity and axisymmetry, we can always choose coordinates such that the line element for the exterior geometry takes the Weyl-Papapetrou form [31, 231]:

$$ds^2 = -P\,\mathrm{d}t^2 + 2Q\,\mathrm{d}t\,\mathrm{d}\phi + H\,\mathrm{d}\phi^2 + W\left(\mathrm{d}\rho^2 + \mathrm{d}z^2\right), \tag{2.18}$$

where the only off diagonal component of the metric is $g_{t\phi} = Q$. As a result, $\mathrm{d}\Sigma_t = \mathrm{d}\Sigma_\phi = \mathrm{d}\Sigma^t = \mathrm{d}\Sigma^\phi = 0$ on the horizon hypersurface $r = r_{\rm H}$. In addition, using the assumptions (iii)-(iv), one can show in general that $J_t = J_\phi = 0$, and thus also $J^t = J^\phi = 0$, everywhere, and in particular at the horizon. This can be checked explicitly for the Horndeski current in Eq. (2.15), while a general proof holding for any theory that satisfies the above requirements can be found in Appendix A.1. Thus, we can write

$$\mathrm{d}\Sigma_\mu\, g^{\mu\nu}\, J_\nu = \mathrm{d}\Sigma_i g^{ij} J_j \tag{2.19}$$

as an inner product in a three-dimensional space.

Using Eq. (2.18), one obtains, more explicitly,

$$\begin{aligned}(\mathrm{d}\Sigma_i\, g^{ij}\, J_j)^2 &= W^{-2}\left(\mathrm{d}\Sigma_\rho J_\rho + \mathrm{d}\Sigma_z J_z\right)^2 \\ &\leq W^{-2}\left(\mathrm{d}\Sigma_\rho^2 + \mathrm{d}\Sigma_z^2\right)\left(J_\rho^2 + J_z^2\right) = \\ &= \left(J_i\, g^{ij}\, J_j\right)\left(\mathrm{d}\Sigma_k\, g^{kl}\, \mathrm{d}\Sigma_l\right),\end{aligned} \tag{2.20}$$

where we have used the Cauchy-Schwarz inequality. From the regularity of $J_i\, g^{ij}\, J_j$, which follows from the assumption (v) and the fact that $J_t = J_\phi = 0$, and from the vanishing of $\mathrm{d}\Sigma_k\, g^{kl}\, \mathrm{d}\Sigma_l$ at $r = r_{\rm H}$ by definition of null hypersurface, it follows that the right-hand side of Eq. (2.20) vanishes at the horizon. As a consequence, the left-hand side of Eq. (2.20) must vanish as well. This proves that in $d = 4$ there is no flux at the horizon contributing to the integral in Eq. (2.17).[4]

Let us now focus on the constant-time boundaries of the region in Fig. 2.1. On the hypersurfaces $t = t_0$, or $t = t_1$, one has $\mathrm{d}\Sigma_\mu \propto \delta^t_\mu$ [231]. Therefore, since $J_t = J_\phi = 0$, $\mathrm{d}\Sigma_\mu\, g^{\mu\nu}\, J_\nu = 0$ at both $t = t_0$ and $t = t_1$.[5]

We are therefore left only with the boundary contribution at large radii. Choosing the boundary to be at $r = r_{\rm out} \to \infty$, the flux reads

$$\oint_{\partial\mathcal{M}} \mathrm{d}\Sigma_\mu\, g^{\mu\nu}\, J_\nu = \int_{\{r\to\infty\}} \mathrm{d}\Sigma_r\, g^{rr}\, J_r\,. \tag{2.21}$$

At large distances, we can express the scalar profile as $\psi = \sum_\ell \psi_\ell(r) P_\ell(\cos\theta)$, where P_ℓ are the Legendre polynomials and ψ_ℓ (because of asymptotic flatness) go at leading order as[6]

$$\psi_\ell \sim \frac{a_\ell}{r^{\ell+1}}\,, \tag{2.22}$$

[4] The vanishing of this contribution can also be proven, in $d = 4$ dimensions and for Horndeski theories, by assuming that the surface gravity of the horizon is constant and the scalar field is regular [232, 233].

[5] It is actually not necessary that J_t and J_ϕ vanish. It is enough that they are independent of t and ϕ, as required by stationarity and axisymmetry. In fact, $\mathrm{d}\Sigma_\mu$ points in opposite directions at $t = t_0$ and $t = t_1$; thus, for J_t and J_ϕ independent of t and ϕ, the fluxes at the time boundaries are guaranteed to cancel each other.

[6] We are using here the assumption that the scalar equations of motion reduce, at large distances from the BH, to those of a free scalar field, and we are disregarding the other independent solution with falloff $\sim r^\ell$.

for constant a_ℓ. In particular, the coefficient a_0 of the monopole term with $\ell = 0$ is related to the scalar charge, or "hair", Q_S via $a_0 = Q_S M$, where M is the BH mass [195, 199, 234]. Let us now use assumption (vi) and write [121, 173]

$$J_r \sim -\partial_r \psi \tag{2.23}$$

at large distances from the BH. Furthermore, from assumption (ii) we have $g^{rr} = 1 + \mathcal{O}(1/r)$. Computing the integral (2.21) using spherical polar coordinates one gets

$$\int_{\{r\to\infty\}} \mathrm{d}\Sigma_r \, g^{rr} \, J_r = \lim_{r\to\infty} r^2 \int \mathrm{d}t \, \mathrm{d}\Omega_{S^2} \, J_r = (t_1 - t_0)\, 4\pi M Q_S = 0 \,, \tag{2.24}$$

which implies $Q_S = 0$.

Hence, we have shown that under the assumptions (i)-(vi) above, the scalar charge is always zero in four dimensions. This result is independent of the particular form of the (shit-symmetric) scalar action and can be generalized to arbitrary dimensions, as we will discuss in the next section. In this sense, it is a generalization of the no-hair theorem of Ref. [219] - which applies to non-rotating BHs in shift-symmetric scalar-tensor theories - as well as of the theorem of Refs. [214, 231, 235] - which applies to rotating BHs, but which holds only in theories with at most single derivatives acting on the scalar field. However, our result is weaker because it rules out only the monopole scalar hair, but does not exclude the possibility of nonvanishing subleading multipole terms in the scalar profile.

2.3 Generalization to higher dimensions

We will now generalize the results of the previous section to arbitrary spacetime dimensions $d > 4$. The landscape of vacuum solutions in higher-dimensional GR is richer than in four dimensions. In $d > 4$ there exist black objects with extended horizons, such as black strings and black p-branes, as well as solutions presenting horizons with nontrivial topology, such as black rings. See, e.g., Ref. [236] for a review. For simplicity, we will focus here on spacetimes with horizons that have the topology of a sphere, and restrict our analysis to the class of Myers-Perry BHs (with single or multiple spins) [236, 237], leaving the generalization to different types of solutions for future work.

The fundamental assumptions will be the same as in the previous section, properly generalized. In particular, we will assume that (i) the metric has $n+1$ commuting Killing vectors given by ∂_t and ∂_{ϕ_a}, for $a = 1, \ldots, n$, with $n \leq d-2$, and is invariant under the symmetry transformation $\{t \to -t, \phi_1 \to -\phi_1, \ldots, \phi_n \to -\phi_n\}$. In addition, we require (ii) asymptotic flatness, with subleading corrections scaling now as $1/r^{d-3}$ for $h_{\mu\nu}$ and ψ. The assumptions (iii)-(vi) of Sec. 2.2 are instead unchanged, with the only obvious remark that (iv) should be now understood to apply to all $n+1$ Killing vectors of the metric.

Note that Eqs. (2.16) and (2.17) (where now $\partial\mathcal{M}$ is the generalization of the boundary hypersurface in Fig. 2.1 to higher dimensions) hold in any spacetime dimension. Therefore, the first part of the argument is identical up to Eq. (2.17). Let us thus reconsider the different contributions to the flux in Eq. (2.17). First, notice that the contribution from the boundaries at fixed t_0 and t_1 vanishes for the same reason discussed above. Regarding the boundary at $r = r_H$, one can define the null directed surface element $\mathrm{d}\Sigma_\mu$ orthogonal to the horizon, where $\mathrm{d}\Sigma_t = \mathrm{d}\Sigma_{\phi_a} = 0$ because of (i). Hence Eq. (2.19) also remains true. However, showing that g^{ij} is positive-definite requires slightly adjusted considerations, because one cannot generically guarantee that g^{ij} can be put in diagonal form. We shall thus proceed as follows. First, from the positivity of the spatial line element $\mathrm{d}l^2 = g_{ij}\mathrm{d}x^i\mathrm{d}x^j$,

where latin indices here denote the $n-1$ spatial coordinates, it follows that g_{ij} with lower spatial indices is positive-definite everywhere in the BH exterior. Furthermore, one can choose the coordinates in such a way that the only off diagonal terms in the metric tensor are those that mix time with the angles ϕ_a associated with the spin direction(s). In reference to this, see e.g. the explicit form of the Myers–Perry line element in Appendix A.2. Hence, the metric can be expressed as

$$(g_{\mu\nu}) = \begin{pmatrix} g_{tt} & u_j \\ u_i & \gamma_{ij} \end{pmatrix} , \tag{2.25}$$

where the only nonvanishing components of the vector u are those corresponding to the coordinates ϕ_i, and where γ is a positive-definite $(d-1)\times(d-1)$ matrix, defined as $\gamma_{ij} = g_{ij}$. Note that the spatial indices of the metric blocks are raised/lowered as

$$u^i = \gamma^{ij} u_j \,, \qquad\qquad \gamma_{ik}\gamma^{kj} = \delta_i^j \,. \tag{2.26}$$

Using the inversion rule for a block matrix, we get the spatial part of the inverse metric as

$$g^{ij} = \gamma^{ij} + \frac{\gamma^{ik}\, u_k\, u_l\, \gamma^{lj}}{g_{tt} - u_k\, \gamma^{kl}\, u_l} \,. \tag{2.27}$$

From the symmetries of the BH solution, it follows that γ^{-1} is block diagonal and does not mix the ϕ_a directions with the other spatial coordinates. Therefore, $\mathrm{d}\Sigma_i \gamma^{ik}\, u_k = J_i\, \gamma^{ik}\, u_k = 0$. Furthermore, $\mathrm{d}\Sigma_t = \mathrm{d}\Sigma_{\phi_a} = J_t = J_{\phi_a} = 0$ (see Appendix A.1). Hence, in analogy with the $d = 4$ case, we have

$$\mathrm{d}\Sigma_\alpha\, g^{\alpha\beta}\, J_\beta = \mathrm{d}\Sigma_i\, \gamma^{ij}\, J_j \,. \tag{2.28}$$

At this point, since γ^{-1} is positive definite, we can safely apply the Cauchy–Schwarz inequality

$$(\mathrm{d}\Sigma_i\, \gamma^{ij}\, J_j)^2 \leq (J_i\, \gamma^{ij}\, J_j)\, (\mathrm{d}\Sigma_k\, \gamma^{kl}\, \mathrm{d}\Sigma_l) \,. \tag{2.29}$$

From the regularity of $J^\mu J_\mu$ at the horizon [assumption (v)] and $J_t = J_{\phi_a} = 0$, the right-hand side of Eq. (2.29) is zero, as $\mathrm{d}\Sigma$ is null and has therefore vanishing norm at the horizon.[7] This shows that the contribution to the integral (2.17) from this boundary is zero, just like in the $d = 4$ case.

At large distances, we can decompose the scalar field as $\psi = \sum_L \tilde{\psi}_L(r) Y_L(\theta)$, where Y_L are hyperspherical harmonics, θ is a shorthand for the angles on the $(d-2)$-dimensional hypersphere (see, e.g., Ref. [238]), and ψ_L scale at leading order as

$$\tilde{\psi}_L \sim \frac{a_L}{r^{L+d-3}} \,, \tag{2.30}$$

for constant a_L. The scalar charge can be defined via $a_0 = Q_S\, \mu$, where μ is the d-dimensional mass parameter defined in Appendix A.2, which reduces to $2GM$ in four dimensions.

Computing the flux at spatial infinity yields

$$\begin{aligned} \int_{\{r\to\infty\}} \mathrm{d}\Sigma_r\, g^{rr}\, J_r &= \lim_{r\to\infty} r^{d-2} \int \mathrm{d}t\, \mathrm{d}\Omega_{S^{d-2}}\, g^{rr}\, J_r \\ &= (t_1 - t_0) \frac{8\pi}{(d-2)} M Q_S = 0 \,, \end{aligned} \tag{2.31}$$

which generalizes (2.24) to higher dimensions.

[7] Actually, one needs to apply the argument slightly away from the horizon, and a limit must be taken.

2.4 Evading the no-hair theorem

In this section, we study how the no-hair theorem formulated in Sec. 2.2 is affected if we drop some of its underlying assumptions. We will consider in particular two cases: a linear time dependence in the scalar profile, and a coupling to the Gauss–Bonnet operator, which violate the conditions (iv) and (v) respectively. We will also mention the possibility that assumption (i) is violated.

2.4.1 Introducing a linear time dependence

Let us start by relaxing the condition (iv). It is in general not strictly necessary for the scalar field solution ψ to have the same symmetries as the background metric: one can in fact allow for a linear dependence in t and/or ϕ_a while keeping the isometries of the spacetime unchanged. In practice, this happens because the shift symmetry ensures that the stress energy tensor depends on ψ only through its derivatives. Said differently, although time translations and/or rotations in ϕ_a are spontaneously broken, it is possible to find, for each broken generator, a "diagonal" combination with a suitable shift in ψ that is unbroken on the background solution.

It has been shown in [239] that a linear time dependence in the scalar profile is actually not allowed around stationary asymptotically flat BHs in the context of K-essence. However, the proof assumes a field ψ that is backreacting on the metric through its SET, while it is possible to find counterexamples to this statement in the test field limit. The simplest and most notable example of this is given by Jacobson's solution [215] (see also [216]), where the scalar field carries a linear dependence on time. More general examples of such "stealth" solutions beyond K-essence have been later found also in the context of e.g. Schwarzschild-(A)dS BHs [240–244] and Lorentz-violating gravity [245].

Given these preliminary considerations, let us consider a scalar profile of the form[8]

$$\psi = S(r,\theta) + E\,t\,, \tag{2.32}$$

where we have included a linear dependence on time, and where we have denoted generically with θ the angles that do not correspond to Killing directions. Note that at large r, S admits the multipole expansion given by Eq. (2.30).

Let us start again from Eq. (2.17). The contributions to the integral from the fluxes through the hypersurfaces at $t = t_0$ and $t = t_1$ cancel out for the same reason as in the previous sections. A crucial difference is instead arising from the contribution at the horizon. To understand why, let us focus on the inequality in Eq. (2.29). In Sec. 2.3 it was crucial that $J_t = J_{\phi_a} = 0$ to be able to use the assumption (v) and conclude that $J_i g^{ij} J_i$ is finite at the horizon. This is no longer true now, as a profile of the form in Eq. (2.32) will in general induce a nonzero J_t, allowing $J_i g^{ij} J_i$ to be singular at $r = r_{\rm H}$ without invalidating the regularity of $J^\mu J_\mu$.

An example of this is given by Ref. [215]. That solution is valid in the limit in which the scalar field backreaction on the geometry is neglected; i.e. it is an exact solution of the Klein–Gordon equation $\Box\psi = 0$ on a Schwarzschild background. It reads explicitly

$$\psi(t,r) = Q_S \left[\frac{t}{r_s} + \ln\left(1 - \frac{r_s}{r}\right)\right], \tag{2.33}$$

where $r_s = 2GM$ denotes the Schwarzschild EH radius. The conserved shift-symmetry current in this case is simply $J^\mu = \partial^\mu\psi$. The squared norm $J^\mu J_\mu$ is thus just the standard

[8] For simplicity, we considered only a linear term in t. Adding linear terms in the angles ϕ_a would not formally change our conclusions.

kinetic term $\partial_\mu\psi\partial^\mu\psi$, which is regular at $r = r_s$, as can easily be verified using Eq. (2.33). However, computing the left-hand side of Eq. (2.29) explicitly, we see that it does not vanish at $r = r_s$. In fact,

$$\int_{r=r_s} \mathrm{d}\Sigma_r \, g^{rr} \, J_r = -4\pi \, r_s \, Q_S \,, \tag{2.34}$$

which is nonzero, as a result of the linear time dependence in Eq. (2.33). Furthermore, the surface integral at $r_{\rm out} \to \infty$ yields a contribution equal in magnitude but with opposite sign. Therefore, Stokes' theorem is trivially satisfied and cannot be used to constrain the scalar charge Q_S. There are cases in which one can also have nontrivial contributions from the linear time dependence at $r = r_{\rm out}$. To see this, let us study the asymptotic behavior of the current at large radii, keeping in mind the asymptotic expansion of the metric introduced in assumption (ii). The kinetic term now reads

$$\begin{aligned} X &= -\frac{1}{2}\left[- E^2 + (\partial_r S)^2 + \frac{(\partial_\theta S)^2}{r^2} + h^{\alpha\beta}\partial_\alpha\psi\,\partial_\beta\psi \right] = \\ &= -\frac{1}{2}\left[-E^2 + h^{\alpha\beta}\partial_\alpha\psi\,\partial_\beta\psi + \mathcal{O}\left(\frac{1}{r^{2d-4}}\right)\right] , \end{aligned} \tag{2.35}$$

and its derivative is given by

$$\partial_r X = -\frac{1}{2}\partial_r\left[-(1-h^{tt})E^2 + \mathcal{O}\left(\frac{1}{r^{2d-4}}\right)\right] = -\frac{E^2}{2}\partial_r h^{tt} + \mathcal{O}\left(\frac{1}{r^{2d-3}}\right) . \tag{2.36}$$

Regardless of its full expression, the metric component h_{tt} at large distances must yield the Newtonian potential in d-dimensions, i.e.,

$$\partial_r h^{tt} \sim \mathcal{O}\Big(\frac{1}{r^{d-2}}\Big) . \tag{2.37}$$

It is thus clear that another important difference with the time-independent case [c.f. Eq. (2.23)] is showing up at large radii: the gradient of the kinetic term now yields an additional contribution of the same order as the gradient of the scalar field. Note that this effect can arise if the theory includes a cubic Galileon interaction. In the case of (2.15), the current is given asymptotically by

$$J_r = -\partial_r S\,(K_X + \mathcal{O}(1/r^{d-1})) - \partial_r X\,(G_{3X} + \mathcal{O}(1/r^{d-1})) + \mathcal{O}(1/r^{d+1}) . \tag{2.38}$$

The Stokes' theorem then yields

$$\begin{aligned} &\oint_{\partial\mathcal{M}} \mathrm{d}\Sigma_\mu \, g^{\mu\nu} \, J_\nu = 0 = \int_{r=r_{\rm H}} \mathrm{d}\Sigma_r \, g^{rr} \, J_r + \int_{\{r\to\infty\}} \mathrm{d}\Sigma_r \, g^{rr} \, J_r = \\ &= \int_{r=r_{\rm H}} \mathrm{d}\Sigma_r \, g^{rr} \, J_r - \int_{\{r\to\infty\}} \mathrm{d}\Sigma_r \Big(\partial_r S \, K_X + \partial_r X \, G_{3X}\Big) . \end{aligned} \tag{2.39}$$

Let us now specialize to $d = 4$ dimensions and assume

$$K_X \to 1 \,, \qquad\qquad G_{3X} \to g_3 \,, \tag{2.40}$$

at large distances, as expected from asymptotic flatness [246], where g_3 is the coupling associated with the cubic Galileon interaction. Then, Eq. (2.39) provides one with a general expression for the scalar charge,

$$Q_S = g_3 \, E^2 - \frac{2}{M}\int_{r=r_{\rm H}} \mathrm{d}\Sigma_r \, g^{rr} \, J_r \,. \tag{2.41}$$

Depending on the specific model, this constraint can be verified trivially (as in the case of Jacobson's solution), or it can yield nontrivial relations between the scalar charge and the scalar time gradient E. In particular, this second possibility can give rise to hairy solutions in the presence of cubic Galileon interactions, if the horizon contribution vanishes.

2.4.2 Coupling to GB

It is well known that a linear coupling of the scalar field ψ to the GB invariant $\mathcal{G}$, defined in Eq. (1.17) can source a nontrivial hair around spherically symmetric BH solutions in $d = 4$, while preserving the shift symmetry [222]. In this case, the assumption that is violated is (v). In fact, the squared norm $J^\mu J_\mu$ of the shift-symmetry current diverges at the horizon. This is however not an issue since J^μ is not a diffeomorphism-invariant current in the presence of the Gauss–Bonnet term, and therefore $J^\mu J_\mu$ is not a physical scalar quantity [247].

The same conclusion is expected to hold for rotating solutions. Note that the divergence of $J^\mu J_\mu$ at the horizon prevents one from claiming that the right-hand side of Eq. (2.20) is zero at $r = r_{\rm H}$, invalidating our no-hair theorem of Sec. 2.2.

2.4.3 Deviations from circularity

We conclude this section with an additional cautionary note. The first assumption that we made was circularity, i.e. we required that besides possessing two Killing vectors, the metric is also reflection symmetric. The existence of physically meaningful noncircular stationary, asymptotically flat rotating BHs seems to be excluded for a wide class of theories [248]. In an EFT context, Ref. [249] showed that BH solutions must be circular if they reduce to GR solutions in a proper limit (in other words, if there are no separate branches).

In principle, however, in theories beyond GR one should not take circularity for granted [250]. Evidence for deviations from circularity is found numerically by Ref. [218] in cubic Galileon gravity. Other cases can be found for instance in DHOST theories [251, 252]. These solutions involve a stealth time dependence of the scalar field, which does not show up in the Einstein equations. Furthermore, separate branches of solutions could exist in the presence of a coupling between the scalar and a curvature invariant like the GB term. (We will discuss this case in more detail in Sec. 2.5.)

In summary, while examples of hairy BHs that violate our assumption (i) do exist, they also seem to violate our assumptions (iv) or (v).

2.5 No-hair theorem for quasi-K-essence theory

In this section, we review the no-hair theorem of Ref. [214], which shows that in K-essence theories the scalar field must be trivial and generalize it to generic spacetime dimensions d. For simplicity, we again restrict the analysis to the class of Myers-Perry BHs, with single or multiple spins. We stress that the proof is stronger than the one discussed so far, in the sense that it rules out not only a nonvanishing scalar charge at infinity, but also a nontrivial scalar profile. It is, however, less general, as it applies only to K-essence theories, i.e. ones with first-order derivative self-interactions. In more general theories, the presence of higher derivative operators may invalidate the proof, as it will become clear later on. Nevertheless, we will show that if the higher derivative operators provide perturbative corrections to the K-essence action, the proof can be generalized (with some subtle caveats). We will discuss this aspect at the end of the section.

Let us start from the action[9]

$$S = \frac{M_{\rm Pl}^2}{2}\int {\rm d}^d x\sqrt{-g}\,\left[R + K(\psi, X)\right]\,, \tag{2.42}$$

where $X \equiv -\frac{1}{2}\nabla_\mu\psi\nabla^\mu\psi$. Let us assume that there may exist a stationary BH solution with nontrivial scalar profile, sharing the same symmetries as the geometry. The scalar equations of motion are

$$\nabla_\alpha\big(K_X\,\partial^\alpha\psi\big) + K_\psi = 0\,. \tag{2.43}$$

Now, let us multiply Eq. (2.43) by ψ and integrate it over the volume of the BH exterior region $\mathcal{M}$. Then, integrating by parts and using Stokes' theorem, we obtain

$$\int_{\mathcal{M}} {\rm d}^d x\,\sqrt{-g}\,\left(K_X\,\partial_\alpha\psi\partial^\alpha\psi - \psi\,K_\psi\right) = \int_{\partial\mathcal{M}} {\rm d}\Sigma_\alpha\,V^\alpha \tag{2.44}$$

where we have introduced the vector

$$V^\alpha \equiv K_X\,\psi\,\partial^\alpha\psi\,. \tag{2.45}$$

Let us focus first on the right-hand side of Eq. (2.44). The treatment of the surface terms is analogous to our previous discussion in Sec. 2.2: the flux at the horizon is zero because of the vanishing of ${\rm d}\Sigma_\alpha{\rm d}\Sigma^\alpha$ and the regularity of $V_\alpha V^\alpha$ at $r = r_{\rm H}$; the contributions from the integral over the time boundaries cancel out because V_α is time independent; the flux across the hypersurface $r = r_{\rm out} \to \infty$ is zero because we are considering asymptotically flat solutions and hence $\psi \to 0$ at large radii. As a result, the right-hand side of Eq. (2.44) vanishes.

Let us then focus on the terms on the left-hand side of Eq. (2.44). For a ψ solution that has the same symmetries as the geometry, we can write $\partial_\alpha\psi\partial^\alpha\psi = \partial_i\psi\,g^{ij}\partial_j\psi$, which is positive definite outside the horizon [see the discussion around Eqs. (2.25)–(2.27)]. Furthermore, the energy-momentum tensor of the scalar field is $T_{\mu\nu} = K_X\partial_\mu\psi\partial_\nu\psi + K g_{\mu\nu}$. Assuming the null energy condition, i.e. $n^\mu T_{\mu\nu}n^\nu \geq 0$ for any null vector n^μ [253, 254], one obtains $K_X \geq 0$, which means that the term $K_X\,\partial_\alpha\psi\partial^\alpha\psi$ in Eq. (2.44) is positive (semi)definite. Then, unless ψK_ψ in Eq. (2.44) is also positive (semi)definite,[10] the left-hand side of Eq. (2.44) can vanish only if ψ is the trivial solution [214].

Now, starting from this result, let us add a cubic Galileon term to the Lagrangian:

$$\frac{\Delta\mathcal{L}}{\sqrt{-g}} = -\frac{M_{\rm Pl}^3}{\Lambda^3}G_3(\psi, X)\Box\psi\,, \tag{2.46}$$

Note that in Eq. (2.1) the energy scales $M_{\rm Pl}$ and Λ are absorbed in the definition of G_3, while we show them explicitly here. With this definition, G_3 has the dimensions of an energy squared, like X and K.

The dynamics of the system is associated with a characteristic scale, set by the mass of the BH, M. Let us therefore rescale the coordinates as $x^\mu \to x^\mu M_{\rm Pl}^2/M$. The scalar equation of motion then reads

$$\nabla_\alpha\big(K_X\,\partial^\alpha\psi\big) + \left(\frac{M}{M_{\rm Pl}^2}\right)^2 K_\psi = \varepsilon\left[\nabla_\alpha\big(G_{3X}\Box\psi\,\partial^\alpha\psi + G_{3X}\,\partial^\alpha X\big) + \left(\frac{M}{M_{\rm Pl}^2}\right)^2 G_{3\psi}\Box\psi\right]. \tag{2.47}$$

[9] As opposed to the previous sections, we relax here the assumption of shift symmetry, allowing K to be a function of both X and ψ.

[10] Note that, for $K = X - V(\psi)$, requiring $\psi K_\psi = -\psi V_\psi$ to be positive semidefinite is equivalent to having a potential V that is unbounded from below.

where we defined the dimensionless parameter

$$\varepsilon \equiv \frac{M_{\rm Pl}^5}{M^2\Lambda^3}\,. \tag{2.48}$$

By requiring that the Galileon strong coupling scale Λ is relevant for the cosmological dynamics, one gets $\Lambda^3 \sim M_{\rm Pl}\,H^2$, with H the Hubble parameter.[11] Then, the parameter ε becomes the ratio of the Hubble and BH radii. This is of course a huge number for astrophysical BHs. Therefore, considering Galileon-like interactions in the scalar sector with a cutoff scale producing a non-negligible dynamics on cosmological scales, we can expect highly nonperturbative corrections to the K-essence solution $\psi = 0$.

However, one may consider the same interaction with a cutoff Λ large enough to make $\varepsilon \ll 1$ [188]. In this case, we will have small perturbative corrections to the K-essence scalar solution; i.e. we can write

$$\psi = \sum_{n=1}^{\infty} \varepsilon^n \psi^{(n)}\,. \tag{2.49}$$

Plugging this ansatz into Eq. (2.47), at $\mathcal{O}(\varepsilon)$ one obtains

$$\nabla_\alpha\big(K_X(\psi=0)\,\partial^\alpha\psi^{(1)}\big) = 0\,, \tag{2.50}$$

while the backreaction of the scalar field onto the metric through the Einstein equations is subleading. From this equation, one can conclude that $\psi^{(1)} = 0$. The procedure can be carried out iteratively for successive orders in ε. In more detail, at $\mathcal{O}(\varepsilon^n)$ one has

$$\nabla_\alpha\big(K_X(\psi=0)\,\partial^\alpha\psi^{(n)}\big) + \mathcal{C}(\psi^{(1)},\dots,\psi^{(n-1)}) = 0\,, \tag{2.51}$$

where the corrections $\mathcal{C}$ vanish, as lower order corrections are zero.

Therefore, we can conclude that adding the Galileon term (2.46) in the action does not spoil the no-hair theorem proven for K-essence, as long as the coupling is perturbative. This holds straightforwardly also for the higher order Galileon interactions in the action (2.1).

The situation is different if we introduce, e.g., a coupling of the form

$$\frac{\Delta\mathcal{L}}{\sqrt{-g}} = \alpha\, f(\psi) I \tag{2.52}$$

where I is a curvature invariant. The only invariants which can be relevant are the Ricci and the mth order Euler density, where $m = d/2$, d being the dimension of the manifold. The former is zero on the trivial K-essence solution, and therefore it can induce deviations from that solution only at order α^2. However, the latter is generally nonzero, even in vacuum, and can yield nontrivial contributions to the perturbative calculation. In $d = 4$, the $m = 2$ Euler density is the Gauss–Bonnet invariant $\mathcal{G}$. In the following we will focus for simplicity on the case $I = \mathcal{G}$ in $d = 4$, but the argument in a generic higher dimensional manifold would be completely analogous.

The contribution to the scalar equation is

$$\frac{\delta}{\delta\psi}\left(\frac{\Delta\mathcal{L}}{\sqrt{-g}}\right) = \alpha_{\rm GB} f_\psi\,\mathcal{G}\,. \tag{2.53}$$

[11] This can be found heuristically by equating the kinetic and Galileon energies, and estimating the derivatives with the Hubble rate $\partial \sim H$.

One can rescale the coordinates as done earlier, and define the dimensionless parameter $\tilde{\alpha} = \alpha_{\rm GB}(M_{\rm Pl}^2/M)^2$. Carrying out the perturbative expansion with this parameter, one can see that the contribution to the equation of motion can be $\mathcal{O}(\tilde{\alpha})$ if $f_\psi = \partial f/\partial\psi = \mathcal{O}(\tilde{\alpha}^0)$. This is the case for shift-symmetric and dilatonic scalar-Gauss–Bonnet coupling functions, i.e.,

$$f_{\text{Shift-Symm}} \sim \psi\,, \qquad\qquad f_{\text{Dilatonic}} \sim \mathrm{e}^{\psi}\,. \tag{2.54}$$

In these cases, one finds perturbative corrections to the K-essence solution $\psi = 0$ at all orders. For instance, at first order, one has

$$\nabla_\alpha\big(K_X(\psi=0)\,\partial^\alpha\psi^{(1)}\big) = -\mathcal{G}\,. \tag{2.55}$$

This result is not surprising, as these coupling functions do not admit GR solutions, and the formation of a scalar hair is already evident at the perturbative level.

There are, however, examples of coupling functions $f(\psi)$ admitting GR solutions, alongside "scalarized" ones [226, 227, 255, 256]. Consider for instance BHs in scalar-GB gravity, with $f(\psi) = \psi^2$ and a canonical kinetic term $K(X) = X$. The scalar field obeys the Klein-Gordon equation

$$\left(\Box + m_{\rm eff}^2\right)\psi = 0\,, \tag{2.56}$$

with the effective mass $m_{\rm eff}^2 = 2\alpha_{\rm GB}\,\mathcal{G}$. The trivial GR configuration $\psi = 0$ is clearly a solution, but nontrivial solutions can also exist. In fact, $\mathcal{G} > 0$ for the Schwarzschild solution and $\mathcal{G} < 0$ for the Kerr one (at large spins). Therefore, depending on the sign of $\alpha_{\rm GB}$, the effective mass can become tachyonic, in which case the GR solution is unstable. The instability's endpoint is a scalarized nontrivial solution.

This solution is missed by our perturbative argument, which formally does apply to a theory with $f(\psi) = \psi^2$ and $K(X) = X$ (predicting incorrectly that scalarized solutions should not exist). The reason is that the scalarized solution is a nonperturbative correction of the GR one, i.e. it lives on a different branch of solutions. For this reason, our perturbative proof, which assumes a small deviation from the K-essence solution, does not apply.

Another important caveat is that BHs can dynamically evolve away from the GR configuration (even in the presence of no-hair theorems). This is the case for instance for a nontachyonic mass term (produced by a quadratic coupling to the Gauss–Bonnet invariant, or simply by a scalar potential). For rotating BHs, a mass term can give rise to superradiant instabilities, i.e. highly spinning GR solutions which, while allowed by no-hair theorems, may be unstable to superradiance [150, 257–260].

2.6 Conclusions

We proved a no-hair theorem for stationary, asymptotically flat BHs in shift-symmetric scalar-tensor theories. The theorem prevents the BHs from developing a scalar charge, defined as the coefficient of the $1/r$ falloff at large distances in the scalar profile. The proof is based on six fundamental assumptions and holds for general shift-symmetric theories, including Horndeski and DHOST theories as particular examples.[12] Our result extends the no-hair theorem of Ref. [219] to rotating BHs , as well as the results of Refs. [214, 231, 235], which apply only to theories with at most single derivatives acting on the scalar field.

[12] In the simplest case of a massless, noninteracting scalar field, note that the theorem is consistent with the symmetry arguments of [261, 262].

Under the assumption that the higher-derivative operators in the theory provide only perturbative corrections to the solution, we showed, following [214], that there exists a stronger version of the theorem forbidding not only the scalar charge, but any nontrivial scalar profile.

Moreover, we discussed loopholes to the theorem, revisiting, in the context of rotating BHs, some known results in the literature. In particular, we discussed the case of a scalar field with linear dependence in time, and a coupling to the GB operator.

In addition, we showed how our no-hair theorem can be extended to higher spacetime dimensions in the class of Myers-Perry BHs with one or multiple spins. In this context, it would be interesting to study to what extent the theorem applies also to rotating BHs with nontrivial topologies, which exist in $d > 4$ [236]. We leave this research direction for future work.

We conclude the discussion with a few remarks about the phenomenological implications of this result. Our theorem, unlike those of Refs. [214, 219, 231, 235], does not exclude possible subleading falloff terms in the scalar profile, unless we assume perturbative couplings. However, the absence of a scalar charge automatically proves that no deviations from GR are to be expected in the GW fluxes at leading (i.e., dipole) order [263].

Furthermore, given the structure of Eq. (2.41), it would be interesting to find models of hairy BHs with linear time growth yielding a vanishing horizon term. In this case, the scalar charge would be independent of the geometry, and it would allow one to constrain the coupling g_3, assuming a growth rate for the scalar field at infinity comparable to the Hubble rate.

Part II

Testing gravity through black hole oscillations

Chapter 3

Black hole perturbation theory

3.1 Introduction

The second part of the present work will be mainly devoted to the study of the BH ringdown, namely the final stage of the GW signal emitted by a binary system of coalescing BHs. As the name suggests, the remnant BH, *rings* for a short time after the merger, as it settles down to an equilibrium configuration [264–269]. More specifically, the duration of this process scales inversely with the mass of the BH.

The ringdown signal is particularly suited for a certain class of tests of gravity. In particular, its sensitivity to the background BH spacetime geometry renders it the best tool to perform tests of the no-hair conjecture discussed in the previous chapter, or, more generally, to probe the spacetime geometry close to EH [270].

In a technical perspective, the physics of the ringdown can be well understood within the framework of BH perturbation theory (BHPT) [271–276], that we are going to introduce in this chapter. In a nutshell, BHPT provides relatively simple equations that can usually be solved in the frequency domain as eigenvalue problems. The general solution appears as an infinite sum of quasinormal modes (QNMs), that are shaped as damped sinusoids in the time domain [264, 265, 277]. This scheme has already been proven to provide a solid analytical procedure and yield accurate predictions [40, 103, 278–280]. At the same time, the ringdown can also be simulated numerically, both with full-fledged numerical relativity (NR) simulations or integrating in the time domain the equations of BHPT [281–284]. Some physical problems related to the BH ringdown require, in fact, a critical comparison between these two kinds of analysis [1]

The spectrum of the ringdown in the frequency domain is quite rich already at the linear level of BHPT [286]. Since QNMs are characterized by different damping times, in practice, we are only able to detect a subset of them, namely those that are longer-lived. In principle, the detection of shorter lived modes, i.e. overtone modes, could be possible with future observations, if one considers the signal close enough to the start of the ringdown, usually defined at the peak of GW luminosity [287–289]. However, despite exhibiting a higher signal-to-noise (SNR) ratio, the early part of the ringdown signal is expected to contain contributions beyond linear perturbation theory [289–292]. Some important results have already been obtained in the context of second-order BHPT and quadratic QNMs [293–297]. However, the relevance of these contributions, as well as the proper initial time of the perturbative regime, is not yet fully understood. A particularly intriguing higher-order effect is the evolution of the BH mass due to gravitational radiation absorption. The

[1] See, for instance, the question of QNM spectral (in)stability [285], that we will not cover here.

impact of this phenomenon on the QNM spectrum has been explored in [298–300], but its full implications are still under debate.

At late times, the ringdown signal is expected to be dominated by a non-QNM, power law contribution [301–305]. This effect is usually called late-time tail. While in the past this tails was deemed irrelevant for observational purposes, recent work showed that they can be enhanced by several orders of magnitude in eccentric systems [305, 306]. Thus, having access to high-SNR detections raises the question of the detectability of these terms and the importance of including them in the data analysis templates.

Moreover, as discussed in Chapter 1 and 2, some theories of gravity beyond GR, such as HDG or some specific theories within ST gravity, predict BH solutions that are different from those predicted by GR [81, 222–224, 256]. Although deviations from GR are already tightly constrained [103], it possible, in principle, that their detection will be possible with future GW observations [307, 308]. For this reason, it is crucial to understand how BHPT equations get modified beyond GR.

Finally, in addition to a detailed discussion on the ringdown, we will also briefly address the tidal response of BHs. While the tidal response of a compact object is typically relevant in the inspiral phase, rather than during the post-merger relaxation process [309], both problems involve solving linearized perturbation equations around a background spacetime [310–312], and thus share important structural similarities. In particular, the tidal response of a BH can be computed from the static limit of BHPT master equations [238]. Remarkably, in GR, stationary and asymptotically flat BHs have vanishing tidal deformability [238, 313, 314], while introducing dynamical or environmental effects, or considering a more general theory of gravitation could result in a nontrivial tidal response [300, 315, 316]. In conclusion, the study of tidal deformations, provides complementary insights into the near-horizon geometry and the fundamental nature of compact objects [317].

In the next chapters, we are going to directly address some of the aforementioned open problems. In Chapter 4, based on [300], we are going to discuss the impact of a dynamical BH mass evolution on the QNM spectrum and on the tidal response. In Chapter 5, based on [318], we are going to describe a parametrized framework for studying QNMs of rotating BHs beyond GR. Finally, in Chapter 6, based on [319], we will address the more observation-related problem of systematic biases in the ringdown analysis. However, before turning to these applications, we shall first, in this chapter, collect the mathematical tools for the description of BH perturbations. We will start in Sec. 3.2 with the derivation of the linear perturbation equations in spherical symmetry, the well-known Regge-Wheeler and Zerilli equations. We will then describe their solutions in Sec. 3.3 and the nonlinear corrections in Sec. 3.4. Then, we will outline the generalization to a rotating background case (Teukolsky equation) in Sec. 3.5, and discuss how perturbation equations can be modified in alternative theories of gravity in Sec. 3.6. Finally, we will review the application of BHPT to the computation of tidal response of BHs in Sec. 3.7. From this chapter on, we will adopt the more convenient choice of geometric units $c = G = 1$, instead of the natural units (c$= \hbar = 1$) employed in Chapter 1 and 2.

3.2 Regge-Wheeler and Zerilli equations

Let us consider a spherically symmetric metric $g^B_{\mu\nu}$ and perturb it. Due to the symmetry of the system, it is convenient to work in a frame of spherical polar coordinates (t, r, θ, ϕ). In particular, we will now specialize to the only vacuum static solution in GR, i.e. the Schwarzschild metric.

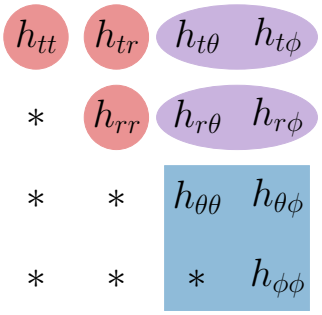

Figure 3.1: Transformation properties of the metric perturbations under rotations around the origin. The red components transform as scalars, the purple ones as vectors, whereas the blue block transforms as a rank-2 tensor. The $*$ symbol indicates symmetric components.

Schematically, the perturbation procedure can be represented as

$$g^B_{\mu\nu} \to g^B_{\mu\nu} + \epsilon h_{\mu\nu} + \mathcal{O}\left(\epsilon^2\right) , \tag{3.1}$$

with ϵ being a dimensionless book-keeping parameter that we consider to be $\ll 1$. Let us now restrict our analysis to the first perturbative order and have a closer look at the geometry of the perturbation. Our purpose is to separate the dependence on the different coordinates within $h_{\mu\nu}(t, r, \theta, \phi)$. First of all, let us consider the two-dimensional manifold, defined by $t = \text{const}, r = \text{const}$. When performing a rotation of the frame around the origin, the components of $h_{\mu\nu}$ have different transformation properties. In particular, the components h_{tt}, h_{tr}, h_{rr} transform as scalars, $(h_{t\theta}, h_{t\phi})$ and $(h_{t\theta}, h_{t\phi})$ transform as vectors, while the remaining block transforms as a rank-2 tensor on the Euclidian two-sphere [271–274]. This structure is depicted in Fig 3.1. In light of this geometrical properties, we can expand the metric components accordingly, introducing an orthonormal basis of generalized spherical harmonics. In practice, one has [271]

$$h_{\mu\nu} = \sum_{\ell m} h^{\ell m}_{\mu\nu} , \tag{3.2}$$

where ℓ and m are the two angular momentum "quantum" numbers. Note that for a gravitational perturbation $\ell \geq 2$, as the lowest-order term in a multipolar expansion is given by the quadrupole [7, 310]. Let us now consider in more detail the different components. A scalar mode can only have the structure $\sim Y_{\ell m}(\theta, \phi)$, while a vector can be generally decomposed in two different modes behaving like [271]

$$\begin{aligned} v^a_P &\sim \partial^a Y_{\ell m}(\theta, \phi) , \\ v^a_A &\sim \varepsilon_b{}^a \partial^b Y_{\ell m}(\theta, \phi) , \end{aligned} \tag{3.3}$$

where we introduced the Levi-Civita tensor on the two-dimensional Euclidian sphere ε. Moreover, a generic tensor mode can be decomposed into a basis given by [271]

$$\begin{aligned} t^{ab}_P &\sim \nabla^a \nabla^b Y_{\ell m}(\theta, \phi) , \\ t^{ab}_S &\sim \gamma^{ab} Y_{\ell m}(\theta, \phi) , \\ t^{ab}_A &\sim \frac{1}{2}\left(\varepsilon_c{}^a t^{cb}_P + \varepsilon_c{}^b t^{ca}_P\right) , \end{aligned} \tag{3.4}$$

where γ_{ij} is the metric on the two-sphere divided by r^2.

The terms described above can be further classified according with their transformation properties under a parity transformation, namely $\theta \to \pi - \theta , \phi \to \phi + \pi$ [271, 272]. The

scalar modes, along with v_P^a, t_P^{ab} and t_S^{ab}, pick a factor $(-1)^\ell$, and are called polar, or even. In contrast, v_A^a and t_A^{ab} pick a factor $(-1)^{\ell+1}$, and are called axial, or odd. In spherical symmetry, the two classes of perturbations do not interact with the each other, and it is therefore possible to separate $h_{\mu\nu}^{\ell m}$ in two independent sectors, namely [271]

$$h_{\mu\nu}^{\ell m} = h_{\mu\nu}^{\ell m\,,\mathrm{odd}} + h_{\mu\nu}^{\ell m\,,\mathrm{even}}\,. \tag{3.5}$$

The most general form for the axial part reads

$$\begin{aligned} &h_{\mu\nu}^{\ell m\,,\mathrm{odd}} = \\ &\begin{pmatrix} 0 & 0 & -\dfrac{h_0}{\sin\theta}\,\partial_\phi & h_0 \sin\theta\,\partial_\theta \\ 0 & 0 & -\dfrac{h_1}{\sin\theta}\,\partial_\phi & h_1 \sin\theta\,\partial_\theta \\ * & * & h_2\left(\dfrac{1}{\sin\theta}\partial_\theta\partial_\phi - \dfrac{\cos\theta}{\sin^2\theta}\partial_\phi\right) & \frac{1}{2}h_2\left(\dfrac{1}{\sin\theta}\partial_\theta\partial_\phi - \sin\theta\,\partial_\theta\partial_\theta + \cos\theta\,\partial_\theta\right) \\ * & * & * & -h_2(t,r)\left(\sin\theta\,\partial_\theta\partial_\phi - \cos\theta\,\partial_\phi\right) \end{pmatrix} \\ &\times Y_{\ell m}(\theta,\phi)\,, \end{aligned} \tag{3.6}$$

while the most general expression for the polar part is

$$\begin{aligned} &h_{\mu\nu}^{\ell m\,,\mathrm{even}} = \\ &\begin{pmatrix} \left(1-\dfrac{r_s}{r}\right)H_0 & H_1 & \mathcal{H}_0\,\partial_\theta & \mathcal{H}_0\,\partial_\phi \\ H_1 & \left(1-\dfrac{r_s}{r}\right)^{-1}H_2 & \mathcal{H}_1\,\partial_\theta & \mathcal{H}_1\,\partial_\phi \\ * & * & r^2\left(k + G\partial_\theta\partial_\theta\right) & r^2 G\left(\partial_\theta\partial_\phi - \dfrac{\cos\theta}{\sin\theta}\partial_\phi\right) \\ * & * & * & r^2\left(k\sin^2\theta + G\left(\partial_\phi\partial_\phi + \sin\theta\cos\theta\partial_\theta\right)\right) \end{pmatrix} \\ &\times Y_{\ell m}(\theta,\phi)\,, \end{aligned} \tag{3.7}$$

where the symbol $*$ indicates symmetric components. Notice that the degrees of freedom appearing in the metric perturbations depend on (t,r), although we did not explicitly indicate this, in order to keep the notation compact. For the same reason, we also suppressed the subscripts ℓm.

The expressions above can be further simplified by exploiting the gauge freedom enjoyed by metric perturbations. In more detail, performing an infinitesimal diffeomorphism $x^\mu \to x^\mu + \xi^\mu$, the metric perturbation transforms as [106–108, 271]

$$h_{\mu\nu} \to h_{\mu\nu} - \left(\nabla_\mu\xi_\nu + \nabla_\nu\xi_\mu\right)\,, \tag{3.8}$$

where ∇_μ indicates covariant differentiation. The vector ξ_μ can also be split in an axial and a polar part, which read

$$\begin{aligned} \xi_\mu^{\mathrm{odd}} &= \left(0,\ 0,\ \xi_V\,\frac{1}{\sin\theta}\,\partial_\phi,\ -\sin\theta\,\xi_V\,\partial_\theta\right)Y_{\ell m}(\theta,\phi)\,, \\ \xi_\mu^{\mathrm{even}} &= \left(-\left(1-\frac{r_s}{r}\right)\xi_0\,,\ \left(1-\frac{r_s}{r}\right)^{-1}\xi_1\,,\ \xi_S\,\partial_\theta,\ \xi_S\,\frac{1}{\sin^2\theta}\partial_\phi\right)Y_{\ell m}(\theta,\phi)\,. \end{aligned} \tag{3.9}$$

With an appropriate choice of the degrees of freedom ξ_0, ξ_1, ξ_S and ξ_V, it is possible to construct a physically equivalent metric perturbation displaying a smaller number of degrees of freedom. A possible gauge choice, results in $h_2(t,r) = \mathcal{H}_0(t,r) = k(t,r) = G(t,r) = 0$ [2].

[2]Note that this is slightly different from the Regge-Wheeler gauge, in which the degree of freedom $\mathcal{H}_1$ is eliminated, while k is kept. The two choices are anyway completely equivalent.

Expanding the Einstein-Hilbert action at quadratic order in the perturbations, with the gauge choice described above, one obtains a quadratic action for the remaining degrees of freedom, that can be split in an axial and a polar part [320]. Schematically, we have

$$S_{\rm quad} = S_{\rm odd}[h_0, h_1] + S_{\rm even}[H_0, H_1, H_2, \mathcal{H}_1]\,. \tag{3.10}$$

Both terms in Eq. (3.10), due to the orthonormality of our polar decomposition, can be expressed in the form

$$S_i = \frac{1}{16\pi}\sum_{\ell,m}\sum_{\ell',m'}\int \mathrm{d}\Omega\, Y_{\ell m}(\theta,\phi)Y^*_{\ell' m'}(\theta,\phi)\,\ell(\ell+1)\mathcal{S}_i^{\ell\ell'} = \frac{1}{16\pi}\sum_{\ell}\ell(\ell+1)\mathcal{S}_i^{\ell}\,, \tag{3.11}$$

where we introduced the reduced actions $\mathcal{S}_i^\ell$, which in spherical symmetry encode all the relevant dynamics. In the second passage we used the orthonormality condition for spherical harmonics and the fact that, due to spherical symmetry, there is no dependence on m in the reduced action. For the axial sector one has

$$\begin{aligned}\mathcal{S}^\ell_{\rm odd}[h_0,h_1] = \int \mathrm{d}t\,\mathrm{d}r\,\Bigg[&(h_0')^2 + \dot{h}_1^2 + 2\dot{h}_1\left(\frac{2h_0}{r} - h_0'\right)\\ &+\frac{h_0^2}{r^2\left(1-\frac{r_s}{r}\right)}\left(\ell(\ell+1) - \frac{2r_s}{r}\right) + h_1^2\left(\frac{2-\ell(\ell+1)}{r^2}\right)\left(1-\frac{r_s}{r}\right)\Bigg]\,.\end{aligned} \tag{3.12}$$

The two degrees of freedom appearing in the reduced action are redundant, and this can be viewed through the introduction of an auxiliary degree of freedom σ. The action can be re-expressed as

$$\begin{aligned}\mathcal{S}^\ell_{\rm odd}[h_0,h_1] = \int \mathrm{d}t\,\mathrm{d}r\,\Bigg[&\frac{(\ell(\ell+1)-2)\,h_0^2}{r^2\left(1-\frac{r_s}{r}\right)} - \frac{(\ell(\ell+1)-2)\,\left(1-\frac{r_s}{r}\right)\,h_1^2}{r^2}\\ &-\frac{\sigma^2}{r^2} + \frac{2\,\sigma}{r}\left(\frac{2h_0}{r^2} + \dot{h}_1 - h_0'\right)\Bigg]\,.\end{aligned} \tag{3.13}$$

Varying Eq. (3.13) with respect to $h_0(t,r)$ and $h_1(t,r)$, one obtains two constraints that allow to integrate them out. Namely

$$\begin{aligned} h_0 &= -\left(1-\frac{r_s}{r}\right)\frac{\sigma + r\sigma'}{\ell(\ell+1)-2}\,,\\ h_1 &= -\left(1-\frac{r_s}{r}\right)^{-1}\frac{r\dot{\sigma}}{\ell(\ell+1)-2}\,.\end{aligned} \tag{3.14}$$

With the redefinition $\tilde{\sigma} = \sigma/\sqrt{\ell(\ell+1)/2-1}$, one has

$$\mathcal{S}^\ell_{\rm odd}[\tilde{\sigma}] = \frac{1}{2}\int \mathrm{d}t\,\mathrm{d}r\left[\frac{\dot{\tilde{\sigma}}^2}{\left(1-\frac{r_s}{r}\right)} - \left(1-\frac{r_s}{r}\right)(\tilde{\sigma}')^2 - V_{\rm RW}(r)\tilde{\sigma}^2\right]\,, \tag{3.15}$$

where we defined the Regge-Wheeler potential

$$V_{\rm RW}(r) = \frac{\ell(\ell+1)}{r^2} - \frac{r_s}{r^3}\,. \tag{3.16}$$

Finally, varying Eq. (3.13) with respect to $\tilde{\sigma}$, one gets the *Regge-Wheeler equation* [271]

$$\left(-\frac{\partial^2}{\partial t^2} + \frac{\partial^2}{\partial r_*^2} - \left(1-\frac{r_s}{r}\right)V_{\rm RW}(r)\right)\tilde{\sigma}(t,r) = 0\,. \tag{3.17}$$

The coordinate $r_* = \int \mathrm{d}r\,(1-r_s/r)^{-1}$ is usually called tortoise coordinate, and sends the location of the EH to $-\infty$.

A similar procedure can be applied to the polar sector. Upon integration by parts, the reduced action can be expressed as

$$\begin{aligned}\mathcal{S}^{\ell}_{\rm even}[h_0,h_1] = \int \mathrm{d}t\,\mathrm{d}r \Bigg[& H_1^2 + \frac{H_2^2}{\ell(1+\ell)} + \frac{2\left(1-\frac{r_s}{2r}\right) H_0\,\mathcal{H}_1}{r} - \frac{2r\left(1-\frac{3r_s}{2r}\right) H_2\,\mathcal{H}_1}{r^2} \\ & + \frac{2\left(1-\frac{r_s}{r}\right)\mathcal{H}_1^2}{r^2} - \frac{H_2\left((2+\ell(\ell+1))H_0 + \frac{r_s}{2}\,H_0'\right)}{\ell(1+\ell)} - \frac{2r\left(1-\frac{3r_s}{4r}\right) H_0 H_2'}{\ell(1+\ell)} \\ & + \frac{2\left(1-\frac{r_s}{r}\right)\mathcal{H}_1 H_2'}{r^2} + 2\left(1-\frac{r_s}{r}\right) H_0\mathcal{H}_1' + \frac{2\left(1-\frac{r_s}{r}\right) H_2\mathcal{H}_1'}{r^2} \\ & + 2H_1\left(\frac{2rH_2'}{\ell(1+\ell)} - \dot{\mathcal{H}}_1\right) + \dot{\mathcal{H}}_1^2\Bigg]\,.\end{aligned} \tag{3.18}$$

As it is evident, the function $H_1(t,r)$ only appears algebraically, and can be therefore easily integrated out through the constraint

$$H_1 = -\frac{2r}{\ell(\ell+1)}\dot{H}_2 + \dot{\mathcal{H}}_1\,. \tag{3.19}$$

It is also convenient to redefine the function $\mathcal{H}_1(t,r)$ as

$$\mathcal{H}_1 = \frac{r}{\ell(\ell+1)}H_2 + \mathcal{A}\,. \tag{3.20}$$

The reduced action now reads

$$\begin{aligned}\mathcal{S}^{\ell}_{\rm even}[h_0,h_1] = \int \mathrm{d}t\,\mathrm{d}r \Bigg[& -\frac{(\ell(\ell+1)-2)\left(1-\frac{r_s}{r}\right) H_2^2}{\ell^2\,(1+\ell)^2} + \frac{2(1-\frac{r_s}{r})\,\mathcal{A}^2}{r^2} \\ & - \frac{\left[2(\ell(\ell+1)-2) - (\ell(\ell+1)-4)\,\frac{r_s}{r}\right]\,H_2\,\mathcal{A}}{\ell\,(1+\ell)\,r} + \frac{4r\,\dot{H}_2\,\dot{\mathcal{A}}}{\ell(1+\ell)} \\ & + H_0\left(\frac{-r\left[(\ell(\ell+1)-2)\,r+3r_s\right]H_2 + \ell(1+\ell)\left[(2r-r_s)\,\mathcal{A} + 2r(r-r_s)\,\mathcal{A}'\right]}{\ell\,(1+\ell)\,r^2}\right)\Bigg]\,.\end{aligned} \tag{3.21}$$

The function H_0 is now a Lagrangian multiplier, that yields the constraint

$$H_2 = \frac{2\,\ell(1+\ell)\,\left(\left(1-\frac{r_s}{2r}\right)\frac{\mathcal{A}}{r} + \left(1-\frac{r_s}{r}\right)\mathcal{A}'\right)}{\ell(\ell+1) - 2 + \frac{3r_s}{r}}\,. \tag{3.22}$$

The resulting reduced action only includes the degree of freedom $\mathcal{A}(t,r)$. Moreover, one can introduce the field redefinition

$$\mathcal{A} = \frac{1}{\sqrt{2}}\left(\frac{\sqrt{\ell(\ell+1)}\left(1-\frac{r_s}{r}\right)}{\ell(\ell+1) - 2 + \frac{3r_s}{r}}\right)^{-1}\tilde{\mathcal{A}}\,. \tag{3.23}$$

The final action reads

$$\mathcal{S}^{\ell}_{\rm even}[\tilde{\mathcal{A}}] = \frac{1}{2}\int \mathrm{d}t\,\mathrm{d}r\,\left[\frac{\dot{\tilde{\mathcal{A}}}^2}{\left(1-\frac{r_s}{r}\right)} - \left(1-\frac{r_s}{r}\right)(\tilde{\mathcal{A}}')^2 - V_{\rm Z}(r)\tilde{\mathcal{A}}^2\right]\,, \tag{3.24}$$

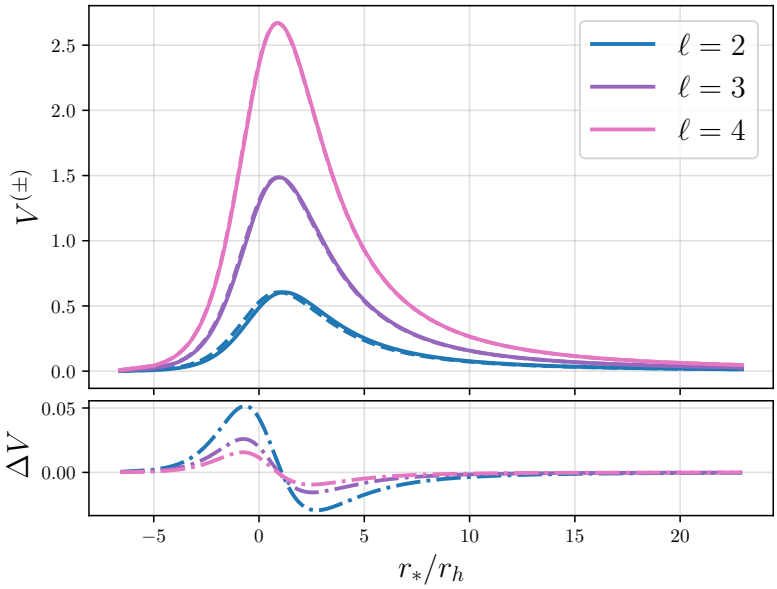

Figure 3.2: Potentials $V^{(+)}$ (continuous line) and $V^{(-)}$ (dashed line), for $\ell = 2, 3, 4$. Notice that, with increasing ℓ, the difference between the two potential decreases.

where we introduced the Zerilli potential

$$V_{\rm Z} = \frac{2\left(\ell(\ell+1)-2\right)^2\left(\ell(\ell+1)+1\right)}{3\,r^2\left(\ell(\ell+1)-2+\frac{3r_s}{r}\right)^2} + \frac{(\ell-1)(\ell+2)}{3\,r^2} + \frac{r_s}{r^3}\,. \tag{3.25}$$

Notice that in the eikonal limit, meaning $\ell \to \infty$, the Regge-Wheeler and Zerilli potentials become the same, namely $V_{\rm RW}, V_{\rm Z} \to \ell^2/r^2$.

The variation of Eq. (3.24) leads to the *Zerilli equation* [272]

$$\left(-\frac{\partial^2}{\partial t^2} + \frac{\partial^2}{\partial r_*^2} - \left(1-\frac{r_s}{r}\right) V_{\rm Z}(r)\right) \tilde{\mathcal{A}}(t,r) = 0\,. \tag{3.26}$$

The Regge-Wheeler and Zerilli equations are separable in time and radial coordinate. The time-dependent part, has the general harmonic behavior $\sim \exp(-i\omega t)$. Hence, the two equations can be rewritten in the Schrödinger form

$$\left(-\frac{\mathrm{d}^2}{\mathrm{d}r_*^2} + V^{(\pm)}\right) \Psi^{(\pm)} = \omega^2\, \Psi^{(\pm)}\,, \tag{3.27}$$

where $\Psi^{(+)} = \tilde{\sigma}$, $\Psi^{(-)} = \tilde{\mathcal{A}}$, and $V^{(\pm)} = (1 - r_s/r) V_{\rm RW,Z}$. The two potentials are represented in Fig. 3.2 for different values of ℓ.

While the dynamics of the two sectors in spherical symmetry is independent, the master equations are connected by a very peculiar duality [230, 321].

In fact, the potentials $V^{(\pm)}$ can be derived by a single *superpotential* W given by

$$W = -\frac{(\ell-1)\,\ell\,(\ell+1)\,(\ell+2)}{6\,r_s} - \frac{3\,r_s\left(1-\frac{r_s}{r}\right)}{r^2\left(\ell(\ell+1)-2+\frac{3r_s}{r}\right)}\,. \tag{3.28}$$

The transformation that generates the axial and polar potentials is given by

$$V^{(\pm)} = W^2 \pm \frac{\mathrm{d}W_{\rm S}}{\mathrm{d}r_*} + \kappa \tag{3.29}$$

with the constant

$$\kappa = -\frac{(\ell-1)^2\,(\ell+2)^2\,\ell^2\,(\ell+1)^2}{36\,r_s^2}\,. \tag{3.30}$$

This intriguing property of the Regge-Wheeler and Zerilli equation is usually referred to as Chandrasekhar symmetry [321]. The corresponding potentials can be formally viewed as "partners" in the language of supersymmetric quantum mechanics [322–324]. In practice, this means that introducing two Hamiltonians $\mathcal{H}^{(\pm)}$ defined as the left-hand side of Eq. (3.27), one can express them as

$$\mathcal{H}^{(+)} = A^\dagger A + \kappa\,, \qquad\qquad \mathcal{H}^{(-)} = A A^\dagger + \kappa\,, \tag{3.31}$$

with the operators

$$A = -\frac{\mathrm{d}^2}{\mathrm{d}r_*^2} + W \qquad\qquad A^\dagger = \frac{\mathrm{d}^2}{\mathrm{d}r_*^2} + W\,. \tag{3.32}$$

The main consequence of Chandrasekhar symmetry, is that the two Eqs. (3.27), while being different, have the same eigenvalue spectrum. It is important to stress, that this property is rather delicate and only holds for vacuum GR in four spacetime dimensions, while even slight deformations of one of the two potential can generally break it.

In a different, but equivalent perspective, the Chandrasekhar symmetry can be viewed as a property of the two wave-functions $\Psi^{(+)}$ and $\Psi^{(-)}$, rather than a symmetry of the potentials. In GR, the wave-functions are, in fact, related by a special class of *Darboux transformations* [325–327]. In more detail, one has

$$\Psi^{(+)} = \left(\frac{\mathrm{d}}{\mathrm{d}r_*} + \mathcal{F}(r_*)\right)\Psi^{(-)}\,, \tag{3.33}$$

with

$$\mathcal{F}(r_*) = \frac{\dfrac{\mathrm{d}}{\mathrm{d}r_*}\left(V^{(+)} + V^{(-)}\right)}{2\left(V^{(+)} - V^{(-)}\right)}\,. \tag{3.34}$$

This relation reflects the fact that axial and polar perturbations carry the same dynamical information, highlighting a sort of redundancy in the description of gravitational perturbations on static backgrounds.

We conclude this section mentioning that the equations for scalar and axial/polar electromagnetic perturbations on the Schwarzschild background can be easily derived from the Klein-Gordon and Maxwell equations. The result can be cast in the same form of Eq. (3.17) and (3.26) just replacing the potential with

$$\begin{aligned} V_{\rm scalar} &= \frac{\ell(\ell+1)}{r^2} + \frac{r_s}{r^3}\,, \\ V_{\rm e.m,axial} &= V_{\rm e.m,polar} = \frac{\ell(\ell+1)}{r^2}\,. \end{aligned} \tag{3.35}$$

Notice that all the potentials become the same in the eikonal limit.

3.3 Quasinormal modes

In this section, we discuss the solutions to the Regge-Wheeler and Zerilli equations. Just like for the well-known Schrödinger equation with a potential well, the boundary conditions that one imposes, select a discrete (infinite) set of eigenvalues. In a compact system, like an oscillating string, or an infinite potential well in quantum mechanics, the eigenfunctions corresponding to this discrete spectrum are called normal modes, and are purely oscillating. However, consider now the Schrödinger equation in three spatial dimensions with a potential well localized in a finite region around one point, and falling off to zero far way from it. In this case, one can look for a different class of solutions, that behave like outgoing spherical waves far away from the well. In the language of quantum mechanics, these states are typically known as *quasistationary* [328]. The eigenvalues of the system in this case are typically complex due to the complexity of the boundary condition at infinity. The imaginary part is related to the inverse of the lifetime of the state. Moreover, the spectrum is not even strictly discrete, but rather quasidiscrete, as it presents broadened energy levels with a width that is related to the imaginary part of the eigenvalues. In other words, the eigenfunctions of quasistationary states behave as damped sinusoids in the time domain, and as Lorentzian functions in the frequency (or energy) domain. This case is similar to the BH perturbations described by Eq. (3.27), with two main differences. The first is that the BH perturbation dissipates not only infinitely far away but also into the BH horizon. The second difference regards the nature of the potential. In fact, the Regge-Wheeler and Zerilli potentials appear as barriers located around the light-ring ($\sim 3r_s$), and decaying away from it. This kind of configuration clearly does not admit bound or quasibound states, but rather waves that are scattered off the potential and propagate both towards infinity and into the BH horizon.

This picture can be naturally translated into the following set of boundary conditions

$$\begin{aligned} &\Psi(t, r_*) \sim e^{-i\omega(t-r_*)} && \text{for} \quad r_* \to +\infty \\ &\Psi(t, r_*) \sim e^{-i\omega(t+r_*)} && \text{for} \quad r_* \to -\infty \,. \end{aligned} \tag{3.36}$$

However, when dealing with a real initial value problem, this kind of analysis in Fourier space presents some issues. First of all, the selected resonant modes do not form a complete set, and the corresponding wave-functions are unbound both at the horizon and at spatial infinity. Secondly, the set the boundary conditions of Eq. (3.36) doeas not allow to dermine a unique solution [301, 329].

3.3.1 The Green's function approach

To try to solve the aforementioned problems, and to gain deeper insight into the physical interpretation of QNMs, let us inspect the Regge-Wheeler/Zerilli equation from a slightly different perspective. As we already discussed, the two master equations have the general form

$$\left(-\frac{\partial^2}{\partial t^2} + \frac{\partial^2}{\partial r_*^2} + V(r_*) \right) \Psi(t, r_*) = 0 \,. \tag{3.37}$$

Let us introduce the Laplace transform of $\Psi(t, r_*)$, defined as

$$\hat{\Psi}(s, r_*) = \int_0^\infty \mathrm{d}t \, e^{-st} \Psi(t, r_*) \,. \tag{3.38}$$

It is possible to show [329] that $\Psi(t, r_*)$ is bounded everywhere if it has a compact support. This guarantees that the Laplace transform exists and is analytic in the complex half-plane

given by $\Re(s) > 0$. Applying the transform to Eq. (3.37), we get

$$\left(\frac{\partial^2}{\partial r_*^2} - s^2 - V(r_*)\right)\hat{\Psi}(s, r_*) = \mathcal{J}(s, r_*)\,, \tag{3.39}$$

with the source term

$$\mathcal{J}(t, r_*) = -\left(s\Psi(t, r_*) + \frac{\partial\Psi(t, r_*)}{\partial t}\right)\bigg|_{t=0}\,, \tag{3.40}$$

explicitly depending on the initial data. A general solution of Eq. (3.39) can be written in terms of the Green's function $\hat{G}(s, r_*, r'_*)$ as

$$\hat{\Psi}(s, r_*) = \int_{-\infty}^{\infty} \mathrm{d}r'_*\, \hat{G}(s, r_*, r'_*)\mathcal{J}(s, r_*)\,. \tag{3.41}$$

The Green's function can be constructed as

$$\hat{G}(s, r_*, r'_*) = \frac{1}{\mathcal{W}(s)}\left(\Theta(r_* - r'_*)\hat{\Psi}_1(s, r'_*)\hat{\Psi}_2(s, r_*) + \Theta(r'_* - r_*)\hat{\Psi}_1(s, r_*)\hat{\Psi}_2(s, r'_*)\right)\,, \tag{3.42}$$

where $\hat{\Psi}_{1,2}(s, r_*)$ are two linearly independent solutions of the homogeneous equation, and Θ is the Heaviside step-function. In more detail, it is convenient to choose the two independent solutions to the homeogeneous equation such that

$$\begin{aligned} \hat{\Psi}_1 &\sim e^{-sr_*} \qquad &&\text{for} \quad r_* \to +\infty \\ \hat{\Psi}_2 &\sim e^{+sr_*} \qquad &&\text{for} \quad r_* \to -\infty\,. \end{aligned} \tag{3.43}$$

On the opposite boundaries we have

$$\begin{aligned} \hat{\Psi}_1 &\sim a_{11}(s)e^{sr_*} + a_{12}(s)e^{-sr_*} \qquad &&\text{for} \quad r_* \to -\infty \\ \hat{\Psi}_2 &\sim a_{21}(s)e^{sr_*} + a_{22}(s)e^{-sr_*} \qquad &&\text{for} \quad r_* \to +\infty\,. \end{aligned} \tag{3.44}$$

Moreover, we defined the Wronskian

$$\mathcal{W}(s) = \hat{\Psi}_1(s, r_*)\frac{\partial\hat{\Psi}_2(s, r_*)}{\partial r_*} - \hat{\Psi}_2(s, r_*)\frac{\partial\hat{\Psi}_1}{\partial r_*}(s, r_*)\,, \tag{3.45}$$

which is conserved, i.e. independent of r_*. For this reason, we compute it at $r_* \to \pm\infty$ and the result must be the same. We obtain

$$\mathcal{W}(s) = -2sa_{12}(s) = -2sa_{21}(s)\,, \tag{3.46}$$

which yields $a_{12}(s) = a_{21}(s)$.

Taking the non-homogeneous solution given by Eq. (3.41) and inverting the Laplace transform, one gets

$$\Psi(t, r_*) = \int_{c-i\infty}^{c+i\infty}\frac{\mathrm{d}s}{2\pi i}\int_{-\infty}^{\infty}\mathrm{d}r'_*\, e^{st}G(s, r_*, r'_*)\mathcal{J}(s, r'_*)\,, \tag{3.47}$$

where c is an infinitesimal positive displacement, chosen in such a way that it is larger than the real part of all singularities. Given the non-trivial structure of the integrand in the complex plane, one should choose an appropriate contour Γ to perform the integration.

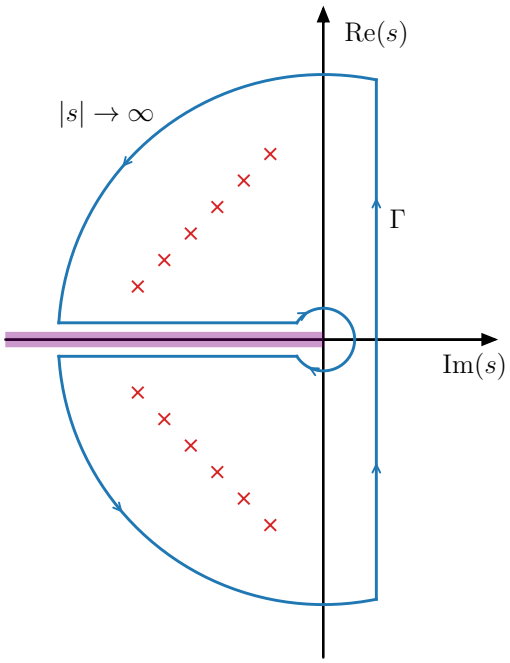

Figure 3.3: Pictorial representation of the integration contour Γ in the complex s plane (blue curve). The poles of the Green's function are represented as red crosses, while the branch-cut along the negative real axis is represented with the purple shaded line.

The integration contour is euristically depicted in Fig. 3.3. We note that a set of simple poles – corresponding to the roots of the Wronskian – are present in the left-half plane, while a branch-cut is running from the origin to $Im(s) \to -\infty$. The contour is chosen in such a way to enclose the singularities and avoid the branch-cut, being then closed into two quarters of circle at infinite distance from the origin.

Let us focus for a moment on the contribution to the integral coming from the poles. Observe that $W(s) = 0$ precisely when the two independent solutions $\hat{\Psi}_1$ and $\hat{\Psi}_2$ become linearly dependent — that is, when $\hat{\Psi}_1 \propto \hat{\Psi}_2$. In this case, the full solution satisfies purely outgoing boundary conditions at spatial infinity and purely ingoing at the horizon simultaneously. By definition, these values of s correspond to the QNMs of the system.

Furthermore, if the potential in the wave equation is real, the QNM spectrum is symmetric under complex conjugation: that is, if $\hat{\Psi}(s_{\rm QNM}, r_*)$ is a QNM solution, then its complex conjugate $\hat{\Psi}(s^*_{\rm QNM}, r_*)$ is also a valid solution of the same equation.

In order to simplify our treatment, let us assume that the source term $\mathcal{J}(s, r_*)$ has compact support, namely that $r_* \in \left[r_*^{\rm in}, r_*^{\rm out}\right]$, and let us study the solution for $r_* > r_*^{\rm out}$. Then the time-domain solution reads

$$\Psi(t, r_*) = \frac{1}{2\pi i} \int_{c-i\infty}^{c+i\infty} \mathrm{d}s\, e^{st}\, \frac{C_2(s)}{\mathcal{W}(s)} \hat{\Psi}_1(s, r_*)\,, \tag{3.48}$$

with

$$C_2(s) = \int_{r_*^{\rm in}}^{r_*^{\rm out}} \mathrm{d}r'_*\, \hat{\Psi}_2(s, r'_*) \mathcal{J}(s, r'_*)\,. \tag{3.49}$$

In the proximity of a zero s_n, the Wronskian can be expanded as

$$\mathcal{W}(s) = \mathcal{W}'(s_n)(s - s_n) + \mathcal{O}(s - s_n)^2\,. \tag{3.50}$$

Plugging this expression into Eq. (3.48), and applying the residue theorem, one obtains

$$\Psi(t, r_*) = \sum_n e^{s_n t} \frac{C_2(s_n)}{\mathcal{W}'(s_n)} \hat{\Psi}_1(s_n, r_*) \,. \tag{3.51}$$

Let us now perform the complex rotation $s = -i\omega$, in order to connect this last result with the more widely employed Fourier transform language. The QNM part of the time domain signal can be expressed as

$$\Psi(t, r_*) = -\int_{-\infty}^{+\infty} \mathrm{d}r'_* \left[\frac{\partial}{\partial t} G(t, r_*, r'_*) \Psi(t = 0, r_*) + G(t, r_*, r'_*) \frac{\partial \Psi}{\partial t}(t = 0, r_*) \right] . \tag{3.52}$$

Furthermore, we can assume that the initial data have a support far away from the BH, i.e. $r_*^{\mathrm{in}} \gg r_s$. In this approximation, the time-domain Green's function reads

$$G(t, r_*, r'_*) \simeq Re \left(\sum_n B_n e^{-i\omega_n (t - r_* - r'_*)} \right) . \tag{3.53}$$

The constant B_n is called QNM excitation factor and reads

$$B_n \equiv - \left(\omega \frac{\mathrm{d}}{\mathrm{d}\omega} a_{21}(-i\omega) \right)^{-1} a_{22}(-i\omega) \mid_{\omega = \omega_n} . \tag{3.54}$$

It is worth noticing that the amplitude of a QNM is roughly given by the product of an excitation factor, that can be fully predicted in the framework of BHPT, and an initial data term. The latter contribution, unlike the excitation factor, is not only dependent on the geometry of the BH spacetime, but carries information about the process that caused the BH ringing. In a merger of compact objects leading to the formation of a ringing BH, the initial data depend on the physical properties of the progenitors. As we will discuss in Chapter 6, in a binary BH merger, the relative contribution from different QNMs to the ringdown signal is strongly affected by the masses and spins of the two merging bodies. As BHPT is not able to fully determine the amplitude of linear QNMs, one has typically to resort to numerical simulations.

Besides the contribution from the poles of the Green's function, one also has to consider the contribution coming from the branch-cut and from the arcs at infinity. It can be shown that the former yields a power-law tail in the time-domain signal [301, 329]. In particular, the tail signal goes as $\sim t^{-2\ell-3}$ for an observer at $t \to \infty$ and fixed r_*, while it falls off as $\sim (t - r_*)^{-\ell-2}$ when observed at future null infinity, i.e. when $t \to \infty$ at fixed t/r_*. This result can be derived analytically, and is in good agreement with the time-domain numerical integration of the Regge-Wheeler and Zerilli equations. In particular, this part of the ringdown signal dominates after QNM have faded away. The presence of a power-law tail appears to be related to the back-scattering of waves off the potential at large distance by the compact object. On the other hand, it seems to be completely independent of the existence of a horizon, and is absent for potentials that decay exponentially at large distance.

Finally, the last contribution to the ringdown time-domain signal, deriving from the arcs at infinity in the left half-complex s plane, is related to the high-frequency components of the initial perturbation, which propagate without "seeing" the potential barrier.

The discussion above clarifies the meaning of non-completeness of the QNMs, as they only reconstruct a part of the full ringdown signal. However, after the merger, in the regime in which BHPT theory is valid, and for a parametrically large time interval, QNMs dominate the signal and constitute a sufficient approximation of the full solution.

3.3.2 WKB approximation and other methods

To conclude this section, we provide a short introduction to the practical computation of QNMs. To this purpose, we start showing an analytical procedure, due to Schutz and Will [277], which is inspired by the well-known *Wentzel-Kramers-Brillouin* (WKB) approximation in quantum mechanics [330–332]. Let us express Eq. (3.27) in a slightly different form, namely

$$\left(\frac{\mathrm{d}^2}{\mathrm{d}r_*^2} + Q(r_*)\right)\Psi(r_*) = 0\,, \tag{3.55}$$

where we consider a generic perturbation sector $\pm$ and removed the superscripts from the potential and the wave-function. We also defined $Q(r_*) \equiv \omega^2 - V(r_*)$.

The general idea is that Eq. (3.55) can be solved in a limit of slowly-varying potential. It is instructive to factor out a term ℓ^2 from $Q(r_*)$, as $Q(r_*) = \ell^2\tilde{Q}(r_*)$. In this way, Eq. (3.55) takes the schematic form

$$\ell^{-2}\Psi'' + \tilde{Q}\Psi = 0\,. \tag{3.56}$$

Notice that if we consider the large ℓ limit, corresponding to the geometric optics regime, we are dealing with a singular perturbation theory problem, in the sense that the order of the differential equation we are solving changes in the limit in which the expansion parameter $\ell^{-1} \to 0$.

Consider now the following ansatz for the wave-function

$$\Psi(x_*) = A(r_*)\exp\left(\frac{i}{\epsilon}\sum_i^\infty \epsilon^i S(r_*)^{(i)}\right)\,, \tag{3.57}$$

introducing the book-keeping parameter ϵ. Notice this should not be confused with the expansion parameters controlling the order of metric perturbations. Plugging this ansatz into the differential equation we get

$$\frac{1}{\ell^2\epsilon^2}(S_0')^2 + \frac{2}{\ell^2\epsilon}(S_1'S_0' + S_0'') + \cdots + \tilde{Q} = 0\,, \tag{3.58}$$

where the dots represent higher-order terms in the double expansion (ℓ^{-1}, ϵ). At this point we can identify $\ell^{-1} = \epsilon$ and compare similar terms. At leading order, we get the eikonal equation

$$(S_0')^2 + \tilde{Q} = 0\,, \tag{3.59}$$

which is solved by $S_0 \sim \exp\left(\pm i\int \mathrm{d}r_*'\sqrt{\tilde{Q}(r_*')}\right)$. At the successive order, we have instead the so-called transport equation

$$2S_0'S_1' + S_0'' = 0\,, \tag{3.60}$$

solved by $S_1 = -(1/4)\ln Q(r_*)$, modulo an integration constant. Putting everything together, one gets the leading order WKB solution

$$\Psi \sim Q^{-1/4}\exp\left(\pm i\int \mathrm{d}r_*\sqrt{Q(r_*)}\right)\,. \tag{3.61}$$

Let us now split the domain of r_* in three regions I, II, III (Fig. 3.4), divided by the matching points r_*^- and r_*^+. In the two external regions I and III, the wave-function is

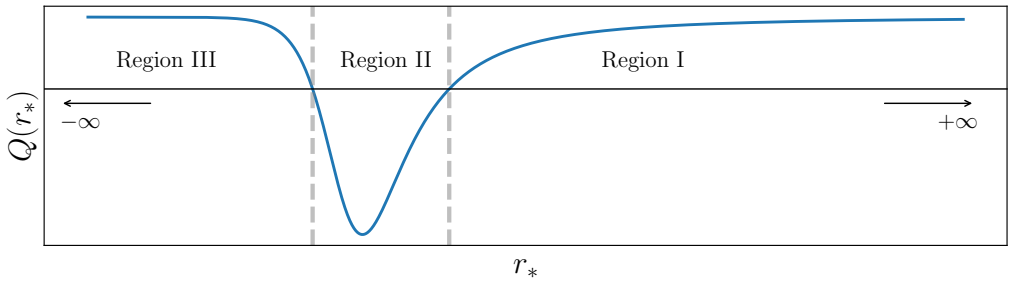

Figure 3.4: Three regions of the domain of the Schrödinger potential. Region I and III represent the regime in which the WKB solution holds.

described by the WKB solution of Eq. (3.61), choosing the appropriate QNM boundary conditions

$$\begin{aligned}\Psi_{\rm I} &\simeq Q(r_*)^{-1/4}\exp\left(\pm i\int_{r_*^-}^{r_*}\mathrm{d}r'_*\sqrt{Q(r'_*)}\right)\\ \Psi_{\rm III} &\simeq Q(r_*)^{-1/4}\exp\left(\pm i\int_{r_*}^{r_*^+}\mathrm{d}r'_*\sqrt{Q(r'_*)}\right)\,.\end{aligned} \tag{3.62}$$

In the intermediate region II, if the turning points are closely spaced, i.e. $(-Q(r_*))_{\rm max} \ll |Q(\pm\infty)|$, we can use the following quadratic approximation for the potential

$$Q(x) = Q_0 + \frac{1}{2}Q_0''(r_*-\bar{r}_*)^2 + \mathcal{O}(r_*-\bar{r}_*)^3\,, \tag{3.63}$$

where $\bar{r}_*$ corresponds to the location of the potential minimum, and $Q_0 \equiv Q(\bar{r}_*) < 0$, $Q_0'' \equiv \mathrm{d}^2Q/\mathrm{d}r_*^2\,|_{\bar{r}_*} > 0$.

Eq. (3.55) can be cast in the more convenient form

$$\left[\frac{\mathrm{d}^2}{\mathrm{d}y^2} + \left(\nu+\frac{1}{2}-\frac{y^2}{4}\right)\right]\Psi(y) = 0\,, \tag{3.64}$$

where we introduced

$$y \equiv (2Q_0'')^{1/4}e^{i\pi/4}(r_*-\bar{r}_*)\,, \qquad \nu+\frac{1}{2} \equiv -\frac{iQ_0}{\sqrt{2Q_0''}}\,. \tag{3.65}$$

Eq. (3.65), also known as Weber equation [333], admits the general analytic solution $\Psi(y) = A_pD_\nu(y)+B_pD_{-\nu-1}(iy)$, where A_p and B_p are constant coefficients and $D_\nu(y)$ is a parabolic cylinder function. The solution has the following asymptotic expansion for $r \gg r_*^+$

$$\begin{aligned}\Psi(r_*) \simeq& B_p e^{-3\pi i(\nu+1)/4}(2Q_0'')^{-(\nu+1)/4}(r_*-\bar{r}_*)^{-\nu-1}\exp\left(\frac{i}{2}\sqrt{\frac{Q_o''}{2}}(r_*-\bar{r}_*)^2\right)\\ &+\left(A_p + B_p\frac{\sqrt{2}e^{-\pi i\nu}}{\Gamma(\nu+1)}\right)e^{\pi i\nu/4}(2Q_0'')^{\nu/4}(r_*-\bar{r}_*)^\nu\times\\ &\times\exp\left(-\frac{i}{2}\sqrt{\frac{Q_o''}{2}}(r_*-\bar{r}_*)^2\right)\,,\end{aligned} \tag{3.66}$$

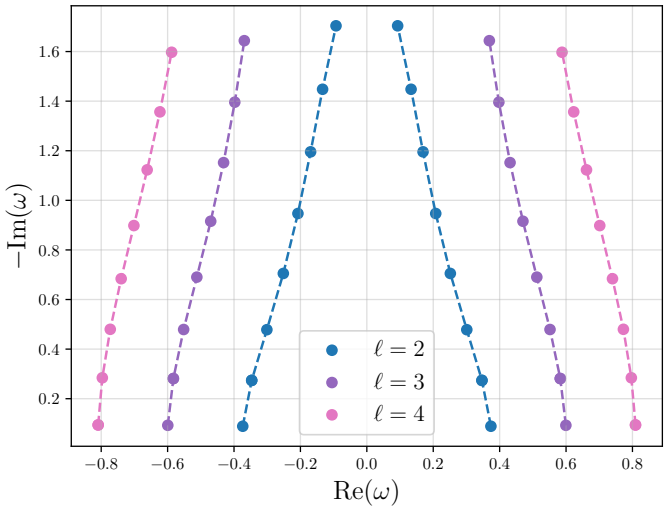

Figure 3.5: QNM spectrum of the Schwarzschild BH in the complex ω plane. Different colors indicate different values of ℓ. Moving upwards, for the same ℓ, the different points represent the eigenvalues for increasing overtone number, from $n = 0$, to $n = 8$. Notice how the increase in ℓ produces an increase in the oscillation frequency, while the increase in the overtone number produces a stronger damping.

while for $r \ll r_*^-$ one has

$$\begin{aligned}\Psi(r_*) \simeq & A_p e^{-3\pi i\nu/4}(2Q_0'')^{\nu/4}(r_*-\bar{r}_*)^{\nu}\exp\left(-\frac{i}{2}\sqrt{\frac{Q_o''}{2}}(r_*-\bar{r}_*)^2\right) \\ & + \left(B_p - iA_p\frac{\sqrt{2}e^{-\pi i\nu}}{\Gamma(-\nu)}\right)e^{\pi i(\nu+1)/4}(2Q_0'')^{-(\nu+1)/4}(r_*-\bar{r}_*)^{-\nu-1}\times \\ & \times\exp\left(\frac{i}{2}\sqrt{\frac{Q_o''}{2}}(r_*-\bar{r}_*)^2\right)\,,\end{aligned} \tag{3.67}$$

where $\Gamma(x)$ is the Euler Gamma function. Imposing that these asymptotic expansions match with the WKB solutions in region I and III, one gets the conditions $B_p = 0$ and $\Gamma(-\nu) = \infty$. In particular, the latter condition implies that $\nu = n$, with n being a positive integer. Together with Eq. (3.65), this constraint leads to a sort of Bohr-Sommerfeld quantization condition, namely

$$\frac{Q_0}{\sqrt{2Q_0''}} = i\left(n+\frac{1}{2}\right)\,. \tag{3.68}$$

Since the left-hand side of Eq. (3.68) depends on the frequency, the relation can be inverted to obtain the discrete QNM spectrum. At leading order, for Schwarzschild, the spectrum reads

$$r_s\,\omega_{n\ell} \simeq \frac{2}{\sqrt{3}\,3}\left[\left(\ell+\frac{1}{2}\right) - i\left(n+\frac{1}{2}\right)\right]\,. \tag{3.69}$$

This procedure can be carried on to higher accuracy [334, 335]. Notice that the real part of the QNM frequency grows linearly with the multipole order, while the imaginary part becomes more and more negative as we increase the integer n. This corresponds to an increasingly severe suppression in the time domain. The integer n is generally called *overtone number*.

It is important to stress that the result of Eq. (3.69) is more accurate for large ℓ, due to the connection between WKB expansion and the geometric optics regime.

In summary, the WKB/eikonal approximation, being fully analytical, allows for a nice visualization of the dependence of the QNM frequencies on the different parameters. However, several more accurate semi-analytical and numerical methods have been developed for the computation of the QNM spectrum. Some examples are inverted potential methods [336, 337], direct integration [338, 339], spectral and pseudo-spectral methods [340–342], and continued-fraction (Leaver) method [286]. In this work, we extensively employed the last one, due to the high degree of accuracy that it yields. We are going to describe it in more detail in the next two chapters.

The spectrum of the Schwarzschild BH is represented in Fig. 3.5. The different colors represent different values of ℓ, while the overtone number increases moving upwards. The core features discussed in the WKB approximation, i.e. imaginary parts decreasing with the overtone number and real parts increasing with the multipole order, are evident. Notice also the mirror symmetry relating frequencies with positive and negative real part.

3.4 Nonlinear perturbation theory

Before finally delving into the generalization of the BHPT framework to rotating backgrounds, we provide an euristic overview of BHPT and QNMs beyond linear order.

Let us first consider quadratic order in the metric perturbation, i.e.

$$g^B_{\mu\nu} \to g^B_{\mu\nu} + \epsilon h^{(1)}_{\mu\nu} + \epsilon^2 h^{(2)}_{\mu\nu} + \mathcal{O}\left(\epsilon^3\right) . \tag{3.70}$$

The Einstein equation at linear order in perturbations reads schematically [271–274]

$$G^{(1)}_{\mu\nu}\left[h^{(1)}_{\mu\nu}\right] = 0 . \tag{3.71}$$

Notice that the linearization of the Einstein equation is equivalent to the expansion of the Einstein-Hilbert action up to quadratic order, that we previously employed for the derivation of Regge-Wheeler and Zerilli equations.

On the other hand, the expansion of Einstein equation to quadratic order has the schematic structure [343–346]

$$G^{(1)}_{\mu\nu}\left[h^{(2)}_{\mu\nu}\right] = -G^{(2)}_{\mu\nu}\left[h^{(1)}_{\mu\nu}, h^{(1)}_{\mu\nu}\right] . \tag{3.72}$$

Notice that the operator on the left-hand side is the same as the one appearing at the linear order, while now we have a source term that is quadratic in the linear metric perturbation.

In practice, the procedure for deriving the quadratic master perturbation equations closely tracks the approach used to obtain the Regge-Wheeler and Zerilli equations. One starts by fixing a convenient gauge at both linear and quadratic order, so that redundant degrees of freedom disappear. Then, in the same fashion, two second-order master scalar variables, denoted $\Psi^{(2)}_{(\pm)}$, can be defined for the the odd and even-parity sector [344, 345]. The equations governing $\Psi^{(2)}_{(\pm)}$ are finally solved with the usual QNM boundary conditions. These solutions can subsequently be translated back into the metric perturbations in the physical TT gauge, where one can compute the observable GW amplitude at null infinity [346].

The resulting equations for the second-order master fields take the form [344, 345]:

$$\left[-\frac{\mathrm{d}^2}{\mathrm{d}r_*^2} + \left(V^{(\pm)} - \omega^2\right)\right] \Psi^{(2)}_{(\pm)} = \mathcal{S}^{(2)}_{\pm} . \tag{3.73}$$

As expected, the left-hand side is precisely the Regge-Wheeler/Zerilli operator, while the right-hand side features a source term $\mathcal{S}^{(2)}_{\pm}$, which is quadratic in the first-order perturbations. The fact that the perturbation equation at quadratic order, unlike the ones at linear order, are not homogeneous has an important consequence. The amplitude of linear modes, as we discussed in the previous section is roughly given by a product of an excitation factor, which can be fully predicted within BHPT, and a initial data-dependent part. In contrast, the amplitude of quadratic QNMs can in principle be completely reconstructed from the amplitudes of linear modes. We briefly mention that a technical complication is met when working in the standard gauge and imposing QNM boundary conditions at quadratic order. In fact, one finds that the source term is divergent at the boundaries [294, 295]. However, the divergence is not physical and can be cured by an appropriate field redefinition of the master variables [294, 347]. With this choice, the ratio of quadratic to linear amplitudes $\mathcal{R}$ can be computed, for instance whith the aforementioned continued-fraction method [286]. Typically, the loudest quadratic QNM, excited in a binary BH merger, is given by the coupling of the linear mode $\ell = 2, n = 0$ (with positive real part) with itself. The ratio is $\mathcal{R} \simeq 0.154\, e^{-0.068 i}$.

The quadratic QNM frequencies are trivially related to the ones of linear modes [347]. Consider the quadratic coupling of the two linear modes (ℓ_1, n_1) and (ℓ_2, n_2). This combination can source the quadratic frequencies

$$\omega^{(2)} = \omega^{(1)}_{\ell_1 n_1} + \omega^{(1)}_{\ell_2 n_2}, \quad \text{or} \quad \omega^{(2)} = \omega^{(1)}_{\ell_1 n_1} - (\omega^{(1)}_{\ell_2 n_2})^*. \tag{3.74}$$

This structure arises because the physical metric perturbations are real, but they are mathematically constructed as the real part of a complexified field.

The negative-sign case in the frequency combination above can equivalently be interpreted as arising from the coupling of a linear mode with a mirror mode.

As we discussed in the Chapter 1, GWs can back-react on the background, producing a dynamical evolution of the spacetime [106–110]. This process also happens during the ringdown, and in particular, part of the waves produced close to light-ring are falling into the BH horizon, increasing its energy content [348–351]. Indeed, while this effect is highly subleading during the inspiral, it could be relevant at the ringdown stage [298, 352].

Let us for simplicity consider the simple case of a monochromatic scalar wave ψ impinging on a static BH of mass M. Close to the horizon, one has [259]

$$\psi \sim A_{\rm H} e^{-i\omega v}\, Y_{\ell m}(\theta, \phi)\,, \tag{3.75}$$

where v is the null Eddington-Finkelstein horizon-penetrating coordinate defined as $t + r_*$. The time-like Killing vector fields t_μ, generates the conserved current [259]

$$J^\mu = -T^{\mu\nu} t_\nu\,, \tag{3.76}$$

where T_{ab} is the SET of the scalar field. The flux of energy through the horizon produces the mass variation [259, 298]

$$M'(v) = -\int_{\rm Horizon} {\rm d}\Omega\, t_\mu J^\mu = \frac{\omega^2}{8\pi} |A_{\rm H}|^2 e^{2v Im(\omega)}\,. \tag{3.77}$$

The mass derivative is then quadratic in the perturbation. The same procedure can be generalized to more modes and to different perturbation fields.

The effect of this evolution of the BH background on the spectrum of gravitational perturbations, appears then at the third BHPT order, and is two-fold. On the one hand, it can modify the QNM spectrum *adiabatically*. In the language of quantum mechanics, this means that the energy levels are slightly deformed without any mixing. This typically happens if the background evolution time-scale is much larger than the one of the ringdown dynamics. On the other hand, GW back-reaction can also alter the mode content of the ringdown. This process is known as absorption-induced mode excitation and can be understood as follows. In the new background spacetime, the original seed mode of the BH with mass M is no longer a pure QNM of the BH with mass $M + \delta M$. Instead, it decomposes into a superposition of modes belonging to the spectrum of the new BH. As a consequence, additional modes are excited. In the next chapter, we will focus on the first effect, namely on an adiabatic deformation of the QNM spectrum due to a smooth evolution of the BH mass. Moreover, in Chapter 6, we will perform a detailed analysis of the BH ringdown waveform, also including quadratic QNMs.

3.5 The Teukolsky equation

In the previous section, we described how the gravitational perturbation equations can be derived on a static background. However, real astrophysical BHs are in general spinning [47, 48]. For this reason, in order to have an accurate description of real ringdown signals, it is crucial to generalize the technology developed so far to the case of a more general stationary spacetime. In this section, we will schematically address the procedure for deriving the master equation for gravitational perturbations on a rotating BH background. Such equation is generally known as Teukolsky equation [276], and its derivation requires a different and more complicated strategy. We are going to summarize here the main steps. However, readers primarily interested in the final form of the Teukolsky equation can skip the derivation, and proceed directly to Eq. (3.96).

The metric of a stationary rotating BH, i.e. the Kerr metric [16], is given by Eq. (3.114), with $Q = 0$. Remarkably, due to the complexity of the Kerr metric, if one tries to proceed in analogy to the scheme adopted in spherical symmetry, they will not succeed in deriving decoupled master equations for the propagating degrees of freedom. Nevertheless, a way out of this problem was found in [353] by Newman and Penrose. The technology that they introduced is indeed the well-known Newmann-Penrose (NP) formalism. The basic idea, is to project the curvature tensors onto a tetrad basis, and to perturb its elements, rather then the components of the metric. In more detail, in the NP formalism, one has to consider a null tetrad, composed of two null real vectors n_μ and l_μ and a complex one m_μ with its complex conjugate $\bar{m}_\mu$. These vectors must satisfy the orthogonality properties

$$\begin{aligned} &l^\mu l_\mu = n^\mu n_\mu = m^\mu m_\mu = \bar{m}^\mu \bar{m}_\mu = 0\,, \\ &l^\mu n_\mu = -m^\mu \bar{m}_\mu = -1\,, \\ &l^\mu m_\mu = l^\mu \bar{m}_\mu = n^\mu m_\mu = n^\mu \bar{m}_\mu = 0\,. \end{aligned} \tag{3.78}$$

A possible choice is the Kinnersley tetrad [354], given by

$$\mu^\mu = \frac{1}{\Delta}\left(r^2 + a^2,\, \Delta,\, 0,\, a\right), \tag{3.79}$$

$$n^\mu = \frac{1}{2\rho^2}\left(r^2 + a^2,\, -\Delta,\, 0,\, a\right), \tag{3.80}$$

$$m^\mu = \frac{1}{\sqrt{2}}\frac{1}{r + ia\cos\theta}\left(ia\sin\theta,\, 0,\, 1,\, \frac{i}{\sin\theta}\right). \tag{3.81}$$

The Kerr metric can be expressed using the Kinnersley tetrad as

$$g^{\mu\nu} = m^\mu \bar{m}^\nu + m^\nu \bar{m}^\mu - n^\mu l^\nu - n^\nu l^\mu \,. \tag{3.82}$$

For a given scalar field ψ, we will use the following notation for the derivatives projected on the elements of null basis:

$$\begin{aligned} D\psi &= \nabla_\mu \psi \, l^\mu \,, & \Delta\psi &= \nabla_\mu \psi \, n^\mu \\ \delta\psi &= \nabla_\mu \psi \, m^\mu \,, & \delta^*\psi &= \nabla_\mu \bar{m}^\mu \,. \end{aligned} \tag{3.83}$$

Let us now introduce the Weyl tensor, corresponding to the traceless part of the Riemann tensor and sharing the same symmetries:

$$C_{\mu\nu\rho\sigma} = R_{\mu\nu\rho\sigma} - \frac{1}{2}\left(g_{\mu[\rho}R_{\sigma]\nu} - g_{\nu[\rho}R_{\sigma]\mu}\right) + \frac{1}{6}R\, g_{\mu[\rho}g_{\sigma]\nu} \,. \tag{3.84}$$

Projecting the Weyl tensor onto the null tetrad defined above, one can define the NP scalars

$$\Psi_0 = C_{\mu\nu\rho\sigma}\, l^\mu m^\nu \, l^\rho m^\sigma \,, \tag{3.85}$$

$$\Psi_1 = C_{\mu\nu\rho\sigma}\, l^\mu n^\nu \, l^\rho m^\sigma \,, \tag{3.86}$$

$$\Psi_2 = \frac{1}{2} C_{\mu\nu\rho\sigma}\, l^\mu n^\nu \, (l^\rho n^\sigma + m^\rho \bar{m}^\sigma) \,, \tag{3.87}$$

$$\Psi_3 = C_{\mu\nu\rho\sigma}\, n^\mu l^\nu \, n^\rho \bar{m}^\sigma \,, \tag{3.88}$$

$$\Psi_4 = C_{\mu\nu\rho\sigma}\, n^\mu \bar{m}^\nu \, n^\rho \bar{m}^\sigma \,. \tag{3.89}$$

In GR, the complex scalar Ψ_4 (or equivalently Ψ_0, that is proportional to Ψ_4^* in the radiation zone) encodes the two graviton degrees of freedom. To illustrate this fact, let us consider a GW propagating on a flat background, along the z axis of a cartesian coordinate frame (t, x, y, z). As discussed in the first chapter, in the TT gauge, the metric perturbation has only four non-vanishing components, that are $h^{\rm TT}_{xx} = -h^{\rm TT}_{yy} = h_+$, and $h^{\rm TT}_{xy} = h^{\rm TT}_{yx} = h_\times$. Moreover, one has

$$R_{0i0j} = -\frac{1}{2}\ddot{h}^{\rm TT}_{ij} \,. \tag{3.90}$$

Projecting the components of the Riemann on the null tetrad, one gets

$$\begin{aligned} \Psi_0 &= -\frac{1}{2}(\ddot{h}_+ + i\ddot{h}_\times) \,, \\ \Psi_4 &= -\frac{1}{2}(\ddot{h}_+ - i\ddot{h}_\times) \,. \end{aligned} \tag{3.91}$$

Similarly to what we did with the Weyl tensor, other complex scalars can be defined from the Ricci tensor, i.e.

$$\begin{aligned} \Phi_{00} &= -\frac{1}{2} R_{\mu\nu}\, l^\mu l^\nu \,, \\ \Phi_{01} &= -\frac{1}{2} R_{\mu\nu}\, l^\mu m^\nu \,, \\ \Phi_{02} &= -\frac{1}{2} R_{\mu\nu}\, m^\mu m^\nu \,, \\ \Phi_{11} &= -\frac{1}{4} R_{\mu\nu}\, (l^\mu n^\nu + m^\mu \bar{m}^\nu) \,, \\ \Phi_{12} &= -\frac{1}{2} R_{\mu\nu}\, n^\mu m^\nu \,, \\ \Phi_{22} &= -\frac{1}{2} R_{\mu\nu}\, n^\mu n^\nu \,. \end{aligned} \tag{3.92}$$

Notice that all the quantities above are vanishing on a Ricci-flat spacetime, such as stationary BHs in GR.

Finally, one can define the twelve spin coefficients

$$\begin{aligned}
\kappa &= \nabla_\nu l^\mu \, m^\nu \, l_\mu, \\
\pi &= -\nabla_\nu n^\mu \, \bar{m}^\nu \, l_\mu, \\
\varepsilon &= \frac{1}{2}\left(\nabla_\nu l^\mu \, n^\nu \, l_\mu - \nabla_\nu m^\mu \, \bar{m}^\nu \, l_\mu\right), \\
\rho &= \nabla_\nu l^\mu \, m^\nu \, \bar{m}_\mu, \\
\lambda &= -\nabla_\nu n^\mu \, \bar{m}^\nu \, \bar{m}_\mu, \\
\alpha &= \frac{1}{2}\left(\nabla_\nu l^\mu \, n^\nu \, \bar{m}_\mu - \nabla_\nu m^\mu \, \bar{m}^\nu \, \bar{m}_\mu\right), \\
\sigma &= \nabla_\nu l^\mu \, m^\nu \, m_\mu, \\
\mu &= -\nabla_\nu n^\mu \, \bar{m}^\nu \, m_\mu, \\
\beta &= \frac{1}{2}\left(\nabla_\nu l^\mu \, n^\nu \, m_\mu - \nabla_\nu m^\mu \, \bar{m}^\nu \, m_\mu\right), \\
\nu &= -\nabla_\nu n^\mu \, \bar{m}^\nu \, n_\mu, \\
\gamma &= \frac{1}{2}\left(\nabla_\nu l^\mu \, n^\nu \, n_\mu - \nabla_\nu m^\mu \, \bar{m}^\nu \, n_\mu\right), \\
\tau &= \nabla_\nu l^\mu \, m^\nu \, n_\mu \, .
\end{aligned} \tag{3.93}$$

Notice that some of the Greek letters here employed for the definition of the spin coefficients, have already been associated to different quantities. However, within this section, there will be no ambiguity.

Now that we are in possess of the basic elements of NP formalism, we can study the perturbation of the metric. In this perspective, as already anticipated, the perturbations are absorbed by the elements of the tetrad. We will express the perturbed vector as, for instance, $l_\mu^{(0)} + l_\mu^{(1)}$, where the superscript $^{(0)}$ indicates the background quantity, whereas the superscript $^{(1)}$ labels the perturbation. All the NP scalar quantities can be perturbed accordingly. The unperturbed tetrad elements correspond to the Kinnersley tetrad, for which one has

$$\Psi_0^{(0)} = \Psi_1^{(0)} = \Psi_3^{(0)} = \Psi_4^{(0)} = 0 \, . \tag{3.94}$$

Since $\Psi_i^{(0),(1)}$ are Lorentz scalars, they are invariant under diffeomorphisms. Furthermore, if we consider an infinitesimal coordinate transformation $x^\mu \to x^\mu + \xi^\mu$, we have $\Psi_i^{(1)} \to \Psi_i^{(1)} - \xi^\mu \partial_\mu \Psi_i^{(0)}$. Hence, for $i = 0, 1, 3, 4$ the perturbations $\Psi_i^{(1)}$ are gauge-invariant.

Applying this machinery to the different components of the Einstein equation in vacuum, and after several nontrivial manipulations, on ends up with the two decoupled equations

$$\begin{aligned}
&[(D - 3\varepsilon + \varepsilon^* - 4\rho - \rho^*)(\triangle - 4\gamma + \mu) \\
&\qquad - (\delta + \pi^* - \alpha^* - 3\beta - 4\tau)(\delta^* + \pi - 4\alpha) - 3\Psi_2^{(0)}]\Psi_0^{(1)} = 0 \, , \\
&[\triangle + 3\gamma - \gamma^* + 4\mu + \mu^*)(D + 4\varepsilon - \rho) \\
&\qquad - (\delta^* - \tau^* + \beta^* + 3\alpha + 4\pi)(\delta - \tau + 4\beta) - 3\Psi_2^{(0)}]\Psi_4^{(1)} = 0 \, .
\end{aligned} \tag{3.95}$$

The two Eqs. (3.95) can be expressed in a unified form, introducing a spin parameter s [3].

$$\begin{aligned}
&\left((r^2+a^2)^2\Delta - a^2\sin^2\theta\right)\frac{\partial^2\tilde{\Psi}^{(1)}}{\partial t^2} \\
&+\frac{2arsr}{\Delta}\frac{\partial^2\tilde{\Psi}^{(1)}}{\partial t\,\partial\phi}+\left(\frac{a^2}{\Delta}-\frac{1}{\sin^2\theta}\right)\frac{\partial^2\tilde{\Psi}^{(1)}}{\partial\phi^2}-\Delta^{-s}\frac{\partial}{\partial r}\left(\Delta^{s+1}\frac{\partial\tilde{\Psi}^{(1)}}{\partial r}\right) \\
&-\frac{1}{\sin\theta}\frac{\partial}{\partial\theta}\left(\sin\theta\frac{\partial\tilde{\Psi}^{(1)}}{\partial\theta}\right)-2s\left(\frac{a(2r-rs)}{2\Delta}+i\frac{\cos\theta}{\sin^2\theta}\right)\frac{\partial\tilde{\Psi}^{(1)}}{\partial\phi} \\
&-2s\left(\frac{rs(r^2-a^2)}{2\Delta}-r-ia\cos\theta\right)\frac{\partial\tilde{\Psi}^{(1)}}{\partial t}+(s^2\cot^2\theta-s)\tilde{\Psi}^{(1)}=0\,.
\end{aligned} \tag{3.96}$$

Eq. (3.96) can be expressed in a compact form as

$$\mathcal{T}\left[\tilde{\Psi}^{(1)}\right]=0\,, \tag{3.97}$$

introducing the Teukolsky operator $\mathcal{T}$. Choosing $s=-2$, the expression describes the dynamics of $\Psi_4^{(1)}$, which is related to the master variable $\tilde{\Psi}^{(1)}$ through $\tilde{\Psi}^{(1)}=(1-ia\cos\theta)^4\Psi_4^{(1)}$. On the other hand, with the choice $s=+2$, the equation describes the dynamics of $\tilde{\Psi}^{(1)}=\Psi_0^{(1)}$. Remarkably, also scalar and electromagnetic perturbations are described by Eq. (3.96), with, respectively $s=0,\pm1$.

Now that we have a single master equation for perturbations on the Kerr background, we proceed with the usual separation of variables. The master function can be expanded as

$$\tilde{\Psi}^{(s)}(t,r,\theta,\phi)=\int_{-\infty}^{+\infty}\mathrm{d}\omega\sum_{\ell m}R^{(s)}_{\ell m}(r,\omega)S^{(s)}_{\ell m}\,e^{im\phi-i\omega t}\,. \tag{3.98}$$

The radial part reads

$$\Delta^{-s}\frac{\mathrm{d}}{\mathrm{d}r}\left[\Delta^{s+1}\left(R^{(s)}_{\ell m}\right)'\right]+V_{\mathrm{T}}R^{(s)}_{\ell m}=0\,, \tag{3.99}$$

with the effective Teukolsky potential

$$V_{\mathrm{T}}=2\mathrm{i}s\frac{\mathrm{d}K}{\mathrm{d}r}-\lambda_{\ell m}+\frac{1}{\Delta}\left(K^2-\mathrm{i}sK\frac{\mathrm{d}\Delta}{\mathrm{d}r}\right)\,, \tag{3.100}$$

and where we defined the quantities

$$\Delta=r^2-r_sr+a^2\,,\qquad K=(r^2+a^2)\omega-am\,, \tag{3.101}$$

$$\lambda_{\ell m}=B_{\ell m}+a^2\omega^2-2am\omega\,. \tag{3.102}$$

It is worth mentioning that the zeros of the function Δ determine the location of the BH inner and outer horizons, given by

$$r_\pm=r_s\left(\frac{1\pm\sqrt{1-\frac{4a^2}{r_s^2}}}{2}\right)\,. \tag{3.103}$$

[3] Again, this should not be confused with the complex variable of the Laplace transform, introduced previously. Within this section, there is no conflict of the two meanings.

The term $B_{\ell m}$ is the separation constant. Unlike the static case, this number does not have a closed analytic form and must be determined numerically.

On the other hand, the angular part reads

$$\begin{aligned}&\frac{\mathrm{d}}{\mathrm{d}y}\left[(1-y^2)\left(S^{(s)}_{\ell m}\right)'\right]\\&\quad+\left[a^2\omega^2y^2-2sa\omega y+B_{\ell m}+s-\frac{(m+sy)^2}{1-y^2}\right]S^{(s)}_{\ell m}=0\,,\end{aligned}\tag{3.104}$$

where $y=\cos\theta$.

The angular functions that solve Eq. (3.104) are called spin-weighted spheroidal harmonics. In practice for obtaining the QNMs of a rotating BH, on has to solve two coupled Schrödinger-like equations, for the two sets of eigenvalues $\{\omega_{\ell mn}, B_{\ell mn}\}$.

The QNM spectrum of the Kerr BH shares the same basic features of the Schwarzschild one, with some extra subtleties. First of all, the dependence on the magnetic number m is nontrivial. The aforementioned mirror symmetry of QNMs in the Kerr case reads

$$\omega_{\ell mn}=-\omega^*_{\ell -mn}\,.\tag{3.105}$$

In the literature, the modes are generally classified as *prograde* if m and $Re(\omega)$ have the same sign, and *retrograde* in the opposite case.

Besides breaking the degeneracy in m, the spin has also the effect of reducing the imaginary part of the QNMs, up to the extremal case in which $Im(\omega)\to 0$.

Finally, the discussion on quadratic BHPT is conceptually similar to the static case, although it requires more technical effort [343]. Consider the perturbation of the NP scalar up to quadratic order

$$\Psi_4=\epsilon\Psi_4^{(1)}+\epsilon^2\Psi_4^{(2)}+\mathcal{O}(\epsilon^3)\,.\tag{3.106}$$

The quadratic master equation takes the form

$$\mathcal{T}\left[\tilde{\Psi}^{(2)}\right]=\mathcal{S}_4\left[h^{(1)}_{\mu\nu},h^{(1)}_{\mu\nu}\right]\,,\tag{3.107}$$

where $\tilde{\Psi}^{(2)}=(1-ia\cos\theta)^4\Psi_4^{(2)}$ and $\mathcal{S}_4$ is an involved function of the linear metric perturbation. The computation of the source term requires that we know the form of the metric perturbation at linear order. In other words, we need to extract the information on $h^{(1)}_{\mu\nu}$ from the projected quantity $\Psi_4^{(1)}$. This process is called *metric reconstruction* [355]. The procedure can be carried out through the derivation of a scalar *Herz potential* that allows to compute the components of the metric perturbation by performing derivative of it along the tetrad directions. Remarkably, this approach yields metric perturbation components in the radiation gauge, so that they are directly related to physically observable quantities.

Finally, with the same logic as in the static case, the quadratic QNM frequencies are fully determined from the linear ones as

$$\omega^{(2)}=\omega^{(1)}_{\ell_1m_1,n_1}+\omega^{(1)}_{\ell_2,m_2n_2},\quad\text{or}\quad\omega^{(2)}=\omega^{(1)}_{\ell_1m_1n_1}-(\omega^{(1)}_{\ell_2m_2n_2})^*,\tag{3.108}$$

while the ratio of the quadratic to linear QNM amplitudes can also be estimated within the BHPT framework, as it is done in the static case.

3.6 Black hole perturbations beyond General Relativity

In Chapter 1, we motivated the importance of exploring deviations from Einstein's GR both at a formal and phenomenological level. In this chapter, we derived the main technical tool to model the ringdown of a real astrophysical BH, namely the Teukolsky equation. Hence, the most natural step forward now, is to try to understand how the perturbation dynamics of BHs is affected if we include (small) modifications of the underlying theory of gravity. In particular, one might wonder whether the nice properties of the Teukolsky equation, such as decoupling of the different degrees of freedom, and separability of radial and angular dependence, can still be recovered beyond GR, given, at least, some reasonable conditions. A seminal work in this context was presented in 2023 [356], and we are going to summarize here the main general findings thereof. Subsequently, we are going to provide a more specific instance of modified Teukolsky equation in a precise modified gravity theory.

Let us start considering the most general modified gravity action

$$S\left[g_{\mu\nu},\psi,\vartheta\right]=S_{\rm EH}\left[g_{\mu\nu}\right]+S_{\rm bEH}\left[g_{\mu\nu},\vartheta\right]+S_{\rm field}\left[g_{\mu\nu},\vartheta\right]+S_{\rm matter}\left[g_{\mu\nu},\Psi_m\right]\,, \tag{3.109}$$

where ϑ is a new dynamical degree of freedom. The part $S_{\rm field}$ includes the minimally coupled terms between ϑ and the metric tensor (kinetic term, and auto-interactions), while the beyond-EH action $S_{\rm bEH}$ represents the non-minimal couplings. This second term, as discussed in Chapter 1, typically appears as a collection of irrelevant operators of an EFT, and comes with one or more dimensionful couplings. Finally, Ψ_m represents a generic matter field belonging to the standard model of particle physics. From now on, we are going to forget about this last contribution, as we will focus on vacuum solutions.

We are now going to design a slightly different perturbation scheme, motivated by the reasonable assumption that the coupling that drives the deviation from GR is small in comparison to the size of the BH. This effect can be naturally expressed by means of a dimensionless parameter ζ, being the ratio of the characteristic energy scale of the gravity modification and the BH mass. Then, a NP scalar such as Ψ_4 can be expanded as

$$\Psi_4=\zeta\Psi_4^{(1,0)}+\epsilon\Psi_4^{(0,1)}+\zeta\epsilon\Psi_4^{(1,1)}+\mathcal{O}\left(\zeta^2,\epsilon^2\right)\,, \tag{3.110}$$

where the superscript $^{(m,n)}$ indicates terms at $\mathcal{O}(\zeta^n,\epsilon^m)$. In the following, we will use both this notation, and the more compact $^{(n)}$, only indicating the order of the expansion in ϵ. It turns out that NP scalars that govern the GW dynamics, namely Ψ_0 and Ψ_4 are generally vanishing at background level, even for known BH spacetime solutions in alternative gravity theories. However, this need not hold for the other scalars Ψ_1, Ψ_2 and Ψ_3. In particular, spacetimes can be classified according with the number of vanishing NP scalars. This grouping is known as Petrov classification [357]. The spacetime types are

$$\begin{aligned}
&\text{Type I}: && \Psi_0=\Psi_4=0\,,\\
&\text{Type II}: && \Psi_0=\Psi_1=\Psi_4=0\,,\\
&\text{Type D}: && \Psi_0=\Psi_1=\Psi_3=\Psi_4=0\,,\\
&\text{Type III}: && \Psi_0=\Psi_1=\Psi_2=\Psi_4=0\,,\\
&\text{Type N}: && \Psi_0=\Psi_1=\Psi_2=\Psi_3=0\,,\\
&\text{Type O}: && \Psi_0=\Psi_1=\Psi_2=\Psi_3=\Psi_4=0\,.
\end{aligned} \tag{3.111}$$

In GR, all stationary BHs belong to the Petrov type D. As we will see, some BH solution beyond GR are still in this category. However, if one drops the stationarity assumption, one can find examples of non-type D BHs also in GR. For instance, the Vaidya spacetime,

representing an accreting or radiating BH, which will be crucial for the discussion in the next chapter, belongs to the Petrov type II. The type O, for which all components of the Weyl tensor vanish, includes flat (Minkowski) and conformally flat (de-Sitter and anti-de Sitter) spacetimes. On the opposite end, one finds the type I, in which only two NP scalars are vanishing. For this reason, spacetimes of Petrov type I are also called *algebraically general*.

The first class of BHs beyond GR that is analyzed in [356], is given by Petrov type D spacetime, that are, however, not Ricci-flat, i.e. their Ricci tensor is $R_{\mu\nu} \sim \mathcal{O}(\zeta)$. In this case, the equations for the different Ψ_i can still be decoupled, but the final Teukolsky equation has, in general, the form

$$\mathcal{T}\left[\tilde{\Psi}^{(1)}\right] = \mathcal{S}_{\rm MT}\,. \tag{3.112}$$

The source term $\mathcal{S}_{\rm MT}$, which is different for $\Psi_0^{(1)}$ and $\Psi_4^{(1)}$, arises because the NP quantities Φ_{ij}, with $i,j = 0,1,2$, are now non-vanishing. Notice that this fact also affects the form of the Teukolsky operator on the left hand-side. This can be viewed by expanding Eq. (3.112) according with the perturbation scheme of Eq. (3.110), i.e.

$$\mathcal{T}^{(0,0)}\tilde{\Psi}^{(1,1)} + \mathcal{T}^{(1,0)}\tilde{\Psi}^{(0,1)} = \mathcal{S}_{\rm MT}^{(1,1)}\,. \tag{3.113}$$

Eq. (3.113), can be further generalized to the case in which the background is algebraically general. In, particular, if one assumes that the background can be expressed as a perturbation of a Petrov type D spacetime, it can be shown that it is still possible to obtain decoupled equation for $\Psi_0^{(1)}$ and $\Psi_4^{(1)}$. The form of the modified Teukolsky equation in this case will have additional terms on the left-hand side in the form $\mathcal{D}^{(0,1)}\Psi_i^{(1,0)}$, where $\mathcal{D}^{(0,1)}$ is some differential operator of the order of the metric perturbation. In particular, at $\mathcal{O}(\zeta)$, the equation for $\Psi_0^{(1)}$ will involve the NP scalar $\Psi_0^{(1,0)}$ and $\Psi_1^{(1,0)}$, while the equation for $\Psi_4^{(1)}$ will involve $\Psi_4^{(1,0)}$ and $\Psi_3^{(1,0)}$. We refer the reader to [356] for further details.

After this quite abstract discussion, it is useful to provide one specific example of modified Teukolsky equation. An interesting case, is again provided by HDG, that we introduced in the first chapter. The line element of rotating BHs in HDG can be expressed as the Kerr one plus some corrections, in the form [81]

$$\begin{aligned} \mathrm{d}s^2 =& -\left(1 - \frac{r_s r}{\Sigma} - H_1\right)\mathrm{d}t^2 - (1+H_2)\frac{2ar_s r\sin^2\theta}{\Sigma}\mathrm{d}t\,\mathrm{d}\phi + (1+H_3)\Sigma\left(\frac{\mathrm{d}r^2}{\Delta} + \mathrm{d}\theta^2\right) \\ &+ (1+H_4)\frac{\left((r^2+a^2)^2 - a^2\Delta\sin^2\theta\right)\sin^2\theta}{\Sigma}\mathrm{d}\phi^2\,, \end{aligned} \tag{3.114}$$

where the functions H_i, which should not be confused with the polar metric perturbation components on a static background, can be defined as series expansions in the spin parameter a as

$$H_i = \sum_{n=0}^{\infty} a^n \sum_{p=0}^{n} \sum_{k=0}^{k_{\rm max}(n)} H_i^{(n,p,k)} \left(\frac{M}{r}\right)^k (\cos\theta)^p\,. \tag{3.115}$$

The coefficients $H_i^{(n,p,k)}$ can then be perturbatively expanded in the dimensionless parameter ζ. This kind of spacetime is, in general, non-Ricci-flat and algebraically general, although the deviation from a Petrov type D can be treated as perturbative. In this framework, the modified Teukolsky equation for the different NP quantities can be decoupled

by means of a metric reconstruction procedure. In particular, at linear order in ζ, the metric reconstruction can be just performed for a metric perturbation in GR. Finally, the equations can be separated using the decomposition of Eq. (3.98). At leading order in ζ, the angular equation is unaffected, while the radial part can be expressed in the nice form

$$\Delta^{-s}\frac{\mathrm{d}}{\mathrm{d}r}\left[\Delta^{s+1}\left(R^{(s)}_{\ell m}\right)'\right]+\left(V_{\rm T}+\zeta\,\delta V\right)R^{(s)}_{\ell m}=0\,. \tag{3.116}$$

For $s=-2$, the correction to the Teukolsky potential can be reduced to

$$\delta V^{-2}=\frac{A_{-2}}{r^2}+A_0+A_1 r+A_2 r^2\,, \tag{3.117}$$

with the coefficients

$$A_k=\sum_{n=0}^{n_{\rm max}}a^n\,A_{k,n}\,. \tag{3.118}$$

In Chapter II, we will consider this example of modified Teukolsky equation, as the main physical application for a parametrized framework for the computation of QNMs of rotating BHs beyond Kerr.

3.7 Tidal response

In this chapter so far, we discussed the general framework of BHPT, focusing on the application to the study of the BH ringdown. In this final section, we introduce a different deployment of BHPT, i.e. the response of a compact object to an external slowly varying tidal field. To do so, let us start with the classical Newtonian description of the problem. Consider an astrophysical object, of density $\rho(\vec{x})$, and radius R, embedded in an external gravitational potential $U_{\rm ext}$, generated by a companion body, and satisfying in the object's neighborhood the Laplace equation

$$\nabla^2 U_{\rm ext}=0\,. \tag{3.119}$$

The tidal field at multipole order ℓ is given by

$$\mathcal{E}_L=-\frac{\partial_{\langle L\rangle}U_{\rm ext}}{(\ell-2)!}\,, \tag{3.120}$$

where we introduced the multi-index $L\equiv i_1 i_2\ldots i_\ell$, with every index i ranging over spatial coordinates, and the brackets $\langle\,\rangle$ indicating the symmetrized traceless part. The mass multipole of the compact object is, in general, defined as

$$I_L\equiv\int \mathrm{d}^3x\,\rho(\vec{x})\,x^{\langle L\rangle}\,, \tag{3.121}$$

For instance, in the quadrupole case, one has

$$Q_{ij}=\int \mathrm{d}^3x\,\rho(\vec{x})\left(x^i x^j-\frac{1}{3}\delta^{ij}r^2\right)\,. \tag{3.122}$$

The tidal field can be connected to the mass multipole at linear order as

$$I_L=-\frac{(l-2)!}{(2l-1)!!}k_l\,R^{2l+1}\mathcal{E}_L\,, \tag{3.123}$$

where k_ℓ is a proportionality factor called linear static *Love number* [311, 317, 358–360]. The Love number quantifies the tidal deformability of an astrophysical object, and can be interpreted as the gravitational analogous of the linear polarizability of a dielectric medium in electrostatics [210]. In general, if we allow for a mild time dependence in the external field $\mathcal{E}_L$, the induced quadrupole, and the tidal response, will also be time-dependent. This effect can be taken into account in the frequency domain with the more general definition of *dynamical* Love number [208, 314, 361]. While static Love numbers are purely real, dynamical Love number possess in general an imaginary part, which represents dissipative effects appearing at next-to-leading order in a small-frequency expansion. Schematically one gets

$$I_L \propto (k_\ell + i\omega\nu_\ell + \dots)\mathcal{E}_L \tag{3.124}$$

where ν_ℓ is usually called *dissipation number*. In the following, we are going to focus only on the static response.

The total gravitational field $U(\vec{x})$ outside the object is given by

$$U(\vec{x}) = -\frac{M}{r} - \sum_{\ell\geq 2} \frac{1}{(\ell-1)\ell}\left[1 + k_\ell \left(\frac{R}{r}\right)^{2\ell+1}\right]\mathcal{E}_L r^L\,, \tag{3.125}$$

with $M = \int \mathrm{d}^3x\,\rho(\vec{x})$ being the total mass of the object. Notice that, we can expand the contraction $\mathcal{E}_L r^L$ as $\sim \sum_\ell \mathcal{E}_\ell r^\ell Y_{\ell 0}(\theta,\phi)$, introducing the tidal moment $\mathcal{E}_\ell$. This Newtonian picture can be generalized to a consistent relativistic treatment in terms of metric components. This allows the computation of the tidal deformation of vacuum spacetimes, such as BHs. Moreover, while in the Newtonian case the tidal deformability is purely polar, in a relativistic context, one typically also has axial tidal perturbations. In an asymptotically mass-centered Cartesian coordinate frame, at large distance from a compact object, the relevant metric components read [310, 362]

$$\begin{aligned} g_{tt} &= -1 + \frac{2M}{r} - \sum_{\ell\geq 2}\left[\frac{2}{\ell(\ell-1)} r^\ell \mathcal{E}_\ell - \frac{2}{r^{\ell+1}}\sqrt{\frac{4\pi}{2\ell+1}}\mathcal{M}_\ell + \dots\right] Y_{\ell 0}(\theta,\phi), \\ g_{t\phi} &= \sum_{\ell\geq 2}\left[\frac{2}{3\ell(\ell-1)} r^{\ell+1}\mathcal{B}_\ell + \frac{2}{r^\ell}\sqrt{\frac{4\pi}{2\ell+1}}\mathcal{S}^\ell_\ell + \dots\right]\sin\theta\frac{\partial}{\partial\theta}Y_{\ell 0}(\theta,\phi), \end{aligned} \tag{3.126}$$

where the dots indicate the contribution from the lower multipoles. We introduced the polar (or-electric-type) and axial (or magnetic-type) tidal moments $\mathcal{E}_\ell$ and $\mathcal{B}_\ell$, and the mass and mass-current multipole moments M_ℓ and $\mathcal{S}_\ell$ respectively. The polar and axial Love numbers can be defined as the ratios of the leading growing and decaying parts in Eq. (3.126), i.e.

$$\begin{aligned} k^{\mathcal{E}}_\ell &= -\ell(\ell-1)R^{-2\ell-1}\sqrt{\frac{4\pi}{2\ell+1}}\frac{M_\ell}{\mathcal{E}_\ell}, \\ k^{\mathcal{B}}_\ell &= -\frac{3\ell(\ell-1)}{(\ell+1)}R^{-2\ell-1}\sqrt{\frac{4\pi}{2\ell+1}}\frac{S_\ell}{\mathcal{B}_\ell}. \end{aligned} \tag{3.127}$$

In the case of a Schwarzschild BH, the tidal Love numbers can be read off from the static limit, i.e. $\omega \to 0$, of Eq. (3.27). Remarkably, in this regime, Eq. (3.27) can be solved analytically in terms of *Hypergeometric functions*. The eigenfunctions $\Psi^{(\pm)}$ at large distance from the horizon read

$$\Psi^{(\pm)} \sim \left(\frac{r}{r_s}\right)^{\ell+1}\left[1 + \mathcal{O}\left(\frac{r_s}{r}\right) + \tilde{k}^{(\pm)}_\ell\left(\frac{r}{r_s}\right)^{-2\ell-1}\left(1 + \mathcal{O}\left(\frac{r_s}{r}\right)\right)\right], \tag{3.128}$$

where the dimensionless factors $\tilde{k}_\ell^{(\pm)}$ can be matched to the polar and axial Love numbers defined previously (with $R = r_s$) as

$$\tilde{k}_\ell^{(+/-)} = \frac{(\ell+1)(\ell+2)}{\ell(\ell-1)} k_\ell^{\mathcal{E}/\mathcal{B}} \,. \tag{3.129}$$

Imposing that the solution be regular at the BH EH, one finds that $\tilde{k}_\ell^{(+)} = \tilde{k}_\ell^{(-)} = 0$, for every value of ℓ. This result can also be shown to hold at quadratic order in BHPT [363–365]. Moreover, not only static BHs, but all stationary, asymptotically-flat BHs in four-dimensional GR appear to have vanishing static Love numbers [238, 312, 313, 358, 363, 366–369]. On the other hand, this general finding need not hold if one considers nontrivial asymptotics [370], or more general theories of gravity [371, 372]. Physically, this means that asymptotically flat BHs in four-dimensional GR do not develop any static tidal deformation under an external field, unlike other compact bodies, such as neutron stars. In the absence of a deep explanation for this fact, in an EFT perspective, this would appear as a fine-tuning problem, similarly to the cosmological constant one [373]. However, recent theoretical progress suggests that this phenomenon is not accidental, but stems from an underlying hidden "Love" symmetry, often characterized as an $\mathrm{SL}(2,\mathbb{R}) \times U(1)$ or Schrödinger-type algebra acting on the near-horizon region [261, 262, 374–377].

The computation of static Love numbers outlined above, while being practical and conceptually straightforward, strongly relies on the choice of an appropriate coordinate frame. As a result, it has been argued that Love numbers introduced in this way are not well defined [366, 378]. To address this issue, it is useful to employ a complementary approach, which is manifestly gauge invariant: the point-particle EFT that we already introduced in Chapter 2. In this framework, finite-size effects, such as tidal deformability, appear as higher-dimensional operators localized on the worldline. This idea is represented with the diagram of Fig. 3.6.

In order to introduce interaction terms on the worldline, it is though convenient to express the point-particle action of Eq. (2.4) in the Polyakov form [379]

$$S_{\rm pp} = \frac{1}{2}\int d\tau\, e \left(e^{-2} \frac{dx^\mu}{d\tau}\frac{dx^\nu}{d\tau} g_{\mu\nu} - m_{\rm pp}^2 \right) \tag{3.130}$$

where we introduced the einbein $e(\tau)$, that can be integrated out to obtain again Eq. (2.4), through the equation of motion

$$e = m_{\rm pp}^{-1} \sqrt{-g_{\mu\nu}\frac{dx^\mu}{d\tau}\frac{dx^\nu}{d\tau}} \,. \tag{3.131}$$

To couple the compact object with an external gravitational field, one can write down the total action, given by the sum of the point-particle action, the gravity action in the bulk, and the interaction operators on the worldline, i.e. $S_{\rm tot} = S_{\rm pp} + S_{\rm bulk} + S_{\rm int}$. The second term is simply given by the Einstein-Hilbert action, that can be expanded up to quadratic order in the metric perturbations. The last contribution can be expanded as

$$\begin{aligned} S_{\rm int} = \sum_{\ell=2}^{\infty} \frac{1}{2\ell!} \int d\tau\, e \Bigg[& \lambda_\ell^{\mathcal{E}} \left(\partial_{\langle a_1} \cdots \partial_{a_{\ell-2}} E^{(2)}_{a_{\ell-1}a_\ell\rangle} \right)^2 \\ & + \frac{1}{2}\lambda_\ell^{\mathcal{B}} \left(\partial_{\langle a_1} \cdots \partial_{a_{\ell-2}} B^{(2)}_{a_{\ell-1}a_\ell\rangle\, |b} \right)^2 \Bigg] \,, \end{aligned} \tag{3.132}$$

where we introduced the electric and magnetic parts of the Weyl tensor respectively as

$$E^{(2)}_{ij} \equiv C_{titj} \,, \qquad\qquad B^{(2)}_{ij|l} \equiv C_{tijl} \,, \tag{3.133}$$

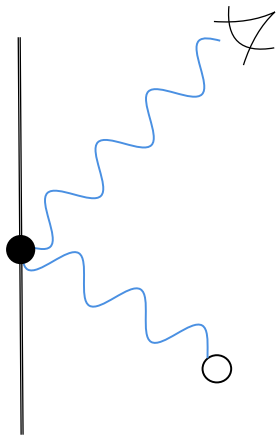

Figure 3.6: Diagrammatic representation of the worldline EFT approach. A generic external field, represented with the wavy line, interacts with the point particle's worldline (represented with the vertical line) and the response can read off at infinity.

and the dimensional couplings $\lambda_\ell^{\mathcal{E},\mathcal{B}}$. The equation of motion for the linear static metric perturbation, obtained by the variation of $S_{\rm tot}$, can be expressed as a set of non-homogeneous Laplace equations for the different components, where the source term is given by the variation of $S_{\rm int}$. Hence, it is useful to expand the metric perturbation as $h_{\mu\nu}^{(1)} = \bar{h}_{\mu\nu} + \delta h_{\mu\nu}$, where $\bar{h}_{\mu\nu}$ is the homogeneous solution, and $\delta h_{\mu\nu}$ is the correction sourced by the interactions on the worldline. In the harmonic gauge, the only nontrivial contribution to the electric-type tidal response comes from the h_{tt} component. The full solution reads [238]

$$h_{tt} = \bar{h}_{tt} + \delta h_{tt} \sim r^\ell Y_{\ell m}(\theta,\phi) \left(1 + \frac{(-1)^\ell 2^{\ell-3}}{\sqrt{\pi}\,\Gamma\left(\frac{1}{2}-\ell\right)} \lambda_\ell^{\mathcal{E}}\, r^{-2\ell-1} \right) . \tag{3.134}$$

The point-particle EFT coupling can then be matched to the electric-type tidal Love number as [238]

$$\lambda_\ell^{\mathcal{E}} = (-1)^\ell \frac{\sqrt{\pi}\,\Gamma\left(\frac{1}{2}-\ell\right)}{2^{\ell-3}} r_s^{2\ell+1} k_\ell^{\mathcal{E}} \,. \tag{3.135}$$

On the other hand, the only components of the metric perturbations that contribute to the magnetic-type tidal response are h_{ti}. Applying a similar reasoning, one ends up with the matching condition [238]

$$\lambda_\ell^{\mathcal{B}} = (-1)^\ell \frac{\ell}{\ell+1} \frac{\sqrt{\pi}\,\Gamma\left(\frac{1}{2}-\ell\right)}{2^{\ell-4}} r_s^{2\ell+1} k_\ell^{\mathcal{B}} \,. \tag{3.136}$$

In the next chapter, we are going to revisit the computation of static Love numbers introduced here, both in the framework of BH perturbation equations and in the point-particle EFT perspective, specializing to the case of a dynamical spacetime.

This section about tidal response concludes our general overview of BHPT.

Chapter 4

Perturbation of a dynamical spacetime

4.1 Introduction

As we discussed in the previous chapter, the emission of GWs produced during the ringdown is generally modelled as perturbations on top of a stationary BH background metric, without accounting for possible evolution of the BH mass. However, realistic BHs are generally non-stationary, as they can dynamically evolve due to the interplay with the surrounding environment. Modelling a dynamical BH background is then crucial for investigating diverse physical scenarios.

Astrophysical BHs are often surrounded by accretion disks, which lead to an increase in the BH mass [380, 381]. It is also known that BHs slowly evaporate through the Hawking mechanism [22, 382, 383]. The timescale of this process grows with the mass of the evaporating BH, hence its effect is likely irrelevant for stellar-origin and SMBHs, while it could in principle play a role in the dynamics of primordial ones. Another process that is capable of removing mass from a BH is given by superradiant instabilities driven by massive boson fields [384, 385]. The unstable production of such particles can in fact be triggered around a BH at the expense of its energy and angular momentum. This effect is related to the very well-known Penrose process [386], and it requires the presence of an ergoregion.

Note that while allowing the extraction of mass/energy from a stationary BH, Hawking evaporation and the Penrose process still satisfy the laws of BH thermodynamics [387, 388]. Moreover, one can consider more exotic scenarios, like accretion of a phantom matter field (i.e., a field violating the dominant energy condition, where BHs can actually lose mass while accreting [389, 390]. Finally, the BH mass is expected to evolve during the ringdown phase also due to the absorption of ringdown GWs themselves [391, 392]. This absorption of GWs is also expected to impact the inspiral dynamics in binary systems in the form of tidal heating [350, 393–397].

Furthermore, as discussed in the last section of the previous chapter, in the inspiral phase, the GW signal is affected by the tidal response of the binary objects. The conservative part of the response is generally quantified in terms of tidal Love numbers [317, 359, 360]. Static tidal Love numbers are zero for stationary, asymptotically-flat BHs in four-dimensional GR [238, 312, 358, 363, 366–369, 398], while they can be be non-vanishing if one considers nontrivial asymptotics, environmental effects, or more general theories of gravity [370–372].

A simple model of spherical, uncharged, dynamical BH spacetimes is provided by the

Vaidya metric (see [399, 400] for a detailed introduction).[1] This model, while relatively simple, provides an effective description of the processes mentioned above, allowing for an estimate of their impact on the astrophysical observables, e.g. the GW signals. A formal discussion of the perturbative dynamics of the Vaidya background can be found in [404–406]. Studies of QNMs for the Vaidya metric have already been carried out in the time domain with a fully numerical approach in [391, 407–411].

In this work, we perform instead a semi-analytic calculation in the frequency domain based on the continued-fraction method (also known as Leaver's method) [286], which is the most accurate technique for computing QNM frequencies, and is capable of handling overtones. Our approach relies on the assumption that the rate of change of the mass is constant. In this way, a proper choice of the coordinates allows to factor out the time dependence in a conformal factor and perform Fourier transforms, as it is usually done in standard BH perturbation theory. In this framework, we also discuss the tidal response of a dynamical BH, arguing that non-vanishing corrections to the Love numbers appear, as a result of the nontrivial mass evolution.

The paper is organized as follows. In section 4.2, we describe the mathematical properties of the Vaidya solution and its conformal structure in the case in which the mass derivative is constant. In section 4.3, we derive the perturbation equations for scalar, electromagnetic and (axial) gravitational fields on such background. In section 4.4, we estimate the QNMs analytically in the eikonal limit, and numerically using Leaver's continued-fraction method. Finally, in section 4.5, we discuss the tidal response of the Vaidya BH. In particular, we will perform the matching with the point-particle effective theory, and show how a small mass derivative provides nontrivial perturbative corrections to the vanishing Schwarzschild Love number couplings.

4.2 The causal structure of the Vaidya black hole

The Vaidya solution describes a (non-empty) spherically symmetric BH spacetime with dynamical mass. A compact way to write its line element is by taking the Schwarzschild line element in ingoing/outgoing Eddington–Finkelstein coordinates (w, r, θ, ϕ) and by promoting the Schwarzschild mass parameter to be a function of the null coordinate w. The latter can either be the advanced time, $w = t + r_*$, or the retarded time, $w = t - r_*$, where r_* is the Schwarzschild tortoise coordinate and t the standard Schwarzschild time.

Concretely, the Vaidya metric takes the form

$$\mathrm{d}s^2 = -\left(1 - \frac{2M(w)}{r}\right)\mathrm{d}w^2 + 2s\,\mathrm{d}w\,\mathrm{d}r + r^2\mathrm{d}\Omega_{S^2}^2\,, \tag{4.1}$$

with s being the sign of the derivative of the mass function $M(w)$, $s \equiv \mathrm{sign}[M'(w)]$, and with $\mathrm{d}\Omega_{S^2}^2 = \mathrm{d}\theta^2 + \sin^2\theta\,\mathrm{d}\phi^2$. In the following, we will assume $M(w)$ to be a monotonic function of w, in such a way that $M'(w)$ has definite sign.

The metric (4.1) describes an absorbing BH by taking $M'(w) > 0$ with $w = t + r_*$ (ingoing Vaidya), while it describes an emitting BH if $M'(w) < 0$ with $w = t - r_*$ (outgoing Vaidya).

The Vaidya BH metric (4.1) solves the non-vacuum Einstein equations

$$R_{\mu\nu} - \frac{1}{2}R\,g_{\mu\nu} = 8\pi T_{\mu\nu}\,, \tag{4.2}$$

[1] The electrically charged generalization was first introduced in [401], while rotating Vaidya solutions have been proposed in [402, 403].

where $R_{\mu\nu}$ and R are the Ricci tensor and Ricci scalar, respectively, while $T_{\mu\nu}$ is the SET

$$T_{\mu\nu} = \frac{|M'(w)|}{4\pi r^2}\partial_\mu w \partial_\nu w \,. \tag{4.3}$$

The latter describes a pure radiation field (e.g., photons or gravitons) in the geometrical optics limit.

The Vaidya BH presents a nontrivial causal structure, related to its departure from stationarity [400, 412, 413]. Unlike in the static case, the apparent horizon (AH), defined as the hypersurface of vanishing expansion, i.e. the boundary at which a congruence of null geodesics starts focusing into a trapped region, does not coincide with the EH. For a null congruence of geodesic curves, the outgoing null expansion $\Theta_{\rm outgoing}$ coincides with the fractional variation of the cross-sectional area Σ of the null congruence itself, with respect to an affine parameter l:

$$\Theta_{\rm outgoing} = \frac{1}{\Sigma}\frac{\delta\Sigma}{\delta l} \,. \tag{4.4}$$

In our case, this simply reads [412]:

$$\Theta_{\rm outgoing} = \frac{1}{r}\left(1 - \frac{2M(w)}{r}\right) . \tag{4.5}$$

The condition $\Theta_{\rm outgoing} = 0$ therefore provides the location of the apparent horizon, namely $r_{\rm AH} = 2M(w)$.

The global EH, instead, cannot be defined locally. However, for a constant rate of increasing/decreasing mass, i.e. $M(w) = M_0 + M'\,(w - w_0)$, with $M' = {\rm const}$, its location can be computed quite easily.

To do so, it is convenient to move to a different coordinate frame, in which the causal structure becomes completely manifest and, at the same time, the equations for the perturbations take a simpler form, as we will discuss in the next section.

Consider first the transformation

$$\begin{cases} w & \to & W \equiv \int \frac{{\rm d}w}{2M(w)} \,, \\ r & \to & x \equiv \frac{r}{2M(w)} \,, \end{cases} \tag{4.6}$$

which rescales both the radial coordinate and the null time. We can then trade the rescaled null time with a timelike coordinate defined as $T = W - s\,x_*$,[2] where

$$x_* = \int \frac{{\rm d}x}{f(x)} \tag{4.7}$$

is a generalized tortoise coordinate with

$$f(x) = 1 - \frac{1}{x} - 4|M'|x \,. \tag{4.8}$$

In these coordinates, the Vaidya metric $g_{\mu\nu}$, defined in (4.1), becomes conformal to a static metric $\tilde{g}_{\mu\nu}$, i.e.,

$$g_{\mu\nu} = 4M(w)^2 \tilde{g}_{\mu\nu}, \tag{4.9}$$

and the line element reads

$${\rm d}s^2 = 4M(w)^2\left[-f(x){\rm d}T^2 + \frac{1}{f(x)}{\rm d}x^2 + x^2 {\rm d}\Omega^2_{S^2}\right] . \tag{4.10}$$

[2]The time coordinate should not be confused with the trace of the SET, which we will denote below, when needed, with $T^\lambda{}_\lambda$.

The location of the EH is now evident in this diagonal form of the metric from the condition $g^{xx} = 0$, which corresponds, in physical coordinates, to

$$r_{\rm EH} = 2M(w)\left(\frac{1-\sqrt{1-16|M'|}}{8|M'|}\right) = 2M(w)\left(1+4|M'|+\mathcal{O}(M'^2)\right)\,, \tag{4.11}$$

where in the second line we have expanded for small values of the mass derivative M' and kept terms only up to linear order. Note that the EH always lies outside the AH.

Notice also that the condition $g^{xx} = 0$ yields at the same time an external "cosmological horizon" (CH), far away from $r_{\rm EH}$ and located at

$$r_{\rm CH} = 2M(w)\left(\frac{1+\sqrt{1-16|M'|}}{8|M'|}\right)\,. \tag{4.12}$$

This is formally similar to the CH present in Schwarzschild-de Sitter spacetime, with the mass derivative playing the role of a positive cosmological constant.

The choice of considering a constant rate of change of the BH mass, which we will adopt in the following, is physically relevant e.g. for accreting BHs (in which case the mass derivative is approximately given by the Eddington rate on timescales much longer than the ringdown). For BHs whose mass changes due to their own ringdown, the mass derivative can also be considered approximately constant on scales shorter than the ringdown decay time, and order corrections depending on the higher time derivatives of the mass can in principle also be included perturbatively.

Finally, note that the condition for the simultaneous existence of the two horizons of Eqs. (4.11) and (4.12) is $|M'| < 1/16$. We will restrict to this case hereafter. This choice is again motivated by the physical assumption that the mass evolution is a subleading effect in the perturbation dynamics.

4.3 Perturbation equations

In this section, we derive the equations of motion for massless scalar, electromagnetic and (axial) gravitational perturbations of the Vaidya spacetime. Thanks to the spherical symmetry of the background geometry (4.1), it will be convenient to adopt spherical coordinates and decompose the field perturbations in spherical harmonics. We will work under the simplifying assumption that the mass rate M' is constant. This will allow us to relate the $M' = \text{const}$ Vaidya metric to a static one through a conformal transformation. As a byproduct, the equations for the perturbations will be time independent in the new coordinates, as we will show explicitly. This fact will allow us to study the solutions in the frequency domain, mirroring the familiar case of perturbations around stationary BHs.

4.3.1 Generalities and scalar case

As an illustrative example, let us start by considering the case of a test massless scalar field. The dynamics is captured by the Klein–Gordon equation

$$\Box\Phi = 0\,, \tag{4.13}$$

where we have defined the d'Alembert operator $\Box = g^{\mu\nu}\nabla_\mu\nabla_\nu$, indicating with ∇ the covariant derivatives.

Under a general conformal transformation of the metric, $g_{\mu\nu} = A^2 \tilde{g}_{\mu\nu}$, a generic field φ transforms as

$$\varphi = A^\chi \tilde{\varphi}\,, \tag{4.14}$$

with χ being the conformal weight. Choosing $\chi = -1$ for the scalar field Φ, one obtains [3]

$$\Box\Phi = \left(\tilde{\Box} - \frac{\tilde{R}}{6}\right)\tilde{\Phi} = 0, \tag{4.15}$$

For the Vaidya metric (4.1), the Ricci scalar R is proportional to the trace of the SET, which is a pure radiation field, and it therefore vanishes, $R = 0$. However, it is nonzero for the conformal metric $\tilde{g}$ in (4.9), which corresponds to choosing $A = 2M(w)$ and yields $\tilde{R} = 24|M'|/x$. Introducing the decomposition

$$\tilde{\Phi}(T, x, \theta, \phi) = \sum_{\ell m} \int \frac{\mathrm{d}\Omega}{2\pi} \mathrm{e}^{-i\Omega T} \frac{u(x)}{x} Y_{\ell m}(\theta, \phi)\,, \tag{4.16}$$

the scalar equation reduces to

$$\left[\frac{\mathrm{d}^2}{\mathrm{d}x_*^2} + \Omega^2 - f(x)\left(\frac{\ell(\ell+1)}{x^2} + \frac{1}{x^3}\right)\right] u(x) = 0\,, \tag{4.17}$$

where we used the tortoise coordinate x_* defined in Eq. (4.7). Note that, for ease of notation, we dropped from $u(x)$ the dependence on the spherical harmonic quantum number ℓ.

4.3.2 Electromagnetic perturbations

Electromagnetic perturbations are described by the Maxwell equations

$$g^{\alpha\mu}\nabla_\alpha F_{\mu\nu} = 0\,, \tag{4.18}$$

where $F_{\mu\nu}$ is the field strength, satisfying $\nabla_{[\alpha} F_{\mu\nu]} = 0$. Unlike the Klein–Gordon equation, the Maxwell equations (4.18) are invariant under conformal transformations, thanks to the scale invariance of electromagnetism in four spacetime dimensions (as it can be explicitly verified by choosing conformal weight $\chi = 0$). Therefore, we can directly consider the equations on the stationary geometry $\tilde{g}_{\mu\nu}$, with the four-potential A_μ transforming trivially as $A_\mu = \tilde{A}_\mu$. Separating the field in axial (odd) and polar (even) parts according to their transformation rules under parity, which acts in polar coordinates as $\theta \to \pi - \theta$, $\phi \to \phi + \pi$, we shall write

$$\begin{aligned} A_\mu\,\mathrm{d}x^\mu &= \left(A_\mu^{(\mathrm{polar})} + A_\mu^{(\mathrm{axial})}\right)\mathrm{d}x^\mu \\ &= \mathrm{e}^{-i\Omega T}\Big[h(x)\,Y_{\ell m}\,\mathrm{d}T + e(x)\,Y_{\ell m}\,\mathrm{d}x \\ &\quad + \left(a(x)\varepsilon_a{}^b\,\partial_b Y_{\ell m} + k(x)\,\partial_a Y_{\ell m}\right)\mathrm{d}x^a\Big]\,, \end{aligned} \tag{4.19}$$

with ε being the Levi-Civita symbol on the two-dimensional Euclidian sphere. In addition, we will make the gauge choice $k(x) = 0$.

The Maxwell equation $\nabla^\mu F_{\mu\phi} = 0$ immediately yields the equation of motion of the odd electromagnetic degree of freedom:

$$\left[\frac{\mathrm{d}^2}{\mathrm{d}x_*^2} + \Omega^2 - f(x)\frac{\ell(\ell+1)}{x^2}\right] a(x) = 0\,. \tag{4.20}$$

On the other hand, from $\nabla^\mu F_{\mu\theta} = 0$, we obtain

$$h(x) = \frac{i}{\Omega} f(x) \frac{\mathrm{d}}{\mathrm{d}x} \left(f(x)\, e(x) \right) . \tag{4.21}$$

Substituting this into $\nabla^\mu F_{\mu x} = 0$,

and introducing the variable $q(x) = f(x)e(x)$, one gets the equation for the electromagnetic polar degree of freedom:

$$\left[\frac{\mathrm{d}^2}{\mathrm{d}x_*^2} + \Omega^2 - f(x) \frac{\ell(\ell+1)}{x^2} \right] q(x) = 0 \, . \tag{4.22}$$

Note that the equation is identical to the one in Eq. (4.20) for the axial mode. This means in particular that the two sectors are isospectral, i.e. they share the same set of QNMs. This result is in fact more general than the case of constant M', which we focused on here. We will explicitly verify this in Appendix B.1 for arbitrary choices of $M(w)$, where we also discuss the connection with electric-magnetic duality.

4.3.3 Gravitational perturbations

Analogously to the electromagnetic case, we perform a similar split in axial and polar components for gravitational perturbations. This will ensure that the dynamics of the two sectors is decoupled at the level of the linearized Einstein equations. Note that, thanks to the structure of the SET of Eq. (4.3), the perturbations of the radiation field couple only to the polar gravitational perturbations, and do not affect the dynamics of the axial gravitational sector. In fact, since $T_{\mu\nu} \propto \partial_\mu w \partial_\nu w$, its fluctuations $\delta T_{\mu\nu}$ can only transform evenly under parity. Hence, for simplicity, we will focus below on the axial gravitational sector only, and leave the analysis of the polar perturbations for a future study.

To obtain the master equation for the axial modes, one can proceed similarly to the derivation of the Regge–Wheeler equation for odd perturbations of Schwarzschild BHs. In the following, we will work in the "Einstein frame" [414], i.e. we will consider the equations of motion for the conformal metric $\tilde{g}_{\mu\nu}$. We will show in Appendix B.1 that this approach is completely equivalent to the derivation of the Regge–Wheeler equation in the Jordan frame, i.e. in terms of the Vaidya metric $g_{\mu\nu}$, satisfying the usual Einstein equations. In the following expressions, we will use the notation $s = \mathrm{sign}(M')$, M' and $|M'|$ to stress the distinction between situations where the mass derivative appears with its sign or in absolute value.

The equations of motion for the conformal metric $\tilde{g}$ read [3]

$$\tilde{R}_{\mu\nu} - 2\nabla_\mu \nabla_\nu \ln A - \tilde{g}_{\mu\nu} \Box \ln A + 2\nabla_\mu \ln A \nabla_\nu \ln A - 2\tilde{g}_{\mu\nu} \nabla_\alpha \ln A \, \nabla^\alpha \ln A = 8\pi T_{\mu\nu} \, , \tag{4.23}$$

where $A = 2M(w)$ and where the SET is

$$T_{\mu\nu} \mathrm{d}x^\mu \mathrm{d}x^\nu = \frac{|M'|}{4\pi x^2} \left[\mathrm{d}T^2 + \frac{2s}{f(x)} \mathrm{d}T \mathrm{d}x + \frac{\mathrm{d}x^2}{f(x)^2} \right] , \tag{4.24}$$

with the logarithmic gradient of the conformal factor reducing to

$$\nabla_\mu \ln A \, \mathrm{d}x^\mu = 2|M'| \left(\mathrm{d}T + \frac{s}{f(x)} \mathrm{d}x \right) . \tag{4.25}$$

Let us consider now a perturbation of the metric in the Einstein frame, i.e. let us write $\tilde{g}+\tilde{h}$, and split the perturbation in axial and polar sectors as $\tilde{h}=\tilde{h}^{(\mathrm{ax})}+\tilde{h}^{(\mathrm{pol})}$. Since $\tilde{h}^{(\mathrm{ax})}$ and $\tilde{h}^{(\mathrm{pol})}$ are decoupled at linear order, it is consistent to set $\tilde{h}^{(\mathrm{pol})}$ to zero and focus only on $\tilde{h}^{(\mathrm{ax})}$.

In the (T,x,θ,ϕ) coordinates and in the Regge–Wheeler gauge [271], we shall write

$$\tilde{h}^{(\mathrm{ax})}_{\mu\nu}=\sum_{\ell m}\int\frac{\mathrm{d}\Omega}{2\pi}\begin{pmatrix}0 & 0 & -\frac{h_0(x)}{\sin\theta}\,\partial_\phi & \sin\theta\, h_0(x)\,\partial_\theta\\ 0 & 0 & -\frac{h_1(x)}{\sin\theta}\,\partial_\phi & \sin\theta\, h_1(x)\,\partial_\theta\\ \mathrm{Sym} & \mathrm{Sym} & 0 & 0\\ \mathrm{Sym} & \mathrm{Sym} & 0 & 0\end{pmatrix}\mathrm{e}^{-i\Omega T}Y_{\ell m}(\theta,\phi)\,. \tag{4.26}$$

The three nontrivial components of the linearized Einstein equations are:

$$\begin{aligned}\frac{f(x)}{x}\left[h_0''(x)+i\Omega\, h_1'(x)\right]+\frac{2i\Omega}{x}\left[f(x)+2|M'|x\right]h_1(x)\\ +\frac{4|M'|}{x}h_0'(x)-\left[\frac{\ell(\ell+1)}{x^2}-\frac{2}{x^3}\right]h_0(x)=0\,,\end{aligned} \tag{4.27}$$

$$h_0'(x)-\frac{2}{x}h_0(x)+s\left[i\Omega-f(x)\frac{\ell(\ell+1)-2}{(4|M'|-i\Omega)x^2}\right]h_1(x)=0\,, \tag{4.28}$$

$$f(x)^2x^2h_1'(x)+sf(x)h_1(x)+(i\Omega-4M')h_0(x)=0\,. \tag{4.29}$$

From the last equation, we can isolate $h_0(x)$ and substitute it in the second one. Then, after introducing the master variable $Q(x)$, defined as $h_1(x)=F(x)Q(x)$, with

$$F(x)=-\frac{x^{\frac{5}{4}}}{f(x)^{\frac{3}{4}}}\exp\left(\frac{\arctan\left(\frac{8|M'|-1}{\sqrt{16|M'|-1}}\right)}{2\sqrt{16|M'|-1}}\right), \tag{4.30}$$

we find the following equation for $Q(x)$:

$$\left[\frac{\mathrm{d}^2}{\mathrm{d}x_*^2}+\tilde{\Omega}^2-f(x)\left(\frac{\ell(\ell+1)}{x^2}-\frac{3}{x^3}\right)\right]Q(x)=0\,, \tag{4.31}$$

with the shifted frequency $\tilde{\Omega}=\Omega+2iM'$ (note that here the mass derivative must be taken with its positive or negative sign).

4.3.4 Master equation

In summary, one can write the equations for all kinds of perturbations (scalars, vectors and axial tensors) as a single master equation for a suitable master variable $R(x)$:

$$\left[\frac{\mathrm{d}^2}{\mathrm{d}x_*^2}+\tilde{\Omega}^2-\,f(x)\left(\frac{\ell(\ell+1)}{x^2}+\frac{\sigma}{x^3}\right)\right]R(x)=0\,, \tag{4.32}$$

where $\tilde{\Omega}=\Omega$ in the scalar and electromagnetic case, and $\tilde{\Omega}=\Omega+2iM'$ in the axial gravitational case. The spin parameter σ reads respectively $1,0,-3$ for scalar, electromagnetic and axial gravitational perturbations. Unlike in the static case ($M'=0$), the potential

$$V(x)=f(x)\left(\frac{\ell(\ell+1)}{x^2}+\frac{\sigma}{x^3}\right) \tag{4.33}$$

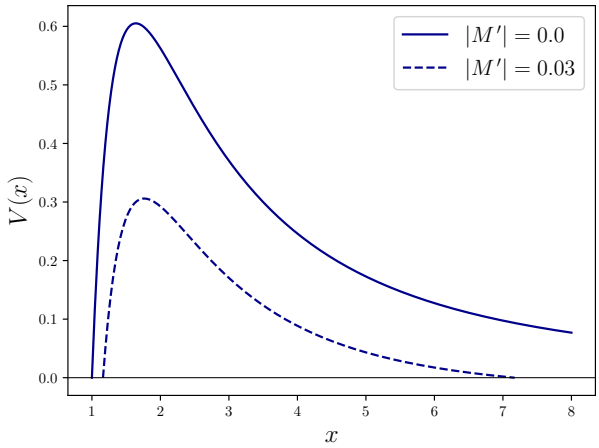

Figure 4.1: Gravitational potential ($\sigma = -3$) for $\ell = 2$. Note that a non-vanishing mass derivative M' shifts the EH outwards, while causing the appearance of an external CH.

vanishes in two points, namely at the EH and at the CH, see Fig. 4.1 for an example.

Note that the main point of our approach is the time-independent form of Eq. (4.32), which can be solved as a boundary value problem in the frequency domain, as we will discuss in the following. In [391, 407–411], time-domain methods have been instead used to solve the wave equation with time-dependent potential (see Appendix B.1 for the expression of the perturbation equations in Eddington–Finkelstein coordinates), given initial conditions and a functional form for the mass evolution function $M(w)$. In most of those works, the time-evolution is performed in double null coordinates u, v, θ, ϕ, where u and v are the retarded and advanced time that we already defined, starting from initial conditions given by a Gaussian wave packet. This procedure allows for a generic time evolution for the mass, but the extraction of the QNM frequencies from the time domain signal can only be performed for the dominant mode, and is generally less accurate than in our frequency domain approach. In the next section, we present the computation of the QNMs in the frequency domain from Eq. (4.32), showing that the full spectrum of frequencies can be obtained in this framework.

4.4 Quasi-Normal Modes

4.4.1 Eikonal approximation

We start here by deriving the Vaidya QNM frequencies in the geometrical optics limit—also known as eikonal limit—while a full numerical computation of the spectrum by means of the continued-fraction method will be presented later on in Sec. 4.4.2. Besides providing a first approximation for the spectrum, the eikonal limit can shed light on the correspondence between the frequencies and the parameters of the unstable photon geodesics at the light-ring. For stationary BHs in GR, it was found [415–417] that the real part of the eikonal QNMs corresponds to multiples of the orbital frequency, while the imaginary part is related to the Lyapunov exponent, which characterizes the instability timescale of the orbit. It is interesting to check whether there are examples of non-stationary BHs for which such correspondence can be recovered.

The potential in Eq. (4.33), in the eikonal limit $\ell \gg 1$, reads

$$V(x) = \left(1 - \frac{1}{x} - 4|M'|\,x\right)\frac{\ell^2}{x^2} + \mathcal{O}(\ell^0)\,. \tag{4.34}$$

It has two stationary points, a global maximum and a global minimum. The latter is located outside the CH. The former corresponds to the light-ring, which is shifted with respect to the Schwarzschild one. Let us consider a small linear evolution of the mass function, namely $M' \to \epsilon M'$, where ϵ is a (positive) book-keeping parameter, which we will take to be small enough such that $\epsilon M' w \ll M_0$. The location of the light-ring r_{lr}, at linear order in ϵ, evolves in time as

$$\begin{aligned} r_{lr} &= 3M(w)\left[1+3|M'|\epsilon+\mathcal{O}(\epsilon^2)\right] = \\ &= 3M_0\left[1+3\left(1+s\frac{w-w_0}{M_0}\right)|M'|\epsilon+\mathcal{O}(\epsilon^2)\right] . \end{aligned} \tag{4.35}$$

This radius can also be obtained from the geodesics equation for photons [418–422]. As already mentioned, the metric $\tilde{g}_{\mu\nu}$ of Eq. (4.10),

which is conformally related to the Vaidya metric, is static and admits the stationarity Killing vector $\xi = \partial_T$.

The equation for null geodesics is the same for both $g_{\mu\nu}$ and $\tilde{g}_{\mu\nu}$, and reads

$$0 = \tilde{g}_{\mu\nu}k^\mu k^\nu = -\left(1-\frac{1}{x}-4|M'|x\right)\frac{\mathrm{d}T}{\mathrm{d}l}+\frac{1}{1-\frac{1}{x}-4|M'|x}\frac{\mathrm{d}x}{\mathrm{d}l}+x^2\frac{\mathrm{d}\phi}{\mathrm{d}l} , \tag{4.36}$$

with l being an affine parameter and k^μ a null vector.

One can then use the conserved quantities associated with the Killing vector ξ and the axial Killing vector $\kappa = \partial_\phi$,

$$\begin{aligned} E &= -\xi_T , \\ L &= \kappa_\phi , \end{aligned} \tag{4.37}$$

to obtain the equation

$$\frac{\mathrm{d}x}{\mathrm{d}l} = E - V_{\text{eff}}(x) . \tag{4.38}$$

The effective potential matches the one appearing in Eq. (4.34):

$$V_{\text{eff}}(x) = \left(1-\frac{1}{x}-4|M'|\,x\right)\frac{L^2}{x^2} . \tag{4.39}$$

This fact shows that the eikonal correspondence between QNMs and null geodesics, which holds for stationary BHs in GR, is recovered in the linear evolution limit of spherically symmetric dynamical BHs described by the Vaidya geometry.

The quasi-normal frequencies can then be estimated analytically in the eikonal approximation (see Sec. 3.3.2 of the previous chapter). In more detail, we have

$$\begin{aligned} \tilde{\Omega}_R^E &= \sqrt{\frac{V(x_M)}{\ell^2}}\left(\ell+\frac{1}{2}\right)+\mathcal{O}(\ell^{-1}), \\ \tilde{\Omega}_I^E &= -\frac{\mathrm{d}x}{\mathrm{d}x_*}\sqrt{\frac{V''(x)}{2V(x)}}\bigg|_{x_M}\left(n+\frac{1}{2}\right)+\mathcal{O}(\ell^{-1}) , \end{aligned} \tag{4.40}$$

where $\tilde{\Omega}_R^E$ and $\tilde{\Omega}_R^E$ are the real and imaginary part of the QNM frequencies computed in the eikonal limit and x_M is the position of the maximum of the potential.

Considering again a small mass derivative, we have, at leading order,

$$\begin{aligned}\tilde{\Omega}_R^E &= \frac{2}{\sqrt{3}}\left(\ell+\frac{1}{2}\right)\left[\frac{1}{3}-3|M'|\,\epsilon+\mathcal{O}(\epsilon^2)\right],\\ \tilde{\Omega}_I^E &= -\frac{2}{\sqrt{3}}\left(n+\frac{1}{2}\right)\left[\frac{1}{3}-4|M'|\,\epsilon+\mathcal{O}(\epsilon^2)\right].\end{aligned} \tag{4.41}$$

These expressions can be directly related to the aforementioned parameters of the unstable circular photon orbit [415–417].

4.4.2 Numerical analysis

In order to find the full frequency spectrum, we solve Eq. (4.32) using Leaver's continued-fraction method. The procedure that we adopt for the Vaidya BH is similar to the Schwarzschild-de Sitter case, in which a study of QNMs with the same approach has been carried out in e.g. [423–425]. This method follows from the more general Frobenius procedure for second-order linear differential equations, which allows for finding solutions in terms of infinite power series. Two of the four singular points of the wave equation (4.32) (the other two being $x=0,\infty$) correspond to the positive zeros of the function $f(x)$, the first being the EH x_H, and the second being the CH $x_C\sim 1/|M'|$. The QNMs can be defined as solutions to the wave equation that are purely ingoing at the EH and purely outgoing at the CH. We can impose these boundary conditions in terms of the tortoise coordinate

$$x_* = \int \frac{\mathrm{d}x}{f(x)} = \frac{1}{4|M'|(x_C-x_H)}\Big[x_H\ln(x-x_H)-x_C\ln(x-x_C)\Big]. \tag{4.42}$$

They read

$$\begin{aligned}R(x_*) &\xrightarrow{x\to x_C} \mathrm{e}^{i\tilde{\Omega}x_*},\\ R(x_*) &\xrightarrow{x\to x_H} \mathrm{e}^{-i\tilde{\Omega}x_*}.\end{aligned} \tag{4.43}$$

Note that we can safely impose these outgoing/ingoing conditions at the horizons in terms of the frequency $\tilde{\Omega}$, as the latter is related to Ω by a shift in the imaginary part, which only affects the amplitude of the mode.

The solution to Eq. (4.32), subject to the boundary conditions (4.43) can then be expressed as the product of a diverging function at the horizons, and a convergent infinite power series in the interval (x_H,x_C). We can therefore use the ansatz

$$R(x) = (x-x_C)^{\rho\,\eta\,x_C}(x-x_H)^{\rho\,\eta\,x_H}\,S(x)\,, \tag{4.44}$$

where we defined $\rho=-i\Omega$ and $\eta=\frac{1}{4|M'|(x_C-x_H)}$, and where $S(x)$ is the Frobenius series

$$S(x) = \sum_{n=0}^{\infty} a_n\left(\frac{x-x_H}{x}\right)^n. \tag{4.45}$$

Inserting this ansatz into the master equation, one obtains the following five-term recurrence relation among the coefficients a_n

$$\alpha_n\,a_{n+1}+\beta_n\,a_n+\gamma_n\,a_{n-1}+\delta_n\,a_{n-2}+\zeta_n\,a_{n-3}=0\,. \tag{4.46}$$

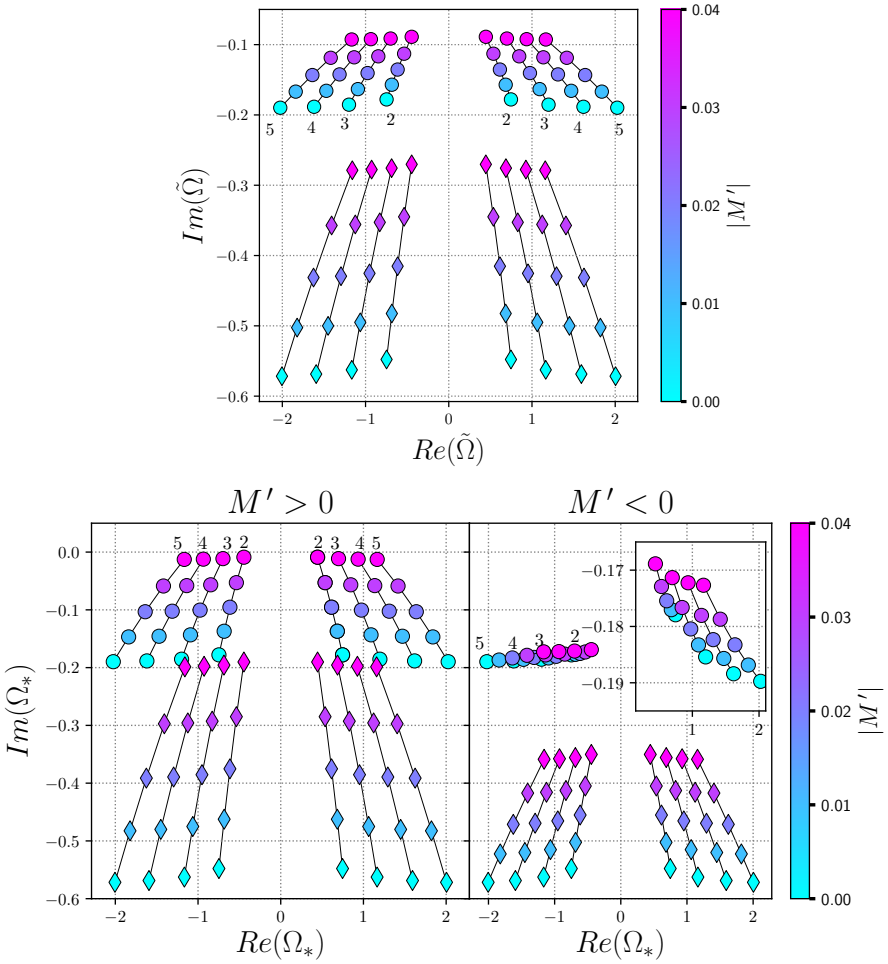

Figure 4.2: QNM rescaled frequencies in the complex plane. The fundamental modes are presented with round points, while the first overtones with diamond-shaped symbols. The small black numbers inside the plot indicate the angular momentum number ℓ, which we vary within the interval $\ell \in [2, 5]$. The color code indicates the modulus of the mass derivative. The upper panel represents the frequencies $\tilde{\Omega}$ in the master equation Eq. (4.32): at this level there is no difference between the increasing and decreasing mass cases. The lower panels represent instead the frequencies $\bar{\Omega}$ which are shifted according with the conformal weight of the gravitational perturbation field: here the spectrum is instead different in the cases in which the mass is increasing (left panel) or decreasing (right panel). Note that for large M' in the lower-left panel the frequencies approach the unstable regime.

The explicit expressions for these coefficients, which are quite lengthy, are presented in Appendix B.2. This five-term relation can be reduced numerically through Gaussian elimination in two steps.

One first define the new coefficients as

$$\begin{aligned}
\alpha'_n &= \alpha_n \,, \\
\beta'_n &= \beta_n - \frac{\alpha'_{n-1}}{\delta'_{n-1}} \zeta_n \,, \\
\gamma'_n &= \gamma_n - \frac{\beta'_{n-1}}{\delta'_{n-1}} \zeta_n \,, \\
\delta'_n &= \delta_n - \frac{\gamma'_{n-1}}{\delta'_{n-1}} \zeta_n \,.
\end{aligned} \tag{4.47}$$

The same procedure can be repeated to obtain the three-term relation

$$\alpha''_n\, a_{n+1} + \beta''_n\, a_n + \gamma''_n\, a_{n-1} = 0\,. \tag{4.48}$$

At this point, one can define the n-th ladder operator from the $(n+1)$-th one, as

$$A_n = \frac{\gamma''_n}{\beta''_n - \alpha''_n\, A_{n+1}}\,. \tag{4.49}$$

Finally, the spectrum is obtained by finding the zeros of the Leaver function

$$\mathcal{F}_{\text{Leaver}}(\tilde{\Omega}, \epsilon) = A_1 - \frac{\beta''_0}{\alpha''_0} = 0\,. \tag{4.50}$$

The frequencies obtained in this way from the spectrum of the master variable in (4.32) do not represent the physical spectrum. To obtain the physical spectrum, two effects must be taken into account. First, the physical perturbations are related to the master variable by a factor $(2M(w))^\chi$, where χ is the conformal weight of the fields. This effect introduces a shift in the frequencies $\tilde{\Omega}$. Second, because we performed a Fourier transform in the dimensionless time variable T, the frequencies must be rescaled by an overall time-dependent factor. This second effect will be discussed in more detail in the next subsection.

In the rescaled coordinates, and ignoring all factors depending on x (which affect the amplitude and not the frequency), the time-dependent mass reads

$$M(w)^\chi \sim \mathrm{e}^{2\chi M' T}\,. \tag{4.51}$$

The physical fields will then oscillate with frequency

$$\Omega_* \equiv \Omega + 2i\chi M'\,, \tag{4.52}$$

where $\Omega = \tilde{\Omega}$ for scalar and electromagnetic perturbations and $\Omega = \tilde{\Omega} - 2iM'$ for gravitational axial perturbations. Again, this is a purely imaginary shift, so it does not affect the boundary conditions of Eq. (4.43). The rescaled frequencies of the axial metric perturbations ($\chi = 2$), which represent the physical gravitational perturbations (in the axial sector), then oscillate with frequency $\tilde{\Omega} + 2iM'$. The overall shift of the gravitational spectrum in the complex plane is represented in Fig 4.2. The fundamental modes are represented with round points, while the first overtones are indicated with diamond-shaped points. The color-code represents the absolute value of the mass-derivative. The upper panel shows the frequency spectrum $\tilde{\Omega}$, i.e. before the shift $2i\chi M'$ is introduced. This spectrum does not depend on the sign of the mass derivative. The lower panels show instead the spectrum Ω_*, which differs when the mass increases or decreases.

4.4.3 Small rate limit and unstable regimes

For small values of the mass derivative the quasi-normal frequencies can be approximated as

$$\Omega_{n\ell} \simeq \Omega^{(0)}_{n\ell} + \delta\Omega_{n\ell}\,\epsilon\,, \tag{4.53}$$

with $\Omega^{(0)}_{n\ell}$ being the Schwarzschild QNMs and $\delta\Omega_{n\ell}$ being a constant complex coefficients. This can be viewed as a Taylor expansion of the frequencies around $\epsilon = 0$, namely

$$\Omega(\epsilon) = \Omega(0) + \left.\frac{\partial\Omega}{\partial\epsilon}\right|_{\epsilon=0} \epsilon + \mathcal{O}(\epsilon^2)\,. \tag{4.54}$$

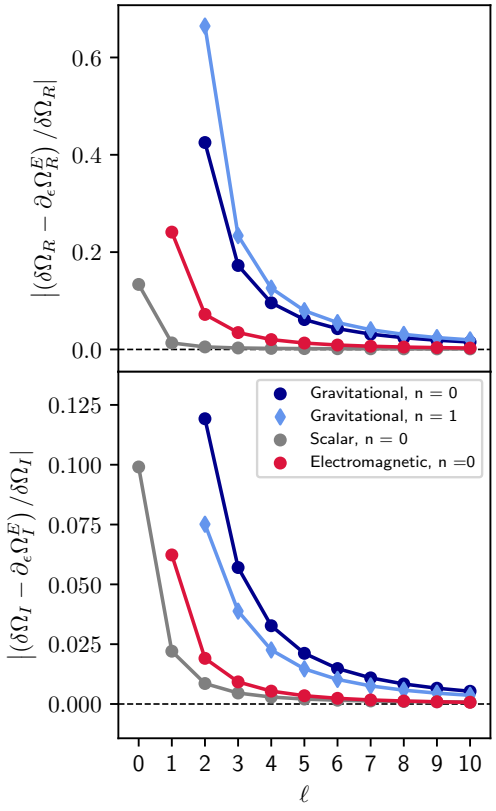

Figure 4.3: Relative error between the linear coefficients $\delta\Omega$ computed numerically with the Leaver method (upper panel) and those computed analytically with the eikonal approximation (lower panel). It can be observed that, as expected, the eikonal approximation becomes better as ℓ increases.

The first order correction can be obtained from a linear fit of the numerical results, and can also be estimated analytically in the eikonal limit from Eq. (4.40).

One can see from Fig. 4.3 that the agreement between the numerical $\delta\Omega$ and the one computed with Eq. (4.40) gets better and better as ℓ increases, exactly as expected.

On the other hand, for high enough values of $|M'|$, the imaginary part of the quasinormal frequencies can change sign due to the shift $2i\chi M'$, leading to the onset of an instability. The sign of the conformal weight χ determines whether this unstable regime can be developed in the increasing or decreasing mass case. Gravitational perturbations can grow unstable for $M' > 0$. Indeed, it is evident from Fig. 4.2 that the rescaled frequencies approach the limit of vanishing imaginary part for positive enough M'. On the other hand, scalar perturbations transform with conformal weight $\chi = -1$, and therefore they can become unstable for negative enough values of M'. Electromagnetic perturbations are instead always stable.

As previously stated, we are only interested in the range $|M'| < 1/16$ for the mass derivative. However, values of M' in this range can produce instabilities. In particular, the instability threshold for the fundamental $\ell = 2$ gravitational mode is $M'_{\rm Tr} \simeq 0.0420$, while for the fundamental $\ell = 0$ scalar mode is $M'_{\rm Tr} \simeq -0.0436$. The stability properties for different perturbations are summarized in Table 4.1.

4.4.4 Time-domain waveforms

In the following analysis we will just consider the small mass derivative case, in order to avoid possible instabilities. As already anticipated, in addition to including the shift in the imaginary part, in order to obtain the physical spectrum, we also have to account for the fact that the physical frequencies present an intrinsic time dependence determined by the

	$M' > 0$	$M' < 0$
Scalar	✗	✓
Electromagnetic	✗	✗
Gravitational axial	✓	✗

Table 4.1: Possibility of developing an instability for different kind of perturbations in the two cases in which the BH mass is increasing and decreasing. The symbol ✓ signals that the quasi-normal frequencies can have an instability for a large enough $|M'|$. On the other hand, the symbol ✗ indicates that this is never the case.

evolution of the mass.

The appearance of a time-depending factor in the physical frequencies can be seen from extracting the time evolution of the signal at $x \to x_C$. One has

$$\begin{aligned}\psi_{\rm CH}(T,x) &= \mathrm{e}^{-i\Omega T}(x-x_C)^{-i\Omega\eta x_C} = \mathrm{e}^{-i\Omega\int\frac{\mathrm{d}w}{2M(w)}}\mathrm{e}^{-i\Omega x_*(x_C)}(x-x_C)^{-i\Omega\eta x_C} \\ &= \mathrm{e}^{-i\Omega\int\frac{\mathrm{d}w}{2M(w)}}(x-x_C)^{-i\Omega x_C(\eta-\eta)} = \mathrm{e}^{-i\int\omega(w)\mathrm{d}w}\,,\end{aligned} \tag{4.55}$$

where in the last line we defined the w-dependent frequency $\omega(w)$. The same computation can be carried out close to the EH:

$$\begin{aligned}\psi_{\rm EH}(T,x) =& \mathrm{e}^{-i\Omega T}(x-x_H)^{-i\Omega\eta x_H} \\ &= \mathrm{e}^{-i\int\omega(w)\mathrm{d}w}(x-x_H)^{-2i\Omega\eta x_H} \\ &= \mathrm{e}^{-i\int\omega(w)\mathrm{d}w}\,\mathrm{e}^{2i\Omega\eta x_H\,\ln(2M(w))}(r-r_H)^{-2i\Omega\eta x_H} \\ &= \mathrm{e}^{-i(1-4\eta x_H M')\int\omega(w)\mathrm{d}w}(r-r_H)^{-2i\Omega\eta x_H}\,,\end{aligned} \tag{4.56}$$

where we used the relation

$$\int\frac{\mathrm{d}w}{2M(w)} = \frac{1}{2M'}\ln(2M(w))\,, \tag{4.57}$$

which is valid in the $M' = \text{const}$ case.

Note that if we introduce again the small parameter $\epsilon \ll 1$, the w-dependent frequency at the horizon gets an order ϵ overall correction with respect to the one measured at the outer horizon. In fact, one has

$$\eta\, x_H M'\epsilon = M'\epsilon + \mathcal{O}(\epsilon^2)\,. \tag{4.58}$$

To summarize, two separate effects modify the QNM frequencies as a consequence of the BH mass evolution. The first is a 'static' effect appearing already at the level of the rescaled coordinates, which displaces the QNMs with respect to the Schwarzschild positions on the complex plane. The second is the time-dependent scaling of the physical frequency with the mass:

$$\omega(w) = \frac{\Omega}{2M(w)}\,. \tag{4.59}$$

At this point, one can reconstruct the physical observable signal, which we show in Fig. 4.4.

Notice that the deviation from the static background signal is more evident in the increasing mass case, because the damping of the real part of the rescaled frequency in the complex plane adds up to the suppression of the physical frequency according to Eq. (4.59). On the other hand, the two effects are competing in the decreasing mass case, canceling out at the beginning, before the time-dependent enhancement starts prevailing.

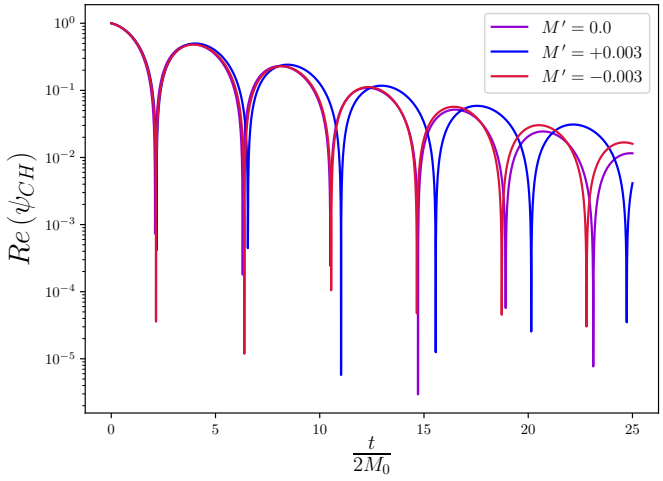

Figure 4.4: Signal evolution at the CH at leading order in ϵ, for different mass derivative values

4.5 Tidal response

In the first part of the work, we have discussed the QNM spectrum of a Vaidya BH, assuming that the BH mass evolves at a constant rate. Here, we study a different type of effect, namely the tidal deformability of the BH induced by an external perturbation.

In a relativistic context, the conservative tidal response of a compact object is parametrized in terms of a set of coefficients, which are often referred to as Love numbers. It is well known that, as opposed to neutron stars or other types of self-gravitating compact sources, asymptotically-flat BHs in GR have vanishing static Love numbers [312, 363, 366, 367]. In the following, we wish to study how this result gets modified for a BH with varying mass, in the particular case of the Vaidya geometry (4.1).

4.5.1 Love numbers

Our starting point is the master equation (4.32). We will work under the assumption that $|M'| = \text{const} \ll 1$: in other words, we will treat terms proportional to M' as small corrections to the Schwarzschild solution. To see how the Vaidya corrections affect the unperturbed Schwarzschild result, it will be enough to keep terms only up to linear order in M'. We will thus drop everywhere terms that are $\mathcal{O}(M'^2)$ or higher.

As opposed to the computation of the QNMs in Sec. 4.4, we are interested here in a different boundary-value problem. In particular, we want to understand how the BH responds when acted upon by an external static perturbation. We will thus start by setting $\tilde{\Omega}$ to zero in (4.32).[3] Note that, as opposed to the case of an asymptotically-flat Schwarzschild spacetime with $M' = 0$ [238, 312, 358, 366, 367], Eq. (4.32) has a different singularity structure. This results in a change in the form of the falloff of the solutions at the asymptotic boundary. In particular, at large values of x, $R(x)$ will not be a simple polynomial. In order to extract the response, we will thus first solve the equation in a region that is sufficiently far from the CH, where the standard x^ℓ and $x^{-\ell-1}$ falloffs hold. Then, we will perform a matching with the point-particle effective theory (see Sec. 4.5.2), where the response coefficients are defined in a way that is independent of the coordinates.

[3] In reality, one might want to set to zero the frequency Ω_* of the physical perturbation (see Eq. (4.52)). However, since $\tilde{\Omega}$ only enters quadratically in the master equation (4.32) and we are interested in the linear order in M', whichever frequency is set to zero among Ω_*, $\tilde{\Omega}$ or Ω is totally immaterial, as this will affect the result only at order $\mathcal{O}(M'^2)$.

Concretely, let us start by recalling the expression of the function $f(x)$, and of its derivative, appearing in Eq. (4.32):

$$\begin{aligned} f(x) &= 4\epsilon|M'|x_C\left(1-\frac{x_H}{x}\right)\left(1-\frac{x}{x_C}\right)\,, \\ f'(x) &= \frac{4\epsilon|M'|x_H x_C}{x^2}\left(1-\frac{x^2}{x_H\,x_C}\right)\,, \end{aligned} \tag{4.60}$$

where ϵ is again a book-keeping parameter to emphasize that we are taking $|M'|$ small. In order to neglect corrections from the singular point at x_C, we will focus on the region $x_H \leq x \ll \sqrt{x_H\,x_C} \ll x_C$. This defines a "near zone" where both terms x/x_C and $x^2/(x_H\,x_C)$ in (4.60) are small, and can thus be neglected.[4] Introducing the variable $z \equiv x/x_H$, in the near-zone approximation Eq. (4.32) then reduces to

$$4x_C x_H \epsilon|M'|\left[\left(1-\frac{1}{z}\right)R''(z)+\frac{1}{z^2}R'(z)\right]-\left[\frac{\ell(\ell+1)x_H}{z^2}+\frac{\sigma}{z^3}\right]R(z)=0\,. \tag{4.61}$$

Note that (4.61) recovers the usual master equation on Schwarzschild spacetime for $\epsilon \to 0$, as $z \to x$, $x_H \to 1$ and $4\epsilon|M'|x_C \to 1$. It is worth emphasizing that, even though x_C no longer appears as a singular point of (4.61), information about M' is still contained in x_H.

Eq. (4.61) can be recast in a more convenient form by employing the following change of variable and field redefinition:

$$\begin{aligned} z \to y &\equiv \frac{1}{z}\,, \\ R(y) \to p(y) &\equiv y^{-\lambda}R(y)\,, \end{aligned} \tag{4.62}$$

with

$$\lambda = \sqrt{\ell(\ell+1)\,x_H+\frac{1}{4}}-\frac{1}{2} = \ell + 4\,\frac{\ell(\ell+1)}{2\ell+1}\,|M'|\,\epsilon+\mathcal{O}(\epsilon^2)\,. \tag{4.63}$$

With this transformation, one recovers the canonical form of the hypergeometric equation [426, 427], i.e.,

$$y(1-y)p''(y)+[c-(a+b+1)y]p'(y)-ab\,p(y)=0\,, \tag{4.64}$$

with $a=\lambda+1-\sqrt{1-\sigma}$, $b=\lambda+1+\sqrt{1-\sigma}$ and $c=2\lambda+2$. This equation has two linearly independent solutions, which can be expressed as

$$\begin{aligned} p_1(y) &= {}_2F_1\left(a,b;c;y\right)\,, \\ p_2(y) &= y^{1-c}{}_2F_1\left(a-c+1,b-c+1;2-c;y\right)\,. \end{aligned} \tag{4.65}$$

Both p_1 and p_2 exhibit a logarithmic divergence at the horizon $z=1$. To obtain the physical solution that is regular at the BH horizon, we take the linear combination[5]

$$p(y)=\frac{\Gamma(2-c)}{\Gamma(a-c+1)\Gamma(b-c+1)}\,p_1(y)-\frac{\Gamma(a+b)}{\Gamma(a)\Gamma(b)}\,p_2(y). \tag{4.66}$$

[4] We stress that, despite the name, the near zone covers a wide region, and is not restricted to values of x close to x_H.

[5] Note that the master variables might not be directly observables. To impose the correct boundary condition at the horizon, one should require that physical observable quantities are regular at x_H. This can be done by looking for instance at scalar quantities constructed with the master variable solutions. See e.g. [238, 261].

Expanding for $z \gg 1$, one obtains

$$R(z) \sim z^{\lambda+1}\left[1 + k\, z^{-2\lambda+1}\right], \tag{4.67}$$

up to an overall constant which corresponds to the amplitude of the external probe tidal field. The relative coefficient k is

$$k = \frac{\Gamma(2-c)\Gamma(a)\Gamma(b)}{\Gamma(a-c+1)\Gamma(b-c+1)\Gamma(a+b)} = (a+b-1)\frac{\Gamma(a)^2\Gamma(b)^2}{\Gamma(a+b)^2}\frac{\sin(\pi a)\sin(\pi b)}{\pi\sin(\pi(a+b))}, \tag{4.68}$$

and is related to the tidal Love numbers of the BH, as we will see more explicitly below. Note that k vanishes for $M' = 0$, which is consistent with the result that Schwarzschild BHs have vanishing static tidal response.

Let us focus for a moment on the growing term in Eq. (4.67). Transforming back to physical coordinates, it reads

$$z^{\lambda+1} = \left(\frac{r}{2M_0}\right)^{\ell+1}\left(1 + \delta_{\rm tf}(w,r)\right), \tag{4.69}$$

where

$$\delta_{\rm tf}(w,r) \equiv -(\ell+1)\left[\left(4 + s\,\frac{w-w_0}{2M_0}\right) - \frac{4\ell}{2\ell+1}\,\ln\left(\frac{r}{2M_0}\right)\right]|M'|\,\epsilon + \mathcal{O}(\epsilon^2). \tag{4.70}$$

The function $\delta_{\rm tf}$ is a correction to the asymptotic profile of the tidal field induced by the adiabatic evolution of the BH. Note that $\delta_{\rm tf}$ is a sum of two terms, a piece that is linear in the null coordinate and a logarithmic term, which both vanish in the $|M'| \to 0$ limit.

Plugging the values of a and b for $\sigma = 1, 0, -3$ in (4.68), we obtain the response coefficients for the various spins, perturbatively in the mass derivative, i.e.,

$$k = k^{(0)} + k^{(1)}\epsilon + \dots, \tag{4.71}$$

where $k^{(0)} = 0$ [238, 312, 358, 363, 366, 367], and the leading-order corrections to the Schwarzschild result for different spins read

$$\begin{aligned}
k^{(1)}_{\rm scalar} &= \frac{\ell^3(\ell+1)}{2(2\ell+1)^2}\frac{\Gamma(\ell)^4}{\Gamma(2\ell)^2}\,|M'|\,,\\
k^{(1)}_{\rm e.m.} &= \frac{\ell(\ell+1)^3}{2(2\ell+1)^2}\frac{\Gamma(\ell)^4}{\Gamma(2\ell)^2}\,|M'|\,,\\
k^{(1)}_{\rm grav.\ axial} &= \frac{\ell(\ell+2)^2(\ell+1)^3}{2(2\ell+1)^2(\ell-1)^2}\frac{\Gamma(\ell)^4}{\Gamma(2\ell)^2}\,|M'|\,,
\end{aligned} \tag{4.72}$$

where we used the trigonometric identities and the property of the Euler's gamma function, $\Gamma(\ell+1) = \ell\,\Gamma(\ell)$.

Note that, at linear order in the mass derivative, the Love numbers are constant, while radial running and time evolution appear at quadratic order.

In summary, at large distances from the BH horizon, but still restricting to the near-zone regime defined above, the solution to the static equation for a perturbation of spin σ is

$$\begin{aligned}
R_\sigma(w,r) \sim \left(\frac{r}{2M_0}\right)^{\ell+1}\Bigg[&1 + \delta_{\rm tf}(w,r) + \mathcal{O}\left(\frac{2M_0}{r}\right)\\
&+ k_\sigma\left(\frac{r}{2M_0}\right)^{-(2\ell+1)}\left(1 + \mathcal{O}\left(\frac{2M_0}{r}\right)\right)\Bigg],
\end{aligned} \tag{4.73}$$

where k_σ can be read off from Eq. (4.72).

4.5.2 Point-particle EFT

In order to gain insight on the physical meaning of the coefficients k_σ computed above, we will now resort to the point-particle EFT [206, 428] (see [207, 429–431] for some reviews). The EFT has the advantage that it defines the induced response in a way that is coordinate independent and more directly related to observable quantities. We will thus introduce the Love numbers as coupling constants of operators localized on the point particle's worldline in the EFT, and compute them by matching with the full solution (4.73). Again, we will work perturbatively in M', i.e. we will treat the Vaidya solution as a small correction to the leading Schwarzschild geometry. We will discuss in detail the scalar-field case, and report the result for spin-1 and spin-2 Love numbers at the end.

Indicating with X^μ a generic set of spacetime coordinates, the point-particle EFT, including finite-size operators, has the following form:

$$S_{\rm EFT} = S_{\rm bulk} + S_{\rm scalar} + S_{\rm pp} + S_{\rm int}\,, \tag{4.74}$$

where $S_{\rm bulk}$ is the gravitational bulk action given by

$$S_{\rm bulk} = \frac{1}{16\pi}\int \mathrm{d}^4X\,\sqrt{-g}\,g^{\mu\nu}\left(R_{\mu\nu} - T_{\mu\nu}\right)\,, \tag{4.75}$$

including the Vaidya SET, $S_{\rm scalar}$ captures the scalar dynamics in the bulk geometry,

$$S_{\rm scalar} = -\frac{1}{2}\int \mathrm{d}^4X\,\sqrt{-g}\,g^{\mu\nu}\partial_\mu\Phi\partial_\nu\Phi\,, \tag{4.76}$$

$S_{\rm pp}$ describes the motion of the point particle, which to leading-order in the small-M' expansion is simply the worldline's Nambu–Goto action on flat space,

$$S_{\rm pp} = -M_0\int \mathrm{d}\tau\,, \tag{4.77}$$

where τ parametrizes the worldline, and $S_{\rm int}$ describes finite-size effects i.e., schematically,

$$S_{\rm int} = \int \mathrm{d}\tau\, e\sum_{\ell=1}^{\infty}\frac{\mu_\ell}{2\ell!}\left(P^{\nu_1}_{(\mu_1}\cdots P^{\nu_\ell}_{\mu_\ell)_T}\nabla_{\nu_1}\cdots\nabla_{\nu_\ell}\Phi\right)^2 \tag{4.78}$$

where P^ν_μ projects onto the point-particle rest frame, e is an einbein enforcing reparametrization invariance of the worldline, and $(\cdots)_T$ denotes the symmetrized traceless component of the enclosed indices (see Refs. [206, 238, 358, 428] for details). The couplings μ_ℓ in $S_{\rm int}$ represent the Love numbers, which we want to match with the k_σ coefficients derived above. Note that the EFT action (4.74) contains Vaidya corrections; however, as we shall see below, it will be enough for the matching to solve the equations to leading order, effectively setting M' to zero.

Let us start by expanding the scalar Φ as $\Phi = \Phi_{\rm tidal} + \Phi_{\rm resp}$, where $\Phi_{\rm tidal}$ represents the external tidal field, which solves the free bulk equation of motion $\Box\Phi_{\rm tidal} = 0$, while $\Phi_{\rm resp}$ encodes the response that we want to compute and which solves the inhomogeneous equation

$$\begin{aligned}\Box\Phi_{\rm resp} =&(-1)^{\ell+1}\frac{\mu_\ell}{\ell!}\nabla^{\rho_1}\cdots\nabla^{\rho_\ell}\Big(\delta^{(3)}_D\left(X - X(\tau)\right)\\ &\times P^{(\mu_1}_{\rho_1}\cdots P^{\mu_\ell)_T}_{\rho_\ell}P^{\nu_1}_{(\mu_1}\cdots P^{\nu_\ell}_{\mu_\ell)_T}\nabla_{\nu_1}\cdots\nabla_{\nu_\ell}\Phi_{\rm tidal}\Big).\end{aligned} \tag{4.79}$$

The idea is to solve (4.79) perturbatively in M'. Concretely, we shall expand each component in powers of ϵ as $\Phi_{\rm tidal} = \Phi^{(0)}_{\rm tidal} + \epsilon\Phi^{(1)}_{\rm tidal} + \ldots$, $\Phi_{\rm resp} = \Phi^{(0)}_{\rm resp} + \epsilon\Phi^{(1)}_{\rm resp} + \ldots$, and

similarly for the Love number couplings, $\mu_\ell = \mu_\ell^{(0)} + \epsilon\mu_\ell^{(1)} + \dots$, and the covariant derivatives. However, since we already know that the induced static response of Schwarzschild BHs is zero in GR [238, 312, 358, 363, 366, 367], we can set $\Phi^{(0)}_{\rm resp} = 0 = \mu_\ell^{(0)}$, and just focus on linear quantities in ϵ. The vanishing of $\mu_\ell^{(0)}$ implies that, at linear order in ϵ, we can replace $\Phi_{\rm tidal}$ on the right-hand side of (4.79) with $\Phi^{(0)}_{\rm tidal}$ and replace the covariant derivatives with simple derivatives in Minkowski space. The zeroth-order tidal field can be written, in cartesian coordinates, as

$$\Phi^{(0)}_{\rm tidal} = c_{a_1\dots a_\ell} X^{a_1}\dots X^{a_\ell}\,, \tag{4.80}$$

or, equivalently, in spherical harmonics as $C_\ell r^\ell Y_{\ell m}(\theta,\phi)$ with some overall ℓ-dependent amplitude coefficient [238]. Similarly, since $\Phi^{(0)}_{\rm resp} = 0$, on the left-hand side of (4.79), we can replace $\Phi_{\rm resp}$ with $\Phi^{(1)}_{\rm resp}$ and the covariant d'Alembert operator with the Laplace operator in flat space. All in all, the response field equation boils down to

$$\vec\nabla^2\Phi^{(1)}_{\rm resp} = J\,, \tag{4.81}$$

with the source term on the right-hand side given, in the rest frame of the point particle, by

$$J = \mu_\ell(-1)^{\ell+1}\, c^{a_1\dots a_\ell}\partial_{(a_1}\dots\partial_{a_\ell)_T}\delta^{(3)}_D(\vec X)\,. \tag{4.82}$$

Eq. (4.81) can be solved in Fourier space. From the Green's function of the Laplace operator in flat space, $G(\vec p) = -|\vec p|^{-2}$, one obtains [238]

$$\tilde\Phi^{(1)}_{\rm resp}(\vec p) = \mu_\ell(-i)^\ell\, c^{a_1\dots a_\ell}\frac{p_{(a_1}\dots p_{a_\ell)_T}}{|\vec p|^2}\,. \tag{4.83}$$

Finally, from the inverse Fourier transform,

$$\begin{aligned}\Phi^{(1)}_{\rm resp} &= \mu_\ell(-i)^\ell\int\frac{{\rm d}^3\vec p}{(2\pi)^3}\,{\rm e}^{i\vec p\cdot\vec X}c^{a_1\dots a_\ell}\frac{p_{(a_1}\dots p_{a_\ell)_T}}{|\vec p|^2}\\ &= \mu_\ell K\, c_{a_1\dots a_\ell}X^{a_1}\dots X^{a_\ell}\left(\frac{|\vec X|^2}{4}\right)^{-\frac12-\ell}\,,\end{aligned} \tag{4.84}$$

with the prefactor

$$K = \frac{(-1)^\ell}{2^{\ell+3}\sqrt{\pi}\,\Gamma\left(\frac12-\ell\right)}\,. \tag{4.85}$$

By comparing the EFT solution $\Phi^{(1)}_{\rm resp}$ with the full solution $\Phi = R(x)Y_{\ell m}(\theta,\phi)/x$ where $R(x)$ can be read off from (4.73), to linear order in ϵ, we can express the EFT Love number coefficients μ_ℓ in terms of $k^{(1)}_{\rm scalar}$ in (4.72). The result is

$$\mu_\ell^{(1)} = \frac{(-1)^\ell\sqrt{\pi}}{2^{\ell-2}}\Gamma\left(\frac12-\ell\right)(2M_0)^{2\ell+1}\;k^{(1)}_{\rm scalar}\,. \tag{4.86}$$

A similar procedure can be followed in the case of electromagnetic and gravitational axial perturbations. To describe electromagnetic response, one has to introduce in the bulk the electromagnetic action

$$S_{\rm em} = -\frac14\int{\rm d}^4x\,\sqrt{-g}F_{\mu\nu}F^{\mu\nu}\,. \tag{4.87}$$

The metric is expanded in perturbations as

$$g_{\mu\nu} = g^{(B)}_{\mu\nu} + h_{\mu\nu} + \dots \,, \tag{4.88}$$

where $g^{(B)}_{\mu\nu}$ is the Minkowski flat metric plus perturbative corrections in M'. The interacting part of the action can be constructed as

$$\begin{aligned} S_{\rm int} = \int \mathrm{d}\tau\, e \sum_\ell \Bigg[& \frac{\mu^E_\ell}{2\ell!} \left(P^{\nu_1}_{(\mu_1} \cdots P^{\nu_\ell}_{\mu_\ell)_T} \nabla_{\nu_1} \cdots \nabla_{\nu_{\ell-1}} E_{\nu_\ell} \right)^2 \\ & + \frac{\mu^B_\ell}{4\ell!} \left(P^{\nu_1}_{(\mu_1} \cdots P^{\nu_\ell}_{\mu_\ell)_T} P^\beta_\alpha \nabla_{\nu_1} \cdots \nabla_{\nu_{\ell-1}} B_{\nu_\ell \beta} \right)^2 \\ & + \frac{\mu^{C_B}_\ell}{4\ell!} \left(P^{\nu_1}_{(\mu_1} \cdots P^{\nu_\ell}_{\mu_\ell)_T} P^\beta_\alpha \nabla_{\nu_1} \cdots \nabla_{\nu_{\ell-2}} B^{(2)}_{\nu_{\ell-1}\nu_\ell|\beta} \right)^2 \Bigg] , \end{aligned} \tag{4.89}$$

where the sum over ℓ starts from $\ell = 1$ for the first two terms and from $\ell = 2$ for the last one. The objects E_μ, $B_{\mu\nu}$ e $B^{(2)}_{\mu\nu\beta}$ are related to the electric and magnetic fields, and the magnetic part of the Weyl tensor, respectively. In the rest frame of the point particle, their only nonzero components, at leading order in the flat-space limit, are

$$\begin{aligned} E_i &= -\partial_i A_t \,, \\ B_{ij} &= \partial_i A_j - \partial_j A_i \,, \\ B^{(2)}_{ij|k} &= C_{0ijk} \,, \end{aligned} \tag{4.90}$$

where A_μ is the electromagnetic potential and $C_{\mu\nu\alpha\beta}$ is the Weyl tensor. This is all that we will need on the EFT side.

As already discussed for the scalar case, one can split the field A_μ and $h_{\mu\nu}$ in a tidal part and a response part, and then expand both to linear order in ϵ. Since the zeroth-order response is vanishing, one obtains an inhomogeneous equation for the linear correction in the form (4.81), with a source term involving derivative computed on a flat background. The relevant equations for linear electromagnetic and gravitational response can be found in [238, 377]. To perform the matching, we shall use the t-component of the four-potential, the angular components of B_{ij} and the components C_{trij} of the Weyl tensor. The latter can be directly related to the Regge–Wheeler master variable ψ defined as auxiliary field in Appendix B.1.3 in the static limit.

The result of the matching is:

$$\begin{aligned} \mu^{E,(1)}_\ell &= \frac{(-1)^{\ell+1}\ell\sqrt{\pi}}{2^{\ell-1}(\ell+1)} \Gamma\left(\frac{1}{2} - \ell\right) (2M_0)^{2\ell+1}\, k^{(1)}_{\rm e.m.} \,, \\ \mu^{B,(1)}_\ell &= \frac{(-1)^{\ell}\ell\sqrt{\pi}}{2^{\ell-1}(\ell+1)} \Gamma\left(\frac{1}{2} - \ell\right) (2M_0)^{2\ell+1}\, k^{(1)}_{\rm e.m.} \,, \\ \mu^{C_B,(1)}_\ell &= \frac{(-1)^{\ell+1}\ell(\ell-1)}{\sqrt{\pi}(\ell+1)(\ell+2)2^{\ell+1}} \Gamma\left(\frac{1}{2} - \ell\right) (2M_0)^{2\ell+1}\, k^{(1)}_{\rm grav} \,. \end{aligned} \tag{4.91}$$

The relations in Eq.(4.85) and Eq.(4.91) are analogous to the ones that hold for the Schwarzschild BH. However, this computation demonstrates the robustness of the result of the previous section, namely that the Vaidya BH, unlike Schwarzschild, exhibits a nontrivial tidal response, quantified by the Love numbers presented in Eqs (4.72).

4.6 Conclusions

In this work, we studied perturbations of Vaidya BHs. In the first part, we revisited the computation of the QNMs. Unlike previous works in the same context [391, 407–411], our analysis was carried out in the frequency domain, under the assumption of a constant rate of change M' of the BH mass.

In this framework, we computed the QNM spectrum both analytically in the eikonal approximation, and with a numerical approach based on Leaver's continued-fraction method. One main advantage of our approach is that, with respect to previous results in the literature, it allowed us to compute the frequencies with higher accuracy. In addition, it provides a more transparent understanding of the physical effects associated with the dynamical BH mass, including the stability properties of the solution.

On the other hand, the fact that the (null) time evolution of the physical frequencies inversely tracks the dynamical BH mass, which was found numerically in [408], is naturally recovered in our formalism, through the scaling of the physical frequencies $\omega \propto M(w)^{-1}$, as discussed in Sec. 4.4.4.

In the second part, we studied tidal effects on Vaidya BHs. As opposed to the QNM analysis, we worked here under the assumption that M' is small (in addition to being constant), and we computed explicitly the tidal Love numbers to linear order in M'. Our result shows that dynamical effects due to a time-dependent mass of the Vaidya BH induce non-vanishing tidal response. This should be contrasted with the case of Schwarzschild BHs, whose Love numbers are exactly zero in GR.

Chapter 5

Parametrized deviations from GR

5.1 Introduction

The procedure known as BH spectroscopy, *i.e.*, the identification of the different QNMs of which the signal is composed in the ringdown [432–434], has been applied to tens of events [103, 435, 436]. The detection of two modes simultaneously, despite being controversial for the first three observing runs [278, 280, 437–443], is expected to be effective for the current O4a run and future ones.

Detecting a second mode is a crucial ingredient for tests of GR. As already discussed in the previous chapters, due to no-hair theorems, the QNM spectrum of a Kerr BH depends uniquely on its mass and spin. If only one mode is detected, this can always be fitted to a QNM frequency of a Kerr BH with a certain mass and angular momentum. However, the measurement of any additional modes provides a consistency test of the Kerr QNM spectrum and hence would allow us to spot deviations from GR. This clear identification of possible beyond-GR effects makes BH spectroscopy one of the most promising ways to test GR.

Currently, ringdown tests employ blind deviations from GR in the frequencies [436], or agnostic deviations constructed assuming small-coupling and slow-spin parametrization [444–446]. On the other hand, theory-specific tests are limited to a handful of cases [447]. This is because the computation of QNMs for rotating solutions beyond-GR is incomplete. The main difficulties arise from: absence of analytic background solution, non-separability of the perturbation equations, additional fields coupled to the metric, different boundary conditions [434]. It turns out that for a vast class of theories, the first problem can be solved performing a double simultaneous expansion in the spin and in the coupling constant of the theory [81, 448–451]. Then, one can choose whether to study perturbations giving priority to slow-spin or small coupling. The former has the advantage of being possible for metric perturbations, for which couplings between different fields are tractable, at the cost of not being able to predict precisely QNMs at high spins (which are relevant for astrophysical purposes) [452–458].

On the other hand, by assuming small-coupling for the perturbations, one can work out a modified Teukolsky equation, which is, in principle, reliable at any spin [88, 356, 459]. The disadvantage comes from the construction itself of the Teukolsky equation, which is based on curvature perturbations, and once one has some perturbations of perturbations, as in the case outlined here, metric reconstruction becomes necessary. This feature strongly hinders one from going beyond the first order in the coupling expansion.

The necessity of having reliable QNMs at high spins and the fact that observations seem to narrow down the size of deviations from GR, make the modified Teukolsky framework

preferable for the study of QNMs beyond GR. The scope of this chapter is to develop a general formalism for the quick computation of QNMs in theories which have a perturbative departure from GR. The framework is based on an assumption similar to one developed in spherical symmetry [460–463]. The advantage of this formalism is that it can be used also for the inverse problem, *i.e.*, if a modification to GR is detected, one wants to be able to reconstruct the potential, the metric, or even the action from which the deviation originated from [462, 464, 465]. In general, this framework opens the path to the development of a theory-informed description of QNM agnostic deviations.

The structure of the chapter is as follows: we first introduce the modified Teukolsky equation and the formalism in section 5.2; then we show how to numerically compute the coefficients with the continued fraction method and their regime of validity in section 5.3; the formalism has already a few notable applications, which we use as a check for our computations in section 5.4; finally, we outline our conclusions in section 5.5. We assume that the background, unmodified metric is a Kerr BH of mass $M = 1/2$ and spin a. It is worth noting that due to the choice of units, the spin parameter a ranges between 0 and 1/2.

5.2 Parametrized formalism

5.2.1 The linear coefficients

Let us start from the radial and angular Teukolsky equation for a spin s field, given respectively by Eq. (3.99) and Eq. (3.104). We now assume that for a modified theory of gravity whose modifications are small with respect to GR the equation governing radial perturbations is the Teukolsky radial equation plus a correction to the potential linear in the coupling constants

$$\frac{1}{\Delta^s R(r)} \frac{\mathrm{d}}{\mathrm{d}r}\left[\Delta^{s+1} R'(r)\right] + V(r) + \Delta V(r) = 0\,, \tag{5.1}$$

and we assume that the modification is expanded in powers of r

$$\Delta V(r) = \frac{1}{\Delta} \sum_{k=-K}^{4} \alpha^{(k)} \left(\frac{r}{r_+}\right)^k\,, \tag{5.2}$$

where K is the most negative coefficient of the power series and $\alpha^{(k)}$ are dimensionful coefficients we assume to be small. This assumption is justified by the recent developments in obtaining modified Teukolsky equations by assuming small coupling corrections to GR [88, 356, 459].

On the other hand, we can also assume that the angular equation remains unchanged. This is due to the fact that the spheroidal harmonics are a complete basis of the 2-sphere angular variables, and it can be shown that if one forces an angular expansion of the Weyl scalars in spin-weighted spheroidal harmonics, all the mixing terms would enter at second order in the coupling constants [88, 466]. Nevertheless, a modification on the QNM frequencies will induce a modification to the separation constant $B_{\ell m}$, hence, we also need to include equation (3.104) in our analysis.

If we assume the couplings to be small [1], we are allowed to perform a Taylor expansion

[1] We will provide a more quantitative comment about this assumption in Sec. 5.3.4. For now just consider these adimensional parameters to be small enough to allow a linearization of the eigenvalues $\omega_{n\ell m}$ and $B_{\ell m}$.

of QNMs and separation constants around their GR values [460, 461]. Hence, we can write

$$\begin{aligned} \omega_{n\ell m} &\simeq \omega^0_{n\ell m} + \sum_k d^{(k)}_{\omega,n\ell m}\alpha^{(k)}\,, \\ B_{\ell m}(a\omega) &\simeq B^0_{\ell m}(a\omega) + \sum_k d^{(k)}_{B,\ell m}\alpha^{(k)}\,. \end{aligned} \tag{5.3}$$

In the following steps, we omit the indices s, n, ℓ, m, a, ω for clarity. The linear coefficients d_ω and d_B can be identified as the derivatives of ω and B with respect to the single coupling α. To compute them, we perform the following steps. In the GR limit, one finds ω and $B_{\ell m}$ as simultaneous roots of two functions constructed from the radial and the angular equation

$$\mathcal{L}_r\left[\omega, B_{\ell m}\right] = 0\,, \qquad \mathcal{L}_\theta\left[\omega, B_{\ell m}\right] = 0\,. \tag{5.4}$$

The exact form of these functions depends on the chosen numerical method. For non-zero modifications, we can perform a Taylor expansion of the two functions around $\alpha = 0$

$$\mathcal{L}_j\big|_{\rm GR} + \alpha \left.\frac{\mathrm{d}\mathcal{L}_j}{\mathrm{d}\alpha}\right|_{\rm GR} + \mathcal{O}(\alpha)^2 = 0\,, \tag{5.5}$$

where $j = [r, \theta]$ and we evaluate the derivative around their GR value $\omega = \omega^0$, $B = B^0$, $\alpha = 0$. By requiring that equations (5.5) is satisfied at each order in α, and expanding the derivative by chain rule, we obtain

$$\begin{aligned} \left.\frac{\partial\mathcal{L}_r}{\partial\alpha} + \frac{\partial\mathcal{L}_r}{\partial\omega}\,d_\omega + \frac{\partial\mathcal{L}_r}{\partial B}\,d_B\right|_{\rm GR} &= 0\,, \\ \left.\frac{\partial\mathcal{L}_\theta}{\partial\omega}\,d_\omega + \frac{\partial\mathcal{L}_\theta}{\partial B}\,d_B\right|_{\rm GR} &= 0\,, \end{aligned} \tag{5.6}$$

where we identified d_ω and d_B from their definition in equation (5.3). By solving the conditions above for d_ω and d_B, we get

$$\begin{aligned} d_\omega &= -\frac{\partial\mathcal{L}_r}{\partial\alpha}\frac{\partial\mathcal{L}_\theta}{\partial B}\left(\frac{\partial\mathcal{L}_r}{\partial\omega}\frac{\partial\mathcal{L}_\theta}{\partial B} - \frac{\partial\mathcal{L}_r}{\partial B}\frac{\partial\mathcal{L}_\theta}{\partial\omega}\right)^{-1}\Bigg|_{\rm GR}\,, \\ d_B &= \frac{\partial\mathcal{L}_r}{\partial\alpha}\frac{\partial\mathcal{L}_\theta}{\partial\omega}\left(\frac{\partial\mathcal{L}_r}{\partial\omega}\frac{\partial\mathcal{L}_\theta}{\partial B} - \frac{\partial\mathcal{L}_r}{\partial B}\frac{\partial\mathcal{L}_\theta}{\partial\omega}\right)^{-1}\Bigg|_{\rm GR}\,. \end{aligned} \tag{5.7}$$

In section 5.3 we show how to numerically define the functions $\mathcal{L}_j$ with Leaver's continued fraction method.

5.2.2 Maximum number of independent coefficients

In reference [467], Kimura realised that in the case of spherically symmetric perturbations, there is always an ambiguity in defining the modified potential, upon a free reparametrization of the field. The same reasoning can be applied to the Teukolsky equation as well. If we perform the following transformation in equation (5.1)

$$R(r) \to \left[1 + \varepsilon X(r)\right] R(r) + \varepsilon\Delta Y(r) R'(r)\,, \tag{5.8}$$

assuming that $\varepsilon \ll 1$, then the equation that $R(r)$ solves is

$$\frac{1}{\Delta^s R}\frac{\mathrm{d}}{\mathrm{d}r}\left[\Delta^{s+1}R'\right] + V + \Delta V + \Delta\overline{V} + \Delta W\frac{R'}{R} = 0\,. \tag{5.9}$$

By imposing $\Delta W = 0$ we uniquely obtain the free function $X(r)$ as

$$X(r) = c + \frac{s}{2}\Delta' Y - \frac{1}{2}\Delta Y' \,, \tag{5.10}$$

which yields the "ambiguous" potential in the form

$$\begin{aligned}\Delta\overline{V} = \varepsilon\Delta\Bigg[Y'\left(\frac{\left(s^2-1\right)\left(\Delta'\right)^2}{2\Delta} + 2s - 2V - 1\right) \\ + Y\left(\frac{s(s+1)\Delta'}{\Delta} - V' - \frac{V\Delta'}{\Delta}\right) - \frac{1}{2}\Delta Y^{(3)} - \frac{3\Delta' Y''}{2}\Bigg] \,.\end{aligned} \tag{5.11}$$

Now, upon suitable choice of the function Y, we can express $\Delta\overline{V}$ in the r basis. It turns out that the ansatz $Y = Y_j = y_j(r_+/r)^j$ yields

$$\Delta\overline{V} = \frac{\varepsilon y_j}{\Delta}\sum_{k=-3}^{5} r_+^k \overline{A}_j^{(k)} \left(\frac{r}{r_+}\right)^{k-j} \,, \tag{5.12}$$

which implies that $j \geq 1$ since the maximum power of r in V is r^4, and the full expression of $\overline{A}_j^{(k)}$ can be found in appendix B.3. In general, one can take a linear combination of the free functions Y_j and still get a potential that is equivalent to the starting one. Each term of this linear combination contains the free parameter y_j, which can be used to set to 0 one of the terms $\alpha^{(k)}$ in equation (5.2). This reasoning allows us to fix the negative limit in the power expansion to be $K = 3$.

It is possible that by choosing a different ansatz for Y one could further reduce the number of coefficients in the equation. In fact, for the case of study of HDG that we treat in another publication [468] the number of independent coefficients reduces to four (being $k = [-2, 0, 1, 2]$) — see also [87]. Although we could not prove this is a general feature of arbitrary modifications of the Teukolsky equation, we suspect that it was possible in that case thanks to the expansion in the spin assumed for every coefficient. Indeed, we believe that the ansatz for Y that would reduce the potential to the lowest number of terms would be, perhaps, a rational function involving powers of a and r. To date, we could not find such reduction.

5.3 Computation of the coefficients: the continued fraction method

5.3.1 Continued fractions for the Teukolsky equation

We start here by recalling the Leaver method to compute the frequencies and the separation constant for a Kerr spacetime. The first step to find a continued fraction expansion is to assume an ansatz for the wavefunctions. Let us start from the radial equation, where we assume the following ansatz [286]

$$R(r) = f^{-\mathrm{i}\sigma-s}(r-r_-)^{p-1-2s}\mathrm{e}^{qr}\sum_{n=0}^{N} R_n f^n \,, \tag{5.13}$$

where $r_\pm$ are the zeros of Δ,

$$f = \frac{r-r_+}{r-r_-} \,, \tag{5.14}$$

and we defined $p = q = \mathrm{i}\omega$ and

$$\sigma = \sigma_{\rm GR} \equiv \frac{r_+(\omega - \omega_c)}{r_+ - r_-}\,, \qquad \omega_c = \frac{am}{r_+}\,, \tag{5.15}$$

$$r_\pm = \frac{1}{2}(1 \pm \beta)\,, \qquad \beta = \sqrt{1 - 4a^2}\,. \tag{5.16}$$

With these definitions, the equation (3.99) takes the form

$$\sum_{n=0}^{N} R_n \left(\frac{\alpha^r_{n-1}}{f} + \beta^r_n + \gamma^r_{n+1} f \right) f^n = 0\,, \tag{5.17}$$

where the coefficients are

$$\begin{aligned}
\alpha^r_n =& (n+1)\,(n+1-s-2\mathrm{i}\sigma) && (5.18)\\
\beta^r_n =& 2n(2\mathrm{i}\sigma + p + q\beta - 1) - 2n^2 - 1 - s - B_{\ell m} \\
&+ q\left(a^2 q + \beta + s\right) - 2i\sigma(p + \beta q + i\omega - 1) \\
&- p(\beta q + q + s - 1) && (5.19)\\
\gamma^r_n =& \,(n - p - \mathrm{i}\omega)\,(n + s - p - 2\mathrm{i}\sigma + \mathrm{i}\omega)\,. && (5.20)
\end{aligned}$$

The equation is satisfied when each term proportional to a power of f vanishes

$$\beta^r_0 R_0 + \alpha^r_0 R_1 = 0\,, \tag{5.21}$$

$$\gamma^r_n R_{n-1} + \beta^r_n R_n + \alpha^r_n R_{n+1} = 0 \quad \text{for } n \geq 1\,. \tag{5.22}$$

The path for the angular equation is similar. We define an ansatz to be finite at the regular singular points $y = \pm 1$ [286]

$$S(y) = (1+y)^{k_1}(1-y)^{k_2}\mathrm{e}^{a\omega y}\sum_{n=0}^{N} S_n (1+y)^n\,, \tag{5.23}$$

where $k_1 = |m-s|/2$ and $k_2 = |m+s|/2$. We can obtain a similar recurrence relation by inserting this ansatz into equation (3.104), which, with an analogous reshuffling, reads

$$\beta^\theta_0 S_0 + \alpha^\theta_0 S_1 = 0\,, \tag{5.24}$$

$$\gamma^\theta_n S_{n-1} + \beta^\theta_n S_n + \alpha^\theta_n S_{n+1} = 0 \quad \text{for } n \geq 1\,, \tag{5.25}$$

where the coefficients are

$$\begin{aligned}
\alpha^\theta_n =& -2(n+1)\,(n+1+2k_1)\,, && (5.26)\\
\beta^\theta_n =& \, n(n-1) + 2n(k_1 + k_2 + 1 - 2a\omega) \\
&- 2a\omega(2k_1 + s + 1) + (k_1 + k_2)(k_1 + k_2 + 1) \\
&- a^2\omega^2 - s(s+1) - B_{\ell m}\,, && (5.27)\\
\gamma^\theta_n =& \, 2a\omega(n + k_1 + k_2 + s)\,. && (5.28)
\end{aligned}$$

To invert the relation we can define the ladder operators which have the following property $R_{n+1} = -\lambda^r_n R_n$ and $S_{n+1} = -\lambda^\theta_n S_n$ as (the superscript r/θ is omitted for clarity)

$$\lambda_n = \frac{\gamma_{n+1}}{\beta_{n+1} - \alpha_{n+1}\lambda_{n+1}}\,. \tag{5.29}$$

By initializing λ_N according to the Nollert expansion (explained in detail in appendix B.4), the equations one needs to solve simultaneously to obtain the eigenfrequency ω and the separation constant $B_{\ell m}$ are

$$\mathcal{L}_r = \lambda_1^r \alpha_0^r - \beta_0^r = 0\,, \tag{5.30}$$

$$\mathcal{L}_\theta = \lambda_1^\theta \alpha_0^\theta - \beta_0^\theta = 0\,, \tag{5.31}$$

which are nothing but (5.21) and (5.24).

5.3.2 Continued fraction beyond Teukolsky

We now turn our attention to the modified Teukolsky equation. It is always possible to bring equation (5.2) into the following form[2]

$$\begin{aligned}\Delta V(r) = \frac{A^{(0)}}{\Delta} + \frac{A^{(1)}}{r_+(r-r_-)} + \frac{1}{r_+^2}\sum_{k=0}^{2}\widetilde{\alpha}^{(k)}\left(\frac{r}{r_+}\right)^k \\ + \frac{1}{\Delta}\sum_{k=1}^{K}\alpha^{(-k)}\left(\frac{r_+}{r}\right)^k\,,\end{aligned} \tag{5.32}$$

where $A^{(0)}$, $A^{(1)}$ and $\widetilde{\alpha}^{(k)}$ are constants that can be obtained from the constants $\alpha^{(k)}$ appearing in equation (5.2), as explained in appendix B.6. First of all, we notice that the terms multiplied by $1/\Delta$ modify the behaviour of the equation at the horizon. In order to take into account of these additional terms, we need to modify the definition of the exponent σ appearing in the ansatz (5.13). By requesting that the solution is regular at the horizon, we must replace the value of σ into

$$\sigma = \frac{\mathrm{i}s}{2} + \sqrt{\left(\sigma_{\mathrm{GR}} - \frac{\mathrm{i}s}{2}\right)^2 + \frac{1}{\beta^2}\sum_{k=-K}^{4}\alpha^{(k)}}\,, \tag{5.33}$$

where we took the positive sign of the square root in order to obtain the correct GR limit. See Appendix B.5 for the derivation of the proper boundary conditions for the beyond-Teukolsky case.

On the other hand, the terms $\widetilde{\alpha}^{(1)}$ and $\widetilde{\alpha}^{(2)}$ modify the behaviour at infinity of the equation. This leads to a modification of the values of p and q into

$$q = \pm\sqrt{-\frac{\widetilde{\alpha}^{(2)}}{r_+^4} - \omega^2}\,, \tag{5.34}$$

$$p = -\frac{r_+\widetilde{\alpha}^{(1)} + \widetilde{\alpha}^{(2)} - 2r_+^4\left(qs - \mathrm{i}s\omega - \omega^2\right)}{2qr_+^4}\,, \tag{5.35}$$

where the sign of q is chosen such that $\mathrm{Re}(q) > 0$. This asymptotic behaviour is the reason why we truncate the series in equation (5.2) at $k = 4$. By repeating the steps done for the GR case, we obtain a modified version of equation (5.17)

$$\begin{aligned}\sum_{n=0}^{N} R_n \Bigg[\frac{\alpha_{n-1}^{\mathrm{bg}}}{f} + \beta_n^{\mathrm{bg}} + \gamma_{n+1}^{\mathrm{bg}} f \\ + \frac{1}{\beta^2}\frac{(1-f)^2}{f}\sum_{k=1}^{K}\alpha^{(-k)}\left(\frac{1-f}{1-\eta f}\right)^k\Bigg] f^n = 0\,,\end{aligned} \tag{5.36}$$

[2] In section 5.2.2 we showed that $K = 3$, but the following analysis works, in principle, for any value of K, hence we keep it unspecified.

where $\eta = r_-/r_+$ and

$$\alpha_n^{\rm bg} = \alpha_n^r - \frac{1}{\beta^2}\sum_{k=1}^{K}\alpha^{(-k)}\,, \tag{5.37}$$

$$\begin{aligned}\beta_n^{\rm bg} =& \beta_n^r - 2\left(\sigma_{\rm GR}-\sigma\right)\left(\sigma_{\rm GR}+\sigma-\omega\right)\,,\\ &- 2\frac{A^{(0)}}{\beta^2} + \frac{A^{(1)}}{r_+\beta} + \frac{\widetilde{\alpha}^{(0)}}{r_+^2}\end{aligned} \tag{5.38}$$

$$\begin{aligned}\gamma_n^{\rm bg} =& \gamma_n^r + 2{\rm i}\left(\sigma_{\rm GR}-\sigma\right)\left(s+{\rm i}\omega\right)\\ &- \frac{1}{\beta^2}\sum_{k=1}^{K}\alpha^{(-k)} - \frac{A^{(1)}}{r_+\beta}\,,\end{aligned} \tag{5.39}$$

and we used the fact that

$$\Delta = \beta^2\frac{f}{(1-f)^2}\,, \qquad r - r_- = \frac{\beta}{1-f}\,. \tag{5.40}$$

If we fix a single modification k, we can get rid of the rational behaviour in f by multiplying the equation by $(1-\eta f)^k$, obtaining the following expression

$$\begin{aligned}\sum_{n=0}^{N} R_n\Bigg[&\left(\frac{\alpha_{n-1}^{\rm bg}}{f} + \beta_n^{\rm bg} + \gamma_{n+1}^{\rm bg} f\right)(1-\eta f)^k\\ &+ \frac{\alpha^{(-k)}}{\beta^2}\frac{(1-f)^{k+2}}{f}\Bigg] f^n = 0\,.\end{aligned} \tag{5.41}$$

We can figure out the coefficient relation (equivalent to that of equation (5.22)), which at a given n takes the form

$$\sum_{j=-1}^{k+1}\left(\widetilde{\gamma}_{n,j-1} + \widetilde{\beta}_{n,j} + \widetilde{\alpha}_{n,j+1}\right) R_{n-j} = 0\,. \tag{5.42}$$

The coefficients appearing in the relation are given by

$$\widetilde{\alpha}_{n,j} = (-\eta)^j\binom{k}{j}\alpha_{n-j}^{\rm bg} + (-1)^j\binom{k+2}{j}\frac{\alpha^{(-k)}}{\beta^2}\,, \tag{5.43}$$

$$\widetilde{\beta}_{n,j} = (-\eta)^j\binom{k}{j}\beta_{n-j}^{\rm bg}\,, \tag{5.44}$$

$$\widetilde{\gamma}_{n,j} = (-\eta)^j\binom{k}{j}\gamma_{n-j}^{\rm bg}\,. \tag{5.45}$$

We notice that, from the definition of the binomial, $\widetilde{\alpha}_{n,j}$ is non-vanishing for $0 \le j \le k+2$, while $\widetilde{\beta}_{n,j}$ and $\widetilde{\gamma}_{n,j}$ are non-zero for $0 \le j \le k$. Now that we have a $k+3$ terms relation, we can perform a Gaussian elimination to reduce it to a three-terms relation (details can be found in the appendix of [462]). Once the three-terms relation is found, one can re-initialize the ladder operator λ_n^r and obtain the modified frequency and separation constant from equations (5.30)–(5.31).

5.3.3 Numerical computation of the coefficients

In the previous two sections we explained how to obtain the functions $\mathcal{L}_r(\omega, B, \alpha)$ and $\mathcal{L}_\theta(\omega, B)$. To compute the coefficients d_ω and d_B as given in equation (5.7), we evaluate the derivatives numerically with a 4-points centered stencil. For each pair of coefficients, we initialize the ladder operators λ_N to some arbitrary low integer N, and then increase it by one until the simultaneous relative change in d_ω and d_B is smaller than a given tolerance (which we chose to be 10^{-7}). We computed numerically all the coefficients for the following values $s = -2$, $n = [0, 2]$, $\ell = [2, 4]$, $m = [-\ell, \ell]$, $k = [-3, 4]$ in a uniform grid in $a = [0, 0.495]$ with spacing $\Delta a = 0.005$. The full list of coefficients is available in a public git folder [469].

In figure 5.1 we show the results from this computation for the real and imaginary parts of the $d_\omega^{(k)}$ coefficients for $s = -2$, $n = 0$, $\ell = 2$, $m = [-2, 2]$ for values of $k = [-3, 4]$ and of the spin a comprised between 0 and 0.45, as well as the real and the imaginary part of $d_B^{(k)}$ for the same n, ℓ, m and $k = [-1, 2]$.

To directly apply our formalism to further studies, e.g., ringdown analysis of nonlinear computations or data analysis, we also provide a `python` code and a `jupyter notebook` with some examples [469]. It allows one to compute the QNMs and the separation constants as function of n, ℓ, m, a and $\alpha^{(k)}$ and can thus, in principle, be efficiently integrated in commonly used code infrastructure. The code also allows one to access some of the earlier results for the parametrized QNM framework for modifications to the Regge-Wheeler and Zerilli potentials, for which coefficients beyond the fundamental mode have been computed in reference [462]. The GR values for the QNMs have been taken from reference [433, 470]. For more details about how the code is structured and how it can be used, we refer to the provided tutorial.

In principle, one should be able to compare the coefficients for $a = 0$ with those computed in [460, 462]. However, we stress that for $a = 0$, equation (5.1) reduces to the non-spinning limit of the Bardeen-Press equation [471], whereas the formalism of [460, 462] was developed for the Regge-Wheeler and the Zerilli equation. The transformation between the Bardeen-Press potential and the Regge-Wheeler/Zerilli potentials was obtained by Chandrasekhar [321], but generalizing this to the case of the modified potential with generic $\alpha^{(k)}$ couplings is non-trivial.

5.3.4 Linearized regime of validity

The framework we developed is motivated by the assumption that any modification of gravity produces only slight deviations from GR in astrophysical observables. In this section, we expand on the regime of validity of the formalism, by providing a quantitative assessment of the accuracy of such approach. It is worth noting that we can only asses the error made by restricting to linear corrections to the frequencies, as defined in equation (5.3) and not taking into account higher-order corrections to the potential, which are beyond the scope of this work.

First of all, we give a heuristic motivation on the maximum size of the coefficients, by requesting that the perturbation equation is not strongly modified at the boundaries of our dominion and that $\omega \simeq \mathcal{O}(1)$. At $r \to \infty$, we have seen from equations (5.34) and (5.35) that the only coefficients modifying the asymptotic structure of the potential are $\alpha^{(3)}$ and $\alpha^{(4)}$. With some simple algebra, we can infer

$$\alpha^{(3)} \lesssim 1\,, \qquad \alpha^{(4)} \lesssim 1\,. \tag{5.46}$$

On the other hand, the modifications in the potential affect the near-horizon expansion as

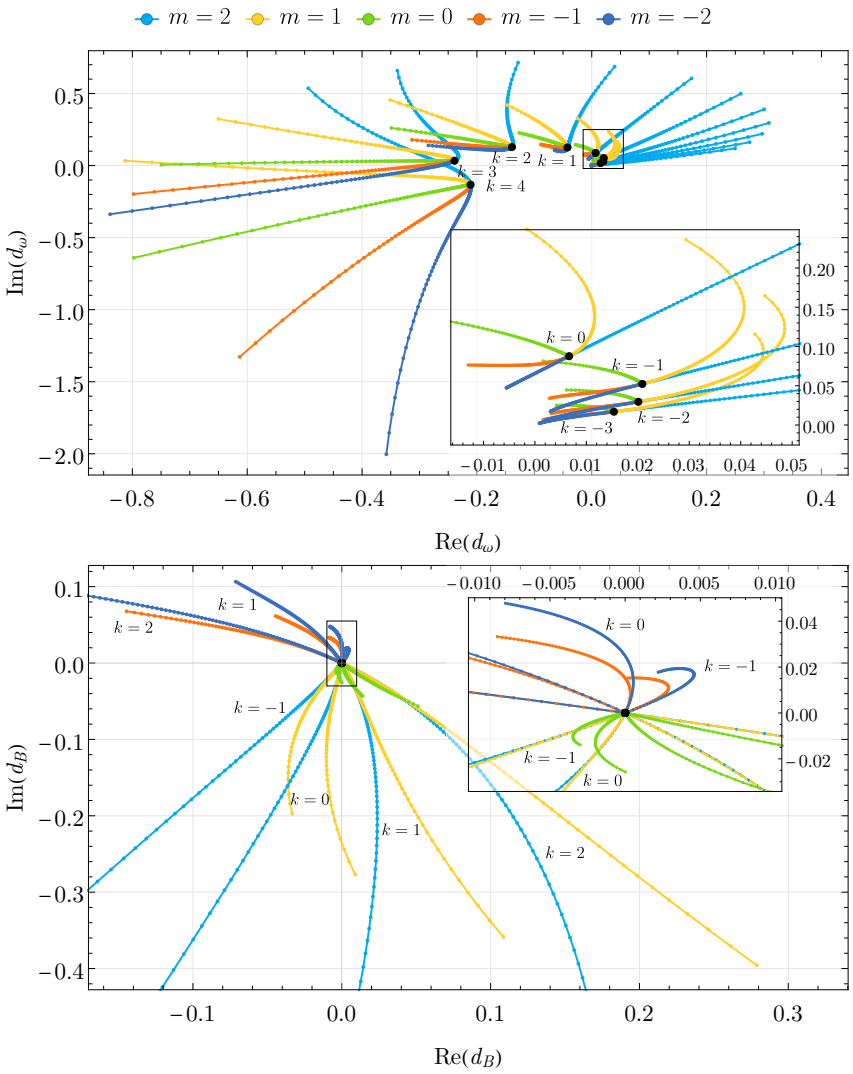

Figure 5.1: In the top panel we show the real and the imaginary part of d_ω for $n = 0$, $\ell = 2$, $m = [-2, 2]$, $k = [-3, 4]$ and values of the spin from $a = 0$ to $a = 0.45$, and each point is on a step of $\Delta a = 0.005$. The inset focuses around the coefficients with $k = [-3, 0]$. In the bottom panel we show the real and the imaginary part of d_B for $n = 0$, $\ell = 2$, $m = [-2, 2]$, $k = [-1, 2]$ and same values of the spin. The inset focuses around the coefficients with $m \leq 0$ and $k = [-1, 0]$. In both plots the black dot signals the coefficient value for $a = 0$.

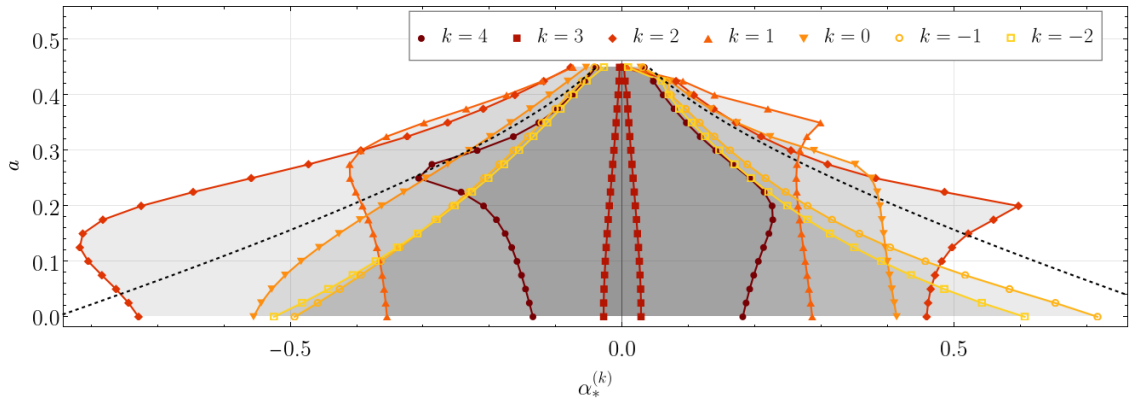

Figure 5.2: We plot the threshold values $\alpha_*^{(k)}$ against the spin for different values of k. With $\alpha_*^{(k)}$, we identify the limit value of a coupling at which an error of 1% the a linear and a nonlinear approximation is obtained. The plot uses as nonlinear estimates the full continued fraction results. The error is evaluated for the $n = 0$, $\ell = m = 2$ mode and different values of k and of the spin a. The black dashed lines correspond to the estimate (5.47)

in equation (5.33). The condition is such that the sum of coefficients must behave as

$$\sum_k \alpha^{(k)} \lesssim \left| 2\beta^2 \sigma_{\rm GR} \left(\sigma_{\rm GR} - \frac{is}{2} \right) \right| . \tag{5.47}$$

It is worth noting that when the superradiant condition $\omega = \omega_c$ is activated, one has $\sigma_{\rm GR} = 0$, and we expect that the formalism is valid only if the sum of the $\alpha^{(k)}$ is approximately 0.

In general, however, each power of k affects in a different way the effective potential. In order to have a more quantitative estimate of the allowed regime of validity, we perform two separate analysis. First, we compare the QNM frequencies computed with the linear approximation against those obtained with a full continued-fraction method discussed above. We estimated the error on the frequencies as

$$\Delta_\omega \equiv \sqrt{\left(\frac{\Delta\omega_R}{\omega_R} \right)^2 + \left(\frac{\Delta\omega_I}{\omega_I} \right)^2} , \tag{5.48}$$

where $\omega_{R,I}$ are respectively the real and imaginary parts of the QNM. We computed the error for several real positive and negative values of the couplings $\alpha^{(k)}$ and extracted the threshold values $\alpha_*^{(k)}$ at which the error reaches 1%. The results are represented in figure 5.2 for the mode $n = 0$, $\ell = m = 2$, for selected values of the spins between $a = 0$ and $a = 0.45$ and for $k = [-2, 4]$.

It can be seen that there is a complicated dependence of the thresholds on the type of modification we introduce in the potential. However, a main qualitative feature can be read off, i.e. that, for any modification, the threshold tends to get smaller for higher spins. The physical interpretation of that, is that, for a given beyond-GR effect in the modified Teukolsky equation, rotation tends to exacerbate the deviation of the linear approximation with respect to the true values of the QNMs. Bearing this caveat in mind, we will still show in the next section that the linear approximation provides very good results in a couple of known models of perturbation of rotating BHs with deviations from Kerr, also for high spin.

Since the computation of QNMs with the continued fraction method is not immediate nor straightforward to implement, we want to provide a quick estimate for the errors of the single-k contributions. In this respect, we compute the diagonal quadratic corrections,

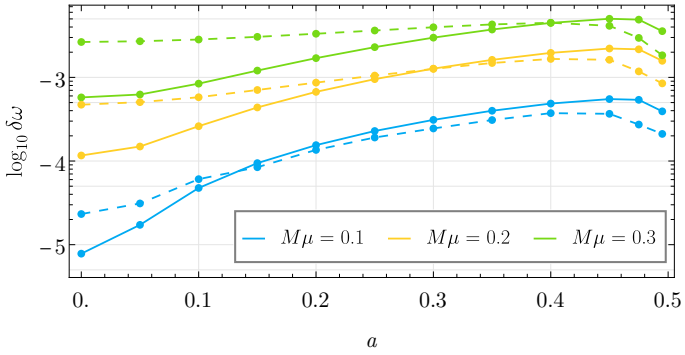

Figure 5.3: Relative difference for the real part (solid line) and imaginary part (dashed line) of the fundamental $\ell = m = 2$ mode for a massive scalar perturbation computed with the linear approximation against the nonlinear results of [259].

as explained in appendix B.7. We checked the estimate $\alpha_*^{(k)}$ by computing the error Δ_ω assuming that the nonlinear frequencies are obtained including quadratic coefficients. By a qualitative comparison, the quadratic estimate works well to capture the error except for $k = 3$, and partially for $k = 4$. Even though it is not as precise as the full nonlinear comparison, the quadratic coefficients can be used as a quick way to understand what threshold value to take for the couplings.

Lastly, we want to stress that the thresholds that we provided in this section, are referred to the contribution of a single modification. Hence, it could be that, depending on the values of the coefficients, the combination of multiple k would need larger or smaller threshold values. This means that for a theory-specific case, the bounds on $\alpha^{(k)}$ might differ from what we inferred in this section, and need to be addressed case-by-case.

5.4 Applications

5.4.1 Massive scalar perturbations

The first example that we provide to test our formalism is for the computation of the QNMs of a massive scalar field, a case extensively studied in the literature [150, 258, 259]. The radial and angular perturbation equations for a massive scalar field ($s = 0$) with mass μ are

$$\frac{\mathrm{d}}{\mathrm{d}r}\left[\Delta R'(r)\right] + \left(\frac{K^2}{\Delta} - \lambda_{\ell m} - \mu^2 r^2\right) R(r) = 0\,, \tag{5.49}$$

$$\begin{aligned}&\frac{\mathrm{d}}{\mathrm{d}y}\left[\left(1-y^2\right) S'(y)\right] \\ &\quad + \left[a^2\left(\omega^2 - \mu^2\right) y^2 + B_{\ell m} - \frac{m^2}{1-y^2}\right] S(y) = 0\,.\end{aligned} \tag{5.50}$$

First of all, we bring the angular equation into the form of equation (3.104) by transforming $\omega \to \omega + \frac{\mu^2}{2\omega}$. Then, by assuming $\mu \ll 1$, the radial equation is automatically brought in the form of (5.1), with the only non-zero $\alpha^{(k)}$ being

$$\alpha^{(1)} = \mu^2 a r_+ \left(a - \frac{m}{\omega_0}\right)\,, \qquad \alpha^{(3)} = \mu^2 r_+^3\,, \tag{5.51}$$

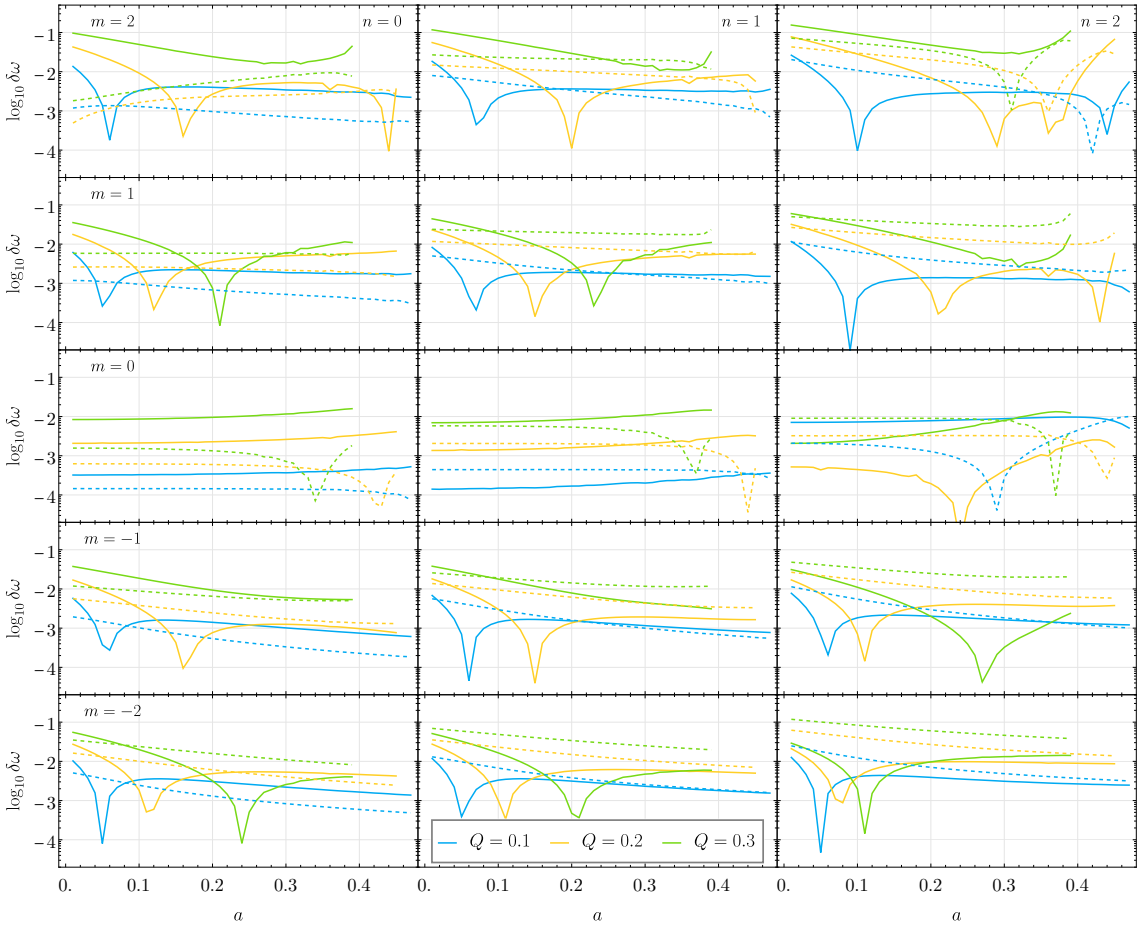

Figure 5.4: Difference between the real (solid lines) and imaginary (dashed lines) part of the Dudley-Finley QNMs computed either with the linear perturbative approach or the full continued fraction method. We show results for $n = 0$ (left panels), $n = 1$ (central panels) and $n = 2$ (right panels), $\ell = 2$, $m = [-2, 2]$ (bottom to top panels) for different values of the spin and of the electric charge. Note that the three curves have different endpoints, as for a given Q the maximum value of a is $a_{\rm max} = \frac{1}{2}\sqrt{1-4Q^2}$

where ω_0 is the unperturbed Kerr frequency. The effect of the mass on the frequency at linear order in μ^2 is given by

$$\omega_{\rm L} = \omega_0 + \frac{\mu^2}{2\omega_0} + d_{(1)}\alpha^{(1)} + d_{(3)}\alpha^{(3)}\,. \tag{5.52}$$

In figure 5.3 we show the difference $\Delta\omega = |\omega_{\rm L} - \omega_{\rm NL}|$ between the linear results in (5.52) and the nonlinear QNMs $\omega_{\rm NL}$ computed in [259] for $\ell = m = 2$ modes.

5.4.2 The Dudley-Finley equation

As a second example, we would like to test our formalism against gravitational perturbation of a Kerr-Newman (KN) BH in the limit of small charge, since the QNMs for a generic electric charge Q have been computed numerically in [472] and fits are available in [447]. Unfortunately, the KN perturbation equation is not explicitly separable, not even in the limit of small charge [473] in which at least electromagnetic and gravitational perturbations decouple. One could apply the algorithm of [88, 356, 459] to obtain a modified Teukolsky operator for the KN solution, but it goes beyond the scopes of this work. For the sake of testing the method, we can restrict ourselves to the Dudley-Finley (DF) equation, a proxy

equation for the perturbations of the Kerr-Newman metric [474–476]. The DF equation is obtained by taking equation (3.99) and performing the following substitution

$$\Delta \to \Delta + Q^2 \,. \tag{5.53}$$

We can then rescale the equation into the form (5.1) by assuming that $Q \ll 1/2$ and by defining a new spin parameter

$$\bar{a} = a + \frac{Q^2}{2a} \,, \tag{5.54}$$

such that $\bar{a}^2 \simeq a^2 + Q^2$. Retaining only the terms quadratic in Q, we can see that the only non-zero $\alpha^{(k)}$ terms that contribute to the equation (5.2) are

$$\alpha^{(0)} = Q^2 \left[\frac{\mathrm{i}s}{2\bar{a}}(m - 2\bar{a}\bar{\omega}_0) - (m - \bar{a}\bar{\omega}_0)^2 \right] , \tag{5.55}$$

$$\alpha^{(1)} = Q^2 r_+ \left[\bar{\omega}_0 \frac{m - \bar{a}\omega_0}{\bar{a}} - \frac{\mathrm{i}s}{\bar{a}}(m - 2\bar{a}\bar{\omega}_0) \right] , \tag{5.56}$$

$$\alpha^{(2)} = -Q^2 r_+^2 \bar{\omega}_0^2 \,, \tag{5.57}$$

where $\bar{\omega}_0$ is the Kerr frequency evaluated at spin $\bar{a}$. The DF linear frequencies at spin a are obtained by

$$\omega_{\mathrm{L}} = \bar{\omega}_0 + \sum_{k=0}^{2} \alpha^{(k)} d_{(k)} \,. \tag{5.58}$$

In Figure 5.4 we show the real and imaginary part of the absolute difference $\Delta\omega = |\omega_{\mathrm{L}} - \omega_{\mathrm{NL}}|$ between the linear results in (5.58) and the nonlinear QNMs ω_{NL} computed via the Leaver method in [476], for various spins and different values of the electric charge. We make the comparison with $\ell = 2$ modes, with all values of $m = [-2, 2]$, for the fundamental and first two overtones. The plot clearly shows that the discrepancy between the linearized QNMs and the full nonlinear results scales with the charge, and the approximation remains valid for all the different values of (n, ℓ, m) surveyed.

Finally, we comment on the fact that the errors grow for small values of the spin. This is due to the fact that in order to bring the equation in the form of (5.1), we performed the transformation (5.54), which brings a term $1/a$ to the denominator when $m \neq 0$. In other words, this transformation is valid as long as $|Q| \ll |a|$. Nevertheless, the smallness of the universal coefficients $d_{(k)}$ is such that the combination in frequency (5.58) is finite and faithful to the nonlinear value.

5.4.3 Higher-Derivative Gravity

Now we want to check the prediction of QNMs in HDG using the parametrized method against the results presented in [87]. In a companion paper [468], focused on the analysis of QNMs in HDG, it is shown how to reduce the radial perturbation equation to the form of equation (5.1), with the only non-vanishing values of $\alpha^{(k)}$ being $k = k^{\mathrm{HD}} = [-2, 0, 1, 2]$

$$\Delta V^{\pm} = \lambda \sum_{k \in k^{\mathrm{HD}}} \alpha_{\pm}^{(k)} \left(\frac{r}{r_+} \right)^k \,, \tag{5.59}$$

where the $\pm$ refers to the polarization of the perturbation and we collected out λ, the normalized coupling constant of the theory.[3] From this, we can compute the frequencies

[3] *cfr.* equation (30) of [468], for which $\alpha^{(k)} = A^{(k)} r_+^k$, and the coupling constant has been previously factorized out. Here we use λ to refer to the coupling constant, to avoid misunderstanding with the α_{q} used in [468].

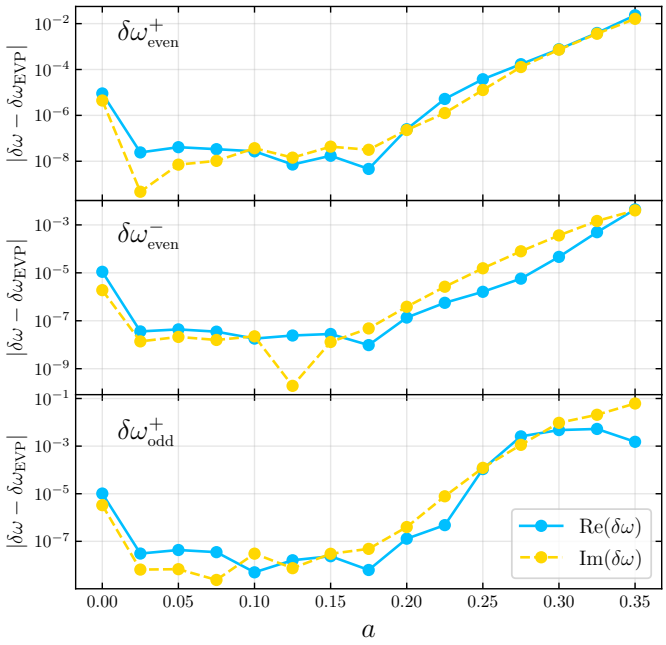

Figure 5.5: Real and imaginary part of the absolute difference between the QNM shifts computed with the eigenvalue perturbation method of [87] and the ones computed with the parametrized formalism for the $\pm$ polarizations of even cubic modes and the $+$ polarization of the odd cubic mode

deviations, normalized by the coupling constant λ

$$\delta\omega = \frac{\omega^{\rm HDG} - \omega^{\rm Kerr}}{\lambda} = \sum_{k\in k^{\rm HDG}} \alpha^{(k)}_{\pm} d_{(k)}\,, \tag{5.60}$$

for each parity, and each realization of the theory. In particular, the parity-preserving operators in HDG, produce QNM shifts with definite parity, i.e. axial and polar. However, the isospectrality between the two sectors is broken. On the other hand, parity-violating operators produce QNM shifts with two different polarizations, that do not have a definite parity. These shifts are equal and opposite [87]. In figure 5.5, we compare our results against the computation of $\delta\omega$ presented in [87], based on the eigenvalue perturbation method [459, 477]. We truncate the analysis at spin $a = 0.35$, since the results for the comparison are only available up to this value. The plot shows remarkable agreement between the corrections computed with two different methods, strengthening the validity of the parametrized formalism. In figure 5.5 we limited to show QNM shifts produced by cubic operators in HDG, for the fundamental $\ell = m = 2$ mode. We indicate polar and axial, $\ell = m = 2$ QNM shifts with $\delta\omega^{\pm}_{\rm even}$, and the two polarizations of parity-violating corrections with $\delta\omega^{\pm}_{\rm odd}$. Notice that, since $\delta\omega^{-}_{\rm odd} = -\delta\omega^{+}_{\rm odd}$, we only represent $\delta\omega^{+}_{\rm odd}$. More details on the definition of these modes can be found in [87] and in the companion paper where an extensive study of QNMs of rotating BHs in HDG is carried out [468].

5.5 Conclusions

In this chapter we have shown how to connect small deviations parametrized by powers of the radial coordinate r in the Teukolsky equation to small deviations in the eigenfrequencies and in the separation constants of modified Kerr BHs. We proved that for each value of n, ℓ, m there are up to nine independent coefficients in the radial parametrization, but

for specific cases they could be less. We presented a robust method to compute the coefficients that control the linear corrections to the QNM frequencies and separation constants through a generalization of Leaver's continued fractions, and used it to compute them for $n = [0, 2]$, $\ell = [2, 4]$, $m = [-\ell, \ell]$ and $k = [-3, 4]$ in a range of spins between 0 and 0.495.[4] These results are available online in a public git repository [469], together with a `python` code and a `jupyter notebook` to compute the QNMs and separation constants. There we also provide a tutorial demonstrating how to use the code, which can in principle be applied to compute QNMs with arbitrary n, l, m, k and angular momentum besides those we computed explicitly here.

We checked the quality of the predictions against three cases known in the literature: perturbations of a massive scalar field around Kerr, the Dudley-Finley equation and the QNMs of BHs in HDG. For all the three cases the frequencies predicted by the formalism show great agreement with respect to the results in the literature.

These coefficients will be particularly useful for the computation of QNMs of rotating BHs in alternative theories of gravity for which a modified Teukolsky equation is obtained, in the spirit of the method developed in [88, 356, 459]. So far, this method has been successfully applied to HDG [87], but other theories like scalar-GB gravity and dynamical-Chern-Simons gravity [478] are good candidates for this computation. In order to study those cases, it would be interesting to generalize our parametrized formalism by including couplings between the Teukolsky equation and a scalar field, analogous to the analysis of [461] in the case of static BHs.

The modified Teukolsky approach of [88, 356, 459] is currently limited by the fact that metric reconstruction is only available for GR, meaning that it is not yet possible to extend the method beyond first order in the coupling. For this reason, we did not explore further the quadratic coefficients as it was done in the non-rotating case [461, 462], and we limited the computation of the diagonal ones just to have a quick estimate of the error of the method itself.

Let us also remark that a different approach to study beyond-GR QNMs based on spectral methods has recently been introduced and successfully demonstrated for a wide range of spins in Refs. [341, 342, 479–481]. These methods have the advantage of being more flexible, but on the other hand, they have a much higher computational complexity and cost than the standard perturbative approaches. In this regard, the results of our method applied to specific theories may be useful to validate the spectral approaches.

The most intriguing open problem from our analysis is whether one can find a better way to exploit the potential ambiguity, as done in section 5.2.2. With the choice we made, we could reduce the number of independent coefficients $\alpha^{(k)}$ to 8. For the case of HDG we have been able to numerically reduce the number of free coefficients to just 4 [468]. One may wonder whether HDG has a special structure of the equations, or if there is a fundamental transformation of the potential that could diminish the number of free parameters.

Such discussion is relevant especially if one wants to use this formalism in a theory-agnostic setup, *e.g.*, to perform ringdown tests of GR or the inverse problem. Since the coefficients $d^{(k)}$ have a spin dependence, it would be interesting to map them to ParSpec [444]. Another useful mapping would be with the WKB deviation coefficients, as done in [464]. Finally, in the upcoming analysis, it would be interesting to compare the detectability of beyond-Teukolsky effects against that of second order QNMs [291, 297, 352].

[4] We recall that in our conventions extremality corresponds to $a = 1/2$

Chapter 6

Systematic bias in the ringdown analysis of massive black holes

6.1 Introduction

In Chapter II, we provided a broad overview of the framework of BHPT. Let us briefly recall here a couple of relevant aspects.

As we discussed, linear superpositions of QNMs provide a valid description of the ringdown at intermediate times after the merger, while at later times, the GW signal is instead dominated by a non-oscillatory power-law tail [304, 305, 482]. On the other hand, at earlier times close to the merger, nonlinear effects determine the signal behavior [290, 483]. The QNM-dominated stage of the ringdown is also affected by (small) contributions beyond linear perturbation theory, such as quadratic QNMs [291–297, 352, 484–488]. Moreover, third-order effects in perturbation theory, such as the dynamical evolution of the BH mass and the ensuing modification of the spectrum, have also been discussed in the recent literature [298–300], as well as in Chapter 4.

Observation of the BH ringdown allows the extraction of crucial physical information, related to the astrophysical properties of the source and to fundamental physics [489–491]. We anticipated in Chapter 1, that thanks to the improvements in ground-based GW detectors and upcoming space-based detectors, we are likely to be able to detect many GW events with a high SNR [137, 142, 143, 145–147, 492, 493].

In particular, LISA [145, 492] is expected to observe anywhere from a few to thousands of massive BH binaries per year (depending on the astrophysical model) [494–499]. Many of these events could have SNRs $\gtrsim 100$ in the ringdown phase [297, 500], enabling precise parameter estimation with statistical uncertainties far smaller than those achievable with the current LIGO-Virgo-KAGRA network. The reduction in statistical errors can potentially expose systematic biases induced by waveform mismodeling of the GW signal.

Such mismodeling can arise because of unaccounted effects from the astrophysical environment or new physics [501] (see also Chapter 5), but also from inaccurate or incomplete modeling of known dynamics or truncation in perturbation methods [502–515].

In this work, we focus on the accuracy of ringdown waveforms, which is needed to perform BH spectroscopy [267, 516, 517] and tests of GR [268, 518–520]. Specifically, we analyze the systematic biases induced by capping the number of modes in the ringdown waveform template. Indeed, given an observed ringdown GW signal in LISA, it is not obvious *a priori* how many modes one should include in the template: too many modes can lead to overfitting issues, while including too few will bias parameter estimation. Starting with a template containing a maximal set of modes $N_{\rm max}$, which we take as our fiducial (or

"true") waveform, we compare it to approximate templates, including only the first $N < N_{\rm max}$ highest-SNR modes. As will be discussed in Sec. 6.3, we use fits of numerical relativity (NR) simulations for 11 linear modes and 2 quadratic modes, for a total of $N_{\rm max} = 13$ modes. We estimate systematic errors using the linear signal approximation [104, 503, 521], comparing them with the statistical errors obtained from the Fisher approximation [522]. We determine the minimum number of modes $N_{\rm min}$ required for the estimation of unbiased parameters and explore how this threshold varies for different systems. We compute $N_{\rm min}$ in two equivalent ways, by checking if the following criteria are satisfied: (i) systematic errors are smaller than the statistical errors, (ii) the mismatch is below an SNR-dependent threshold. Since we work in the frequency domain, we introduce a high-frequency cutoff to avoid windowing artifacts, such as spectral leakage and mode contamination. Thus, our $N_{\rm min}$ is a window-insensitive lower bound (underestimate) of the number of modes needed for accurate parameter estimation.

The work is organized as follows. In Sec. 6.2 we describe the details of our ringdown model. In Sec. 6.3 we provide an overview of the formalism used to assess waveform inaccuracy. Finally, in Sec. 6.4 we present and discuss our results. The appendices contain robustness checks of our calculations and further dependencies of the results on the binary parameters. In Appendix C.1 we explicitly check the validity of the linear signal approximation introduced in Sec. 6.2. In Appendix C.2 we discuss the issue of the starting time. In Appendix C.3 we study the dependence of $N_{\rm min}$ on the individual spins, mass ratio, inclination and angular position of the source. In Appendix C.4, we compare our findings, obtained with a single high-frequency cutoff for all modes, with a different approach, in which a phenomenological mode-dependent tapering in the frequency domain is introduced. We also validate the frequency domain predictions by comparing the results with that for a time domain model.

6.2 The ringdown model

6.2.1 Time and frequency-domain models

The ringdown signal in the time domain can be modeled as an infinite sum of damped sinusoids. Specifically, we write the GW strain in time domain for $t > t_0$ (where t_0 is the starting time of the ringdown) as

$$h_+ - ih_\times = \frac{M}{d_L}\sum_{\ell mn}\Big[\mathcal{A}_{\ell mn}e^{-i\omega_{\ell mn}(t-t_0)}e^{-(t-t_0)/\tau_{\ell mn}} + \mathcal{A}'_{\ell mn}e^{i\omega_{\ell -mn}(t-t_0)}e^{-(t-t_0)/\tau_{\ell -mn}}\Big]{}_{-2}Y_{\ell m}(\iota,\varphi) \tag{6.1}$$

where M is the remnant BH mass in the detector frame, d_L is the luminosity distance to the source, $\omega_{\ell mn}$ and $-1/\tau_{\ell mn}$ are the real and imaginary parts of the QNM frequency, and (ι,φ) are the angular coordinates of the direction of propagation as seen from the remnant BH, with ${}_{-2}Y_{\ell m}$ the spin-weighted spherical harmonics. Note that for a given set of (ℓmn), there are two mode contributions $\mathcal{A}_{\ell mn}$ and $\mathcal{A}'_{\ell mn}$: this is because for any given QNM with frequency $\omega_{\ell mn}$ and damping time $\tau_{\ell mn}$, there exists a "mirror mode" also solving the equations of motion, which corresponds to the second term in Eq. (6.1) [268, 470]. Finally, for this study, we set the starting time to $t_0 = 20M$ after the luminosity peak. For further details on the choice of the starting time, see App. C.2

We will further assume, as common in the literature [523, 524], that the amplitude of

the mirror modes is given by

$$\mathcal{A}'_{\ell mn} = (-1)^{\ell} \mathcal{A}^{*}_{\ell -mn}, \tag{6.2}$$

where $*$ denotes complex conjugation. This property follows from equatorial symmetry [279, 294], i.e. from neglecting orbital precession in the merger waveform.

In the following, we define the Fourier transform of a time series[1] $u(t)$ as

$$\tilde{u}(f) = \int_{-\infty}^{+\infty} \mathrm{d}t\, u(t) e^{2\pi i f t}\,. \tag{6.3}$$

Furthermore, to compute the Fourier transform, following [104, 470], we continuously extend the ringdown for $t < t_0$ by symmetrically mirroring the waveform across $t = t_0$. More precisely, we replace $e^{-(t-t_0)/\tau} \to e^{(t-t_0)/\tau}$ for $t < t_0$, and divide the amplitude by $\sqrt{2}$ to avoid double-counting. By ensuring continuity of the signal in $t = t_0$, this approach improves the behavior of the Fourier transform at high frequencies, preventing the introduction of spurious Fourier components. This procedure gives:

$$\begin{aligned} \tilde{h}_{+,\times}(f) = e^{i\omega t_0} i^{\frac{1\mp 1}{2}} \frac{M}{\sqrt{2} d_L} \\ \times \sum_{\ell mn} \frac{A_{\ell mn} Y^{+,\times}_{\ell m}}{\tau_{\ell mn}} \left(L^{+}_{\ell mn} \pm L^{-}_{\ell mn} \right)\,, \end{aligned} \tag{6.4}$$

where we separate the complex amplitudes in a modulus and a phase, $\mathcal{A}_{\ell mn} = A_{\ell mn} e^{i\Phi_{\ell mn}}$, and we defined the angular functions

$$Y^{+,\times}_{\ell m} = {}_{-2}Y_{\ell m}(\iota, 0) \pm (-1)^{\ell}\, {}_{-2}Y_{\ell -m}(\iota, 0)\,. \tag{6.5}$$

The Lorentzian functions read

$$L^{\pm}_{\ell mn} = \frac{e^{\pm i(m\varphi + \Phi_{\ell mn})}}{\tau^{-2}_{\ell mn} + (2\pi f \mp \omega_{\ell mn})^2}\,. \tag{6.6}$$

Given two times series $u(t)$ and $v(t)$, we define the matched filter inner product as

$$\left(u \,|\, v\right) \equiv 4\mathrm{Re}\left[\int_0^{\infty} \mathrm{d}f\, \frac{\tilde{u}(f) \tilde{v}^{*}(f)}{S_n(f)} \right]\,. \tag{6.7}$$

In Eq. (6.7), $S_n(f)$ is the (one-sided) noise power-spectral density (PSD) of the detector given in [145].

The signal measured by the detector also depends on the response of LISA to the incoming GW, which is encoded in the time-dependent LISA transfer function [525, 526]. For typical sources observed by LISA, the ringdown lasts from minutes to hours, which is negligible compared to the timescale of LISA's motion, thereby making the stationary approximation sufficient for our work. In the stationary approximation, the LISA configuration is effectively described by two detectors [525, 527], which we will label by I, II. The LISA response is then characterized by the antenna response functions (for each GW polarization) of the two detectors, which are given by [525, 527]

$$F^{\mathrm{II}}_{+,\times}(\theta, \phi, \psi) = F^{\mathrm{I}}_{+,\times}\left(\theta, \phi - \pi/4, \psi\right)\,. \tag{6.8}$$

[1] When the time domain data is real, the Fourier components satisfy the relation $\tilde{u}(f) = \tilde{u}^{*}(-f)$.

The antenna response functions depend on the sky position of the source, determined by the angles θ and ϕ, and a polarization angle ψ, and their expressions read [528]

$$\begin{aligned} F_+(\theta,\phi,\psi) =& \frac{\sqrt{3}}{4}\left(1+\cos^2\theta\right)\cos 2\psi\cos 2\phi\,, \\ & -\frac{\sqrt{3}}{2}\cos\theta\sin 2\psi\sin 2\phi \\ F_\times(\theta,\phi,\psi) =& \frac{\sqrt{3}}{4}\left(1+\cos^2\theta\right)\sin 2\psi\cos 2\phi \\ & +\frac{\sqrt{3}}{2}\cos\theta\cos 2\psi\sin 2\phi\,. \end{aligned} \tag{6.9}$$

The signal measured in a single detector is then given by

$$\tilde{h}(f)^{\mathrm{I/II}} = F_+^{\mathrm{I/II}}\tilde{h}_+(f) + F_\times^{\mathrm{I/II}}\tilde{h}_\times(f)\,. \tag{6.10}$$

For the rest of the chapter, to avoid cluttering, we will drop the tilde indicating the Fourier transform.

6.2.2 Validity regime of the QNM model

To assess the number of modes needed to ensure waveform accuracy, it is important to account for the validity regime of the frequency-domain QNM model given by Eq. (6.4). The time-domain damped-sinusoid QNM model given by Eq. (6.1) is only accurate at intermediate times after the merger, because early times are dominated by the prompt response and late times by nonlinear tails [270, 301, 305, 529–531]. In general, to isolate the regime where the QNM model is valid, one needs to apply a window function $W(t)$ to the time-domain signal that removes the early and late time contributions. As a result, the frequency-domain response corresponds to a convolution of Eq. (6.1) with the Fourier transform of the window $W(f)$.

The bandwidth of $W(f)$ is roughly given by $\Delta f \sim 1/\Delta t$, with Δt being the transition time of the window, characterizing how fast the latter rises or drops. A very sharp transition with small Δt would thus result in a large frequency spread of the signal response, leading to spectral leakage. In addition, if the window is discontinuous in its p-th derivative, the high-frequency fall-off goes as $1/f^{p+1}$ (see Appendix C.4 for details). Thus, the smoothness of the window is crucial when trying to mitigate spectral leakage.

Since the choice of window is not unique, in Fig. 6.1 we consider a typical ringdown system and compare the frequency-domain waveforms obtained with the standard Heaviside window and with the mirroring technique adopted in our work. Since the Heaviside filter and the mirroring produce a discontinuity at $t = t0$ respectively in the strain and in its first derivative, the corresponding frequency falloffs are $1/f$ and $1/f^2$. We find that with the Heaviside window, there is significant spectral leakage from the 220 mode, which contaminates the peaks of the higher harmonics, such as the 330 and 550 modes shown in Fig. 6.1. With the mirroring, the 330 mode is much less contaminated, due to suppressed spectral leakage from the 220. However, due to its smaller amplitude, the 550 is still significantly contaminated. More in general, depending on the choice of window function, spectral leakage can contaminate the frequency-domain description of the sub-dominant higher frequency modes.

In practice, to deal with spectral leakage, we use a high-frequency cutoff that ensures that our model is not sensitive to the choice of window. The price that we pay is the loss of information from some sub-dominant higher modes that are potentially contaminated

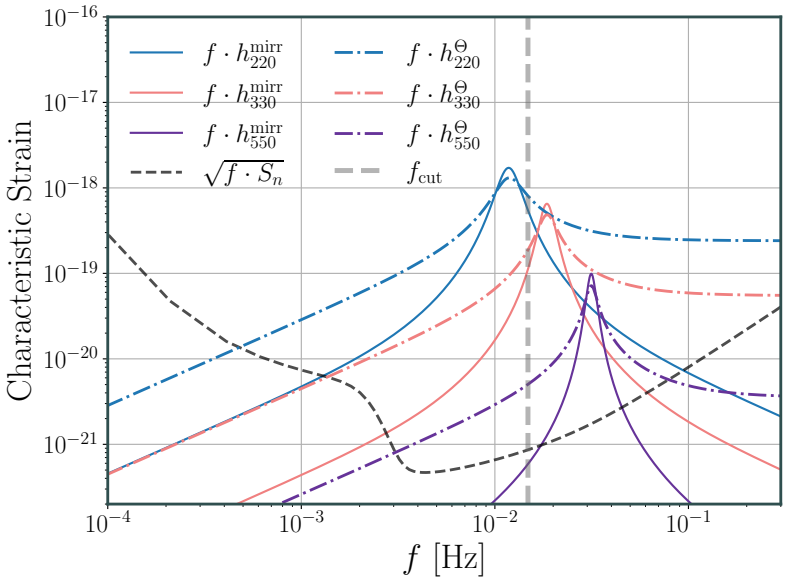

Figure 6.1: Characteristic strain of three QNMs in the ringdown of a BBH with remnant mass $M = 1.44 \times 10^6 M_\odot$ and dimensionless spin $a = 0.66$, observed at redshift $z = 0.1$. The modes h_{220}, h_{330}, and h_{550} are shown in light blue, pink, and purple, respectively. Solid and dot-dashed lines indicate the mirroring technique ($h^{\rm mirr}_{\ell mn}$) and a Heaviside time window ($h^{\Theta}_{\ell mn}$), applied before taking the Fourier transform. The black dashed line represents the LISA strain sensitivity curve, while the thick grey vertical dashed line marks indicates the PhenomA $f_{\rm cut}$. Observe that there is significant spectral leakage from the dominant h_{220} mode into higher-frequency regions above $f_{\rm cut}$.

by spectral leakage from the dominant ones. We adopt the PhenomA [532] high-frequency cutoff for the frequency-domain model, given by

$$f_{\rm cut} = \frac{\sum_{i=0}^{2} c_i \eta^i}{\pi(m_1 + m_2)}\,, \tag{6.11}$$

where c_i are numerical coefficients given in [532], and we introduced the symmetric mass ratio $\eta = m_1 m_2/(m_1 + m_2)^2$. In Fig. 6.1, we see that for $\omega_{220}/(2\pi) < f < f_{\rm cut}$, the frequency-domain model is not sensitive to the choice of window. For $f > f_{\rm cut}$ on the other hand, the frequency-domain model becomes window-dependent. This cutoff is particularly important for high-mass sources with $M \gtrsim 10^8 M_\odot$, as the QNM high-frequency tails will match the low-frequency behavior of the LISA sensitivity curve. Note that $f_{\rm cut}$ is effectively set by the 220 mode, as it dominates the spectral leakage. Specifically, the model is truncated where the 220 mode begins to exhibit windowing artifacts in the frequency domain. While each individual mode is valid within approximately $\sim 1/\tau_{\ell mn}$ of its peak, a common cutoff must be applied across all modes, since the model (and the data) are constructed as sums over them.

To mitigate spectral leakage in a more systematic way, one could optimally tune the transition width Δt for a C^∞ window (such as the Planck-taper [533]). This approach is discussed in Appendix C.4. However, our practical approach with the frequency cutoff still allows us to obtain results that are insensitive to the choice of window. Thus, in our work, we essentially estimate a window-insensitive lower bound for the number of modes $N_{\rm min}$ needed for model accuracy. In Appendix C.4, we show results computed from a phenomenological implementation of a tapered frequency-domain ringdown model that captures features of an optimal window function. We find that the results for $N_{\rm min}$ obtained with the frequency cutoff of the mirrored frequency-domain response are indeed

generically smaller than those obtained with the phenomenological optimal taper. This confirms that our results for $N_{\rm min}$ presented in the main text should be regarded as lower bounds, independent of the choice of window. We have further validated our results by comparing them to those obtained with an analysis of the mismatch in the time domain, for a specific point of the parameter space (M, z) (c.f. Appendix C.4).

6.2.3 Modes

In our work, we use the frequency domain waveform of Eq. (6.4) with the 13 modes listed in Table 6.2.3 as the "true" ringdown signal. These modes can be classified according to the following three criteria:

- **Order in perturbation theory.** We consider both linear and quadratic modes. Linear modes can be labeled with the angular and overtone numbers ℓmn. We choose to label quadratic modes by $(\ell_1 m_1 n_1) \times (\ell_2 m_2 n_2)$, where ℓ_i and m_i are the angular numbers of the linear modes that source them. We will only consider quadratic modes with angular number given by $\ell = \ell_1 + \ell_2$ and $m = m_1 + m_2$. The frequencies and damping timescales of quadratic modes are given by $\omega_{\ell mn} = \omega_{\ell_1 m_1 n_1} + \omega_{\ell_2 m_2 n_2}$ and $\tau^{-1}_{\ell mn} = \tau^{-1}_{\ell_1 m_1 n_1} + \tau^{-1}_{\ell_2 m_2 n_2}$.
- **Overtone number.** We only consider modes with $n = 0$ (fundamental modes) or $n = 1$ (overtone modes).
- **(Counter) rotation.** As shown in Eq. (6.1), given a certain triplet (ℓmn), there are two modes in the waveform with either positive or negative real frequency. We will refer as "prograde" to the modes with $\text{Sign}(\omega) = \text{Sign}(m)$, and as "retrograde" to those satisfying the opposite condition $\text{Sign}(\omega) = -\text{Sign}(m)$. Thus, each ℓmn harmonic contains both a prograde and a retrograde mode.

Due to the homogeneity of the linear Teukolsky equation, the complex amplitudes of linear modes, unlike the frequencies, depend on the binary configuration before the merger. Therefore, they cannot be predicted by perturbation theory for a merger of comparable mass objects, although they can be extracted from NR simulations [484, 530, 534, 535]. We compute the true values of the amplitudes $A_{\ell mn}$ and phases $\Phi_{\ell mn}$ of the linear modes as functions of the masses m_1, m_2 and spins a_1, a_2 of the progenitors using the fits of [530] to NR simulations. To account for a starting time of the ringdown later than the luminosity peak, we multiply all complex amplitudes given in [530] by a suppression factor $e^{-i\omega_{\ell mn} t_0} e^{-t_0/\tau_{\ell mn}}$, which corresponds to evolving the model of Eq. (6.1) for a time t_0.

On the other hand, given the amplitude of linear modes, the amplitudes of quadratic modes can be computed in perturbation theory [293–296, 487, 488, 536]. We use the fits from NR simulations of [488] to obtain the spin-dependent amplitude of the quadratic modes that we include in our model. Notice that our assumption of equatorial symmetry implies that the ratio of quadratic to linear mode amplitudes is a single number independent of the initial conditions [294, 488].

The frequencies and damping times $\omega_{\ell mn}$ and $\tau_{\ell mn}$ are obtained by interpolating numerical values computed with the continued-fraction method [268, 286, 470]. However, as we will explain in the next section, for our analysis we need derivatives of the template with respect to its parameters, which requires computing the derivatives of the QNMs frequencies with respect to the remnant spin. Only for this purpose, we resort to the analytic

fits described in [470], instead of the more accurate interpolation. Those analytic fits are given by

$$\begin{aligned}\omega_{\ell mn} &= f_1 + f_2(1-\chi_{\rm rem})^{f_3}\,;\\ Q_{\ell mn} &= q_1 + q_2(1-\chi_{\rm rem})^{q_3}\,;\\ \tau_{\ell mn} &= \frac{2Q_{\ell mn}}{\omega_{\ell mn}}\,,\end{aligned} \tag{6.12}$$

where $\chi_{\rm rem}$ is the remnant spin, and $\{f_1, f_2, q_1, q_2, q_3\}$ are given in [470]. The mass and spin of the remnant, entering Eqs. (6.12) and (6.4), are computed with the phenomenological formulae of [537, 538].

6.3 Assessing waveform inaccuracy

We will now provide an overview of the general approach for assessing the impact of waveform inaccuracies in GW parameter estimation using the linear signal and Fisher approximations, based on [104, 503, 521, 539], and introduce the relevant notation and definitions.

Following [503], we assume that there exists a template $h_{\rm GR}(\boldsymbol{\theta}; t)$ with parameters $\boldsymbol{\theta}$ which, when evaluated at the true parameters $\boldsymbol{\theta} = \boldsymbol{\theta}_{\rm tr}$, can accurately describe the GW signal. Geometrically, in the absence of noise, this simply means that the GW signal lies on the template manifold spanned by $h_{\rm GR}$ [503, 513, 521]. When using a less accurate template, denoted as $h_{\rm AP}$, even in the absence of noise, we would find that the best-fit parameters $\theta^i_{\rm bf}$ do not match the true parameters $\theta^i_{\rm tr}$, where θ^i are the parameters common to both $h_{\rm GR}$ and $h_{\rm AP}$.

The errors induced by such waveform inaccuracies are a type of *systematic error*. Uncertainties in parameter estimation induced by detector noise are instead a type of *statistical error*. A waveform template is accurate when the systematic errors are smaller than the statistical errors.

In the following, for completeness, we review the derivation for the different errors, along with the waveform accuracy criteria. We set the GW data in a given detector to be $d(t) = h_{\rm GR}(\boldsymbol{\theta}_{\rm tr}; t) + n(t)$, where $n(t)$ is the detector noise. For stationary and Gaussian noise, the likelihood $p(d|\boldsymbol{\theta})$ corresponding to the approximate template $h_{\rm AP}$ is then given by

$$\log p\left(d \,|\, \boldsymbol{\theta}\right) = -\frac{1}{2}\left(d - h_{\rm AP}(\boldsymbol{\theta}) \,|\, d - h_{\rm AP}(\boldsymbol{\theta})\right), \tag{6.13}$$

For the parameters common to both $h_{\rm AP}$ and $h_{\rm GR}$, let $\theta^i_{\rm bf}$ be the best-fit parameters of $h_{\rm AP}$ that maximize the log-likelihood given by Eq. (6.13). We introduce the total error due to both waveform inaccuracy and detector noise as $\Delta\theta^i = \theta^i_{\rm bf} - \theta^i_{\rm tr}$. In the frequency domain, Gaussian and stationary noise is uncorrelated across frequencies [539], i.e.,

$$\langle n(f) n^*(f')\rangle = \frac{1}{2} S_n(f)\delta_D(f - f')\,, \tag{6.14}$$

where δ_D is the Dirac delta function and S_n is the PSD. The symbol $\langle\cdot\rangle$ indicates the ensemble average over all possible noise realizations. For Gaussian and stationary noise, note that Eq. (6.14) also implies the completeness relation given by

$$\langle (u|n)\,(n|v)\rangle = (u|v)\ , \tag{6.15}$$

for two frequency-domain signals $u(f)$ and $v(f)$. Given that stationary noise is uncorrelated across frequencies, we choose to work in the frequency domain to compute $\Delta\theta^i$.

In general, computing $\Delta\theta^i$ requires an exploration of the likelihood surface around the maximum likelihood point. For high-dimensional parameter spaces, this typically requires stochastic methods such as Markov Chain Monte Carlo or nested sampling. However, when the SNR is large, and for small waveform modeling errors, one can simplify the computation of $\Delta\theta^i$ by using a combination of the Fisher approximation and the linear signal approximation.

We introduce the optimal SNR of the approximate template $h_{\rm AP}$ as

$$\rho = \sqrt{(h_{\rm AP} \mid h_{\rm AP})}. \tag{6.16}$$

When $\rho \gg 1$, we can take advantage of the Fisher (or Laplace) approximation [522, 540]. For the parameters that are common to $h_{\rm AP}$ and $h_{\rm GR}$, the likelihood region around $\theta_{\rm bf}$ is well described by a Gaussian distribution, and one can expand the template $h_{\rm AP}$ in terms of $\delta\theta^i = \theta^i - \theta^i_{\rm bf}$ up to leading order. Explicitly, the likelihood then reads

$$p(d|\boldsymbol{\theta}) \approx \mathcal{N} \exp\left[-\frac{1}{2}\Gamma_{ij}\delta\theta^i\delta\theta^j\right], \tag{6.17}$$

where Γ_{ij} is the Fisher Information Matrix (FIM), defined by

$$\Gamma_{ij} \equiv \left(\partial_i h_{\rm AP} \mid \partial_j h_{\rm AP}\right)|_{\theta=\theta_{\rm bf}}, \tag{6.18}$$

where we used the notation $\partial_i = \partial/\partial\theta^i$. The normalization factor is given by $\mathcal{N} = \sqrt{\det\Gamma/(2\pi)}$.

The estimation of $\theta^i_{\rm bf}$ requires maximizing Eq. (6.13), which amounts to solving[2]

$$\left(\partial_j h_{\rm AP}(\boldsymbol{\theta}_{\rm bf}) \mid d - h_{\rm AP}(\boldsymbol{\theta}_{\rm bf})\right) = 0\,, \tag{6.19}$$

where we have $d(f) = h_{\rm GR}(\boldsymbol{\theta}_{\rm tr}; f) + n(f)$. When the difference between $h_{\rm GR}$ and $h_{\rm AP}$ is small, we can also linearize $h_{\rm AP}$ in $\Delta\theta^i$, proceeding as in the linearization in $\delta\theta^i$. By Taylor expanding $h_{\rm AP}$ around $\theta^i_{\rm bf}$ to linear order in $\Delta\theta^i$, inserting it into the waveform difference $d - h_{\rm AP}(\boldsymbol{\theta}_{\rm bf})$, and solving for $\Delta\theta^i$, we obtain

$$\begin{aligned}
\Delta\theta^i &= \Delta^{(n)}\theta^i + \Delta^{(\rm Sys)}\theta^i, \\
\Delta^{(n)}\theta^i &= \left(\Gamma^{-1}\right)^{ij}\left(\partial_j h_{\rm AP} \mid n\right)\Big|_{\theta^i=\theta^i_{\rm tr}}, \\
\Delta^{(\rm Sys)}\theta^i &= \left(\Gamma^{-1}\right)^{ij}\left(\partial_j h_{\rm AP} \mid h_{\rm GR} - h_{\rm AP}\right)\Big|_{\theta^i=\theta^i_{\rm tr}}.
\end{aligned} \tag{6.20}$$

In Eq. (6.20), we have used the fact that in the linear signal approximation, the gradients of the waveform are identical at both $\theta^i_{\rm bf}$ and $\theta^i_{\rm tr}$, which also implies that Γ^{ij} is the same when evaluated at $\theta^i_{\rm bf}$ or $\theta^i_{\rm tr}$. The systematic error due to waveform inaccuracy is given by $\Delta^{(\rm Sys)}\theta^i$. Meanwhile, $\Delta^{(n)}\theta^i$ captures the bias due to a specific noise realization. When averaged over all realizations, the one-point function $\langle\Delta^{(n)}\theta^i\rangle$ vanishes. In other words, averaging over all noise realizations is equivalent to setting the noise realization to zero [541,

[2] Geometrically, the difference between the data and template is normal to the tangent subspace at the maximum-likelihood point [503, 513].

542]. However, the two-point function $\langle \Delta^{(n)}\theta^i \Delta^{(n)}\theta^j \rangle$ will not vanish, and, as we show below, quantifies the ensemble averaged statistical error. We have that

$$\begin{aligned}
&\langle \Delta^{(n)}\theta^i \Delta^{(n)}\theta^j \rangle = \\
&= \langle \left(\Gamma^{-1}\right)^{ik} \left(\Gamma^{-1}\right)^{jl} \left(\partial_k h_{\rm AP} \mid n\right) \left(n \mid \partial_l h_{\rm AP}\right) \rangle \mid_{\theta=\theta_{\rm tr}} = \\
&= \left(\Gamma^{-1}\right)^{ij} \mid_{\theta=\theta_{\rm tr}} ,
\end{aligned} \tag{6.21}$$

where, in the second step, we exploited the completeness relation of Eq. (6.15) and the definition of FIM. The statistical error is quantified through $\Delta^{(\rm St)}\theta^i \equiv \sqrt{\langle (\Delta^{(n)}\theta^i)^2 \rangle}$, resulting in [104, 539, 540]

$$\Delta^{(\rm St)}\theta^i = \sqrt{\left(\Gamma^{-1}\right)^{ii}}. \tag{6.22}$$

We define the waveform template $h_{\rm AP}$ to be accurate when

$$|\Delta^{(\rm Sys)}\theta^i| < \Delta^{(\rm St)}\theta^i, \tag{6.23}$$

and likewise $h_{\rm AP}$ is inaccurate when the inequality in Eq. (6.23) is violated. In our work, we use Eq. (6.23) as a criterion to determine the minimum number of ringdown modes needed to ensure accurate parameter estimation.

Another way to quantify the accuracy of the waveform template $h_{\rm AP}$, relative to $h_{\rm GR}$, is through the *match*, which is given by

$$\mathcal{M} = \max_{t_c,\phi_c} \frac{(h_{\rm AP}|h_{\rm GR})}{\sqrt{(h_{\rm AP}|h_{\rm AP})(h_{\rm GR}|h_{\rm GR})}}. \tag{6.24}$$

The match represents the normalized scalar product between the two templates, maximized over a relative time shift t_c and phase shift ϕ_c. A value of $\mathcal{M}$ close to one indicates that the templates almost perfectly overlap. Note that one needs to align the templates by maximization over ϕ_c and t_c so that any mismatch is entirely attributed to waveform inaccuracy and not to template misalignment.

Requiring Eq. (6.23) for all θ^i translates to [513, 543]

$$1 - \mathcal{M} < \frac{D}{2\rho^2}, \tag{6.25}$$

where $1-\mathcal{M}$ is the *mismatch*, D is the number of parameters of the model $h_{\rm AP}$, and ρ is the optimal SNR. In the mismatch criterion given by Eq. (6.25), we have neglected the contribution from the fitting factor, which makes the criterion conservative [104, 513, 521, 543–545]. In other words, when Eq. (6.25) is satisfied, the approximate waveform is sufficiently accurate.

Following [546], we now discuss how to perform the maximization over ϕ_c and t_c and compute $\mathcal{M}$. Attributing the time and phase shift to the template $h_{\rm AP}$, i.e. defining $\hat{h}_{\rm AP} = e^{-i\phi_c + 2\pi i f t_c} h_{\rm AP}$, the inner product to be maximized is

$$(h_{\rm GR}|\hat{h}_{\rm AP}) = 4{\rm Re}\left[e^{i\phi_c} \int_0^\infty \frac{h_{\rm GR}\, h^*_{\rm AP}}{S_n(f)} e^{-2\pi i f t_c} df \right]. \tag{6.26}$$

We then define $\tilde{G}(f) = h_{\rm GR} \cdot h^*_{\rm AP}/S_n(f)$, so that

$$(h_{\rm GR}|\hat{h}_{AP}) = 4{\rm Re}[e^{i\phi_c} G(t_c)], \tag{6.27}$$

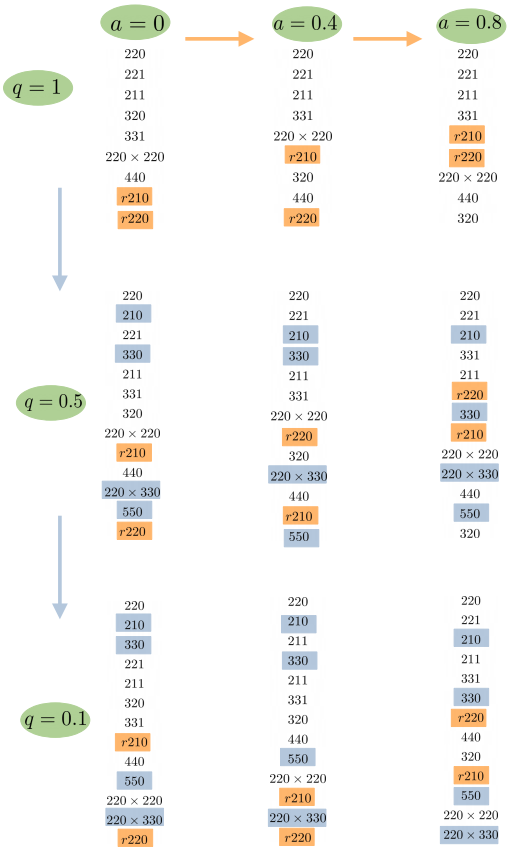

Figure 6.2: QNMs ordered by SNR from the loudest (up) to the quietest (down). We take 3 representative values of spin and mass ratio, fixing the primary mass to $10^6\,M_\odot$, the luminosity distance to 5Gpc, and the angles to $\theta = \psi = \iota = \pi/3$, $\phi = 0$. The odd-m modes are highlighted in blue. Note their absence in a mass-symmetric system, and their increasing relevance as we take a small q. Further observe that they tend to climb the ranking as we consider more spinning systems.

where we used the definition of the inverse Fourier transform. The maximization of $(h_{\rm GR}|\hat{h}_{AP})$ over ϕ_c is carried out by simply taking the modulus of the complex quantity $G(t_c)$. The match then reduces to

$$\mathcal{M} = \mathcal{C} \cdot \max_{t_c} |G(t_c)|, \tag{6.28}$$

with the proportionality constant being $\mathcal{C} = 4/\sqrt{(h_{\rm GR}|h_{\rm GR})(h_{\rm AP}|h_{\rm AP})}$. To maximize the quantity in Eq. (6.28) we employed the `minimize_scalar` function from `scipy`, using the `'bounded'` method. This approach performs a minimization within specified bounds using Brent's algorithm, which does not require derivatives evaluation.

We end this section with a summary of the main points governing how we assess waveform accuracy:

- We use the Fisher and linear signal approximations to estimate the systematic error and statistical error when using the approximate template $h_{\rm AP}$. We then quantify the waveform to be accurate when Eq. (6.23) is satisfied for every parameter in $h_{\rm AP}$.
- We also independently quantify the waveform accuracy using the mismatch criterion given by Eq. (6.25), which is valid for small mismatches and large SNR. Doing so allows us to further validate the use of Eq. (6.23), because the computation of the mismatch does not explicitly use the linear signal approximation.
- Given the approximations made, our use of the waveform accuracy criteria (described by Eq. (6.23) and Eq. (6.25)) is conservative.

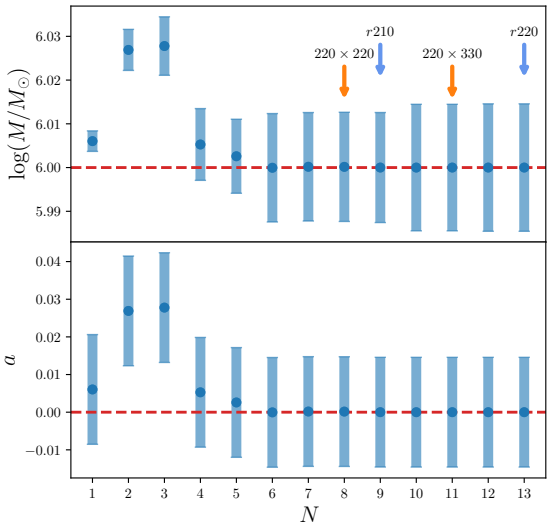

Figure 6.3: Comparison of statistical and systematic error for mass and spin, as a function of the number of modes N for an approximate template $h_{\rm AP}^{(N)}$. The selected system has primary progenitor mass $10^6 M_\odot$ and mass ratio $q = 0.5$ and it is located at a luminosity distance of 10 Gpc. The angles are fixed to the values $\theta = \psi = \iota = \pi/3$ and $\phi = 0$. The true value of the parameters is represented with the red dashed line, while the offset of the round points is given by the systematic error. Finally, the error bars represent the statistical error. The orange and blue arrows indicate respectively the points in which quadratic and linear retrograde modes are included. Observe that the inclusion of more modes tends to tame the systematic error.

6.4 Results

Equipped with the formalism described in the previous sections, we now present the results of our work.

In the context of the ringdown, we will consider $h_{\rm GR}$ to be the template given by Eq. (6.4) including all the 13 modes from the set described in Sec. 6.2.3. On the other hand, we will consider a family of approximate templates $h_{\rm AP}^{(N)}$ including a number $N < 13$ of modes. Recall that the set of parameters $\{\theta^i\}$ of $h_{\rm GR}$ includes all the amplitudes and the phases of the N modes, the logarithm of the remnant mass $\log M$, the spin of the remnant BH $\chi_{\rm rem}$, and the four angles θ, ϕ, ψ and ι, while we restrict ourselves to the case in which $\varphi = 0$, amounting to $D = 2(N + 3)$ free parameters. Notice that we do not include the luminosity distance d_L in the Fisher matrix, as it is completely degenerate with the mode amplitudes. Specifically, only the effective amplitudes $A^{\rm eff}_{\ell mn} = A_{\ell mn}/d_\ell$ are measurable. Rather than working with $A^{\rm eff}_{\ell mn}$, we choose to fix d_ℓ to its true value, in order to keep the amplitudes $\mathcal{O}(1)$. For the same reason, we do not include the angle φ, which has no impact on the observables besides shifting the mode phases $\phi_{\ell mn}$. In practice, we set $\varphi = 0$ for all systems.

In order to study the dependence of the errors on the number of modes N, we adopt the SNR of single-mode template as a criterion for ordering the QNMs. The SNR of each mode, and the resulting hierarchy of the modes, are strongly dependent on the mass ratio and the spin. For instance, highly mass-symmetric systems result in faint odd-ℓ modes, while high spins can affect the spectrum in different ways, e.g. enhancing the contribution from retrograde modes. Additionally, the angles, in particular ι, can influence the luminosity of the QNMs.

In Fig. 6.2, we schematically show the dependence of the QNMs on the mass ratio and spin. Crucially, we note that the overtone modes, described by the fits of [530], tend to become louder and dominate the spectrum when we consider systems with large spin and small mass ratio. We attribute this behavior to the extrapolation of the amplitude values to very early time, where the fitted amplitude is still unstable. Hence, in order to get physically robust results, one should carefully choose the ringdown starting time, which could in principle vary for different systems. In our work, we adopt $t_0 = 20M$ as a conservative choice for systems with non-spinning progenitors, motivated by a comparison with NR waveforms that we describe in more detail in Appendix C.2.

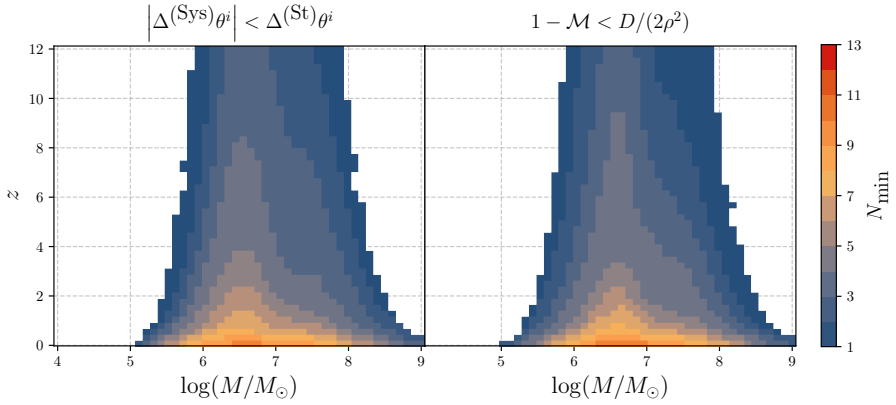

Figure 6.4: Minimum number of modes N_{min}, represented by the color code, as a function of primary mass and redshift. The mass ratio and the progenitor spins have been fixed to $q = 0.5$ and $a_1 = a_2 = 0$, while we have averaged over sky localization. Observe that at low redshift $z < 1$ and for $M/M_\odot \sim \mathcal{O}\left(10^{6-7}\right)$, we need $N_{\mathrm{min}} \in [8, 10]$. Further note that the contours track the behavior of the SNR, given the PSD of LISA.

Given the ordering procedure described above, we proceed to compute the systematic errors $\Delta^{(\mathrm{Sys})}\theta^i$ and statistical errors $\Delta^{(\mathrm{St})}\theta^i$, as described in Sec. 6.3[3]. In order to compute $\Delta^{(\mathrm{Sys})}\theta^i$ and $\Delta^{(\mathrm{St})}\theta^i$, we incorporate Gaussian priors for the parameters of h_{AP}, following [506, 539, 540]. Specifically, we implement these priors by shifting the FIM by a diagonal matrix ε_{ij}, namely $\Gamma_{ij} \to \Gamma_{ij} + \varepsilon_{ij}$. Concretely, one can show that $\varepsilon_{ii} = 1/\sigma_i^2$, where σ_i is the standard deviation of the Gaussian prior for parameter θ^i. A more informative prior on θ^i corresponds to a larger ε_{ii}. Due to the large dimensionality of our FIMs, the inclusion of these terms can also be interpreted as a way of conditioning them for inversion. In practice, we use a prior $\varepsilon_{ii} = 0.01$ for amplitudes and phases of the modes, and $\varepsilon_{ii} = 0.1$ for the logarithms of mass and spin. This choice corresponds to a Gaussian prior with a width $\sigma_i = 10$ for amplitudes and phases and $\sigma_i = 3.16$ for logarithm of the mass and spin. Amplitudes and phases are typically $\sim \mathcal{O}(1)$ or less, the spin ranges in the interval $[0, 1)$, and the error on the mass scales with the mass itself, hence, these priors are uninformative and do not affect the results. For the angles, we set $\varepsilon_{\theta\theta} = \varepsilon_{\iota\iota} = 0.1$ and $\varepsilon_{\phi\phi} = \varepsilon_{\psi\psi} = 0.025$. This corresponds to covering the whole celestial sphere and all the possible values of inclination and polarization angle.

In Fig. 6.3, we show the systematic and statistical errors for mass and spin, computed with Eqs. (6.20) and (6.22). We fixed the primary progenitor mass to $10^6 M_\odot$, the mass ratio q to 0.5 and the spins to $a_1 = a_2 = 0$. The angles are fixed to $\theta = \psi = \iota = \pi/3$ and $\phi = 0$ and the luminosity distance to 10 Gpc. The systematic error can be understood as the difference between the best-fit values, depicted by the blue circles, and the true values, represented by red dashed lines. The statistical error is presented as the blue vertical error bars for each setup. We show both quantities as functions of the number of modes included in the approximate template.

When a large number of modes are included, one can clearly observe that the systematic bias is mitigated. To understand the trend of the systematic bias with N, we first discuss the behavior of the statistical error with increasing N. Here, there are, in fact, two competing effects at play – one due to the increasing dimensionality and another due to the

[3]We also note here that while the formalism in Sec. 6.3 is presented for a single detector, we apply it for the LISA detector network described in Sec. 6.2. We do so by summing over the relevant inner products to obtain the network statistical and systematic errors (see Appendix A of [547]).

increasing SNR. Adding new modes increases the dimensionality of the parameter space, which contributes to an increase in the statistical error. At the same time, the increase in SNR with increasing N has the opposite effect. Overall, the increase in dimensionality is the dominant contribution when N is large, owing to a decreasing SNR contribution from the higher modes.

We now turn to the behavior of the systematic error as a function of N. The early trend for $N < 3$ is oscillatory. In Appendix C.1, we show that this behavior for small N corresponds to the non-perturbative regime, where the linear signal expansion is not valid, owing to the large dephasing between $h_{\rm GR}$ and $h^{(N)}_{\rm AP}$. As we include more modes, specifically when $N > 3$, we see a clear trend of decreasing systematic error with increasing N. Moreover, when $N > 3$, we observe that the systematic bias is negligible, as the true values are contained within the statistical errors.

Given the behavior of the systematic and statistical errors with N for a specific system, we now move on to discuss what is the minimum number of modes $N_{\rm min}$ needed for unbiased parameter estimation across parameter space. We independently compute $N_{\rm min}$ using the two criteria of Eq. (6.23) and Eq. (6.25). Given the non-trivial behavior of both the systematic and statistical errors with N, we implement the following scheme to ensure that our estimate of $N_{\rm min}$ is robust. We start with $h^{(1)}_{\rm AP}$, which includes only the loudest 220 mode and evaluate the criterion given by Eq. (6.23). If the criterion is already satisfied, we estimate $N_{\rm min} = 1$. However, to ensure that this estimate is robust, we add the next two modes, and check whether the criterion is still satisfied. If instead the criterion is not satisfied for $h^{(1)}_{\rm AP}$, we move on to $N = 2$ modes, and repeat the above steps until we find the $h^{(N)}_{\rm AP}$ that satisfies the criterion.

We first focus on the dependence of $N_{\rm min}$ on mass M and redshift z, by fixing the spins to $a_1 = a_2 = 0$, and the mass ratio to $q = 0.5$. We show the dependence on a_1, a_2, and q in Appendix C.3. To compute $N_{\rm min}$ as a function of (M, z), we average over several configurations of sky localization, polarization and inclination angles. In practice, we generate a large number of random configurations [4] of $(\theta, \phi, \psi, \iota)$ and compute the Monte Carlo-averaged $N_{\rm min}$ in both cases. Afterwards, we smooth out the sampling fluctuations n the data with a moving average algorithm in two dimensions.

The final result is then rounded to the closest integer.

In the left panel of Fig. 6.4, we show the resulting $N_{\rm min}$ obtained using Eq. (6.23) (within the linear-signal approximation for the systematic and statistical errors). The dependence of $N_{\rm min}$ on the mass and redshift tracks the SNR behavior, controlled by the LISA PSD. At small redshifts $z < 1$ and for masses $M/M_\odot \sim \mathcal{O}(10^{6-7})$, i.e. in the most sensitive part of the LISA frequency band, a number of modes in the range $N_{\rm min} \in [8, 10]$ will be needed to ensure an unbiased estimate of the parameters. At higher redshift, we find that there is a wide region of parameter space where $N_{\rm min} \in [3, 6]$ is required. For a given mass, increasing the redshift results in a fainter signal, for which fewer modes are required. Similarly, for either very high or low mass, even at low redshift, $N_{\rm min}$ decreases. We checked that if we impose Eq. (6.23) only for the intrinsic parameters (mass, spin, amplitudes and phases), rather than for all parameters (intrinsic and extrinsic), the value of $N_{\rm min}$ is essentially unchanged. In the right panel of Fig. 6.4, we show $N_{\rm min}$ as obtained using the mismatch criterion given by Eq. (6.25). We find strong agreement between the results obtained using the two criteria. The main reason for this, as discussed in Sec. 6.2, is that when Eq. (6.23) is satisfied for every parameter, then Eq. (6.25) is also satisfied. The main difference between the two criteria is that the linear signal approximation is

[4] The number of configurations is chosen so that the error on the Monte Carlo average is under control, typically $\delta N_{\rm min} \ll 1$.

explicitly used in Eq. (6.23), while it is used implicitly in Eq. (6.25). Specifically, we did not use the linear signal approximation in computing $\mathcal{M}$, which results in slightly different estimates for $N_{\rm min}$ in different parts of the parameter space. Overall, we observe that in most of the parameter space, the mismatch criterion results in a slightly lower estimate of $N_{\rm min}$.

6.5 Conclusions

In this work, we carried out an analysis of the systematic bias due to an incomplete description of the GW ringdown signal, as observed by LISA. We employed a frequency-domain waveform template with a maximal set of 13 modes including linear QNMs–considering both fundamental modes and overtones–and two quadratic QNMs. We ranked the QNMs by their single-mode SNR, and superimposed them to construct approximate ringdown templates of increasing accuracy.

Our main result, represented in the waterfall plot of Fig. 6.4, is the minimum number of modes $N_{\rm min}$ required for unbiased parameter estimation. As discussed in Sec. 6.3, due to the high-frequency cutoff introduced in our frequency-domain model to mitigate spectral leakage from the dominant mode, the estimate for $N_{\rm min}$ should be interpreted as a lower bound that is insensitive to the choice of time window, used to isolate the ringdown stage. We determined $N_{\rm min}$ based on two equivalent waveform accuracy criteria: a direct comparison of systematic and statistical errors within the linear-signal approximation, and, separately, via the mismatch criterion given by Eq. (6.25) (with both methods in excellent agreement). Our findings highlight the importance of carefully selecting the waveform template across the LISA parameter space. For sources at redshifts around $z \sim 2$–6, corresponding to the peak in the merger rate of massive BH binary formation and coalescence models [492], we find that a minimum of 3–6 modes are needed to avoid systematic biases. For massive BH binary sources at low redshifts of $z < 1$, as many as 10 modes may be required to ensure unbiased parameter estimation.

While our work provides a robust and conservative estimate of the minimum number of QNMs required for controlling systematics, there are some limitations that should be acknowledged. First, we assume that the true GR signal is a pure linear superposition of QNMs, as given by the waveform in Eq. (6.1). This representation is valid only within an intermediate time window, as it excludes the prompt response at early times and the power-law tails at late times. Although our high-frequency cutoff mitigates spectral leakage due to the windowing, a full Bayesian *time-domain* analysis is an important future direction to further assess the robustness of our results. Second, while there is general agreement across different mode extraction algorithms for the fundamental modes, we observed some discrepancies in the overtone amplitudes predicted by different fits [530, 534, 548, 549] for certain combinations of source parameters. This could be a source of systematic errors *per se*, especially for systems with loud overtones.

We would also like to emphasize that, while the use of the low-frequency approximation — compared to the full LISA response — may have a limited effect on the results, the omission of Time Delay Interferometry (TDI) can have a larger impact. This is particularly relevant for low-mass sources, whose ringdown phase may be shorter than the light travel time across the LISA arms. In general, the TDI response overlaps signals from different times, mixing pre-merger, merger and ringdown components. In order to isolate the ringdown phase and mitigate this issue, the analysis could be started at times later than approximately 68 s [5] after the luminosity peak. However, this delay can span the

[5] This corresponds to the light travel time for a second-generation TDI configuration.

entire ringdown duration for some low-mass sources. Therefore, new methods for analyzing ringdown signals are needed to account for complex detector responses, such as that of LISA.

Part III

Summary and outlook

The rapidly evolving landscape of GW astronomy will provide unprecedented opportunities to test gravity in the inspiral, merger and ringdown regimes [40, 103, 135, 136, 139, 141, 435, 436]. The next decades will see a synergy between ground-based, space-based, and pulsar-timing experiments, enabling multiband observations of BH binaries across an extraordinary mass range [137, 142, 143, 145–151, 491, 550, 551]. The laws governing the Universe — that we try to access through GWs — are shaped both by the fundamental nature of gravity and by the astrophysical properties of source populations. These two aspects are often deeply intertwined, and progress in understanding one is synergistic with advances in the other. Hence, accurate theoretical modeling of GW phenomenology is essential to disentangle fundamental physics from astrophysical effects and to avoid systematic biases in data analysis. In this context, this thesis has been devoted to the theoretical investigation of multiple aspects of GW–based tests of gravity.

In Chapter 1, based on [552], we considered a wide class of theories beyond GR, which include an additional scalar degree of freedom: ST theories. Within this class, some important no-hair theorems, already existing in the literature [214, 219, 231, 235], narrow down the possibility of having BH solutions that differ from GR. However, these theorems do not cover the most general case, as they assume either a restricted subset of ST theories, or static BHs. We partially filled the gap in Chapter 2, demonstrating that in the most general shift-symmetric ST theory, stationary BHs cannot support any scalar charge, defined as the $1/r$ term in the far-field scalar profile. This result can be extended to d-dimensional Myers-Perry BHs (with $d > 4$).

The proof is based on six core assumptions; relaxing some of them leads to well-known loopholes in the theorem. In particular, we revisited solutions admitting scalar charge, such as those where the scalar field has linear time dependence, or where the action includes a coupling to the GB invariant. Moreover, even beyond the shift-symmetric case, we showed that if higher-derivative couplings in the action are treated perturbatively, then the existence of scalar hair can still be excluded. Again, non-trivial solutions may arise if the scalar field couples non-minimally to curvature invariants like the GB term.

These theoretical considerations have important phenomenological implications. The presence of scalar charge implies the emission of dipolar scalar radiation during the inspiral phase of a BH binary, leading to deviations from GR in the GW signal [8, 121]. Although our no-hair theorem significantly limits such effects, the known loopholes motivate focused investigations. For instance, let us consider the case of theories in which the scalar is coupled to the GB invariant through a dimensional coupling λ. In most of the models of this kind, the scalarized branch of BH solutions, while exhibiting a maximum possible value of the ratio of the BH mass and λ, it extends continuously to infinitely small values of this ratio. This means that the best constraints on λ in this scenario come from BHs with small mass [256]. Hence, binaries in the stellar-mass regime expected to be observed by GW detectors such as LIGO-Virgo-Kagra, Einstein Telescope, and Cosmic Explorer, are viable targets for exploring scalarization. In addition, it has recently been shown, that it is possible, with the inclusion of higher-curvature terms, to construct models of BH scalarization in a finite mass window [553]. In this scenario, scalarization could occur only for SMBHs, leaving stellar-mass objects unaffected. This motivates other tests with LISA and PTAs [554].

The second part of the thesis is devoted to BHPT, which provides a complementary avenue for testing gravity. Unlike inspiral-based tests, which are sensitive primarily to long-range interactions, BHPT can probe the full spacetime geometry and is therefore sensitive to a broader class of deviations from GR. Our analysis of the ringdown is twofold. On the one hand, we explored the impact of GR effects beyond linear BHPT. On the other

hand, we also investigate possible beyond GR effects.

In Chapter 4, based on [300], we focus on the impact of a time-dependent BH mass on the QNM spectrum. Such mass evolution may result from GW self-absorption during the ringdown phase, or from environmental effects such as astrophysical accretion. To model this scenario, we adopted the Vaidya metric — a well-known solution of the Einstein equations that describes an absorbing or radiating BH. The novelty of our approach, compared to previous studies, lies in performing a frequency-domain analysis under the assumption of a constant mass accretion or radiation rate.

We found that the QNM frequencies at a fixed time slice exhibit characteristic shifts relative to the Schwarzschild spectrum, approximately linear in the time derivative of the BH mass. Both the real and imaginary parts of the QNM frequencies tend to decrease with an increase in the absolute value of the accretion/radiation rate. Furthermore, our formalism recovers the adiabatic time evolution of QNMs, with frequencies scaling as $\propto M(w)^{-1}$ — a behavior that was previously observed in fully numerical time-domain studies [409, 410].

We also identify linear instabilities in scalar and axial gravitational perturbations in, respectively, the radiating and absorbing cases, if the mass evolution rate exceeds a critical threshold. Additionally, within the same framework, we analyze the tidal response of the Vaidya BH in the static limit of the perturbation equations. We find that the linear static tidal Love numbers acquire perturbative corrections due to the time dependence of the mass, in contrast to the vanishing Love numbers of stationary BHs in GR. Finally, we show how these results can be consistently interpreted within the point-particle EFT framework.

In Chapter 5, based on [318], we developed a new and widely-applicable method for the computation of beyond-GR corrections to the Kerr QNM spectrum. In more detail, we showed how small deviations in the Teukolsky potential, parametrized by powers of the radial coordinate r, translate into linear corrections to the QNM frequencies and separation constants of perturbed Kerr BHs. The linear coefficients of these corrections were computed with a generalized continued-fraction method.

The validity of our predictions was confirmed by comparing with known results for massive scalar perturbations on a Kerr background, the Dudley–Finley equation, and BHs in HDG. This last application, which has been more extensively analyzed in the companion paper [468], represents an important step towards the exploration of the BH ringdown spectrum in modified theories of gravity. The parametrized framework we developed, can in principle be extended to include a larger class of modified gravity theories that admit a perturbed Teukolsky equation, with more coupled degrees of freedom, such as Einstein-scalar-GB or dynamical Chern–Simons gravity [457, 478]. As another possible future direction, it would be interesting to map our formalism to a data-analysis framework, such as ParSpec [444], in order to provide a connection between the theoretical quantification of beyond GR effects and experimental tests thereof.

Finally, in Chapter 6, based on [319], we addressed the problem of theoretical biases due to inaccurate ringdown waveform description in parameter estimation. In particular, we focused on the space-based detector LISA. We used a frequency-domain template incorporating up to 13 QNMs, including both fundamental and overtone modes, along with two quadratic QNMs. Modes were ranked by their single-mode SNR, and combined progressively to build increasingly accurate templates. Employing two different criteria – in excellent agreement – we found that 3–6 modes are necessary for unbiased parameter estimation at redshifts $z \sim 2-6$, where LISA is expected to observe the peak of massive BH merger rates. For lower-redshift systems ($z < 1$), up to 10 modes might be needed. In

the future, it will be important to validate our findings with a full Bayesian time-domain analysis.

Part IV

Supplemental material

Appendix A

Circularity symmetry and higher dimensions

A.1 Conserved current and circular spacetimes

We claimed in Sec. 2.2 that the components J_t and J_ϕ of the Noether current J_μ, associated with the shift symmetry in the scalar action, are zero in our setup. Although not obvious, due to the presence in J_μ of possible higher derivative operators involving the curvature, it is not hard to show that this is in fact the case as long as the conditions (i) and (iv) are fulfilled.

We can express the shift-symmetry current in full generality as

$$J_\mu = F_{\mu\nu}\,\nabla^\nu\psi\,, \tag{A.1}$$

where the tensor $F_{\mu\nu}$ is a function of ψ, $g_{\mu\nu}$ and their derivatives. The idea of the proof, which we formalize better in the following, consists simply in showing that, given $\nabla^t\psi = \nabla^\phi\psi = 0$, it is not possible to construct (using only the building blocks ψ, g and ∇) any nontrivial $F_{\mu\nu}$ with an odd number of indices r or θ if the spacetime has the isometries in (i).[1]

Consider an open subset $\mathcal{U}$ of a four-dimensional spacetime, which has a continuous isometry group associated with two commuting Killing vectors, labeled as $\xi^{(a)}_\mu$, where $a = 1, 2$. We define surface of transitivity [557] a privileged two-dimensional hypersurface, which is everywhere tangent to the Killing vectors. A spacetime is circular if it has a set of Killing vectors and it admits hypersurfaces of conjugate dimension 2, which are everywhere orthogonal to their transitivity surfaces (orthogonal transitivity condition). For a stationary circular BH, we have the Killing vectors $\xi_{(a)} = \partial_t\,,\,\partial_\phi$. We can then define the surfaces of transitivity with the coordinates $i = r,\,\theta$ and choose the coordinates in such a way that the components of the metric $g_{ia} = g_{rt}\,,\,g_{r\phi}\,,\,g_{\theta t}\,,\,g_{\theta\phi}$ vanish.

We then need a further step. Let us define $\zeta_{(i)}$ to be a set of independent vectors orthogonal to the transitivity surface. A tensor T is said to be invertible at a point if all the quantities

$$T_{\mu_1,\dots\mu_p}{}^{\nu_1,\dots\nu_q}\;\xi^{\mu_1}_{(a_1)}\cdots\xi^{\mu_p}_{(a_p)}\,\zeta^{(i_1)}_{\nu_1}\cdots\zeta^{(i_q)}_{\nu_q} \tag{A.2}$$

are zero for odd p.

It can be showed [249] that the circularity of the subset $\mathcal{U}$ implies the invertibility of the Riemann and Ricci tensors on it. Furthermore, it can also be proven that the invertibility property of a tensor is preserved when one takes its covariant derivative.

[1] A similar construction can be found, e.g., in Refs. [555, 556].

Now consider Eq. (A.1). Given $\nabla^t\psi = \nabla^\phi\psi = 0$ and the symmetries of the Riemann tensor, it is easy to check that the only way of having a nonvanishing J_t is to have nonzero tensors constructed from R and covariant derivatives of R and ψ, with an odd number of indices running over (r, θ). In other words, we should be able to construct a noninvertible $F_{\mu\nu}$ on $\mathcal{U}$. However, this cannot happen, thanks to the invertibility of the building blocks.

The same can be shown for J_ϕ. Hence, as long as the condition (iv) is verified, the only nonvanishing components of the current are J_r and J_θ.

Note that the situation is different if we drop the assumption (iv) and allow the scalar field to linearly depend on time. In this case, it is easy to verify that a non-vanishing J_t is not incompatible with circularity anymore.

The same considerations can be extended to higher dimensions for the class of BHs discussed in Sec. 2.3.

A.2 Myers-Perry BHs in d-dimensions

The generalization of the Kerr metric in $d > 4$ dimensions for a BH rotating in a single plane is given by the Myers–Perry line element [237] (see Ref. [236] for a review),

$$\begin{aligned} \mathrm{d}s^2 =& -\mathrm{d}t^2 + \frac{\mu}{r^{d-5}\Sigma}(\mathrm{d}t - a\,\sin^2\theta\,\mathrm{d}\phi)^2 + \frac{\Sigma}{\Delta}\mathrm{d}r^2 \\ &+ \Sigma\,\mathrm{d}\theta^2 + (r^2+a^2)\sin^2\theta\,\mathrm{d}\phi^2 + r^2\cos^2\theta\,\mathrm{d}\Omega^2_{d-4}\,. \end{aligned} \tag{A.3}$$

Besides the angles θ and ϕ defined in the usual way, we have $d-4$ additional angles in $\mathrm{d}\Omega^2_{d-4}$. The functions appearing in the metric are generalizations of the well-known Kerr ones,

$$\Sigma \equiv r^2 + a^2\cos^2\theta\,, \qquad \Delta \equiv r^2 + a^2 - \frac{\mu}{r^{d-5}}\,, \tag{A.4}$$

with the mass and spin parameters being

$$M \equiv \frac{(d-2)\Omega_{d-2}}{16\pi G}\mu\,, \qquad J \equiv \frac{2M}{d-2}a\,. \tag{A.5}$$

In $d > 4$, rotation around more independent planes is allowed. In the most general case, the number of planes can be up to $N = (d-1)/2$. The metric is different for odd and even d. In particular, we have for odd d:

$$\begin{aligned} \mathrm{d}s^2 =& -\mathrm{d}t^2 + (r^2+a_i^2)(\mathrm{d}\mu_i^2 + \mu_i^2\mathrm{d}\phi_i) + \frac{\mu r^2}{\Pi\,F}(\mathrm{d}t - a_i\,\mu_i^2\,\mathrm{d}\phi_i)^2 \\ &+ \frac{\Pi\,F}{(\Pi - \mu r^2)}\mathrm{d}r^2\,, \end{aligned} \tag{A.6}$$

where $i = 1, \ldots, N$, a_i is the spin associated to the i-th rotation plane and μ_i the corresponding direction cosine. Summation over i is assumed and $\mu_i^2 = 1$.

For even d we have instead,

$$\begin{aligned} \mathrm{d}s^2 =& -\mathrm{d}t^2 + r^2\mathrm{d}\alpha^2 + (r^2+a_i^2)(\mathrm{d}\mu_i^2 + \mu_i^2\mathrm{d}\phi_i) + \frac{\mu r^2}{\Pi\,F}(\mathrm{d}t - a_i\,\mu_i^2\,\mathrm{d}\phi_i)^2 \\ &+ \frac{\Pi\,F}{(\Pi - \mu r^2)}\mathrm{d}r^2\,. \end{aligned} \tag{A.7}$$

where the functions Π and F are defined as

$$\begin{aligned} \Pi(r) &= \prod_I^N (r^2 + a_i^2)\,, \\ F(r, \mu_i) &= 1 - \frac{a_i^2\mu_i^2}{r^2 + a_i^2}\,, \end{aligned} \tag{A.8}$$

and $\mu_i^2 + \alpha^2 = 1$.

Appendix B

Perturbation equations and the continued-fraction method

B.1 Perturbation equation in Eddington-Finkelstein coordinates

In the following, we derive the equations for perturbations of various spin in the Jordan frame and in the Eddington–Finkelstein coordinates. We will mainly work at the level of the action, and show that the result recovers the equations obtained in the main text, after transforming into rescaled coordinates. For the sake of the presentation, we just illustrate the decreasing mass case (where w is the retarded time), as the increasing mass case is completely analogous.

B.1.1 Scalars and photons

The dynamics of scalar perturbations obeys the Klein–Gordon equation

$$\partial_\mu \left(\sqrt{-g}\, g^{\mu\nu}\partial_\nu \Phi\right) = 0\,. \tag{B.1}$$

The scalar field can be expanded as

$$\Phi(w, r, \theta, \phi) = \sum_{\ell,m} \frac{f(w,r)}{r} Y_{\ell m}(\theta, \phi)\,. \tag{B.2}$$

With this ansatz, on the Vaidya background
Eq. (B.1) reads:

$$\begin{aligned}\left(1 - \frac{2M(w)}{r}\right)\frac{\partial^2 f(w,r)}{\partial r^2} - 2\frac{\partial^2 f(w,r)}{\partial w \partial r} + \frac{2\,M(w)}{r^2}\frac{\partial f(w,r)}{\partial r} \\ - \left(\frac{\ell(\ell+1)}{r^2} + \frac{2M(w)}{r^3}\right) f(w,r) = 0\,.\end{aligned} \tag{B.3}$$

Note that this equation is equivalent to the one derived in the Einstein frame in Sec. 4.3.1. In fact, the master variable of Eq. (B.2) implicitly introduces a conformal factor $(2M(w))^{-1}$ encoded in the term r^{-1}. This corresponds to the conformal weight $\chi = -1$ that we choose for the scalar field in the main text.

Electromagnetic perturbations are described by the Maxwell action

$$S_{\rm EM}[A, g] = -\frac{1}{4}\int \mathrm{d}^4x\, \sqrt{-g}\, F_{\mu\nu}F^{\mu\nu}\,, \tag{B.4}$$

with the field strength $F_{\mu\nu} = \partial_{[\mu} A_{\nu]}$. The four-potential in the coordinates (w, r, θ, ϕ) can be decomposed with the ansatz

$$A = A^{(\text{polar})} + A^{(\text{axial})} = \begin{pmatrix} h(w,r)\, Y_{\ell m} \\ e(w,r)\, Y_{\ell m} \\ a(w,r)\varepsilon_i{}^j\, \partial_j Y_{\ell m} + k(w,r)\, \partial_i Y_{\ell m} \end{pmatrix} . \tag{B.5}$$

Note that the ℓ, m dependence has been left implicit in the functions h, e, k and a. Adopting the gauge choice $k(w,r) = 0$, and after integrating out the angular part, one obtains the reduced action

$$S_{\text{red}} = \int \mathrm{d}w\, \mathrm{d}r\, \mathcal{L}[a,\, h,\, e\,] , \tag{B.6}$$

with

$$\begin{aligned} \mathcal{L}[a,\, h,\, e\,] = \frac{\ell(\ell+1)}{2} \Bigg[& -\ell(\ell+1)\frac{a^2}{r^2} + 2\partial_u a \partial_r a - \left(1 - \frac{2M(w)}{r}\right) \partial_r a^2 \\ & - \left(1 - \frac{2M(w)}{r}\right) e^2 + \frac{r^2\, (\partial_r h - \partial_u e)^2}{\ell(\ell+1)} + 2e\, h \Bigg] = \\ = \mathcal{L}[a] + \mathcal{L}[h,\, e] , & \end{aligned} \tag{B.7}$$

where we defined the Lagrangians $\mathcal{L}[a]$ and $\mathcal{L}[h,\, e]$ describing the axial degree of freedom a, and the polar modes $(h,\, e)$, respectively.

Varying $\mathcal{L}[a]$ with respect to a, one gets the equation of motion

$$\begin{aligned} \left(1 - \frac{2M(w)}{r}\right) \frac{\partial^2 a(w,r)}{\partial r^2} - 2\frac{\partial^2 a(w,r)}{\partial w \partial r} + \frac{2\, M(w)}{r^2} \frac{\partial a(w,r)}{\partial r} \\ - \frac{\ell(\ell+1)}{r^2} a(w,r) = 0 . \end{aligned} \tag{B.8}$$

Instead, $\mathcal{L}[h,\, e]$ can be conveniently rewritten, introducing an auxiliary field q, as

$$\begin{aligned} \mathcal{L}[h,\, e,\, q] = \frac{\ell(\ell+1)}{2} \Bigg[& -\frac{\ell(\ell+1) q^2}{2r^2} + q\, (\partial_r h - \partial_w e) + 2eh \\ & + \left(\frac{2M(w)}{r} - 1\right) e^2 \Bigg] . \end{aligned} \tag{B.9}$$

It is straightforward to check that (B.9) is equivalent to $\mathcal{L}[h,\, e]$ upon using the q's equation of motion,

$$q(w,r) = \frac{r^2}{\ell(\ell+1)} \left(\partial_r\, h(w,r) - \partial_u e(w,r)\right) . \tag{B.10}$$

The introduction of the field q is convenient because it makes it easier to integrate out the fields e and h from (B.9). Computing the equations of motion of e and h, and plugging the solutions back into (B.9), one finds the following action for the single degree of freedom q:

$$\mathcal{L}[q] = -\frac{\ell(\ell+1)}{2} \left[\ell(\ell+1)\frac{q^2}{r^2} + \left(1 - \frac{2M(w)}{r}\right) \partial_r q^2 - 2\partial_w q \partial_r q \right] , \tag{B.11}$$

yielding the equation of motion

$$\left(1-\frac{2M(w)}{r}\right)\frac{\partial^2 q(w,r)}{\partial r^2}-2\frac{\partial^2 q(w,r)}{\partial w\partial r}+\frac{2\,M(w)}{r^2}\frac{\partial f(w,r)}{\partial r} - \frac{\ell(\ell+1)}{r^2}q(w,r)=0\,. \tag{B.12}$$

Note that this has the same for as Eq. (B.8). This fact, which is responsible for isospectrality of the even and odd electromagnetic modes, is a consequence of the electric-magnetic duality, as we will now explicitly show, mirroring exactly the Schwarzschild case [238].

Notice also that, like in the scalar case, we are implicitly introducing a conformal factor through the master variable of Eq. (B.10). The conformal weight is related to the power of r that appears in the definition on $q(w,r)$. Indeed, $q\sim(2M(w))\,h$, and, since $F\sim\partial q$ we have the implicit transformation law for the field strength $F\to F$. This corresponds to the choice of $\chi=0$ that we made in the Einstein frame in Sec. 4.3.2.

B.1.2 Electric-magnetic duality

The two electromagnetic degrees of freedom $a(w,r)$ and $q(w,r)$ can be joined in the $SO(2)$ doublet

$$\xi(w,r)=\begin{pmatrix} a(w,r)\\ q(w,r)\end{pmatrix}\,, \tag{B.13}$$

whose dynamics is described by the action

$$S[\xi]=-\frac{\ell(\ell+1)}{2}\int \mathrm{d}w\,\mathrm{d}r\left[\frac{\ell(\ell+1)}{r^2}\xi^T\,\xi+\left(1-\frac{2M(w)}{r}\right)\partial_r\xi^T\,\partial_r\xi + 2\,\partial_u\xi^T\,\partial_r\xi\right]. \tag{B.14}$$

The Maxwell equations can be written concisely using differential forms as

$$\mathrm{d}F=0\,,\qquad \mathrm{d}\star F=0\,, \tag{B.15}$$

where $\star$ represents the Hodge dual operation. This form makes it evident that the equations are symmetric under $F\leftrightarrow\star F$, which is the well-known electric-magnetic duality.

The components of the field strength can be computed explicitly from the four-potential in Eq. (4.19)

$$\begin{aligned} F_{wr}&=-\frac{\ell(\ell+1)}{2r^2}q\,Y_{\ell m}\\ F_{wa}&=\partial_w a\,\varepsilon_a{}^b\,\partial_b Y_{\ell m}-\left[\left(1-\frac{2M(w)}{r}\right)\partial_r q-\partial_w q\right]\partial_a Y_{\ell m}\\ F_{ra}&=\partial_r a\,\varepsilon_a{}^b\,\partial_b Y_{\ell m}-\partial_r q,\partial_a Y_{\ell m}\\ F_{ab}&=-\frac{\ell(\ell+1)}{2}\varepsilon_{ab}\,a\,Y_{\ell m}\,, \end{aligned} \tag{B.16}$$

where the indices a,b run over the angular coordinates. One can compute the dual components $\star F_{\alpha\beta}=\frac{1}{2}\epsilon_{\alpha\beta\mu\nu}F^{\mu\nu}$ and verify that they yield precisely the same expressions, upon exchanging $a\leftrightarrow q$.

B.1.3 Regge–Wheeler equation

The gravitational perturbations, like the electromagnetic ones, can be decomposed into axial and polar sectors [271]. Such decomposition is useful as the spherical symmetry of the Vaidya geometry ensures that the two sectors are decoupled at the level of the linearized dynamics. In the following, we will focus on the axial sector only.

The axial metric perturbations can be expressed, in the coordinates (w, r, θ, ϕ), and in the Regge–Wheeler gauge [271], as

$$h_{\mu\nu}^{(\text{axial})} = \sum_{\ell m} \begin{pmatrix} 0 & 0 & -\frac{h_0}{\sin\theta}\,\partial_\phi & \sin\theta\, h_0\,\partial_\theta \\ 0 & 0 & -\frac{h_1}{\sin\theta}\,\partial_\phi & \sin\theta\, h_1\,\partial_\theta \\ \text{Sym} & \text{Sym} & 0 & 0 \\ \text{Sym} & \text{Sym} & 0 & 0 \end{pmatrix} Y_{\ell m}(\theta, \phi)\,, \tag{B.17}$$

where h_0 and h_1 are functions of w and r. The dynamics of the odd fields can be obtained from the action

$$S_{\text{grav}} = \frac{M_{\text{Pl}}^2}{2} \int \mathrm{d}^4x\, \sqrt{-g}\big(R - T^\lambda{}_\lambda\big)\,, \tag{B.18}$$

where $T^\lambda{}_\lambda$ is the trace of the SET of Eq. (4.3)), sourcing the Vaidya geometry.

Expanding (B.18) to quadratic order in the fields, and integrating over the solid angle, one finds an action for h_0 and h_1 which is again more conveniently rewritten in terms of an auxiliary field ψ as

$$S_{\text{axial}}^{(2)} = -\frac{\ell(\ell+1)M_{\text{Pl}}^2}{2} \int \mathrm{d}w\, \mathrm{d}r\, \mathcal{L}[h_0,\, h_1,\, \psi]\,, \tag{B.19}$$

where

$$\begin{aligned} \mathcal{L}[h_0, h_1, \psi] = \frac{r^2\psi^2}{2} &+ \psi\left(-2h_0 + r(\partial_r h_0 - \partial_w h_1)\right) \\ &+ \frac{(\ell+2)(\ell-1)}{r^2}\left[\left(1 - \frac{2M(w)}{r}\right)\frac{h_1^2}{2} - h_0 h_1\right], \end{aligned} \tag{B.20}$$

where the auxiliary field ψ is expressed in terms of h_0 and h_1 via the relation

$$\psi(w, r) = 2h_0(w, r) + r\left(\partial_w h_1(w, r) - \partial_r h_0(w, r)\right)\,. \tag{B.21}$$

Integrating out h_0 and h_1 from (B.20), one finally finds a quadratic action for the single degree of freedom ψ:

$$\mathcal{L}[\psi] = -\left(1 - \frac{2M(w)}{r}\right)\frac{\partial_r\psi^2}{2} + \partial_r\psi\partial_w\psi - \left(\frac{\ell(\ell+1)}{r^2} - \frac{6M(w)}{r^3}\right)\frac{\psi^2}{2}\,, \tag{B.22}$$

which yields the equation of motion

$$\begin{aligned} \left(1 - \frac{2M(w)}{r}\right)\frac{\partial^2\psi(w,r)}{\partial r^2} - 2\frac{\partial^2\psi(w,r)}{\partial w\partial r} + \frac{2\,M(w)}{r^2}\frac{\partial\psi(w,r)}{\partial r} \\ - \left(\frac{\ell(\ell+1)}{r^2} - \frac{6M(w)}{r^3}\right)\psi(w,r) = 0\,, \end{aligned} \tag{B.23}$$

representing the generalization of the Regge–Wheeler equation to Vaidya BHs.

B.1.4 Master equation and spectrum

All in all, we can write down a single master equation (holding for both the increasing and decreasing mass cases) for massless scalar, (polar and axial) electromagnetic and (axial) gravitational perturbations on a Vaidya background in Eddington–Finkelstein coordinates [391, 409, 558]:

$$\left(1-\frac{2M(w)}{r}\right)\frac{\partial^2\psi(w,r)}{\partial r^2}+2s\,\frac{\partial^2\psi(w,r)}{\partial u\partial r}+\frac{2\,M(w)}{r^2}\frac{\partial\psi(w,r)}{\partial r}+ \\ -\left(\frac{\ell(\ell+1)}{r^2}+\frac{2\,\sigma M(w)}{r^3}\right)\psi(w,r)=0\,, \tag{B.24}$$

where $\sigma=1,0,-3$ holds respectively for scalar, (polar and axial) electromagnetic and axial gravitational perturbations.

Consider now the change of coordinates introduced in Eq. (4.6). The derivatives transform as

$$\begin{aligned}
&\frac{\partial}{\partial r}\to\frac{1}{2M(w)}\frac{\partial}{\partial x}\\
&\frac{\partial}{\partial w}\to\frac{1}{2M(w)}\frac{\partial}{\partial W}-x\frac{M'(w)}{M(w)}\frac{\partial}{\partial x}\\
&\frac{\partial^2}{\partial r^2}\to\frac{1}{4M(w)^2}\frac{\partial^2}{\partial x^2}\\
&\frac{\partial^2}{\partial r\partial w}\to\frac{1}{4M(w)^2}\frac{\partial^2}{\partial W\partial x}-\frac{M'(w)}{2M(w)^2}\frac{\partial}{\partial x}-x\frac{M'(w)}{2M(w)^2}\frac{\partial^2}{\partial x^2}
\end{aligned} \tag{B.25}$$

Note that the term $\partial M(w)/\partial x$ is vanishing (from the inverse Jacobian of the coordinate transformation). Approximating the mass evolution with a linear growth in the null time, we get that,

modulo an overall factor, Eq. (B.24) becomes independent of u:

$$\frac{\left(x-1-4|M'|\,x^2\right)}{x}\frac{\partial^2\psi(W,x)}{\partial x^2}+2s\,\frac{\partial^2\psi(W,x)}{\partial U\partial x}+\frac{\left(1-4|M'|\,x^2\right)}{x^2}\frac{\partial\psi(W,x)}{\partial x} \\ -\left(\frac{\ell(\ell+1)}{x^2}+\frac{\sigma}{x^3}\right)\psi(W,x)=0\,. \tag{B.26}$$

Given the time-independent form of Eq. (B.26), we can further change coordinate from W to $T=W-s\,x_*$, and obtain

$$\begin{aligned}
&\frac{\partial}{\partial x}\to-\frac{s}{f(x)}\frac{\partial}{\partial T}+\frac{\partial}{\partial x}\\
&\frac{\partial}{\partial W}\to\frac{\partial}{\partial T}\\
&\frac{\partial^2}{\partial x^2}\to\frac{1}{f(x)^2}\frac{\partial^2}{\partial T^2}-\frac{2s}{f(x)}\frac{\partial^2}{\partial T\partial x}+s\,\frac{f'(x)}{f(x)^2}\frac{\partial}{\partial T}+\frac{\partial^2}{\partial x^2}\\
&\frac{\partial^2}{\partial W\partial x}\to-\frac{s}{f(x)}\frac{\partial^2}{\partial T^2}+\frac{\partial^2}{\partial T\partial x}\,.
\end{aligned} \tag{B.27}$$

Finally, we can use separation of variables in x and T by writing the usual Fourier $\psi(T,x)=\exp\left(-i\Omega_\psi T\right)\Psi(x)$. Introducing again the generalized tortoise coordinate, we

get the very simple master equation

$$\left[\frac{\mathrm{d}^2}{\mathrm{d}x_*^2} + \left(\Omega_\psi^2 - V(x)\right)\right]\Psi(x_*) = 0\,, \tag{B.28}$$

with

$$V(x) = f(x)\left(\frac{\ell(\ell+1)}{x^2} + \frac{\sigma}{x^3}\right)\,. \tag{B.29}$$

Note that this equation recovers Eq. (4.32), upon identifying $\tilde{\Omega} = \Omega_\psi$. From the discussion of Sec. 4.3.3, in the gravitational case, we thus expect the following relation between the frequencies:

$$\Omega_\psi = \Omega + 2iM'\,. \tag{B.30}$$

This relation can be understood as follows.

The master variable of Eq. (B.21) has the same spectrum of the component of the metric perturbations in the Jordan frame $h_{\mu\nu}$. On the other hand, the derivation of Eq. (4.32) was performed in the Einstein frame, namely in terms of the metric perturbation $\tilde{h} \sim h/(2M(w))^2$. However, one also has to account for an extra $2M(w)$ factor relating the off-diagonal metric perturbation components h_{tj}, where t is a "physical" time coordinate and $j = \theta, \phi$, with the components h_{Tj}, where T is the rescaled time coordinate, i.e.,

$$h_{tj} = (2M(w))^{-1}\, h_{Tj} = 2M(w)\,\tilde{h}_{Tj}\,. \tag{B.31}$$

As we discussed in the main text, a factor $2M(w)$ provides the shift $2iM'$ (see Eq. (4.52)) and hence this relation yields exactly the expected connection between the two spectra.

B.2 Coefficients of the five-term recurrence relation

In this appendix, we report the full expressions for the coefficients of the initial five-term recurrence relation introduced in the continued-fraction method for the perturbation equations of the Vaidya spacetime. As an example, we show explicitly the decreasing mass case, corresponding to the outgoing Vaidya metric, but the increasing mass case works analogously:

$$\begin{aligned}
\alpha_n = &-(n+1)\left(16\left|M'\right|-1\right)\Bigg[2\left|M'\right|\Big[8\left|M'\right|\left(-16(n+1)\left|M'\right|\right.\\
&+n\left(3-2\sqrt{1-16\left|M'\right|}\right)\ \left.-2\sqrt{1-16\left|M'\right|}+4\rho+3\right)\\
&+n\left(\sqrt{1-16\left|M'\right|}-1\right)+2\rho\left(3\sqrt{1-16\left|M'\right|}-5\right)\\
&\left.+\sqrt{1-16\left|M'\right|}-1\Big]+\rho\left(-\sqrt{1-16\left|M'\right|}\right)+\rho\Bigg]\,,
\end{aligned} \tag{B.32}$$

$$
\begin{aligned}
\beta_n =& 2\left|M'\right|\Bigg[-4\left|M'\right|\Bigg(16\left|M'\right|\Bigg(-2\ell(\ell+1)\left(\sqrt{1-16\left|M'\right|}-2\right)\\
&+16\left(6n^2+3n+\sigma\right)\left|M'\right|+(5n(2n+1)+\sigma)\sqrt{1-16\left|M'\right|}\\
&-2(5n(2n+2\rho+1)+2\rho+\sigma)\Big)+\ell(\ell+1)\left(6\sqrt{1-16\left|M'\right|}-8\right)\\
&-\sqrt{1-16\left|M'\right|}(3n(6n+16\rho+3)+8\rho+\sigma)+22n^2+n(84\rho+11)\\
&+4\rho(4\rho+3)+\sigma\Bigg)+\ell(\ell+1)\left(\sqrt{1-16\left|M'\right|}-1\right)\\
&-\left(2n^2+20n\rho+n+2\rho(6\rho+1)\right)\sqrt{1-16\left|M'\right|}\\
&+2n^2+24n\rho+n+2\rho(10\rho+1)\Bigg]+\rho(n+2\rho)\left(\sqrt{1-16\left|M'\right|}-1\right),
\end{aligned}
\tag{B.33}
$$

$$
\begin{aligned}
\gamma_n =& 2\left|M'\right|\Bigg[4\left|M'\right|\Bigg(8\left|M'\right|\Bigg(2\ell(\ell+1)\left(5-3\sqrt{1-16\left|M'\right|}\right)\\
&+16(13(n-1)n+5\sigma)\left|M'\right|+4(4(n-1)n+\sigma)\sqrt{1-16\left|M'\right|}\\
&+n(-33n-32\rho+33)+20\rho-9\sigma)+\ell(\ell+1)\left(7\sqrt{1-16\left|M'\right|}-9\right)\\
&-2\sqrt{1-16\left|M'\right|}(2n(3n+7\rho-3)-9\rho+\sigma)\\
&+2\left(20n\rho+7(n-1)n+4\rho^2-13\rho+\sigma\right)\Bigg)\\
&-\left(\sqrt{1-16\left|M'\right|}-1\right)\left(\ell(\ell+1)-n(n+6\rho-1)-4(\rho-1)\rho\right)\Bigg],
\end{aligned}
\tag{B.34}
$$

$$
\begin{aligned}
\delta_n =& 8\left|M'\right|^2\Bigg[8\left|M'\right|\Big[2\ell(\ell+1)\left(\sqrt{1-16\left|M'\right|}-1\right)\\
&-16(3n(2n-5)+4\sigma+6)\left|M'\right|-2(n(2n-5)+\sigma)\sqrt{1-16\left|M'\right|}\\
&-4\sqrt{1-16\left|M'\right|}+n(10n+8\rho-25)-12\rho+6\sigma+10\Big]\\
&-\left(\sqrt{1-16\left|M'\right|}-1\right)\left(\ell(\ell+1)+n(-2n-4\rho+5)+6\rho-\sigma-2\right)\Bigg],
\end{aligned}
\tag{B.35}
$$

$$
\zeta_n = 64\epsilon^3(16\epsilon+1)((n-4)n+\sigma+3). \tag{B.36}
$$

B.3 Ambiguity of the potential modifications

Here we list the explicit form of the coefficients of equation (5.12) when one transforms the radial Teukolsky function as (5.8). These values hold for $s=-2$:

$$\overline{A}_j^{(-3)} = \frac{a^6}{2} j(j+1)(j+2)\,, \qquad \overline{A}_j^{(-2)} = -\frac{3a^4}{2} j(j+1)^2\,, \tag{B.37}$$

$$\overline{A}_j^{(-1)} = \frac{a^4}{2} j\left[3j(j+1) - 4B + 4m^2 - 8i\omega + 10\right] + 4ia^3 jm \tag{B.38}$$

$$+ \frac{3}{2} a^2 j\left(j^2 + j - 1\right)\,, \tag{B.39}$$

$$\overline{A}_j^{(0)} = a^3(2j-1)\left[a\omega(\omega - 4i) - 2m(\omega + 2i)\right]$$

$$- a^2\left[3j^3 - j\left(4B - 2m^2 + 4i\omega - 1\right) + B + 2\right] \tag{B.40}$$

$$- 4iajm - \frac{1}{2} j\left(j^2 - 4\right)\,, \tag{B.41}$$

$$\overline{A}_j^{(1)} = 2a^4(j-1)\omega^2 + \frac{1}{2} a^2\Big[3j^2(j-1) + 4B + 2\omega(\omega - 16i) + 8 \tag{B.42}$$

$$+ j\left(-8B + 4m^2 - 4\omega(\omega - 8i) + 2\right)\Big]$$

$$+ 2am\left[2j(\omega + 3i) - \omega - 2i\right] \tag{B.43}$$

$$+ \frac{1}{2} j\left[3(j-1)j - 4B - 11\right] + B + 2\,, \tag{B.44}$$

$$\overline{A}_j^{(2)} = a^2\omega\left[\omega - 16i(j-1)\right] - 2a(2j-1)m(\omega + 2i) \tag{B.45}$$

$$+ \frac{1}{2} j(-3(j-2)j + 8B - 24i\omega + 13) - 3(B - 4i\omega + 2)\,, \tag{B.46}$$

$$\overline{A}_j^{(3)} = 2a^2(2j-3)\omega^2 + \frac{1}{2}(j-1)\left[(j-2)j - 4(B+2)\right] + 4i(5j-6)\omega\,, \tag{B.47}$$

$$\overline{A}_j^{(4)} = 2\omega\left[2(\omega + 3i) - j(\omega + 4i)\right]\,, \qquad \overline{A}_j^{(5)} = 2(j-2)\omega^2\,. \tag{B.48}$$

B.4 Nollert's improvements of continued fraction

The procedure to numerically solve Teukolsky equation through Leaver's method requires in practice an initialization for the radial ladder operator λ_n^r. Such quantity can be expanded for large initialization number N as

$$\lambda_N^r = \sum_{j=0}^{J} C_j N^{-j/2} + \mathcal{O}\left(N\right)^{-(J+1)/2}\,. \tag{B.49}$$

One can initialize the ladder operator just retaining the first term $C_0 = -1$. However, this approximation requires in general a very high initial value for N (which means long computational time) and appears to be insufficient for frequencies with large imaginary part (namely higher overtones). In [559], it was shown that adding further corrections to the initial λ_N^r improves the accuracy of the method, also allowing to capture higher overtones. The $(k+3)$-terms recurrence relation of equation (5.42) for $n = N$ can be expressed as

$$\sum_{j=-1}^{k+1} M_{N,j}\, R_{N-j} = 0\,, \tag{B.50}$$

where we defined

$$M_{N,j} \equiv \widetilde{\gamma}_{N,j-1} + \widetilde{\beta}_{N,j} + \widetilde{\alpha}_{N,j+1}\,. \tag{B.51}$$

Dividing it by R_{N-k-1} and using the definition of ladder operator $\lambda^r_N = -a_{N+1}/a_N$ one obtains the equation

$$\sum_{j=-1}^{k+1} (-1)^j \, M_{N,j} \prod_{i=j+1}^{k+2} \lambda^r_{N-i} = 0 \,. \tag{B.52}$$

Plugging the definition (B.49) into the above formula, one can solve for the coefficients order by order. By the definition of $\widetilde{\gamma}_{N,j}$, $\widetilde{\beta}_{N,j}$ and $\widetilde{\alpha}_{N,j}$, they scale with N as

$$\widetilde{\alpha}_{N,j} = N^2 + \widetilde{\alpha}_1 N + \widetilde{\alpha}_0 \tag{B.53}$$

$$\widetilde{\beta}_{N,j} = -2N^2 + \widetilde{\beta}_1 N + \widetilde{\beta}_0 \tag{B.54}$$

$$\widetilde{\gamma}_{N,j} = N^2 + \widetilde{\gamma}_1 N + \widetilde{\gamma}_0 \tag{B.55}$$

If we fix $C_0 = -1$, then the other coefficients up to $J = 5$ can be written as

$$C_1 = \pm \sqrt{-\widetilde{\alpha}_1 - \widetilde{\beta}_1 - \widetilde{\gamma}_1} \,, \tag{B.56}$$

$$C_2 = \widetilde{\alpha}_1 + \frac{\widetilde{\beta}_1}{2} - \frac{1}{4} \,, \tag{B.57}$$

$$C_3 = \frac{C_2^2}{2C_1} - \frac{C_2}{4C_1} - \frac{\widetilde{\alpha}_0 + \widetilde{\beta}_0 + \widetilde{\gamma}_0}{2C_1} - \frac{1 + 2\widetilde{\alpha}_1}{4} C_1 \,, \tag{B.58}$$

$$C_4 = \widetilde{\alpha}_0 - \frac{4\widetilde{\alpha}_1 - 8\widetilde{\beta}_0 + 1}{16} - \frac{1 + 4\widetilde{\alpha}_1}{4} C_2 - \frac{C_3}{2C_1} \,, \tag{B.59}$$

$$\begin{aligned} C_5 = {} & \frac{2\widetilde{\alpha}_1 + 3}{4C_1} C_2^2 - \frac{8\widetilde{\alpha}_0 + 4\widetilde{\alpha}_1 + 3}{16} C_1 - \frac{C_3^2}{2C_1} \\ & - \frac{4\widetilde{\alpha}_1 + 3}{16C_1} C_2 + C_3 \left(\frac{C_2}{2C_1^2} - \widetilde{\alpha}_1 - 1 \right) + \left(\frac{C_2}{C_1} - \frac{3}{4C_1} \right) C_4 \,, \end{aligned}$$

and the sign of C_1 is chosen such that $\mathrm{Re}\,(C_1) > 0$.

We can do the same expansion for the angular part, by expanding

$$\lambda^\theta_N = \sum_{j=0}^{J} D_j N^{-j/2} + \mathcal{O}\,(N)^{-(J+1)/2} \,. \tag{B.60}$$

From equations (5.26)–(5.28) we can schematically say that

$$\alpha^\theta_N = -2N^2 + \alpha_1 N + \alpha_0 \tag{B.61}$$

$$\beta^\theta_N = N^2 + \beta_1 N + \beta_0 \tag{B.62}$$

$$\gamma^\theta_N = \gamma_1 N + \gamma_0 \tag{B.63}$$

By solving perturbatively in $1/N$ the relation (5.29), we obtain the following expression for the coefficients D_j up to $J = 4$

$$D_0 = 0 \tag{B.64}$$

$$D_1 = \gamma_1 \tag{B.65}$$

$$D_2 = \gamma_0 - \gamma_1 \,(1 + \beta_1 + 2\gamma_1) \tag{B.66}$$

$$\begin{aligned} D_3 = {} & \gamma_1^2(\alpha_1 - 2) - \gamma_1(1 + \beta_0 + \beta_1) - D_2(\beta_1 + 4\gamma_1 + 2) \\ D_4 = {} & \alpha_0\gamma_1^2 + \frac{2D_2^2\,(\beta_1 + 3\gamma_1 + 2)}{\gamma_1} + D_2\,(\beta_0 + \beta_1 + 2\gamma_1 + 1) \\ & + D_3 \left(\frac{2D_2}{\gamma_1} - \beta_1 - 4\gamma_1 - 2 \right) \end{aligned} \tag{B.67}$$

B.5 Derivation of the appropriate boundary conditions

The correct implementation of the continued fraction method requires that the ansatz that one assumes properly encodes the behavior of the solution close to the singular points of the equation. We will now show how such ansätze are properly derived in the beyond-Teukolsky case.

Following [276], it is convenient to introduce the new master field

$$Y(r) = \Delta^{\frac{s}{2}} \left(r^2 + a^2\right)^{\frac{1}{2}} R(r)\,, \tag{B.68}$$

and the tortoise coordinate r_* defined by

$$\frac{\mathrm{d}r_*}{\mathrm{d}r} = \frac{r^2 + a^2}{\Delta}\,, \tag{B.69}$$

Note that this tortoise coordinate has the asymptotic behavior

$$\begin{aligned} r_* &\xrightarrow{r\to\infty} r\,, \\ r_* &\xrightarrow{r\to r_+} \frac{r_+}{\beta}\ln(r - r_+)\,. \end{aligned} \tag{B.70}$$

This choice allows to rewrite the modified Teukolsky equation in a form in which the first derivative of the master variable does not appear.

For $r \to \infty$ it reads

$$\frac{\mathrm{d}^2}{\mathrm{d}r_*^2}Y + \left[\left(\omega^2 + \frac{\tilde{\alpha}^{(2)}}{r_*^4}\right) + \left(2is\omega + \frac{\tilde{\alpha}^{(1)}}{r_*^3} - \frac{\tilde{\alpha}^{(2)}}{r_*^4}\right) r^{-1}\right] Y = 0\,. \tag{B.71}$$

According with the boundary conditions for QNMs, we choose the outgoing solution, which reads $Y \sim r^{p-s}e^{qr_*}$, where the parameter p and q are the ones introduced in Eq. (5.34) and (5.35).

On the other hand, as $r \to r_+$, the modified Teukolsky equation reads

$$\frac{\mathrm{d}^2}{\mathrm{d}r_*^2}Y + r_+^{-2}\left[\left(k_+ - is\frac{\beta}{2}\right)^2 + \sum_{-K}^{4}\alpha^{(k)}\right] Y = 0\,, \tag{B.72}$$

where $k_+ = r_+\omega - am = \beta\sigma_{\mathrm{GR}}$. In this case, we want the solution to be purely ingoing, so we have

$$Y \sim \exp\left(-\frac{ir_*}{r_+}\sqrt{\left(k_+ - is\frac{\beta}{2}\right)^2 + \sum_{-K}^{4}\alpha^{(k)}}\right) \sim (r - r_+)^{-i\sigma - \frac{is}{2}}\,, \tag{B.73}$$

where σ is defined in Eq. (5.33).

Considering the factor relating the master fields Y and R, we obtain

$$\begin{aligned} R &\xrightarrow{r\to\infty} e^{iqr}r^{p-2s-1}\,, \\ R &\xrightarrow{r\to r_+} (r - r_+)^{-i\sigma - s}\,. \end{aligned} \tag{B.74}$$

One can then easily verify that the ansatz of Eq. (5.13), with the generalized definitions of σ, p and q, correctly encodes the behavior of the solution $R(r)$ at the boundaries.

B.6 Splitting of the potential

In this section of the appendix we show how to transform the potential (5.2) into the potential (5.32). We start by splitting equation (5.2) into

$$\begin{aligned}\Delta V(r) &= \frac{1}{\Delta}\sum_{k=-K}^{4}\alpha^{(k)}\left(\frac{r}{r_+}\right)^k \\ &= \frac{1}{\Delta}\sum_{k=0}^{4}\alpha^{(k)}\left(\frac{r}{r_+}\right)^k + \frac{1}{\Delta}\sum_{k=1}^{K}\alpha^{(-k)}\left(\frac{r_+}{r}\right)^k \end{aligned} \tag{B.75}$$

For $k \geq 1$, the first generic term in k of the sum can be rewritten as

$$\begin{aligned}\frac{\alpha^{(k)}}{\Delta}\left(\frac{r}{r_+}\right)^k &= \frac{\alpha^{(k)}}{\Delta}\left(\frac{r^k - r_+^k}{r_+^k} + 1\right) \\ &= \alpha^{(k)}\left[\frac{1}{\Delta} + \frac{1}{r_+(r-r_-)}\sum_{j=0}^{k-1}\left(\frac{r}{r_+}\right)^j\right] \end{aligned} \tag{B.76}$$

For $k \geq 2$ we can further simplify this term as

$$\begin{aligned}\frac{\alpha^{(k)}}{\Delta}\left(\frac{r}{r_+}\right)^k &= \alpha^{(k)}\left[\frac{1}{\Delta} + \frac{1}{r_+(r-r_-)}\sum_{j=0}^{k-1}\frac{r^j - r_-^j + r_-^j}{r_+^j}\right] \\ &= \alpha^{(k)}\left[\frac{1}{\Delta} + \frac{1}{r_+(r-r_-)}\sum_{j=0}^{k-1}\left(\frac{r_-}{r_+}\right)^j + \frac{1}{r_-r_+}\sum_{j=1}^{k-1}\left(\frac{r_-}{r_+}\right)^j\sum_{n=0}^{j-1}\left(\frac{r}{r_-}\right)^n\right] \\ &= \alpha^{(k)}\left[\frac{1}{\Delta} + \frac{1}{r_+(r-r_-)}\sum_{j=0}^{k-1}\left(\frac{r_-}{r_+}\right)^j + \frac{1}{r_+^2}\sum_{j=0}^{k-2}\left(\frac{r}{r_-}\right)^j\sum_{n=j}^{k-2}\left(\frac{r_-}{r_+}\right)^n\right] \end{aligned} \tag{B.77}$$

where we obtained the last line by expanding the series and collecting the terms in r to the same power. Summing over all the non-negative values of k yields

$$\frac{1}{\Delta}\sum_{k=0}^{4}\alpha^{(k)}\left(\frac{r}{r_+}\right)^k = \frac{1}{\Delta}\sum_{k=0}^{4}\alpha^{(k)} + \frac{1}{r_+(r-r_-)}\sum_{k=1}^{4}\alpha^{(k)}\sum_{j=0}^{k-1}\left(\frac{r_-}{r_+}\right)^j \tag{B.78}$$

$$+ \frac{1}{r_+^2}\sum_{k=0}^{2}\left(\frac{r}{r_+}\right)^k\sum_{j=k}^{2}\alpha^{(j+2)}\sum_{n=0}^{j}\left(\frac{r_-}{r_+}\right)^n \tag{B.79}$$

Now, we can perform a mapping between the coefficients $\alpha^{(k)}$ of equation (5.2) and the coefficients $A^{(0)}$, $A^{(1)}$ and $\widetilde{\alpha}^{(k)}$ introduced in equations (5.32). From a direct comparison we have

$$A^{(0)} = \sum_{k=0}^{4}\alpha^{(k)} \tag{B.80}$$

$$A^{(1)} = \sum_{k=1}^{4}\alpha^{(k)}\sum_{j=0}^{k-1}\left(\frac{r_-}{r_+}\right)^j \tag{B.81}$$

$$\widetilde{\alpha}^{(k)} = \sum_{j=k}^{2}\alpha^{(j+2)}\sum_{n=0}^{j}\left(\frac{r_-}{r_+}\right)^n \tag{B.82}$$

B.7 Diagonal quadratic coefficients

We show here how to compute the quadratic diagonal coefficients, defined from the next-to-leading-order expansion

$$\begin{aligned}\omega &\simeq \omega^0 + \sum_k d_\omega^{(k)}\alpha^{(k)} + \frac{1}{2}e_\omega^{(k)}\alpha^{(k)^2}\,,\\ B &\simeq B^0 + \sum_k d_B^{(k)}\alpha^{(k)} + \frac{1}{2}e_B^{(k)}\alpha^{(k)^2}\,.\end{aligned} \tag{B.83}$$

By extending the Taylor expansion (5.5) to the second order in α, we obtain

$$\mathcal{L}_j\big|_{\rm GR} + \alpha\,\frac{\mathrm{d}\mathcal{L}_j}{\mathrm{d}\alpha}\bigg|_{\rm GR} + \frac{\alpha^2}{2}\,\frac{\mathrm{d}^2\mathcal{L}_j}{\mathrm{d}\alpha^2}\bigg|_{\rm GR} + \mathcal{O}(\alpha)^3 = 0\,. \tag{B.84}$$

By expanding with the chain rule the total derivative $\mathrm{d}^2\mathcal{L}_j/\mathrm{d}\alpha^2|_{\rm GR}$, one can read off the quadratic coefficients as

$$\begin{aligned}
e_\omega = &\left(\frac{\partial\mathcal{L}_r}{\partial B}\frac{\partial\mathcal{L}_\theta}{\partial\omega} - \frac{\partial\mathcal{L}_r}{\partial\omega}\frac{\partial\mathcal{L}_\theta}{\partial B}\right)^{-1}\left[\frac{\partial^2\mathcal{L}_r}{\partial\alpha^2}\frac{\partial\mathcal{L}_\theta}{\partial B} + 2d_\omega\,\frac{\partial^2\mathcal{L}_r}{\partial\alpha\partial\omega}\frac{\partial\mathcal{L}_\theta}{\partial B}\right.\\
&+ 2d_B\,\frac{\partial^2\mathcal{L}_r}{\partial\alpha\partial B}\frac{\partial\mathcal{L}_\theta}{\partial B} - d_\omega^2\left(\frac{\partial^2\mathcal{L}_\theta}{\partial\omega^2}\frac{\partial\mathcal{L}_r}{\partial B} - \frac{\partial^2\mathcal{L}_r}{\partial\omega^2}\frac{\partial\mathcal{L}_\theta}{\partial B}\right)\\
&- d_B^2\left(\frac{\partial^2\mathcal{L}_\theta}{\partial B^2}\frac{\partial\mathcal{L}_r}{\partial B} - \frac{\partial^2\mathcal{L}_r}{\partial B^2}\frac{\partial\mathcal{L}_\theta}{\partial B}\right)\\
&\left.+ 2d_\omega\,d_B\left(\frac{\partial^2\mathcal{L}_r}{\partial\omega\partial B}\frac{\partial\mathcal{L}_\theta}{\partial B} - \frac{\partial^2\mathcal{L}_\theta}{\partial\omega\partial B}\frac{\partial\mathcal{L}_r}{\partial B}\right)\right],\\
e_B = &-\left(\frac{\partial\mathcal{L}_r}{\partial B}\frac{\partial\mathcal{L}_\theta}{\partial\omega} - \frac{\partial\mathcal{L}_r}{\partial\omega}\frac{\partial\mathcal{L}_\theta}{\partial B}\right)^{-1}\left[\frac{\partial^2\mathcal{L}_r}{\partial\alpha^2}\frac{\partial\mathcal{L}_\theta}{\partial\omega} + 2d_\omega\,\frac{\partial^2\mathcal{L}_r}{\partial\alpha\partial\omega}\frac{\partial\mathcal{L}_\theta}{\partial\omega}\right.\\
&+ 2d_B\,\frac{\partial^2\mathcal{L}_r}{\partial\alpha\partial B}\frac{\partial\mathcal{L}_\theta}{\partial\omega} - d_\omega^2\left(\frac{\partial^2\mathcal{L}_r}{\partial\omega^2}\frac{\partial\mathcal{L}_\theta}{\partial\omega} - \frac{\partial^2\mathcal{L}_\theta}{\partial\omega^2}\frac{\partial\mathcal{L}_r}{\partial\omega}\right)\\
&- d_B^2\left(\frac{\partial^2\mathcal{L}_r}{\partial B^2}\frac{\partial\mathcal{L}_\theta}{\partial\omega} - \frac{\partial^2\mathcal{L}_\theta}{\partial B^2}\frac{\partial\mathcal{L}_r}{\partial\omega}\right)\\
&\left.+ 2d_\omega\,d_B\left(\frac{\partial^2\mathcal{L}_r}{\partial\omega\partial B}\frac{\partial\mathcal{L}_\theta}{\partial\omega} - \frac{\partial^2\mathcal{L}_\theta}{\partial\omega\partial B}\frac{\partial\mathcal{L}_r}{\partial\omega}\right)\right],
\end{aligned} \tag{B.85}$$

Appendix C

Systematic biases: validation tests and further exploration of the parameter space

C.1 Reliability of the linear signal regime

In Sec. 6.3, we used the linear signal approximation to estimate both, statistical and systematic errors. For an accurate estimation of the statistical error, the validity of the linear signal approximation coincides with the validity of the Fisher approximation [540]. Typically, when the SNR is large, considering linear deviations in the template around the maximum likelihood is equivalent to approximating the likelihood surface around the maximum as Gaussian.

We also used the linear signal approximation to estimate $\Delta^{(\mathrm{Sys})}\theta^i$, which is the systematic error caused by the waveform inaccuracy.

Essentially, we made the approximation that the difference between $h_{\mathrm{AP}}(\boldsymbol{\theta}_{\mathrm{bf}}; f)$ and $h_{\mathrm{AP}}(\boldsymbol{\theta}_{\mathrm{tr}}; f)$ is linear in $\Delta^{(\mathrm{Sys})}\theta^i$. The validity criteria of the linear signal approximation for estimating statistical errors (as given in [540]) does not apply for estimating systematic errors (which are induced by waveform inaccuracy). A fundamental reason for this is that the systematic error is independent of the SNR, which can be seen from the fact that $\Delta^{(\mathrm{Sys})}\theta^i$ given Eq. (6.20) is SNR scale invariant. The SNR scale invariance of the systematic error holds even beyond the linear signal approximation because Eq. (6.19) is SNR scale invariant, making the estimation of θ^i_{bf} (which is a solution to Eq. (6.19)) also SNR scale invariant. The validity of the linear signal approximation for computing the systematic error is essentially tied to the magnitude of difference between the two waveform templates. When the difference between h_{GR} and h_{AP} is "large", we expect that the simple linear approximation should not hold.

To further quantify the validity regime of the linear signal approximation, we obtain the explicit dependence of $\Delta\theta^i$ on the template difference by considering linear changes between h_{GR} and h_{AP}. Following [503, 513], we first express $h_{\mathrm{GR}}(\boldsymbol{\theta}_{\mathrm{tr}}; f) = A_{\mathrm{GR}}(\boldsymbol{\theta}_{\mathrm{tr}}; f) \exp\left[i\Psi_{\mathrm{GR}}(\boldsymbol{\theta}_{\mathrm{tr}}; f)\right]$ and $h_{\mathrm{AP}}(\boldsymbol{\theta}_{\mathrm{tr}}; f) = A_{\mathrm{AP}}(\boldsymbol{\theta}_{\mathrm{tr}}; f) \exp\left[i\Psi_{\mathrm{AP}}(\boldsymbol{\theta}_{\mathrm{tr}}; f)\right]$, where recall that h_{AP} is only evaluated at the parameters common with h_{GR}. Introducing $\Delta A(\boldsymbol{\theta}_{\mathrm{tr}}; f) \approx A_{\mathrm{GR}}(\boldsymbol{\theta}_{\mathrm{tr}}; f) - A_{\mathrm{AP}}(\boldsymbol{\theta}_{\mathrm{tr}}; f)$, and likewise $\Delta\Psi(\boldsymbol{\theta}_{\mathrm{tr}}; f) \approx \Psi_{\mathrm{GR}}(\boldsymbol{\theta}_{\mathrm{tr}}; f) - \Psi_{\mathrm{AP}}(\boldsymbol{\theta}_{\mathrm{tr}}; f)$, the systematic error $\Delta^{(\mathrm{Sys})}\theta^i$ simpli-

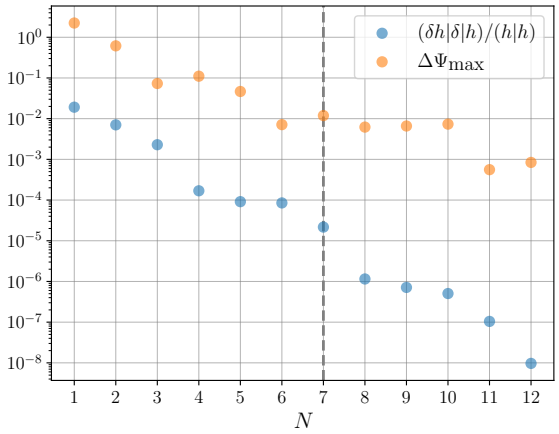

Figure C.1: Relative waveform error (blue dots) and the maximum dephasing (orange dots) between $h_{\rm AP}$ and the fiducial template, as a function of the number of modes. The system has primary mass $5\times10^6\,M_\odot$ and is located at luminosity distance 5 Gpc, with fixed $\theta=\psi=\iota=\pi/3$ and $\phi=0$. $N_{\rm min}=7$ is shown with the vertical dashed line. Observe that with increasing N, the dephasing and relative waveform errors decrease appreciably, allowing for the use of the linear signal approximation in estimating $N_{\rm min}$.

fies to

$$\Delta^{(\rm Sys)}\theta^a \approx \underbrace{\left(\Gamma^{-1}\right)^{ab}\left([\Delta A + iA_{\rm AP}\Delta\Psi]\,e^{i\Psi_{\rm AP}}\middle|\partial_b h_{\rm AP}\right)}_{\theta^a=\theta^a_{\rm tr}}. \tag{C.1}$$

Since $\Delta^{(\rm Sys)}\theta^a$ scales linearly with both ΔA and $\Delta\Psi$, neglecting $\mathcal{O}((\Delta^{(\rm Sys)}\theta^a)^2)$ is formally equivalent to neglecting $\mathcal{O}((\Delta\Psi)^2)$, $\mathcal{O}((\Delta A)^2)$, and $\mathcal{O}((\Delta\Psi)(\Delta A))$ terms. Thus, the linear regime is determined by $\Delta\Psi\ll1$ and $\Delta A\ll A_{\rm AP}$ (or $\Delta A\ll A_{\rm GR}$). For instance, when $\Delta\Psi\gtrsim1$, we expect significant dephasing between the two templates, resulting in large biases and a breakdown of the linear signal approximation. The amplitude corrections are small when the relative waveform error $(\delta h|\delta h)/\rho^2$ is small, where $\delta h=h_{\rm GR}-h_{\rm AP}$. Indeed, when the relative waveform error is small and the SNR ratio of $h_{\rm GR}$ and $h_{\rm AP}$ is close to 1, we also have that [104, 508, 513, 521] $(\delta h|\delta h)/(2\rho^2)\approx(1-\mathcal{M})$. In the mismatch criterion given by Eq. (6.25), we essentially neglect relative waveform and relative SNR errors, and work in the limit of the match being close to 1. Thus, by checking when $(\delta h|\delta h)/\rho^2$, we validate the linear signal approximation, which is explicitly used in Eq. (6.20), and implicitly used in Eq. (6.25).

In Fig. C.1, using the fiducial ringdown template described by Eq. (6.4), we illustrate the dependence of the maximum dephasing $\Delta\Psi_{\rm max}$ and the relative waveform error $(\delta h|\delta h)/\rho^2$ on the number of modes N. We consider the same system as the one in Fig. 6.3, where we fixed $\theta=\psi=\iota=\pi/3$ and $\phi=0$. Recall that we estimated the minimum number of modes for this system to be $N_{\rm min}=7$. As expected, with increasing N, both $\Delta\Psi_{\rm max}$ and $(\delta h|\delta h)/\rho^2$ decrease, implying that the absolute and relative errors are increasingly negligible when more modes are included.

We see that when $N<3$, although relative waveform errors are at the percent level, the maximum dephasing is close to 1, suggesting that the linear signal approximation is not valid. Recall that one of the features that we observed in Fig. 6.3 was the oscillatory behavior of $\Delta^{(\rm Sys)}\theta^i$ with increasing N for $N<3$. Such an oscillatory behavior is tied to the breakdown of the linear signal approximation. We can see this through the oscillatory $\exp(i\Delta\Psi)$ dependence in $\Delta^{(\rm Sys)}\theta^i$ (when one does not further linearize $\Delta^{(\rm Sys)}\theta^i$ in $\Delta\Psi$). As N increases to $3\leq N<6$, we observe that $\Delta\Psi_{\rm max}$ drops to $\mathcal{O}(10^{-1})$, and we enter the regime where the linear signal approximation is valid. Crucially, for $N\geq6$, $\Delta\Psi_{\rm max}$ is $\mathcal{O}(10^{-2})$, ensuring that the linear signal approximation is indeed valid in estimating the minimum number of modes, and that our estimate of $N_{\rm min}=7$ is robust. While we demonstrated this validity for a particular system in Fig. C.1, the arguments apply across

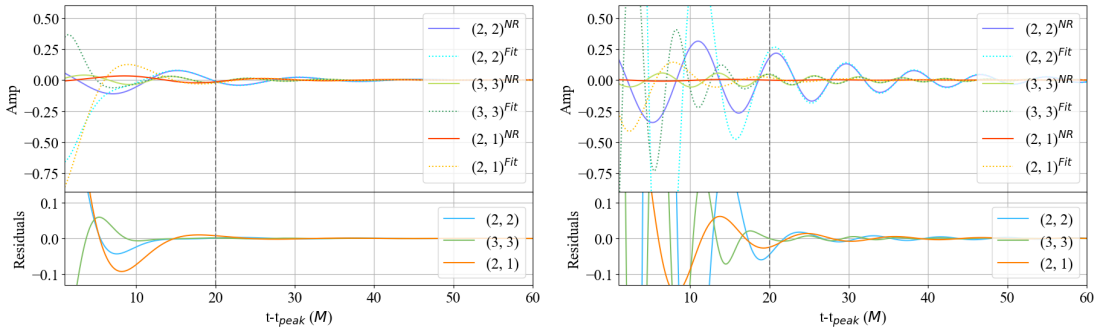

(a) SXS:BBH:0303 with non-rotating BHs and q=0.1. (b) SXS:BBH:0257 with $a_1 = a_2 = 0.85$ and $q = 0.5$.

Figure C.2: Comparison of multipoles drawn from NR simulations with multipoles obtained from Eq. (C.2).

parameter space. The agreement between our estimate of $N_{\rm min}$ based on the (explicit linear signal approximation) criteria in Eq. (6.23) and the (implicit linear signal approximation) criteria in Eq. (6.25) further strengthens the robustness and self-consistency obtained within the linear signal approximation.

C.2 Comparison with NR waveforms

When fitting numerical simulations using a superposition of QNMs, the analysis typically begins at progressively later times until the linear regime associated with a particular QNM emerges within the nonlinear numerical solution [530, 534, 549]; see, however, [535] for a different perspective. Thus, one natural approach to assess the presence of a QNM consists in observing a stable amplitude for a given time duration. This generally occurs at intermediate times, with the exception of the dominant mode 220. Once the amplitude is stable, its value is extracted and extrapolated to t$_{peak}$, with t$_{peak}$ the time of the luminosity peak of the $(2, 2)$ mode. Therefore, highly damped QNMs, such as the overtones, present fitted amplitudes much larger than actually present in the numerical solution. This means that if one were to compute the SNR of the individual QNMs close to $t = t_{\rm peak}$, the SNR of the overtones would be larger than for the fundamental tones.

As explained in Sec. 6.3, to prevent this effect and, more generally, back-extrapolation from corrupting our analysis, we choose the ringdown starting time $t = t_0$ by comparing the ringdown model in Eq. (6.4) (with the fits in [488, 530]) directly with NR simulations. In particular, we require that, for each (ℓ, m), the difference between the amplitude obtained from the fits and that extracted from the simulation to be smaller than a prescribed tolerance. We select two sources from the catalog of the SXS collaboration [560], SXS:BBH:0303 and SXS:BHB:0257, which correspond to $(a_1 = a_2 = 0, q = 0.1)$ and $(a_1 = a_2 = 0.85, q = 0.5)$ respectively. To compare the amplitudes, we first decompose the NR signal into its multipole (ℓ, m) components and then compare them with $h^{Fit}_{\ell m}$, obtained from the fitted amplitudes after summing over the overtone number, i.e.

$$h^{Fit}_{\ell m} = \sum_{\ell'=-\ell}^{\ell'=\ell} \mu_{\ell\ell' m' n'} h_{\ell' m' n'} \delta_{m m'}, \tag{C.2}$$

where $\mu_{\ell\ell' m' n'}$ are the spherical-spheroidal mixing coefficients [561, 562]. Note that in this expression, the linear perturbation framework is respected and only the modes that fulfill $m' = m$ are considered. To give some context, modes with $m' \neq m$ (known as 'recoil' modes) are present in several NR waveforms due to extrapolation at null infinity.

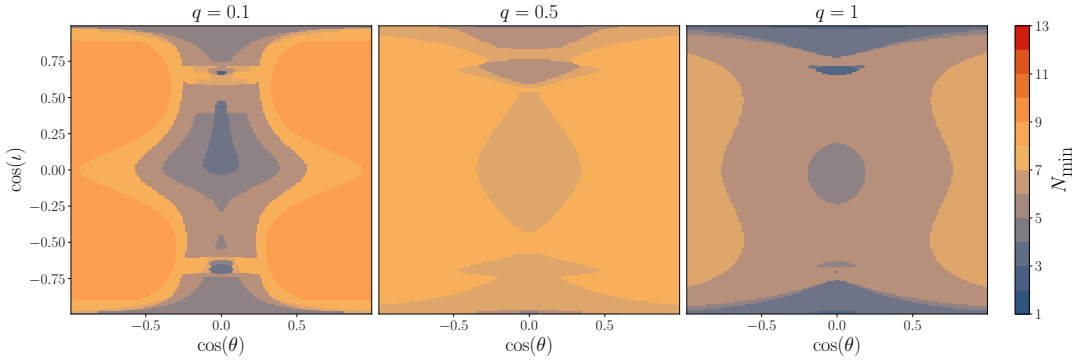

Figure C.3: Dependence of $N_{\rm min}$ on the cosine of the angles θ and ι, for three values of the mass ratio of the progenitors q and $a_1 = a_2 = 0$. The primary BH mass and the luminosity distance have been fixed respectively to $5 \times 10^6 M_\odot$ and 5 Mpc. $N_{\rm min}$ is represented by the color code. Observe that the color pattern is symmetric with respect to $\cos\theta = 0$, while the corresponding symmetry about $\cos\iota = 0$ is slightly broken. Observe also that some patterns present in the right panel disappear in the middle one, to appear again in the mass-symmetric case (left panels). This is the consequence of the competing effects at play when the progenitor mass ratio changes, namely (de)excitation of odd-m modes against changes in the global SNR.

If, instead, one extracts the numerical waveforms with the Cauchy-characteristic extraction technique in the superrest (BMS) frame [548, 563, 564], these recoil modes vanish.

The amplitude residuals and the two waveforms are shown in Fig. C.2. Note that at early times, the overtones from the fitted model dominate the signal, while matching the NR waveform as the time increases. Considering two different sets of parameters, we decide to set the starting time of the ringdown to $t_0 = 20M$ as a compromise between the residuals and the loss of SNR in both cases.

C.3 The impact of spins, mass ratio and angles on $N_{\rm min}$

In this Appendix, we comment more extensively on the dependence of $N_{\rm min}$ on the other parameters, which we briefly discussed in the main text. We restrict the discussion to binary systems with fixed primary BH mass of $5 \times 10^6 M_\odot$ at luminosity distance $d_L =$ 5Mpc.

In Fig. C.3, we show the dependence of $N_{\rm min}$ on the angles ι and θ, fixing the progenitors spins to $a_1 = a_2 = 0$ and $q = 0.1, 0.5, 1$. First, we notice that the patterns are completely symmetric around $\cos\theta = 0$, whereas there is a slight symmetry breaking in the two hemispheres defined by $\cos\iota = 0$. This is indeed what we expect, as two configurations with opposite sky localization with respect to the horizon are completely equivalent, while the corresponding symmetry in the BH frame is broken by the direction of the spin. Furthermore, it can be observed that the case with $q = 0.5$ represents an optimal configuration, where more modes are needed on average, compared to the other two cases. This happens because, as we decrease the mass ratio starting from $q = 1$, the QNM spectrum becomes richer, as odd-m modes are switched on. On the other hand, as we go to smaller mass ratios while keeping the primary mass fixed, the size of the region in which $N_{\rm min} < 5$ increases again. This happens because we are decreasing the total SNR of the event, although many modes are excited. For $q = 0.1$ there are still, however, marginal regions in which $N_{\rm min} > 6$.

In Fig. C.4, we show the dependence of $N_{\rm min}$ on the spin (upper panel) and mass ratio (lower panel) of the progenitors, for a system with primary mass $m_1 = 5 \times 10^6 M_\odot$ and

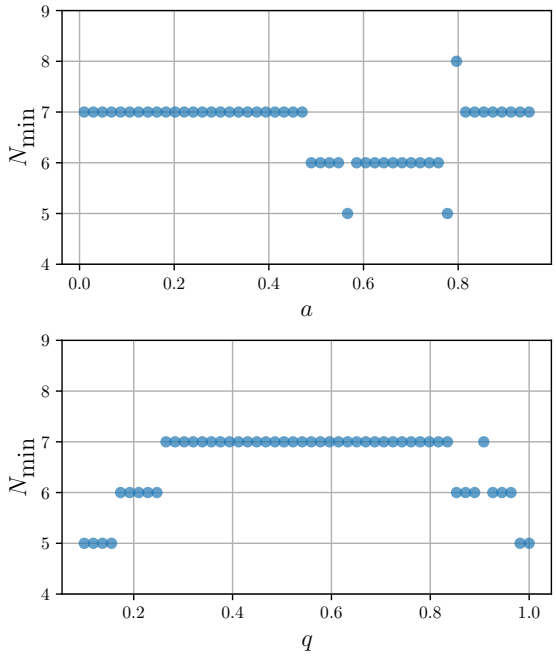

Figure C.4: Dependence of $N_{\rm min}$ on progenitor spins and mass ratio. The primary BH mass and the luminosity distance have been fixed respectively to $5 \times 10^6 M_\odot$ and 10 Gpc, while the angles have been fixed to $\theta = \psi = \iota = \pi/3$, $\phi = 0$. The jumps correspond to crossing of two or more modes in the single-mode SNR ordering.

luminosity distance $dL = 10\,\text{Gpc}$. The angles are fixed to $\theta = \psi = \iota = \pi/3$, $\phi = 0$, and we consider equal spins. The discontinuous behavior that can be observed in both panels reflects the evolution of the modes ordering. In particular, the sudden jumps correspond to the exchange of two or more modes in the SNR ranking.

We do not observe a clear trend of $N_{\rm min}$ in any of the two cases. Overall, the impact of spin and mass ratio is mainly on the ordering of the modes, and only changes $N_{\rm min}$ of ± 1 mode, a smaller fluctuation with respect to the variability introduced by the orientation angles and shown in Fig. C.3. For very loud sources requiring a large $N_{\rm min}$, variations due to spin and mass ratio become larger but remain mostly subdominant compared to those from sky location and inclination.

C.4 A mode-dependent exponential tapering in the frequency domain

In Sec. 6.2 we discussed and motivated our choice for the high-frequency cutoff. In this appendix, we briefly present a different possible approach. In order to better mitigate the spectral leakage due to mirroring, we modify the frequency-domain templates with the replacement $\Lambda^{+,\times}_{\ell mn} \to \tilde{\Lambda}^{+,\times}_{\ell mn}$, introducing the functions

$$\begin{aligned}
\tilde{\Lambda}^{+}_{\ell mn} &= \frac{2L^{+}_{\ell mn}}{\exp\left(\frac{2\pi f}{\omega_{\ell mn}} - 1\right) + 1} + \frac{2L^{-}_{\ell mn}}{\exp\left(\frac{2\pi f}{\omega_{\ell mn}} + 1\right) + 1} \\
\tilde{\Lambda}^{\times}_{\ell mn} &= \frac{2L^{+}_{\ell mn}}{\exp\left(\frac{2\pi f}{\omega_{\ell mn}} - 1\right) + 1} - \frac{2L^{-}_{\ell mn}}{\exp\left(\frac{2\pi f}{\omega_{\ell mn}} - 1\right) + 1}\,.
\end{aligned} \tag{C.3}$$

Recall that for $f \gg \omega_{\ell mn}, f \gg 1/\tau_{lmn}$, the high frequency tails due to mirroring scale as

$$\Lambda^{+}_{\ell mn} \sim \tau^{-1}_{\ell mn} f^{-2}\ ,\ \Lambda^{\times}_{\ell mn} \sim \omega_{\ell mn}\tau^{-1}_{\ell mn} f^{-3}. \tag{C.4}$$

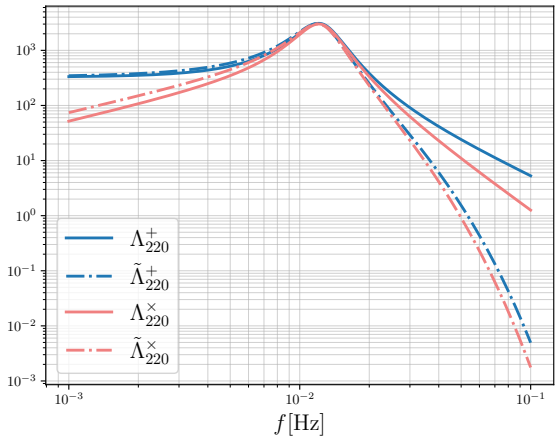

Figure C.5: Comparison between the functions $\Lambda^+_{\ell mn}$ (continuous lines) and $\tilde{\Lambda}^+_{\ell mn}$ (dot-dashed lines) for the 220 mode. The exponentially tapered functions recover the behavior of the standard combinations of Lorentzian combinations, while introducing a sharper cutoff at higher frequencies.

On the other hand, the phenomenologically tapered functions scale as

$$\tilde{\Lambda}^+_{\ell mn} \sim \frac{e^{-2\pi f/\omega_{\ell mn}}}{\tau_{\ell mn} f^2} \ , \ \tilde{\Lambda}^\times_{\ell mn} \sim \frac{\omega_{\ell mn} e^{-2\pi f/\omega_{\ell mn}}}{\tau_{\ell mn} f^3}. \tag{C.5}$$

Thus, our phenomenological tapering mimics a faster than exponential fall-off (due to $1/f^2$ and $1/f^3$ for the + and × polarizations respectively). This approach is conceptually similar to the frequency-domain tapering of IMR waveforms [565–567].

The comparison of these exponentially tapered functions and the standard combinations of Lorentzian functions is shown in Fig. C.5 for the 220 mode and a BH mass of $10^6\, M_\odot$.

Our tapering can be motivated by constructing a time-domain Planck window [533] for each mode. With a Planck window $W_{\rm Planck}(t)$, the high frequency fall-off is at most exponential, which can be sketched out in the following way. The Fourier transform of a C^∞ window function $W(t)$ with compact support, upon integration by parts p times, can be expressed as $W(f) = W^{(p)}(f)/(i2\pi f)^p$, where $W^{(p)}(f)$ is the Fourier transform of the p-th derivative of $W(t)$. Since every derivative exists due to $W(t)$ being C^∞ and $W(t)$ has compact support, we have that $|W(f)| \leq A/f^p$, suggesting that $W(f)$ decays faster than every polynomial in frequency. In other words, $|W(f)|$ can at most have an exponential fall-off. This implies that the C^∞ Planck window will satisfy $|W_{\rm Planck}(f)| \leq A\exp(-Bf)$, where $B \sim \Delta t$ with Δt being the characteristic transition time of the window . With our phenomenological tapering, for each mode, the corresponding mode-dependent Planck window would then have an exponential fall-off $B_{\ell mn} \sim 1/\omega_{\ell mn}$. However, by tuning the mode-dependent transition time $\Delta t_{\ell mn}$, in practice, one can get a faster exponential fall-off with a mode-dependent Planck window.

As a corollary, we can also obtain the frequency fall-off when $W(t)$ is discontinuous in its p-th derivative at $t = t_0$. The Fourier transform $W^{(p)}(f)$, without loss of generality, will contain a term

$$W^{(p)}(f) \supset \int_{t_0}^{\infty} g(t) \exp^{-i2\pi f t}, \tag{C.6}$$

where $g(t)$ is C^∞ and has compact support. Upon integrating by parts, we have that

$$W^{(p)}(f) \supset g(t_0) \frac{e^{-i2\pi f t_0}}{i2\pi f} \left[1 + \mathcal{O}(f^{-1})\right], \tag{C.7}$$

which is also equivalent to Taylor expanding $g(t)$. Given that $W(f) = W^{(p)}(f)/(i2\pi f)^p$, to leading order for the frequency fall-off, we simply have that $|W(f)| \sim 1/f^{p+1}$. For

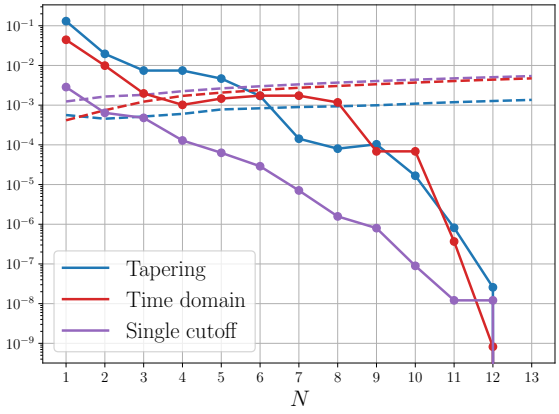

Figure C.6: Mismatch obtained with three different approaches as a function of the number of modes. The remnant mass and spin of the system are respectively $2.66 \times 10^7\, M_\odot$ and 0.60, while the angles have been fixed to $\theta = 3\pi/4$, $\phi = \psi = 0$, $\iota = \pi/3$ and $\varphi = \pi$. The dashed lines correspond to the threshold given by the right-hand side of Eq. (6.25). The blue, red and purple curves show the mismatch obtained respectively with the phenomenological tapering of Eq. (C.3), with the time-domain approach described in Sec. 6.3, and with the single high-frequency cutoff from PhenomA.

the commonly used Heaviside window for ringdown analysis, this means that the spectral leakage fall-off is only $1/f$. Instead, we use a frequency domain ringdown model obtained from mirroring [104, 470] at $t = t_0$. Although mirroring is not identical to a window function multiplying the damped sinusoid, due to the mirrored waveform being C^0 at $t = t_0$, it mimics the use of a C^0 window, and thus leads to a $1/f^2$ fall-off (cf. Eq. (6.4)). Note, however, that $\Lambda^{\times}_{\ell mn}$ scales as $1/f^3$ instead of $1/f^2$ as is the case for $\Lambda^{+}_{\ell mn}$. This is due to the fact that $\Lambda^{\times}_{\ell mn}$ is an anti-symmetric combination which makes the leading $1/f^2$ term cancel out, leaving the next-to-leading $1/f^3$ scaling.

A major caveat of using the phenomenological tapering is that one cannot simply construct a time-domain window $W^{(\ell mn)}(t)$ for each mode. This is because $W^{(\ell mn)}(t)$ would also convolve with modes $(\ell', m', n') \neq (\ell, m, n)$, which are not included in our phenomenologically tapered frequency-domain model. However, we checked that results obtained with our phenomenologically tapered frequency-domain model agree well with a pure time-domain analysis.

To enable the comparison, we generate the waveform in the time domain as described by Eq. (6.1), including the low-frequency approximation for the LISA response. In order to compute the inner product of two strains in the time domain, one needs to compute the two-point correlation function $C(t' - t)$ from the frequency-domain noise PSD, and combine it with the two strain series as described, for example, in Ref. [568].

For a source with remnant mass and spin of $2.66 \times 10^7\, M_\odot$ and 0.60 respectively, and angles $\theta = 3\pi/4$, $\phi = \psi = 0$, $\iota = \pi/3$ and $\varphi = \pi$, we apply the mismatch criterion given by Eq. (6.25) with the two methods (time and frequency domain). We show the result in Fig. C.6. The mismatch $1 - \mathcal{M}$ is shown by solid lines, while its threshold (right-hand side of Eq. (6.25)) is shown by dashed lines. The comparison is presented for different models,

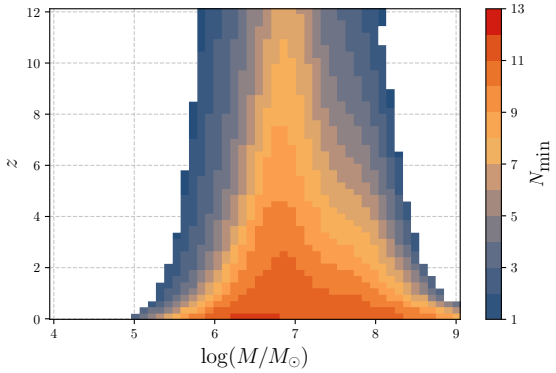

Figure C.7: $N_{\rm min}$ obtained with the criterion of Eq. (6.23) and using the tapered functions in (C.3) as a function of primary mass and redshift. While the qualitative behavior is similar to the one in Fig. 6.4, it is evident how $N_{\rm min}$ is boosted to higher values with this approach.

namely: the time domain (TD) mismatch in red; the frequency domain mismatch with a common single cutoff in purple; and the frequency domain mismatch with optimal tapering in blue. With the cutoff mismatch, two modes are sufficient for a correct estimation of the parameters, while seven modes are needed with the optimal taper. For the time-domain mismatch, four modes are sufficient to fulfill this requirement. We can therefore conclude that with the single cutoff, we can conservatively estimate the minimum number of modes needed for unbiased parameter estimation with damped-sinusoids waveforms.

Bibliography

[1] Albert Einstein. "The Field Equations of Gravitation". In: *Sitzungsber. Preuss. Akad. Wiss. Berlin (Math. Phys.)* 1915 (1915), pp. 844–847.

[2] Sean M. Carroll. *Spacetime and Geometry: An Introduction to General Relativity*. Cambridge University Press, July 2019. ISBN: 978-0-8053-8732-2, 978-1-108-48839-6, 978-1-108-77555-7. DOI: 10.1017/9781108770385.

[3] Robert M. Wald. *General Relativity*. Chicago, USA: Chicago Univ. Pr., 1984. DOI: 10.7208/chicago/9780226870373.001.0001.

[4] Leopold Infeld. "Equations of Motion in General Relativity Theory and the Action Principle". In: *Rev. Mod. Phys.* 29 (1957), pp. 398–411. DOI: 10.1103/RevModPhys.29.398.

[5] D. Lovelock. "The Einstein tensor and its generalizations". In: *J. Math. Phys.* 12 (1971), pp. 498–501. DOI: 10.1063/1.1665613.

[6] F. J. Belinfante. "On the current and the density of the electric charge, the energy, the linear momentum and the angular momentum of arbitrary fields". In: *Physica* 7.5 (May 1940), pp. 449–474. DOI: 10.1016/S0031-8914(40)90091-X.

[7] L. D. Landau and E. M. Lifschits. *The Classical Theory of Fields*. Vol. Volume 2. Course of Theoretical Physics. Oxford: Pergamon Press, 1975. ISBN: 978-0-08-018176-9.

[8] Clifford M. Will. "The Confrontation between General Relativity and Experiment". In: *Living Rev. Rel.* 17 (2014), p. 4. DOI: 10.12942/lrr-2014-4. arXiv: 1403.7377 [gr-qc].

[9] Irwin I. Shapiro. "Fourth Test of General Relativity". In: *Phys. Rev. Lett.* 13 (1964), pp. 789–791. DOI: 10.1103/PhysRevLett.13.789.

[10] Albert Einstein. "Explanation of the Perihelion Motion of Mercury from the General Theory of Relativity". In: *Sitzungsber. Preuss. Akad. Wiss. Berlin (Math. Phys.)* 1915 (1915), pp. 831–839.

[11] Albert Einstein. "On The influence of gravitation on the propagation of light". In: *Annalen Phys.* 35 (1911), pp. 898–908. DOI: 10.1002/andp.200590033.

[12] F. W. Dyson, A. S. Eddington, and C. Davidson. "A Determination of the Deflection of Light by the Sun's Gravitational Field, from Observations Made at the Total Eclipse of May 29, 1919". In: *Phil. Trans. Roy. Soc. Lond. A* 220 (1920), pp. 291–333. DOI: 10.1098/rsta.1920.0009.

[13] Richard C. Tolman. "Static solutions of Einstein's field equations for spheres of fluid". In: *Phys. Rev.* 55 (1939), pp. 364–373. DOI: 10.1103/PhysRev.55.364.

[14] J. R. Oppenheimer and G. M. Volkoff. "On massive neutron cores". In: *Phys. Rev.* 55 (1939), pp. 374–381. DOI: 10.1103/PhysRev.55.374.

[15] Karl Schwarzschild. "On the gravitational field of a mass point according to Einstein's theory". In: *Sitzungsber. Preuss. Akad. Wiss. Berlin (Math. Phys.)* 1916 (1916), pp. 189–196. arXiv: physics/9905030.

[16] Roy P. Kerr. "Gravitational field of a spinning mass as an example of algebraically special metrics". In: *Phys. Rev. Lett.* 11 (1963), pp. 237–238. DOI: 10.1103/PhysRevLett.11.237.

[17] Remo Ruffini and John A. Wheeler. "Introducing the black hole". In: *Phys. Today* 24.1 (1971), p. 30. DOI: 10.1063/1.3022513.

[18] Richard L. Arnowitt, Stanley Deser, and Charles W. Misner. "The Dynamics of general relativity". In: *Gen. Rel. Grav.* 40 (2008), pp. 1997–2027. DOI: 10.1007/s10714-008-0661-1. arXiv: gr-qc/0405109.

[19] Roger Penrose. "Gravitational collapse and space-time singularities". In: *Phys. Rev. Lett.* 14 (1965), pp. 57–59. DOI: 10.1103/PhysRevLett.14.57.

[20] M. D. Kruskal. "Maximal extension of Schwarzschild metric". In: *Phys. Rev.* 119 (1960), pp. 1743–1745. DOI: 10.1103/PhysRev.119.1743.

[21] G. Szekeres. "On the singularities of a Riemannian manifold". In: *Publ. Math. Debrecen* 7 (1960), pp. 285–301.

[22] S. W. Hawking. "Black hole explosions?" In: 248.5443 (Mar. 1974), pp. 30–31. DOI: 10.1038/248030a0.

[23] S. W. Hawking. "Particle Creation by Black Holes". In: *Commun. Math. Phys.* 43 (1975). Ed. by G. W. Gibbons and S. W. Hawking. [Erratum: Commun.Math.Phys. 46, 206 (1976)], pp. 199–220. DOI: 10.1007/BF02345020.

[24] S. W. Hawking and R. Penrose. "The Singularities of gravitational collapse and cosmology". In: *Proc. Roy. Soc. Lond. A* 314 (1970), pp. 529–548. DOI: 10.1098/rspa.1970.0021.

[25] Stephen W. Hawking and George F. R. Ellis. *The Large Scale Structure of Space-Time*. Cambridge Monographs on Mathematical Physics. Cambridge University Press, Feb. 2023. ISBN: 978-1-009-25316-1, 978-1-009-25315-4, 978-0-521-20016-5, 978-0-521-09906-6, 978-0-511-82630-6, 978-0-521-09906-6. DOI: 10.1017/9781009253161.

[26] Martin Bojowald. "Singularities and Quantum Gravity". In: *AIP Conf. Proc.* 910.1 (2007). Ed. by Mario Novello and Santiago E. Perez Bergliaffa, pp. 294–333. DOI: 10.1063/1.2752483. arXiv: gr-qc/0702144.

[27] Benjamin Koch and Frank Saueressig. "Black holes within Asymptotic Safety". In: *Int. J. Mod. Phys. A* 29.8 (2014), p. 1430011. DOI: 10.1142/S0217751X14300117. arXiv: 1401.4452 [hep-th].

[28] Luca Buoninfante. "Ghost and singularity free theories of gravity". In: (Oct. 2016). arXiv: 1610.08744 [gr-qc].

[29] E. T. Newman et al. "Metric of a Rotating, Charged Mass". In: *Journal of Mathematical Physics* 6.6 (June 1965), pp. 918–919. DOI: 10.1063/1.1704351.

[30] Werner Israel. "Event horizons in static vacuum space-times". In: *Phys. Rev.* 164 (1967), pp. 1776–1779. DOI: 10.1103/PhysRev.164.1776.

[31] B. Carter. "Axisymmetric Black Hole Has Only Two Degrees of Freedom". In: *Phys. Rev. Lett.* 26 (6 1971), pp. 331–333. DOI: 10.1103/PhysRevLett.26.331. URL: https://link.aps.org/doi/10.1103/PhysRevLett.26.331.

[32] D. C. Robinson. "Uniqueness of the Kerr Black Hole". In: *Phys. Rev. Lett.* 34 (14 1975), pp. 905–906. DOI: 10.1103/PhysRevLett.34.905. URL: https://link.aps.org/doi/10.1103/PhysRevLett.34.905.

[33] D. C. Robinson. "A Simple Proof of the Generalization of Israel's Theorem". In: *General Relativity and Gravitation* 8 (1977), pp. 695–699. DOI: 10.1007/BF00762792.

[34] R. Genzel et al. "The Dark Mass Concentration in the Central Parsec of the Milky Way". In: *Astrophys. J.* 472 (1996), p. 153. DOI: 10.1086/178051.

[35] A. M. Ghez et al. "High proper motion stars in the vicinity of Sgr A*: Evidence for a supermassive black hole at the center of our galaxy". In: *Astrophys. J.* 509 (1998), pp. 678–686. DOI: 10.1086/306528. arXiv: astro-ph/9807210.

[36] Y. Tanaka et al. "Gravitationally Redshifted Emission Implying an Accretion Disk and Massive Black Hole in the Active Galaxy MCG:-6-30-15". In: *Nature* 375 (1995), p. 659. DOI: 10.1038/375659a0.

[37] C. T. Bolton. "Identification of Cygnus X-1 with HDE 226868". In: 235.5336 (Feb. 1972), pp. 271–273. DOI: 10.1038/235271b0.

[38] B. Louise Webster and Paul Murdin. "Cygnus X-1-a Spectroscopic Binary with a Heavy Companion ?" In: *Nature* 235 (1972), pp. 37–38. DOI: 10.1038/235037a0.

[39] Kazunori Akiyama et al. "First M87 Event Horizon Telescope Results. I. The Shadow of the Supermassive Black Hole". In: *Astrophys. J. Lett.* 875 (2019), p. L1. DOI: 10.3847/2041-8213/ab0ec7. arXiv: 1906.11238 [astro-ph.GA].

[40] B. P. Abbott et al. "Observation of Gravitational Waves from a Binary Black Hole Merger". In: *Phys. Rev. Lett.* 116.6 (2016), p. 061102. DOI: 10.1103/PhysRevLett.116.061102. arXiv: 1602.03837 [gr-qc].

[41] Rudolf Kippenhahn, Alfred Weigert, and Achim Weiss. *Stellar structure and evolution*. Astronomy and Astrophysics Library. Springer, Aug. 2012. ISBN: 978-0-387-58013-5, 978-3-642-30255-8, 978-3-642-30304-3. DOI: 10.1007/978-3-642-30304-3.

[42] S. L. Shapiro and S. A. Teukolsky. *Black holes, white dwarfs, and neutron stars: The physics of compact objects*. 1983. ISBN: 978-0-471-87316-7, 978-3-527-61766-1. DOI: 10.1002/9783527617661.

[43] J. R. Oppenheimer and H. Snyder. "On Continued gravitational contraction". In: *Phys. Rev.* 56 (1939), pp. 455–459. DOI: 10.1103/PhysRev.56.455.

[44] John Kormendy and Luis C. Ho. "Coevolution (Or Not) of Supermassive Black Holes and Host Galaxies". In: *Ann. Rev. Astron. Astrophys.* 51 (2013), pp. 511–653. DOI: 10.1146/annurev-astro-082708-101811. arXiv: 1304.7762 [astro-ph.CO].

[45] Martin J. Rees. "Black Hole Models for Active Galactic Nuclei". In: *Ann. Rev. Astron. Astrophys.* 22 (1984), pp. 471–506. DOI: 10.1146/annurev.aa.22.090184.002351.

[46] G. W. Gibbons. "Vacuum polarization and the spontaneous loss of charge by black holes". In: *Communications in Mathematical Physics* 44.3 (1975), pp. 245–264. DOI: 10.1007/BF01609829.

[47] Gitika Mall et al. "Measuring Black Hole Spins through X-ray Reflection Spectroscopy and the Relativistic Precession Model: the case of XTE J1859+226". In: *Mon. Not. Roy. Astron. Soc.* 527 (2024), pp. 12053–12064. DOI: 10.1093/mnras/stad3933. arXiv: 2309.05018 [astro-ph.HE].

[48] Cosimo Bambi. "Astrophysical Black Holes: A Compact Pedagogical Review". In: *Annalen Phys.* 530 (2018), p. 1700430. DOI: 10.1002/andp.201700430. arXiv: 1711.10256 [gr-qc].

[49] Klaas Landsman. "Penrose's 1965 singularity theorem: from geodesic incompleteness to cosmic censorship". In: *Gen. Rel. Grav.* 54.10 (2022), p. 115. DOI: 10.1007/s10714-022-02973-w. arXiv: 2205.01680 [physics.hist-ph].

[50] Gerard 't Hooft and M. J. G. Veltman. "One loop divergencies in the theory of gravitation". In: *Ann. Inst. H. Poincare A Phys. Theor.* 20 (1974), pp. 69–94.

[51] Marc H. Goroff and Augusto Sagnotti. "QUANTUM GRAVITY AT TWO LOOPS". In: *Phys. Lett. B* 160 (1985), pp. 81–86. DOI: 10.1016/0370-2693(85)91470-4.

[52] John F. Donoghue. "General relativity as an effective field theory: The leading quantum corrections". In: *Phys. Rev. D* 50 (1994), pp. 3874–3888. DOI: 10.1103/PhysRevD.50.3874. arXiv: gr-qc/9405057.

[53] Y. Fukuda et al. "Evidence for oscillation of atmospheric neutrinos". In: *Phys. Rev. Lett.* 81 (1998), pp. 1562–1567. DOI: 10.1103/PhysRevLett.81.1562. arXiv: hep-ex/9807003.

[54] R. N. Mohapatra and P. B. Pal. *Massive neutrinos in physics and astrophysics. Second edition.* Vol. 60. 1998.

[55] P. A. Zyla et al. "Review of Particle Physics". In: *PTEP* 2020.8 (2020), p. 083C01. DOI: 10.1093/ptep/ptaa104.

[56] Steven Weinberg. "Implications of Dynamical Symmetry Breaking". In: *Phys. Rev. D* 13 (1976). [Addendum: Phys.Rev.D 19, 1277–1280 (1979)], pp. 974–996. DOI: 10.1103/PhysRevD.19.1277.

[57] Gian Francesco Giudice. "Naturally Speaking: The Naturalness Criterion and Physics at the LHC". In: (Jan. 2008). Ed. by Gordon Kane and Aaron Pierce, pp. 155–178. DOI: 10.1142/9789812779762_0010. arXiv: 0801.2562 [hep-ph].

[58] Riccardo Barbieri. "Electroweak theory after the first Large Hadron Collider phase". In: *Phys. Scripta T* 158 (2013). Ed. by Tord Ekelöf, p. 014006. DOI: 10.1088/0031-8949/2013/T158/014006. arXiv: 1309.3473 [hep-ph].

[59] Michael E. Peskin and Daniel V. Schroeder. *An Introduction to quantum field theory.* Reading, USA: Addison-Wesley, 1995. ISBN: 978-0-201-50397-5, 978-0-429-50355-9, 978-0-429-49417-8. DOI: 10.1201/9780429503559.

[60] K. Becker, M. Becker, and J. H. Schwarz. *String theory and M-theory: A modern introduction.* Cambridge University Press, Dec. 2006. ISBN: 978-0-511-25486-4, 978-0-521-86069-7, 978-0-511-81608-6. DOI: 10.1017/CBO9780511816086.

[61] Steven Weinberg. "ULTRAVIOLET DIVERGENCES IN QUANTUM THEORIES OF GRAVITATION". In: *General Relativity: An Einstein Centenary Survey.* 1980, pp. 790–831.

[62] Carlo Rovelli and Francesca Vidotto. *Covariant Loop Quantum Gravity: An Elementary Introduction to Quantum Gravity and Spinfoam Theory.* Cambridge Monographs on Mathematical Physics. Cambridge University Press, Nov. 2014. ISBN: 978-1-107-06962-6, 978-1-316-14729-0.

[63] Petr Horava. "Quantum Gravity at a Lifshitz Point". In: *Phys. Rev. D* 79 (2009), p. 084008. DOI: 10.1103/PhysRevD.79.084008. arXiv: 0901.3775 [hep-th].

[64] S. W. Hawking. "Breakdown of Predictability in Gravitational Collapse". In: *Phys. Rev. D* 14 (1976), pp. 2460–2473. DOI: 10.1103/PhysRevD.14.2460.

[65] Don N. Page. "Information in black hole radiation". In: *Phys. Rev. Lett.* 71 (1993), pp. 3743–3746. DOI: 10.1103/PhysRevLett.71.3743. arXiv: hep-th/9306083.

[66] Vera C. Rubin, W. Kent Ford Jr., and Norbert Thonnard. "Extended rotation curves of high-luminosity spiral galaxies. IV. Systematic dynamical properties, Sa through Sc". In: *Astrophys. J. Lett.* 225 (1978), pp. L107–L111. DOI: 10.1086/182804.

[67] A. Bosma. "21-cm line studies of spiral galaxies. I - Observations of the galaxies NGC 3198 and NGC 2403". In: *The Astronomical Journal* 86 (1981), pp. 1791–1824.

[68] P. J. E. Peebles. "Large scale background temperature and mass fluctuations due to scale invariant primeval perturbations". In: *Astrophys. J. Lett.* 263 (1982). Ed. by M. A. Srednicki, pp. L1–L5. DOI: 10.1086/183911.

[69] George R. Blumenthal et al. "Formation of Galaxies and Large Scale Structure with Cold Dark Matter". In: *Nature* 311 (1984). Ed. by M. A. Srednicki, pp. 517–525. DOI: 10.1038/311517a0.

[70] Wayne Hu and Scott Dodelson. "Cosmic Microwave Background Anisotropies". In: *Ann. Rev. Astron. Astrophys.* 40 (2002), pp. 171–216. DOI: 10.1146/annurev.astro.40.060401.093926. arXiv: astro-ph/0110414.

[71] N. Aghanim et al. "Planck 2018 results. VI. Cosmological parameters". In: *Astron. Astrophys.* 641 (2020). [Erratum: Astron.Astrophys. 652, C4 (2021)], A6. DOI: 10.1051/0004-6361/201833910. arXiv: 1807.06209 [astro-ph.CO].

[72] S. Perlmutter et al. "Measurements of Ω and Λ from 42 high redshift supernovae". In: *Astrophys. J.* 517 (1999), pp. 565–586. DOI: 10.1086/307221. arXiv: astro-ph/9812133.

[73] Adam G. Riess and et al. "Observational Evidence from Supernovae for an Accelerating Universe and a Cosmological Constant". In: *The Astronomical Journal* 116.3 (1998), pp. 1009–1038. DOI: 10.1086/300499. URL: https://doi.org/10.1086/300499.

[74] P. A. R. Ade et al. "Planck 2015 results. XIV. Dark energy and modified gravity". In: *Astron. Astrophys.* 594 (2016), A14. DOI: 10.1051/0004-6361/201525814. arXiv: 1502.01590 [astro-ph.CO].

[75] Steven Weinberg. "The Cosmological Constant Problem". In: *Rev. Mod. Phys.* 61 (1989). Ed. by Jong-Ping Hsu and D. Fine, pp. 1–23. DOI: 10.1103/RevModPhys.61.1.

[76] Jerome Martin. "Everything You Always Wanted To Know About The Cosmological Constant Problem (But Were Afraid To Ask)". In: *Comptes Rendus Physique* 13 (2012), pp. 566–665. DOI: 10.1016/j.crhy.2012.04.008. arXiv: 1205.3365 [astro-ph.CO].

[77] S. E. Rugh and H. Zinkernagel. "The Quantum vacuum and the cosmological constant problem". In: *Stud. Hist. Phil. Sci. B* 33 (2002), pp. 663–705. DOI: 10.1016/S1355-2198(02)00033-3. arXiv: hep-th/0012253.

[78] M. Abdul Karim et al. "DESI DR2 Results II: Measurements of Baryon Acoustic Oscillations and Cosmological Constraints". In: (Mar. 2025). arXiv: 2503.14738 [astro-ph.CO].

[79] C. P. Burgess. *Introduction to Effective Field Theory*. Cambridge University Press, Dec. 2020. ISBN: 978-1-139-04804-0, 978-0-521-19547-8. DOI: 10.1017/9781139048040.

[80] Solomon Endlich et al. "An effective formalism for testing extensions to General Relativity with gravitational waves". In: *JHEP* 09 (2017), p. 122. DOI: 10.1007/JHEP09(2017)122. arXiv: 1704.01590 [gr-qc].

[81] Pablo A. Cano and Alejandro Ruipérez. "Leading higher-derivative corrections to Kerr geometry". In: *JHEP* 05 (2019). [Erratum: JHEP 03, 187 (2020)], p. 189. DOI: 10.1007/JHEP05(2019)189. arXiv: 1901.01315 [gr-qc].

[82] A. Gruzinov and M. Kleban. "Causality Constrains Higher Curvature Corrections to Gravity". In: *Class. Quant. Grav.* 24 (2007), pp. 3521–3524. DOI: 10.1088/0264-9381/24/13/N02. arXiv: hep-th/0612015.

[83] Calvin Y. R. Chen et al. "A cautionary case of casual causality". In: *JHEP* 03 (2022), p. 025. DOI: 10.1007/JHEP03(2022)025. arXiv: 2112.05031 [hep-th].

[84] Claudia de Rham, Andrew J. Tolley, and Jun Zhang. "Causality Constraints on Gravitational Effective Field Theories". In: *Phys. Rev. Lett.* 128.13 (2022), p. 131102. DOI: 10.1103/PhysRevLett.128.131102. arXiv: 2112.05054 [gr-qc].

[85] M. Ostrogradsky. "Mémoires sur les équations différentielles, relatives au problème des isopérimètres". In: *Mem. Acad. St. Petersbourg* 6.4 (1850), pp. 385–517.

[86] Richard P. Woodard. "Avoiding dark energy with 1/r modifications of gravity". In: *Lect. Notes Phys.* 720 (2007). Ed. by Lefteris Papantonopoulos, pp. 403–433. DOI: 10.1007/978-3-540-71013-4_14. arXiv: astro-ph/0601672.

[87] Pablo A. Cano et al. "Quasinormal modes of rotating black holes in higher-derivative gravity". In: *Phys. Rev. D* 108.12 (2023), p. 124032. DOI: 10.1103/PhysRevD.108.124032. arXiv: 2307.07431 [gr-qc].

[88] Pablo A. Cano et al. "Universal Teukolsky equations and black hole perturbations in higher-derivative gravity". In: *Phys. Rev. D* 108.2 (2023), p. 024040. DOI: 10.1103/PhysRevD.108.024040. arXiv: 2304.02663 [gr-qc].

[89] C. Wetterich. "Cosmology and the Fate of Dilatation Symmetry". In: *Nucl. Phys. B* 302 (1988), pp. 668–696. DOI: 10.1016/0550-3213(88)90193-9. arXiv: 1711.03844 [hep-th].

[90] Bharat Ratra and P. J. E. Peebles. "Cosmological Consequences of a Rolling Homogeneous Scalar Field". In: *Phys. Rev. D* 37 (1988), p. 3406. DOI: 10.1103/PhysRevD.37.3406.

[91] Shinji Tsujikawa. "Modified gravity models of dark energy". In: *Lect. Notes Phys.* 800 (2010), pp. 99–145. DOI: 10.1007/978-3-642-10598-2_3. arXiv: 1101.0191 [gr-qc].

[92] Lavinia Heisenberg. "Generalization of the Proca Action". In: *JCAP* 05 (2014), p. 015. DOI: 10.1088/1475-7516/2014/05/015. arXiv: 1402.7026 [hep-th].

[93] S. F. Hassan and Rachel A. Rosen. "Bimetric Gravity from Ghost-free Massive Gravity". In: *JHEP* 02 (2012), p. 126. DOI: 10.1007/JHEP02(2012)126. arXiv: 1109.3515 [hep-th].

[94] Ted Jacobson and David Mattingly. "Gravity with a dynamical preferred frame". In: *Phys. Rev. D* 64 (2001), p. 024028. DOI: 10.1103/PhysRevD.64.024028. arXiv: gr-qc/0007031.

[95] Claudia de Rham, Gregory Gabadadze, and Andrew J. Tolley. "Resummation of Massive Gravity". In: *Phys. Rev. Lett.* 106 (2011), p. 231101. DOI: 10.1103/PhysRevLett.106.231101. arXiv: 1011.1232 [hep-th].

[96] Tomi Koivisto. "Dynamics of Nonlocal Cosmology". In: *Phys. Rev. D* 77 (2008), p. 123513. DOI: 10.1103/PhysRevD.77.123513. arXiv: 0803.3399 [gr-qc].

[97] Th. Kaluza. "Zum Unitätsproblem der Physik". In: *Sitzungsber. Preuss. Akad. Wiss. Berlin (Math. Phys.)* 1921 (1921), pp. 966–972. DOI: 10.1142/S0218271818700017. arXiv: 1803.08616 [physics.hist-ph].

[98] Oskar Klein. "Quantum Theory and Five-Dimensional Theory of Relativity. (In German and English)". In: *Z. Phys.* 37 (1926). Ed. by J. C. Taylor, pp. 895–906. DOI: 10.1007/BF01397481.

[99] Lisa Randall and Raman Sundrum. "A Large mass hierarchy from a small extra dimension". In: *Phys. Rev. Lett.* 83 (1999), pp. 3370–3373. DOI: 10.1103/PhysRevLett.83.3370. arXiv: hep-ph/9905221.

[100] G. R. Dvali, Gregory Gabadadze, and Massimo Porrati. "4-D gravity on a brane in 5-D Minkowski space". In: *Phys. Lett. B* 485 (2000), pp. 208–214. DOI: 10.1016/S0370-2693(00)00669-9. arXiv: hep-th/0005016.

[101] Ramesh Narayan and Jeffrey E. McClintock. "Observational Evidence for Black Holes". In: (Dec. 2013). arXiv: 1312.6698 [astro-ph.HE].

[102] Clifford M. Will. *Theory and Experiment in Gravitational Physics*. Cambridge: Cambridge University Press, 1993. ISBN: 9780511564246. DOI: 10.1017/CBO9780511564246.

[103] B. P. Abbott et al. "Tests of general relativity with GW150914". In: *Phys. Rev. Lett.* 116.22 (2016). [Erratum: Phys.Rev.Lett. 121, 129902 (2018)], p. 221101. DOI: 10.1103/PhysRevLett.116.221101. arXiv: 1602.03841 [gr-qc].

[104] Eanna E. Flanagan and Scott A. Hughes. "Measuring gravitational waves from binary black hole coalescences: 2. The Waves' information and its extraction, with and without templates". In: *Phys. Rev. D* 57 (1998), pp. 4566–4587. DOI: 10.1103/PhysRevD.57.4566. arXiv: gr-qc/9710129.

[105] Albert Einstein. "Über Gravitationswellen". In: *Sitzungsber. Preuss. Akad. Wiss. Berlin (Math. Phys.)* 1918 (1918), pp. 154–167.

[106] Hermann Bondi. "Plane gravitational waves in general relativity". In: *Nature* 179 (1957), pp. 1072–1073. DOI: 10.1038/1791072a0.

[107] H. Bondi, F. A. E. Pirani, and I. Robinson. "Gravitational waves in general relativity. 3. Exact plane waves". In: *Proc. Roy. Soc. Lond. A* 251 (1959), pp. 519–533. DOI: 10.1098/rspa.1959.0124.

[108] R. K. Sachs. "Gravitational waves in general relativity. 8. Waves in asymptotically flat space-times". In: *Proc. Roy. Soc. Lond. A* 270 (1962), pp. 103–126. DOI: 10.1098/rspa.1962.0206.

[109] Richard A. Isaacson. "Gravitational Radiation in the Limit of High Frequency. I. The Linear Approximation and Geometrical Optics". In: *Phys. Rev.* 166 (1968), pp. 1263–1271. DOI: 10.1103/PhysRev.166.1263.

[110] Richard A. Isaacson. "Gravitational Radiation in the Limit of High Frequency. II. Nonlinear Terms and the Ef fective Stress Tensor". In: *Phys. Rev.* 166 (1968), pp. 1272–1279. DOI: 10.1103/PhysRev.166.1272.

[111] Katerina Chatziioannou, Nicolás Yunes, and Neil Cornish. "Model-independent test of general relativity: An extended post-Einsteinian framework with complete polarization content". In: *Physical Review D* 86.2 (July 2012). ISSN: 1550-2368. DOI: 10.1103/physrevd.86.022004. URL: http://dx.doi.org/10.1103/PhysRevD.86.022004.

[112] P. C. Peters and J. Mathews. "Gravitational radiation from point masses in a Keplerian orbit". In: *Phys. Rev.* 131 (1963), pp. 435–439. DOI: 10.1103/PhysRev.131.435.

[113] R. O. Hansen. "Postnewtonian gravitational radiation from point masses in a hyperbolic kepler orbit". In: *Phys. Rev. D* 5 (1972), pp. 1021–1023. DOI: 10.1103/PhysRevD.5.1021.

[114] S. Bonazzola and J. A. Marck. "Astrophysical sources of gravitational radiation". In: *Ann. Rev. Nucl. Part. Sci.* 44 (1994), pp. 655–717. DOI: 10.1146/annurev.ns.44.120194.003255.

[115] Luc Blanchet. "Gravitational radiation from post-Newtonian sources and inspiralling compact binaries". In: *Living Rev. Rel.* 9 (2006), p. 4.

[116] Rainer Weiss. "Republication of: Electromagnetically coupled broadband gravitational antenna". In: *Gen. Rel. Grav.* 54.11 (2022), p. 153. DOI: 10.1007/s10714-022-03021-3.

[117] R. L. Forward. "Wide Band Laser Interferometer Gravitational Radiation Experiment". In: *Phys. Rev. D* 17 (1978), pp. 379–390. DOI: 10.1103/PhysRevD.17.379.

[118] Peter R. Saulson. *Fundamentals of Interferometric Gravitational Wave Detectors*. 2nd. ed. World Scientific, 2017. ISBN: 978-981-314-307-4, 978-981-314-620-4. DOI: 10.1142/10116.

[119] Kip S. Thorne. "Gravitational radiation: A New window onto the universe". In: (Apr. 1997). arXiv: gr-qc/9704042.

[120] P. C. Peters. "Gravitational Radiation and the Motion of Two Point Masses". In: *Phys. Rev.* 136 (1964), B1224–B1232. DOI: 10.1103/PhysRev.136.B1224.

[121] Thibault Damour and Gilles Esposito-Farese. "Tensor multiscalar theories of gravitation". In: *Class. Quant. Grav.* 9 (1992), pp. 2093–2176. DOI: 10.1088/0264-9381/9/9/015.

[122] M. Khlopunov and D. V. Gal'tsov. "Leakage of gravitational waves into an extra dimension in the DGP model". In: *JCAP* 10 (2022), p. 062. DOI: 10.1088/1475-7516/2022/10/062. arXiv: 2209.04262 [gr-qc].

[123] Chris Clarkson and Sanjeev S. Seahra. "A gravitational wave window on extra dimensions". In: *Class. Quant. Grav.* 24 (2007), F33–F40. DOI: 10.1088/0264-9381/24/9/F01. arXiv: astro-ph/0610470.

[124] A. Hewish et al. "Observation of a rapidly pulsating radio source". In: *Nature* 217 (1968), pp. 709–713. DOI: 10.1038/217709a0.

[125] T. Gold. "Rotating neutron stars as the origin of the pulsating radio sources". In: *Nature* 218 (1968), pp. 731–732. DOI: 10.1038/218731a0.

[126] R. A. Hulse and J. H. Taylor. "Discovery of a pulsar in a binary system." In: 195 (Jan. 1975), pp. L51–L53. DOI: 10.1086/181708.

[127] J. M. Weisberg and J. H. Taylor. "Gravitational Radiation From an Orbiting Pulsar". In: *Gen. Rel. Grav.* 13 (1981), pp. 1–6.

[128] Joel M. Weisberg and Joseph H. Taylor. "Relativistic binary pulsar B1913+16: Thirty years of observations and analysis". In: *ASP Conf. Ser.* 328 (2005), p. 25. arXiv: astro-ph/0407149.

[129] Subhendra Mohanty and Prafulla Kumar Panda. "Particle physics bounds from the Hulse-Taylor binary". In: *Physical Review D* 53.10 (May 1996), 5723–5726. ISSN: 1089-4918. DOI: 10.1103/physrevd.53.5723. URL: http://dx.doi.org/10.1103/PhysRevD.53.5723.

[130] Paulo C. C. Freire et al. "The relativistic pulsar-white dwarf binary PSR J1738+0333 II. The most stringent test of scalar-tensor gravity". In: *Mon. Not. Roy. Astron. Soc.* 423 (2012), p. 3328. DOI: 10.1111/j.1365-2966.2012.21253.x. arXiv: 1205.1450 [astro-ph.GA].

[131] M. Kramer et al. "Tests of general relativity from timing the double pulsar". In: *Science* 314 (2006), pp. 97–102. DOI: 10.1126/science.1132305. arXiv: astro-ph/0609417 [astro-ph].

[132] John Antoniadis et al. "A Massive Pulsar in a Compact Relativistic Binary". In: *Science* 340 (2013), p. 6131. DOI: 10.1126/science.1233232. arXiv: 1304.6875 [astro-ph.HE].

[133] Carlos Palenzuela and Steven L. Liebling. "Constraining scalar-tensor theories of gravity from the most massive neutron stars". In: *Phys. Rev. D* 93.4 (2016), p. 044009. DOI: 10.1103/PhysRevD.93.044009. arXiv: 1510.03471 [gr-qc].

[134] B.P. Abbott et al. "GW170817: Observation of Gravitational Waves from a Binary Neutron Star Inspiral". In: *Phys. Rev. Lett.* 119.16 (2017), p. 161101. DOI: 10.1103/PhysRevLett.119.161101. arXiv: 1710.05832 [gr-qc].

[135] B. P. Abbott et al. "GW190425: Observation of a Compact Binary Coalescence with Total Mass $\sim 3.4 M_{\odot}$". In: *Astrophys. J. Lett.* 892.1 (2020), p. L3. DOI: 10.3847/2041-8213/ab75f5. arXiv: 2001.01761 [astro-ph.HE].

[136] R. Abbott et al. "GWTC-3: Compact Binary Coalescences Observed by LIGO and Virgo During the Second Part of the Third Observing Run". In: *arXiv e-prints* (Nov. 2021). arXiv: 2111.03606 [gr-qc].

[137] B. P. Abbott et al. "Prospects for observing and localizing gravitational-wave transients with Advanced LIGO, Advanced Virgo and KAGRA". In: *Living Rev. Rel.* 19 (2016), p. 1. DOI: 10.1007/s41114-020-00026-9. arXiv: 1304.0670 [gr-qc].

[138] R. Abbott et al. "GWTC-3: Compact Binary Coalescences Observed by LIGO and Virgo during the Second Part of the Third Observing Run". In: *Phys. Rev. X* 13.4 (2023), p. 041039. DOI: 10.1103/PhysRevX.13.041039. arXiv: 2111.03606 [gr-qc].

[139] B. P. Abbott et al. "Gravitational Waves and Gamma-rays from a Binary Neutron Star Merger: GW170817 and GRB 170817A". In: *Astrophys. J. Lett.* 848.2 (2017), p. L13. DOI: 10.3847/2041-8213/aa920c. arXiv: 1710.05834 [astro-ph.HE].

[140] B. P. Abbott et al. "Tests of General Relativity with GW170817". In: *Phys. Rev. Lett.* 123.1 (2019), p. 011102. DOI: 10.1103/PhysRevLett.123.011102. arXiv: 1811.00364 [gr-qc].

[141] B. P. Abbott et al. "Tests of General Relativity with the Binary Black Hole Signals from the LIGO-Virgo Catalog GWTC-1". In: *Phys. Rev.* D100.10 (2019), p. 104036. DOI: 10.1103/PhysRevD.100.104036. arXiv: 1903.04467 [gr-qc].

[142] M. Punturo et al. "The Einstein Telescope: A third-generation gravitational wave observatory". In: *Class. Quant. Grav.* 27 (2010). Ed. by Fulvio Ricci, p. 194002. DOI: 10.1088/0264-9381/27/19/194002.

[143] David Reitze et al. "Cosmic Explorer: The U.S. Contribution to Gravitational-Wave Astronomy beyond LIGO". In: *Bull. Am. Astron. Soc.* 51.7 (2019), p. 035. arXiv: 1907.04833 [astro-ph.IM].

[144] C. J. Moore, R. H. Cole, and C. P. L. Berry. "Gravitational-wave sensitivity curves". In: *Class. Quant. Grav.* 32.1 (2015), p. 015014. DOI: 10.1088/0264-9381/32/1/015014. arXiv: 1408.0740 [gr-qc].

[145] Pau Amaro-Seoane et al. "Laser Interferometer Space Antenna". In: (Feb. 2017). arXiv: 1702.00786 [astro-ph.IM].

[146] Jun Luo et al. "TianQin: a space-borne gravitational wave detector". In: *Class. Quant. Grav.* 33.3 (2016), p. 035010. DOI: 10.1088/0264-9381/33/3/035010. arXiv: 1512.02076 [astro-ph.IM].

[147] Ziren Luo et al. "The Taiji program: A concise overview". In: *PTEP* 2021.5 (2021), 05A108. DOI: 10.1093/ptep/ptaa083.

[148] Seiji Kawamura et al. "Current status of space gravitational wave antenna DECIGO and B-DECIGO". In: *PTEP* 2021.5 (2021), 05A105. DOI: 10.1093/ptep/ptab019. arXiv: 2006.13545 [gr-qc].

[149] Mikhail V. Sazhin. "Opportunities for detecting ultralong gravitational waves". In: *Sov. Astron.* 22 (1978), pp. 36–38.

[150] Steven L. Detweiler. "Klein-Gordon equation and rotating black holes". In: *Phys. Rev. D* 22 (1980), pp. 2323–2326. DOI: 10.1103/PhysRevD.22.2323.

[151] George Hobbs and Shi Dai. "Gravitational wave research using pulsar timing arrays". In: *Natl. Sci. Rev.* 4.5 (2017), pp. 707–717. DOI: 10.1093/nsr/nwx126. arXiv: 1707.01615 [astro-ph.IM].

[152] F. Jenet et al. "The North American Nanohertz Observatory for Gravitational Waves". In: (Sept. 2009). arXiv: 0909.1058 [astro-ph.IM].

[153] Michael Kramer and David J. Champion. "The European Pulsar Timing Array and the Large European Array for Pulsars". In: *Class. Quant. Grav.* 30 (2013), p. 224009. DOI: 10.1088/0264-9381/30/22/224009.

[154] R. N. Manchester. "The Parkes Pulsar Timing Array Project". In: *Highlights Astron.* 15 (2010). Ed. by Ian F. Corbett, p. 233. DOI: 10.1017/S1743921310008987.

[155] Pratik Tarafdar et al. "The Indian Pulsar Timing Array: First data release". In: *Publ. Astron. Soc. Austral.* 39 (2022), e053. DOI: 10.1017/pasa.2022.46. arXiv: 2206.09289 [astro-ph.IM].

[156] George Hobbs et al. "The International Pulsar Timing Array project: using pulsars as a gravitational wave detector". In: *Class. Quant. Grav.* 27 (2010), p. 084013. DOI: 10.1088/0264-9381/27/8/084013. arXiv: 0911.5206 [astro-ph.SR].

[157] Xuce Niu and Moinul Hossain Rahat. "NANOGrav signal from axion inflation". In: *Phys. Rev. D* 108.11 (2023), p. 115023. DOI: 10.1103/PhysRevD.108.115023. arXiv: 2307.01192 [hep-ph].

[158] Ziwei Wang et al. "The nanohertz stochastic gravitational wave background from cosmic string loops and the abundant high redshift massive galaxies". In: *Sci. China Phys. Mech. Astron.* 66.12 (2023), p. 120403. DOI: 10.1007/s11433-023-2262-0. arXiv: 2306.17150 [astro-ph.HE].

[159] M. R. Gangopadhyay et al. "Is the NANOGrav detection evidence of resonant particle creation during inflation?" In: *JHEAp* 47 (2025), p. 100358. DOI: 10.1016/j.jheap.2025.100358. arXiv: 2309.03101 [astro-ph.CO].

[160] Ved Kenjale and Tina Kahniashvili. "Connecting inflation to the NANOGrav 15-year dataset via massive gravity". In: *Phys. Rev. D* 111.10 (2025), p. 103515. DOI: 10.1103/PhysRevD.111.103515. arXiv: 2410.09658 [astro-ph.CO].

[161] EPTA Collaboration and InPTA Collaboration et al. "The second data release from the European Pulsar Timing Array - III. Search for gravitational wave signals". In: *A&A* 678 (2023), A50. DOI: 10.1051/0004-6361/202346844. URL: https://doi.org/10.1051/0004-6361/202346844.

[162] Gabriella Agazie et al. "The NANOGrav 15 yr Data Set: Evidence for a Gravitational-wave Background". In: *The Astrophysical Journal Letters* 951.1 (June 2023), p. L8. ISSN: 2041-8213. DOI: 10.3847/2041-8213/acdac6. URL: http://dx.doi.org/10.3847/2041-8213/acdac6.

[163] Daniel J. Reardon et al. "Search for an Isotropic Gravitational-wave Background with the Parkes Pulsar Timing Array". In: *The Astrophysical Journal Letters* 951.1 (June 2023), p. L6. ISSN: 2041-8213. DOI: 10.3847/2041-8213/acdd02. URL: http://dx.doi.org/10.3847/2041-8213/acdd02.

[164] Heng Xu et al. "Searching for the Nano-Hertz Stochastic Gravitational Wave Background with the Chinese Pulsar Timing Array Data Release I". In: *Research in Astronomy and Astrophysics* 23.7 (June 2023), p. 075024. ISSN: 1674-4527. DOI: 10.1088/1674-4527/acdfa5. URL: http://dx.doi.org/10.1088/1674-4527/acdfa5.

[165] Matthew T Miles et al. "The MeerKAT Pulsar Timing Array: the 4.5-yr data release and the noise and stochastic signals of the millisecond pulsar population". In: *Monthly Notices of the Royal Astronomical Society* 536.2 (Dec. 2024), 1467–1488. ISSN: 1365-2966. DOI: 10.1093/mnras/stae2572. URL: http://dx.doi.org/10.1093/mnras/stae2572.

[166] R. W. Hellings and G. S. Downs. "Upper limits on the isotropic gravitational radiation background from pulsar timing analysis." In: *The Astrophysical Journal Letters* 265 (Feb. 1983), pp. L39–L42. DOI: 10.1086/183954.

[167] A. M. Cruise and R. M. J. Ingley. "A correlation detector for very high frequency gravitational waves". In: *Class. Quant. Grav.* 22 (2005). Ed. by O. Jennrich, S479–S481. DOI: 10.1088/0264-9381/22/10/046.

[168] Nancy Aggarwal et al. "Challenges and opportunities of gravitational-wave searches at MHz to GHz frequencies". In: *Living Rev. Rel.* 24.1 (2021), p. 4. DOI: 10.1007/s41114-021-00032-5. arXiv: 2011.12414 [gr-qc].

[169] M. Fierz. "On the physical interpretation of P.Jordan's extended theory of gravitation". In: *Helv. Phys. Acta* 29 (1956), pp. 128–134.

[170] Pascual Jordan. "The present state of Dirac's cosmological hypothesis". In: *Z. Phys.* 157 (1959), pp. 112–121. DOI: 10.1007/BF01375155.

[171] C. Brans and R. H. Dicke. "Mach's principle and a relativistic theory of gravitation". In: *Phys. Rev.* 124 (1961). Ed. by Jong-Ping Hsu and D. Fine, pp. 925–935. DOI: 10.1103/PhysRev.124.925.

[172] Thibault Damour and Gilles Esposito-Farese. "Nonperturbative strong field effects in tensor - scalar theories of gravitation". In: *Phys. Rev. Lett.* 70 (1993), pp. 2220–2223. DOI: 10.1103/PhysRevLett.70.2220.

[173] Thibault Damour and Joseph H. Taylor. "Strong field tests of relativistic gravity and binary pulsars". In: *Phys. Rev.* D45 (1992), pp. 1840–1868. DOI: 10.1103/PhysRevD.45.1840.

[174] Pierre Astier and Reynald Pain. "Observational Evidence of the Accelerated Expansion of the Universe". In: *Comptes Rendus Physique* 13 (2012), pp. 521–538. DOI: 10.1016/j.crhy.2012.04.009. arXiv: 1204.5493 [astro-ph.CO].

[175] Alberto Nicolis, Riccardo Rattazzi, and Enrico Trincherini. "The Galileon as a local modification of gravity". In: *Phys. Rev. D* 79 (2009), p. 064036. DOI: 10.1103/PhysRevD.79.064036. arXiv: 0811.2197 [hep-th].

[176] David Pirtskhalava et al. "Weakly Broken Galileon Symmetry". In: *JCAP* 09 (2015), p. 007. DOI: 10.1088/1475-7516/2015/09/007. arXiv: 1505.00007 [hep-th].

[177] Luca Santoni, Enrico Trincherini, and Leonardo G. Trombetta. "Behind Horndeski: structurally robust higher derivative EFTs". In: *JHEP* 08 (2018), p. 118. DOI: 10.1007/JHEP08(2018)118. arXiv: 1806.10073 [hep-th].

[178] Gregory Walter Horndeski. "Second-order scalar-tensor field equations in a four-dimensional space". In: *Int. J. Theor. Phys.* 10 (1974), pp. 363–384. DOI: 10.1007/BF01807638.

[179] Jérôme Gleyzes et al. "Healthy theories beyond Horndeski". In: *Phys. Rev. Lett.* 114.21 (2015), p. 211101. DOI: 10.1103/PhysRevLett.114.211101. arXiv: 1404.6495 [hep-th].

[180] Miguel Zumalacárregui and Juan García-Bellido. "Transforming gravity: from derivative couplings to matter to second-order scalar-tensor theories beyond the Horndeski Lagrangian". In: *Phys. Rev. D* 89 (2014), p. 064046. DOI: 10.1103/PhysRevD.89.064046. arXiv: 1308.4685 [gr-qc].

[181] David Langlois and Karim Noui. "Degenerate higher derivative theories beyond Horndeski: evading the Ostrogradski instability". In: *JCAP* 02 (2016), p. 034. DOI: 10.1088/1475-7516/2016/02/034. arXiv: 1510.06930 [gr-qc].

[182] David Langlois and Karim Noui. "Hamiltonian analysis of higher derivative scalar-tensor theories". In: *JCAP* 07 (2016), p. 016. DOI: 10.1088/1475-7516/2016/07/016. arXiv: 1512.06820 [gr-qc].

[183] Marco Crisostomi et al. "Horndeski: beyond, or not beyond?" In: *JCAP* 03 (2016), p. 038. DOI: 10.1088/1475-7516/2016/03/038. arXiv: 1601.04658 [hep-th].

[184] Jibril Ben Achour et al. "Degenerate higher order scalar-tensor theories beyond Horndeski up to cubic order". In: *JHEP* 12 (2016), p. 100. DOI: 10.1007/JHEP12(2016)100. arXiv: 1608.08135 [hep-th].

[185] Jibril Ben Achour, David Langlois, and Karim Noui. "Degenerate higher order scalar-tensor theories beyond Horndeski and disformal transformations". In: *Phys. Rev. D* 93.12 (2016), p. 124005. DOI: 10.1103/PhysRevD.93.124005. arXiv: 1602.08398 [gr-qc].

[186] Marco Crisostomi, Kazuya Koyama, and Gianmassimo Tasinato. "Extended Scalar-Tensor Theories of Gravity". In: *JCAP* 04 (2016), p. 044. DOI: 10.1088/1475-7516/2016/04/044. arXiv: 1602.03119 [hep-th].

[187] David Langlois. "Dark energy and modified gravity in degenerate higher-order scalar–tensor (DHOST) theories: A review". In: *Int. J. Mod. Phys. D* 28.05 (2019), p. 1942006. DOI: 10.1142/S0218271819420069. arXiv: 1811.06271 [gr-qc].

[188] Johannes Noller et al. "Black Hole Ringdown as a Probe for Dark Energy". In: *Phys. Rev. D* 101 (2020), p. 084049. DOI: 10.1103/PhysRevD.101.084049. arXiv: 1911.11671 [gr-qc].

[189] B.P. Abbott et al. "Gravitational Waves and Gamma-rays from a Binary Neutron Star Merger: GW170817 and GRB 170817A". In: *Astrophys. J. Lett.* 848.2 (2017), p. L13. DOI: 10.3847/2041-8213/aa920c. arXiv: 1710.05834 [astro-ph.HE].

[190] Paolo Creminelli et al. "Gravitational Wave Decay into Dark Energy". In: *JCAP* 1812 (2018), p. 025. DOI: 10.1088/1475-7516/2018/12/025. arXiv: 1809.03484 [astro-ph.CO].

[191] Paolo Creminelli et al. "Resonant Decay of Gravitational Waves into Dark Energy". In: *JCAP* 10 (2019), p. 072. DOI: 10.1088/1475-7516/2019/10/072. arXiv: 1906.07015 [gr-qc].

[192] Paolo Creminelli et al. "Dark-Energy Instabilities induced by Gravitational Waves". In: *JCAP* 05 (2020), p. 002. DOI: 10.1088/1475-7516/2020/05/002. arXiv: 1910.14035 [gr-qc].

[193] Guillermo Lara et al. "Robustness of kinetic screening against matter coupling". In: *Phys. Rev. D* 107.4 (2023), p. 044019. DOI: 10.1103/PhysRevD.107.044019. arXiv: 2207.03437 [gr-qc].

[194] Enrico Barausse et al. "Neutron-star mergers in scalar-tensor theories of gravity". In: *Phys. Rev. D* 87 (2013), p. 081506. DOI: 10.1103/PhysRevD.87.081506. arXiv: 1212.5053 [gr-qc].

[195] Carlos Palenzuela et al. "Dynamical scalarization of neutron stars in scalar-tensor gravity theories". In: *Phys. Rev. D* 89.4 (2014), p. 044024. DOI: 10.1103/PhysRevD.89.044024. arXiv: 1310.4481 [gr-qc].

[196] C. Armendariz-Picon, Viatcheslav F. Mukhanov, and Paul J. Steinhardt. "A Dynamical solution to the problem of a small cosmological constant and late time cosmic acceleration". In: *Phys. Rev. Lett.* 85 (2000), pp. 4438–4441. DOI: 10.1103/PhysRevLett.85.4438. arXiv: astro-ph/0004134.

[197] E. Babichev, C. Deffayet, and R. Ziour. "k-Mouflage gravity". In: *Int. J. Mod. Phys. D* 18 (2009), pp. 2147–2154. DOI: 10.1142/S0218271809016107. arXiv: 0905.2943 [hep-th].

[198] Lotte ter Haar et al. "Dynamics of Screening in Modified Gravity". In: *Phys. Rev. Lett.* 126 (2021), p. 091102. DOI: 10.1103/PhysRevLett.126.091102. arXiv: 2009.03354 [gr-qc].

[199] Miguel Bezares et al. "Kinetic screening in nonlinear stellar oscillations and gravitational collapse". In: *Phys. Rev. D* 104.4 (2021), p. 044022. DOI: 10.1103/PhysRevD.104.044022. arXiv: 2105.13992 [gr-qc].

[200] Miguel Bezares et al. "No Evidence of Kinetic Screening in Simulations of Merging Binary Neutron Stars beyond General Relativity". In: *Phys. Rev. Lett.* 128.9 (2022), p. 091103. DOI: 10.1103/PhysRevLett.128.091103. arXiv: 2107.05648 [gr-qc].

[201] D. M. Eardley. "Observable effects of a scalar gravitational field in a binary pulsar". In: *Astrophys. J.* 196 (1975). DOI: 10.1086/181744.

[202] Clifford M. Will and Helmut W. Zaglauer. "Gravitational Radiation, Close Binary Systems, and the Brans-dicke Theory of Gravity". In: *Astrophys. J.* 346 (1989), p. 366. DOI: 10.1086/168016.

[203] E. T. Newman and A. I. Janis. "Note on the Kerr Spinning-Particle Metric". In: *Journal of Mathematical Physics* 6.6 (1965), pp. 915–917. DOI: 10.1063/1.1704350. eprint: https://doi.org/10.1063/1.1704350. URL: https://doi.org/10.1063/1.1704350.

[204] Brandon Carter. "Global Structure of the Kerr Family of Gravitational Fields". In: *Phys. Rev.* 174 (5 1968), pp. 1559–1571. DOI: 10.1103/PhysRev.174.1559. URL: https://link.aps.org/doi/10.1103/PhysRev.174.1559.

[205] Walter D. Goldberger and Ira Z. Rothstein. "An Effective field theory of gravity for extended objects". In: *Phys. Rev. D* 73 (2006), p. 104029. DOI: 10.1103/PhysRevD.73.104029. arXiv: hep-th/0409156.

[206] Walter D. Goldberger and Ira Z. Rothstein. "Dissipative effects in the worldline approach to black hole dynamics". In: *Phys. Rev. D* 73 (2006), p. 104030. DOI: 10.1103/PhysRevD.73.104030. arXiv: hep-th/0511133.

[207] Rafael A. Porto. "The effective field theorist's approach to gravitational dynamics". In: *Phys. Rept.* 633 (2016), pp. 1–104. DOI: 10.1016/j.physrep.2016.04.003. arXiv: 1601.04914 [hep-th].

[208] Walter D. Goldberger, Jingping Li, and Ira Z. Rothstein. "Non-conservative effects on spinning black holes from world-line effective field theory". In: *JHEP* 06 (2021), p. 053. DOI: 10.1007/JHEP06(2021)053. arXiv: 2012.14869 [hep-th].

[209] Rafael A. Porto and Ira Z. Rothstein. "The Hyperfine Einstein-Infeld-Hoffmann potential". In: *Phys. Rev. Lett.* 97 (2006), p. 021101. DOI: 10.1103/PhysRevLett.97.021101. arXiv: gr-qc/0604099.

[210] L. D. Landau and E. M. Lifshitz. *Electrodynamics of Continuous Media*. 2nd. Vol. 8. Course of Theoretical Physics. See Section 6 for discussion of polarizability. Oxford: Pergamon Press, 1984.

[211] Tetsuo Goto. "Relativistic quantum mechanics of one-dimensional mechanical continuum and subsidiary condition of dual resonance model". In: *Prog. Theor. Phys.* 46 (1971), pp. 1560–1569. DOI: 10.1143/PTP.46.1560.

[212] S. W. Hawking. "Black holes in the Brans-Dicke theory of gravitation". In: *Communications in Mathematical Physics* 25.2 (1972), pp. 167 –171. DOI: cmp/1103857885. URL: https://doi.org/.

[213] Antoine Lehébel, Eugeny Babichev, and Christos Charmousis. "A no-hair theorem for stars in Horndeski theories". In: *JCAP* 07 (2017), p. 037. DOI: 10.1088/1475-7516/2017/07/037. arXiv: 1706.04989 [gr-qc].

[214] Alexander A. H. Graham and Rahul Jha. "Nonexistence of black holes with non-canonical scalar fields". In: *Phys. Rev. D* 89.8 (2014). [Erratum: Phys.Rev.D 92, 069901 (2015)], p. 084056. DOI: 10.1103/PhysRevD.89.084056. arXiv: 1401.8203 [gr-qc].

[215] Ted Jacobson. "Primordial black hole evolution in tensor scalar cosmology". In: *Phys. Rev. Lett.* 83 (1999), pp. 2699–2702. DOI: 10.1103/PhysRevLett.83.2699. arXiv: astro-ph/9905303.

[216] Christos Charmousis et al. "Rotating Black Holes in Higher Order Gravity". In: *Phys. Rev. D* 100.8 (2019), p. 084020. DOI: 10.1103/PhysRevD.100.084020. arXiv: 1903.05519 [hep-th].

[217] Kazufumi Takahashi and Hayato Motohashi. "General Relativity solutions with stealth scalar hair in quadratic higher-order scalar-tensor theories". In: *JCAP* 06 (2020), p. 034. DOI: 10.1088/1475-7516/2020/06/034. arXiv: 2004.03883 [gr-qc].

[218] Karim Van Aelst et al. "Hairy rotating black holes in cubic Galileon theory". In: *Class. Quant. Grav.* 37.3 (2020), p. 035007. DOI: 10.1088/1361-6382/ab6391. arXiv: 1910.08451 [gr-qc].

[219] Lam Hui and Alberto Nicolis. "No-Hair Theorem for the Galileon". In: *Phys. Rev. Lett.* 110 (2013), p. 241104. DOI: 10.1103/PhysRevLett.110.241104. arXiv: 1202.1296 [hep-th].

[220] Dražen Glavan and Chunshan Lin. "Einstein-Gauss-Bonnet Gravity in Four-Dimensional Spacetime". In: *Phys. Rev. Lett.* 124.8 (2020), p. 081301. DOI: 10.1103/PhysRevLett.124.081301. arXiv: 1905.03601 [gr-qc].

[221] Pedro G. S. Fernandes et al. "The 4D Einstein–Gauss–Bonnet theory of gravity: a review". In: *Class. Quant. Grav.* 39.6 (2022), p. 063001. DOI: 10.1088/1361-6382/ac500a. arXiv: 2202.13908 [gr-qc].

[222] Thomas P. Sotiriou and Shuang-Yong Zhou. "Black hole hair in generalized scalar-tensor gravity". In: *Phys. Rev. Lett.* 112 (2014), p. 251102. DOI: 10.1103/PhysRevLett.112.251102. arXiv: 1312.3622 [gr-qc].

[223] Thomas P. Sotiriou and Shuang-Yong Zhou. "Black hole hair in generalized scalar-tensor gravity: An explicit example". In: *Phys. Rev. D* 90 (2014), p. 124063. DOI: 10.1103/PhysRevD.90.124063. arXiv: 1408.1698 [gr-qc].

[224] P. Kanti et al. "Dilatonic black holes in higher curvature string gravity". In: *Phys. Rev. D* 54 (1996), pp. 5049–5058. DOI: 10.1103/PhysRevD.54.5049. arXiv: hep-th/9511071.

[225] Metin Gurses. "Some solutions of the Gauss-Bonnet gravity with scalar field in four dimensions". In: *Gen. Rel. Grav.* 40 (2008), pp. 1825–1830. DOI: 10.1007/s10714-007-0579-z. arXiv: 0707.0347 [gr-qc].

[226] Carlos A. R. Herdeiro et al. "Spin-induced scalarized black holes". In: *Phys. Rev. Lett.* 126.1 (2021), p. 011103. DOI: 10.1103/PhysRevLett.126.011103. arXiv: 2009.03904 [gr-qc].

[227] Alexandru Dima et al. "Spin-induced black hole spontaneous scalarization". In: *Phys. Rev. Lett.* 125.23 (2020), p. 231101. DOI: 10.1103/PhysRevLett.125.231101. arXiv: 2006.03095 [gr-qc].

[228] J. M. Bardeen. "Rapidly rotating stars, disks, and black holes." In: *Black Holes (Les Astres Occlus)*. Jan. 1973, pp. 241–289.

[229] G. Darboux. *Leçons sur les systémes orthogonaux et les coordonnées curvilignes*. Cours de geometrie de la faculté des sciences. GAuthier Villars, 1910. URL: https://books.google.it/books?id=vmZbAAAAcAAJ.

[230] S. Chandrasekhar. *The Mathematical Theory of Black Holes*. International series of monographs on physics. Oxford University Press, 1992. ISBN: 9780198512912. URL: https://books.google.it/books?id=mLMYAQAAMAAJ.

[231] J. D. Bekenstein. "Nonexistence of baryon number for black holes. ii". In: *Phys. Rev. D* 5 (1972), pp. 2403–2412. DOI: 10.1103/PhysRevD.5.2403.

[232] Mehdi Saravani and Thomas P. Sotiriou. "Classification of shift-symmetric Horndeski theories and hairy black holes". In: *Phys. Rev. D* 99.12 (2019), p. 124004. DOI: 10.1103/PhysRevD.99.124004. arXiv: 1903.02055 [gr-qc].

[233] Robert Benkel et al. "Causal structure of black holes in shift-symmetric Horndeski theories". In: *Phys. Rev. D* 98.6 (2018), p. 064006. DOI: 10.1103/PhysRevD.98.064006. arXiv: 1806.08214 [gr-qc].

[234] Kent Yagi. "New constraint on scalar Gauss-Bonnet gravity and a possible explanation for the excess of the orbital decay rate in a low-mass x-ray binary". In: *Physical Review D* 86 (2012), p. 081504. URL: https://api.semanticscholar.org/CorpusID:118441569.

[235] Jacob D. Bekenstein. "Nonexistence of baryon number for static black holes". In: *Phys. Rev. D* 5 (1972), pp. 1239–1246. DOI: 10.1103/PhysRevD.5.1239.

[236] Roberto Emparan and Harvey S. Reall. "Black Holes in Higher Dimensions". In: *Living Rev. Rel.* 11 (2008), p. 6. DOI: 10.12942/lrr-2008-6. arXiv: 0801.3471 [hep-th].

[237] Robert C. Myers and M. J. Perry. "Black Holes in Higher Dimensional Space-Times". In: *Annals Phys.* 172 (1986), p. 304. DOI: 10.1016/0003-4916(86)90186-7.

[238] Lam Hui et al. "Static response and Love numbers of Schwarzschild black holes". In: *JCAP* 04 (2021), p. 052. DOI: 10.1088/1475-7516/2021/04/052. arXiv: 2010.00593 [hep-th].

[239] Alexander A. H. Graham and Rahul Jha. "Stationary Black Holes with Time-Dependent Scalar Fields". In: *Phys. Rev. D* 90.4 (2014), p. 041501. DOI: 10.1103/PhysRevD.90.041501. arXiv: 1407.6573 [gr-qc].

[240] Shinji Mukohyama. "Black holes in the ghost condensate". In: *Phys. Rev. D* 71 (2005), p. 104019. DOI: 10.1103/PhysRevD.71.104019. arXiv: hep-th/0502189.

[241] Eugeny Babichev and Christos Charmousis. "Dressing a black hole with a time-dependent Galileon". In: *JHEP* 08 (2014), p. 106. DOI: 10.1007/JHEP08(2014)106. arXiv: 1312.3204 [gr-qc].

[242] Tsutomu Kobayashi and Norihiro Tanahashi. "Exact black hole solutions in shift symmetric scalar–tensor theories". In: *PTEP* 2014 (2014), 073E02. DOI: 10.1093/ptep/ptu096. arXiv: 1403.4364 [gr-qc].

[243] Jibril Ben Achour and Hongguang Liu. "Hairy Schwarzschild-(A)dS black hole solutions in degenerate higher order scalar-tensor theories beyond shift symmetry". In: *Phys. Rev. D* 99.6 (2019), p. 064042. DOI: 10.1103/PhysRevD.99.064042. arXiv: 1811.05369 [gr-qc].

[244] Hayato Motohashi and Masato Minamitsuji. "Exact black hole solutions in shift-symmetric quadratic degenerate higher-order scalar-tensor theories". In: *Phys. Rev. D* 99.6 (2019), p. 064040. DOI: 10.1103/PhysRevD.99.064040. arXiv: 1901.04658 [gr-qc].

[245] Oscar Ramos and Enrico Barausse. "Constraints on Hořava gravity from binary black hole observations". In: *Phys. Rev. D* 99.2 (2019). [Erratum: Phys.Rev.D 104, 069904 (2021)], p. 024034. DOI: 10.1103/PhysRevD.99.024034. arXiv: 1811.07786 [gr-qc].

[246] Enrico Barausse and Kent Yagi. "Gravitation-Wave Emission in Shift-Symmetric Horndeski Theories". In: *Phys. Rev. Lett.* 115.21 (2015), p. 211105. DOI: 10.1103/PhysRevLett.115.211105. arXiv: 1509.04539 [gr-qc].

[247] Paolo Creminelli et al. "Hairy Black-holes in Shift-symmetric Theories". In: *JHEP* 08 (2020), p. 045. DOI: 10.1007/JHEP08(2020)045. arXiv: 2004.02893 [hep-th].

[248] Keisuke Nakashi and Masashi Kimura. "Towards rotating noncircular black holes in string-inspired gravity". In: *Phys. Rev. D* 102.8 (2020), p. 084021. DOI: 10.1103/PhysRevD.102.084021. arXiv: 2008.04003 [gr-qc].

[249] Yiqi Xie et al. "Square Peg in a Circular Hole: Choosing the Right Ansatz for Isolated Black Holes in Generic Gravitational Theories". In: *Phys. Rev. Lett.* 126.24 (2021), p. 241104. DOI: 10.1103/PhysRevLett.126.241104. arXiv: 2103.03925 [gr-qc].

[250] Timothy Anson et al. "Disforming the Kerr metric". In: *JHEP* 01 (2021), p. 018. DOI: 10.1007/JHEP01(2021)018. arXiv: 2006.06461 [gr-qc].

[251] Jibril Ben Achour et al. "On rotating black holes in DHOST theories". In: *JCAP* 11 (2020), p. 001. DOI: 10.1088/1475-7516/2020/11/001. arXiv: 2006.07245 [gr-qc].

[252] Yohsuke Takamori et al. "Testing the Non-circularity of the Spacetime around Sagittarius A* with Orbiting Pulsars". In: (Aug. 2021). DOI: 10.1093/pasj/psac003. arXiv: 2108.13026 [gr-qc].

[253] V. A. Rubakov. "The Null Energy Condition and its violation". In: *Phys. Usp.* 57 (2014), pp. 128–142. DOI: 10.3367/UFNe.0184.201402b.0137. arXiv: 1401.4024 [hep-th].

[254] Gabriele Franciolini et al. "Stable wormholes in scalar-tensor theories". In: *JHEP* 01 (2019), p. 221. DOI: 10.1007/JHEP01(2019)221. arXiv: 1811.05481 [hep-th].

[255] Hector O. Silva et al. "Spontaneous scalarization of black holes and compact stars from a Gauss-Bonnet coupling". In: *Phys. Rev. Lett.* 120.13 (2018), p. 131104. DOI: 10.1103/PhysRevLett.120.131104. arXiv: 1711.02080 [gr-qc].

[256] Daniela D. Doneva and Stoytcho S. Yazadjiev. "New Gauss-Bonnet Black Holes with Curvature-Induced Scalarization in Extended Scalar-Tensor Theories". In: *Phys. Rev. Lett.* 120 (13 2018), p. 131103. DOI: 10.1103/PhysRevLett.120.131103. URL: https://link.aps.org/doi/10.1103/PhysRevLett.120.131103.

[257] T. Damour, N. Deruelle, and R. Ruffini. "On Quantum Resonances in Stationary Geometries". In: *Lett. Nuovo Cim.* 15 (1976), pp. 257–262. DOI: 10.1007/BF02725534.

[258] T. J. M. Zouros and D. M. Eardley. "Instabilities of massive scalar perturbations of a rotating black hole". In: *Annals Phys.* 118 (1979), pp. 139–155. DOI: 10.1016/0003-4916(79)90237-9.

[259] Sam R. Dolan. "Instability of the massive Klein-Gordon field on the Kerr spacetime". In: *Phys. Rev. D* 76 (2007), p. 084001. DOI: 10.1103/PhysRevD.76.084001. arXiv: 0705.2880 [gr-qc].

[260] Alexandru Dima and Enrico Barausse. "Numerical investigation of plasma-driven superradiant instabilities". In: *Class. Quant. Grav.* 37.17 (2020), p. 175006. DOI: 10.1088/1361-6382/ab9ce0. arXiv: 2001.11484 [gr-qc].

[261] Lam Hui et al. "Ladder symmetries of black holes. Implications for love numbers and no-hair theorems". In: *JCAP* 01.01 (2022), p. 032. DOI: 10.1088/1475-7516/2022/01/032. arXiv: 2105.01069 [hep-th].

[262] Lam Hui et al. "Near-zone symmetries of Kerr black holes". In: *JHEP* 09 (2022), p. 049. DOI: 10.1007/JHEP09(2022)049. arXiv: 2203.08832 [hep-th].

[263] Enrico Barausse, Nicolás Yunes, and Katie Chamberlain. "Theory-Agnostic Constraints on Black-Hole Dipole Radiation with Multiband Gravitational-Wave Astrophysics". In: *Phys. Rev. Lett.* 116.24 (2016), p. 241104. DOI: 10.1103/PhysRevLett.116.241104. arXiv: 1603.04075 [gr-qc].

[264] C. V. Vishveshwara. "Scattering of Gravitational Radiation by a Schwarzschild Black-hole". In: 227.5261 (Aug. 1970), pp. 936–938. DOI: 10.1038/227936a0.

[265] S. Chandrasekhar and S. Detweiler. "The Quasi-Normal Modes of the Schwarzschild Black Hole". In: *Proceedings of the Royal Society of London. Series A, Mathematical and Physical Sciences* 344.1639 (1975), pp. 441–452. ISSN: 00804630. URL: http://www.jstor.org/stable/78902 (visited on 02/09/2024).

[266] Peter Anninos et al. "Collision of two black holes". In: *Physical Review Letters* 71.18 (Nov. 1993), 2851–2854. ISSN: 0031-9007. DOI: 10.1103/physrevlett.71.2851. URL: http://dx.doi.org/10.1103/PhysRevLett.71.2851.

[267] Kostas D. Kokkotas and Bernd G. Schmidt. "Quasinormal modes of stars and black holes". In: *Living Rev. Rel.* 2 (1999), p. 2. DOI: 10.12942/lrr-1999-2. arXiv: gr-qc/9909058.

[268] Emanuele Berti, Vitor Cardoso, and Andrei O Starinets. "Quasinormal modes of black holes and black branes". In: *Classical and Quantum Gravity* 26.16 (July 2009), p. 163001. ISSN: 1361-6382. DOI: 10.1088/0264-9381/26/16/163001. URL: http://dx.doi.org/10.1088/0264-9381/26/16/163001.

[269] R. A. Konoplya and Alexander Zhidenko. "Quasinormal modes of black holes: From astrophysics to string theory". In: *Reviews of Modern Physics* 83.3 (July 2011), 793–836. ISSN: 1539-0756. DOI: 10.1103/revmodphys.83.793. URL: http://dx.doi.org/10.1103/RevModPhys.83.793.

[270] Emanuele Berti et al. "Black hole spectroscopy: from theory to experiment". In: (May 2025). arXiv: 2505.23895 [gr-qc].

[271] Tullio Regge and John A. Wheeler. "Stability of a Schwarzschild Singularity". In: *Phys. Rev.* 108 (4 1957), pp. 1063–1069. DOI: 10.1103/PhysRev.108.1063. URL: https://link.aps.org/doi/10.1103/PhysRev.108.1063.

[272] Frank J. Zerilli. "Effective Potential for Even-Parity Regge-Wheeler Gravitational Perturbation Equations". In: *Phys. Rev. Lett.* 24 (13 1970), pp. 737–738. DOI: 10.1103/PhysRevLett.24.737. URL: https://link.aps.org/doi/10.1103/PhysRevLett.24.737.

[273] V. Moncrief. "Gravitational perturbations of spherically symmetric systems. I. The exterior problem." In: *Annals Phys.* 88 (1974), pp. 323–342. DOI: 10.1016/0003-4916(74)90173-0.

[274] Ulrich H. Gerlach and Uday K. Sengupta. "Gauge-invariant perturbations on most general spherically symmetric space-times". In: *Phys. Rev. D* 19 (8 1979), pp. 2268–2272. DOI: 10.1103/PhysRevD.19.2268. URL: https://link.aps.org/doi/10.1103/PhysRevD.19.2268.

[275] Karl Martel and Eric Poisson. "Gravitational perturbations of the Schwarzschild spacetime: A Practical covariant and gauge-invariant formalism". In: *Phys. Rev. D* 71 (2005), p. 104003. DOI: 10.1103/PhysRevD.71.104003. arXiv: gr-qc/0502028.

[276] Saul A. Teukolsky. "Perturbations of a rotating black hole. 1. Fundamental equations for gravitational electromagnetic and neutrino field perturbations". In: *Astrophys. J.* 185 (1973), pp. 635–647. DOI: 10.1086/152444.

[277] Bernard F. Schutz and Clifford M. Will. "BLACK HOLE NORMAL MODES: A SEMIANALYTIC APPROACH". In: *Astrophys. J. Lett.* 291 (1985), pp. L33–L36. DOI: 10.1086/184453.

[278] Maximiliano Isi et al. "Testing the no-hair theorem with GW150914". In: *Phys. Rev. Lett.* 123.11 (2019), p. 111102. DOI: 10.1103/PhysRevLett.123.111102. arXiv: 1905.00869 [gr-qc].

[279] Maximiliano Isi and Will M. Farr. "Analyzing black-hole ringdowns". In: (July 2021). arXiv: 2107.05609 [gr-qc].

[280] Maximiliano Isi and Will M. Farr. "Revisiting the ringdown of GW150914". In: (Feb. 2022). arXiv: 2202.02941 [gr-qc].

[281] Frans Pretorius. "Evolution of binary black hole spacetimes". In: *Phys. Rev. Lett.* 95 (2005), p. 121101. DOI: 10.1103/PhysRevLett.95.121101. arXiv: gr-qc/0507014.

[282] Carlos O. Lousto. "A time-domain fourth-order-convergent numerical algorithm to integrate black hole perturbations in the extreme-mass-ratio limit". In: *Class. Quant. Grav.* 22 (2005), S543–S568. DOI: 10.1088/0264-9381/22/15/001. arXiv: gr-qc/0503001.

[283] Enrique Pazos-Avalos and Carlos O. Lousto. "Numerical integration of the Teukolsky equation in the time domain". In: *Phys. Rev. D* 72 (2005), p. 084022. DOI: 10.1103/PhysRevD.72.084022. arXiv: gr-qc/0409065.

[284] William Krivan et al. "Dynamics of perturbations of rotating black holes". In: *Phys. Rev. D* 56 (1997), pp. 3395–3404. DOI: 10.1103/PhysRevD.56.3395. arXiv: gr-qc/9702048.

[285] Emanuele Berti et al. "Stability of the fundamental quasinormal mode in time-domain observations against small perturbations". In: *Physical Review D* 106.8 (Oct. 2022). ISSN: 2470-0029. DOI: 10.1103/physrevd.106.084011. URL: http://dx.doi.org/10.1103/PhysRevD.106.084011.

[286] E. W. Leaver. "An Analytic representation for the quasi normal modes of Kerr black holes". In: *Proc. Roy. Soc. Lond. A* 402 (1985), pp. 285–298. DOI: 10.1098/rspa.1985.0119.

[287] Halston Lim et al. "Exciting black hole modes via misaligned coalescences: II. The mode content of late-time coalescence waveforms". In: *Phys. Rev. D* 100.8 (2019), p. 084032. DOI: 10.1103/PhysRevD.100.084032. arXiv: 1901.05902 [gr-qc].

[288] Matthew Giesler et al. "Black Hole Ringdown: The Importance of Overtones". In: *Phys. Rev. X* 9.4 (2019), p. 041060. DOI: 10.1103/PhysRevX.9.041060. arXiv: 1903.08284 [gr-qc].

[289] Matthew Giesler et al. "Overtones and nonlinearities in binary black hole ringdowns". In: *Phys. Rev. D* 111.8 (2025), p. 084041. DOI: 10.1103/PhysRevD.111.084041. arXiv: 2411.11269 [gr-qc].

[290] Maria Okounkova. "Revisiting non-linearity in binary black hole mergers". In: (Apr. 2020). arXiv: 2004.00671 [gr-qc].

[291] Keefe Mitman et al. "Nonlinearities in Black Hole Ringdowns". In: *Phys. Rev. Lett.* 130.8 (2023), p. 081402. DOI: 10.1103/PhysRevLett.130.081402. arXiv: 2208.07380 [gr-qc].

[292] Jaime Redondo-Yuste et al. "Spin dependence of black hole ringdown nonlinearities". In: (Aug. 2023). arXiv: 2308.14796 [gr-qc].

[293] Bruno Bucciotti et al. "Nonlinear quasi-normal modes: uniform approximation". In: *JHEP* 12 (2023), p. 048. DOI: 10.1007/JHEP12(2023)048. arXiv: 2309.08501 [hep-th].

[294] Bruno Bucciotti et al. "Amplitudes and polarizations of quadratic quasi-normal modes for a Schwarzschild black hole". In: *JHEP* 09 (2024), p. 119. DOI: 10.1007/JHEP09(2024)119. arXiv: 2406.14611 [hep-th].

[295] Bruno Bucciotti et al. "Quadratic quasinormal modes of a Schwarzschild black hole". In: *Phys. Rev. D* 110.10 (2024), p. 104048. DOI: 10.1103/PhysRevD.110.104048. arXiv: 2405.06012 [gr-qc].

[296] Bruno Bucciotti et al. "Ringdown nonlinearities in the eikonal regime". In: (Jan. 2025). arXiv: 2501.17950 [gr-qc].

[297] Sophia Yi et al. "Nonlinear quasinormal mode detectability with next-generation gravitational wave detectors". In: *Phys. Rev. D* 109.12 (2024), p. 124029. DOI: 10.1103/PhysRevD.109.124029. arXiv: 2403.09767 [gr-qc].

[298] Laura Sberna et al. "Nonlinear effects in the black hole ringdown: Absorption-induced mode excitation". In: *Phys. Rev. D* 105 (6 2022), p. 064046. DOI: 10.1103/PhysRevD.105.064046. URL: https://link.aps.org/doi/10.1103/PhysRevD.105.064046.

[299] Jaime Redondo-Yuste, David Pereñiguez, and Vitor Cardoso. "Ringdown of a dynamical spacetime". In: *Phys. Rev. D* 109 (4 2024), p. 044048. DOI: 10.1103/PhysRevD.109.044048. URL: https://link.aps.org/doi/10.1103/PhysRevD.109.044048.

[300] Lodovico Capuano, Luca Santoni, and Enrico Barausse. "Perturbations of the Vaidya metric in the frequency domain: Quasinormal modes and tidal response". In: *Phys. Rev. D* 110 (8 2024), p. 084081. DOI: 10.1103/PhysRevD.110.084081. URL: https://link.aps.org/doi/10.1103/PhysRevD.110.084081.

[301] Edward W. Leaver. "Spectral decomposition of the perturbation response of the Schwarzschild geometry". In: *Phys. Rev. D* 34 (2 1986), pp. 384–408. DOI: 10.1103/PhysRevD.34.384. URL: https://link.aps.org/doi/10.1103/PhysRevD.34.384.

[302] Richard H. Price. "Nonspherical perturbations of relativistic gravitational collapse. 1. Scalar and gravitational perturbations". In: *Phys. Rev. D* 5 (1972), pp. 2419–2438. DOI: 10.1103/PhysRevD.5.2419.

[303] Richard H. Price. "Nonspherical Perturbations of Relativistic Gravitational Collapse. II. Integer-Spin, Zero-Rest-Mass Fields". In: *Phys. Rev. D* 5 (1972), pp. 2439–2454. DOI: 10.1103/PhysRevD.5.2439.

[304] Sizheng Ma et al. "Merging black holes with Cauchy-characteristic matching: Computation of late-time tails". In: (Dec. 2024). arXiv: 2412.06906 [gr-qc].

[305] Marina De Amicis et al. “Late-time tails in nonlinear evolutions of merging black holes”. In: (Dec. 2024). arXiv: 2412.06887 [gr-qc].

[306] Marina De Amicis, Simone Albanesi, and Gregorio Carullo. “Inspiral-inherited ringdown tails”. In: *Phys. Rev. D* 110 (10 2024), p. 104005. DOI: 10.1103/PhysRevD.110.104005. URL: https://link.aps.org/doi/10.1103/PhysRevD.110.104005.

[307] Leor Barack et al. “Black holes, gravitational waves and fundamental physics: a roadmap”. In: *Class. Quant. Grav.* 36.14 (2019), p. 143001. DOI: 10.1088/1361-6382/ab0587. arXiv: 1806.05195 [gr-qc].

[308] Nicolas Yunes, Xavier Siemens, and Kent Yagi. “Gravitational-Wave Tests of General Relativity with Ground-Based Detectors and Pulsar-Timing Arrays”. In: (Aug. 2024). arXiv: 2408.05240 [gr-qc].

[309] Eanna E. Flanagan and Tanja Hinderer. “Constraining neutron star tidal Love numbers with gravitational wave detectors”. In: *Phys. Rev. D* 77 (2008), p. 021502. DOI: 10.1103/PhysRevD.77.021502. arXiv: 0709.1915 [astro-ph].

[310] K. S. Thorne. “Multipole Expansions of Gravitational Radiation”. In: *Rev. Mod. Phys.* 52 (1980), pp. 299–339. DOI: 10.1103/RevModPhys.52.299.

[311] Tanja Hinderer. “Tidal Love numbers of neutron stars”. In: *Astrophys. J.* 677 (2008). [Erratum: Astrophys.J. 697, 964 (2009)], pp. 1216–1220. DOI: 10.1086/533487. arXiv: 0711.2420 [astro-ph].

[312] Taylor Binnington and Eric Poisson. “Relativistic theory of tidal Love numbers”. In: *Phys. Rev. D* 80 (2009), p. 084018. DOI: 10.1103/PhysRevD.80.084018. arXiv: 0906.1366 [gr-qc].

[313] Alexandre Le Tiec, Marc Casals, and Edgardo Franzin. “Tidal Love Numbers of Kerr Black Holes”. In: *Phys. Rev. D* 103.8 (2021), p. 084021. DOI: 10.1103/PhysRevD.103.084021. arXiv: 2010.15795 [gr-qc].

[314] Horng Sheng Chia. “Tidal deformation and dissipation of rotating black holes”. In: *Phys. Rev. D* 104.2 (2021), p. 024013. DOI: 10.1103/PhysRevD.104.024013. arXiv: 2010.07300 [gr-qc].

[315] Vitor Cardoso and Francisco Duque. “Environmental effects in gravitational-wave physics: Tidal deformability of black holes immersed in matter”. In: *Phys. Rev. D* 101.6 (2020), p. 064028. DOI: 10.1103/PhysRevD.101.064028. arXiv: 1912.07616 [gr-qc].

[316] Pablo A. Cano. “Love numbers beyond GR from the modified Teukolsky equation”. In: *JHEP* 07 (2025), p. 152. DOI: 10.1007/JHEP07(2025)152. arXiv: 2502.20185 [gr-qc].

[317] E. Franzin et al. “Testing strong gravity with gravitational waves and Love numbers”. In: *J. Phys. Conf. Ser.* 841.1 (2017). Ed. by Fabio Agostini, p. 012035. DOI: 10.1088/1742-6596/841/1/012035.

[318] Pablo A. Cano et al. “Parametrized quasinormal mode framework for modified Teukolsky equations”. In: *Phys. Rev. D* 110.10 (2024), p. 104007. DOI: 10.1103/PhysRevD.110.104007. arXiv: 2407.15947 [gr-qc].

[319] Lodovico Capuano et al. “Systematic bias in LISA ringdown analysis due to waveform inaccuracy”. In: (June 2025). arXiv: 2506.21181 [gr-qc].

[320] Rachel A. Rosen and Luca Santoni. "Black hole perturbations of massive and partially massless spin-2 fields in (anti) de Sitter spacetime". In: *JHEP* 03 (2021), p. 139. DOI: 10.1007/JHEP03(2021)139. arXiv: 2010.00595 [hep-th].

[321] Subrahmanyan Chandrasekhar. "On the equations governing the perturbations of the Schwarzschild black hole". In: *Proc. Roy. Soc. Lond. A* 343.1634 (1975), pp. 289–298. DOI: 10.1098/rspa.1975.0066.

[322] Avinash Khare. "Supersymmetry in quantum mechanics". In: *AIP Conf. Proc.* 744.1 (2004). Ed. by Roelof Bijker et al., pp. 133–165. DOI: 10.1063/1.1853201. arXiv: math-ph/0409003.

[323] P. T. Leung et al. "SUSY transformations for quasinormal and total transmission modes of open systems". In: (Sept. 1999). arXiv: math-ph/9909030.

[324] Alec Maassen van den Brink. "Analytic treatment of black hole gravitational waves at the algebraically special frequency". In: *Phys. Rev. D* 62 (2000), p. 064009. DOI: 10.1103/PhysRevD.62.064009. arXiv: gr-qc/0001032.

[325] G. Darboux. *On a proposition relative to linear equations*. 1999. arXiv: physics/9908003 [physics.hist-ph]. URL: https://arxiv.org/abs/physics/9908003.

[326] V. G. Bagrov and B. F. Samsonov. "Darboux transformation of the Schrodinger equation". In: *Phys. Part. Nucl.* 28 (1997), pp. 374–397. DOI: 10.1134/1.953045.

[327] Kostas Glampedakis, Aaron D. Johnson, and Daniel Kennefick. "Darboux transformation in black hole perturbation theory". In: *Phys. Rev. D* 96.2 (2017), p. 024036. DOI: 10.1103/PhysRevD.96.024036. arXiv: 1702.06459 [gr-qc].

[328] L. D. Landau and E. M. Lifshitz. *Quantum Mechanics: Non-Relativistic Theory*. 3rd. Vol. 3. Course of Theoretical Physics. Pergamon Press, 1977. ISBN: 9780750635394.

[329] Hans-Peter Nollert and Bernd G. Schmidt. "Quasinormal modes of Schwarzschild black holes: Defined and calculated via Laplace transformation". In: *Phys. Rev. D* 45.8 (1992), p. 2617. DOI: 10.1103/PhysRevD.45.2617.

[330] Gregor Wentzel. "Eine Verallgemeinerung der Quantenbedingungen für die Zwecke der Wellenmechanik". In: *Zeitschrift für Physik* 38.6-7 (1926), pp. 518–529. DOI: 10.1007/BF01397171.

[331] H.A. Kramers. "Wellenmechanik und halbzahlige Quantisierung". In: *Zeitschrift für Physik* 39.10-11 (1926), pp. 828–840. DOI: 10.1007/BF01390892.

[332] Léon Brillouin. "La mécanique ondulatoire de Schrödinger; une méthode générale de résolution par approximations successives". In: *Comptes Rendus de l'Académie des Sciences (Paris)* 183 (1926), pp. 24–26.

[333] Carl M. Bender and Steven A. Orszag. *Advanced Mathematical Methods for Scientists and Engineers I*. Springer, 1999. DOI: 10.1007/978-1-4757-3069-2.

[334] Sai Iyer and Clifford M. Will. "Black Hole Normal Modes: A WKB Approach. 1. Foundations and Application of a Higher Order WKB Analysis of Potential Barrier Scattering". In: *Phys. Rev. D* 35 (1987), p. 3621. DOI: 10.1103/PhysRevD.35.3621.

[335] R. A. Konoplya. "Quasinormal behavior of the d-dimensional Schwarzschild black hole and higher order WKB approach". In: *Phys. Rev. D* 68 (2003), p. 024018. DOI: 10.1103/PhysRevD.68.024018. arXiv: gr-qc/0303052.

[336] Valeria Ferrari and Bahram Mashhoon. "Oscillations of a Black Hole". In: *Phys. Rev. Lett.* 52.16 (1984), p. 1361. DOI: 10.1103/PhysRevLett.52.1361.

[337] Valeria Ferrari and Bahram Mashhoon. "New approach to the quasinormal modes of a black hole". In: *Phys. Rev. D* 30 (1984), pp. 295–304. DOI: 10.1103/PhysRevD.30.295.

[338] S. Chandrasekhar and Steven L. Detweiler. "The quasi-normal modes of the Schwarzschild black hole". In: *Proc. Roy. Soc. Lond. A* 344 (1975), pp. 441–452. DOI: 10.1098/rspa.1975.0112.

[339] Steven L. Detweiler. "Resonant oscillations of a rapidly rotating black hole". In: *Proc. Roy. Soc. Lond. A* 352 (1977), pp. 381–395. DOI: 10.1098/rspa.1977.0005.

[340] Sean Fortuna and Ian Vega. "Bernstein spectral method for quasinormal modes and other eigenvalue problems". In: *Eur. Phys. J. C* 83.12 (2023), p. 1170. DOI: 10.1140/epjc/s10052-023-12350-9. arXiv: 2003.06232 [gr-qc].

[341] Adrian Ka-Wai Chung, Pratik Wagle, and Nicolas Yunes. "Spectral method for the gravitational perturbations of black holes: Schwarzschild background case". In: *Phys. Rev. D* 107.12 (2023), p. 124032. DOI: 10.1103/PhysRevD.107.124032. arXiv: 2302.11624 [gr-qc].

[342] Adrian Ka-Wai Chung, Pratik Wagle, and Nicolas Yunes. "Spectral method for metric perturbations of black holes: Kerr background case in general relativity". In: *Phys. Rev. D* 109.4 (2024), p. 044072. DOI: 10.1103/PhysRevD.109.044072. arXiv: 2312.08435 [gr-qc].

[343] Manuela Campanelli and Carlos O. Lousto. "Second order gauge invariant gravitational perturbations of a Kerr black hole". In: *Phys. Rev. D* 59 (1999), p. 124022. DOI: 10.1103/PhysRevD.59.124022. arXiv: gr-qc/9811019.

[344] Reinaldo J Gleiser et al. "Second-order perturbations of a Schwarzschild black hole". In: *Classical and Quantum Gravity* 13.10 (1996), pp. L117–L124. DOI: 10.1088/0264-9381/13/10/001. URL: https://doi.org/10.1088%2F0264-9381%2F13%2F10%2F001.

[345] Reinaldo J. Gleiser et al. "Gravitational radiation from Schwarzschild black holes: the second-order perturbation formalism". In: *Physics Reports* 325.2 (2000), pp. 41–81. DOI: 10.1016/s0370-1573(99)00048-4. URL: https://doi.org/10.1016%2Fs0370-1573%2899%2900048-4.

[346] Alcides Garat and Richard H. Price. "Gauge invariant formalism for second order perturbations of Schwarzschild space-times". In: *Phys. Rev. D* 61 (2000), p. 044006. DOI: 10.1103/PhysRevD.61.044006. arXiv: gr-qc/9909005.

[347] Hiroyuki Nakano and Kunihito Ioka. "Second-order quasinormal mode of the Schwarzschild black hole". In: *Physical Review D* 76.8 (2007). DOI: 10.1103/physrevd.76.084007. URL: https://doi.org/10.1103%2Fphysrevd.76.084007.

[348] Eric Poisson and Misao Sasaki. "Gravitational radiation from a particle in circular orbit around a black hole. 5: Black hole absorption and tail corrections". In: *Phys. Rev. D* 51 (1995), pp. 5753–5767. DOI: 10.1103/PhysRevD.51.5753. arXiv: gr-qc/9412027.

[349] Hideyuki Tagoshi, Shuhei Mano, and Eiichi Takasugi. "PostNewtonian expansion of gravitational waves from a particle in circular orbits around a rotating black hole: Effects of black hole absorption". In: *Prog. Theor. Phys.* 98 (1997), pp. 829–850. DOI: 10.1143/PTP.98.829. arXiv: gr-qc/9711072.

[350] Eric Poisson. "Absorption of mass and angular momentum by a black hole: Time-domain formalisms for gravitational perturbations, and the small-hole or slow-motion approximation". In: *Physical Review D* 70.8 (Oct. 2004). ISSN: 1550-2368. DOI: 10.1103/physrevd.70.084044. URL: http://dx.doi.org/10.1103/PhysRevD.70.084044.

[351] Sebastiano Bernuzzi, Alessandro Nagar, and Anil Zenginoglu. "Horizon-absorption effects in coalescing black-hole binaries: An effective-one-body study of the non-spinning case". In: *Phys. Rev. D* 86 (2012), p. 104038. DOI: 10.1103/PhysRevD.86.104038. arXiv: 1207.0769 [gr-qc].

[352] Mark Ho-Yeuk Cheung et al. "Nonlinear Effects in Black Hole Ringdown". In: *Phys. Rev. Lett.* 130.8 (2023), p. 081401. DOI: 10.1103/PhysRevLett.130.081401. arXiv: 2208.07374 [gr-qc].

[353] Ezra Newman and Roger Penrose. "An Approach to gravitational radiation by a method of spin coefficients". In: *J. Math. Phys.* 3 (1962), pp. 566–578. DOI: 10.1063/1.1724257.

[354] William Kinnersley. "Type D Vacuum Metrics". In: *J. Math. Phys.* 10 (1969), pp. 1195–1203. DOI: 10.1063/1.1664958.

[355] P. L. Chrzanowski. "Vector Potential and Metric Perturbations of a Rotating Black Hole". In: *Phys. Rev. D* 11 (1975), pp. 2042–2062. DOI: 10.1103/PhysRevD.11.2042.

[356] Dongjun Li et al. "Perturbations of Spinning Black Holes beyond General Relativity: Modified Teukolsky Equation". In: *Phys. Rev. X* 13.2 (2023), p. 021029. DOI: 10.1103/PhysRevX.13.021029. arXiv: 2206.10652 [gr-qc].

[357] A. Z. Petrov. "The Classification of spaces defining gravitational fields". In: *Gen. Rel. Grav.* 32 (2000), pp. 1661–1663. DOI: 10.1023/A:1001910908054.

[358] Barak Kol and Michael Smolkin. "Black hole stereotyping: Induced gravito-static polarization". In: *JHEP* 02 (2012), p. 010. DOI: 10.1007/JHEP02(2012)010. arXiv: 1110.3764 [hep-th].

[359] Sayan Chakrabarti, Térence Delsate, and Jan Steinhoff. "New perspectives on neutron star and black hole spectroscopy and dynamic tides". In: *arXiv e-prints*, arXiv:1304.2228 (Apr. 2013), arXiv:1304.2228. DOI: 10.48550/arXiv.1304.2228. arXiv: 1304.2228 [gr-qc].

[360] Vitor Cardoso et al. "Testing strong-field gravity with tidal Love numbers". In: *Phys. Rev. D* 95.8 (2017). [Addendum: Phys.Rev.D 95, 089901 (2017)], p. 084014. DOI: 10.1103/PhysRevD.95.084014. arXiv: 1701.01116 [gr-qc].

[361] M. V. S. Saketh, Zihan Zhou, and Mikhail M. Ivanov. "Dynamical tidal response of Kerr black holes from scattering amplitudes". In: *Phys. Rev. D* 109.6 (2024), p. 064058. DOI: 10.1103/PhysRevD.109.064058. arXiv: 2307.10391 [hep-th].

[362] Kip S. Thorne. "Tidal stabilization of rigidly rotating, fully relativistic neutron stars". In: *Phys. Rev. D* 58 (1998), p. 124031. DOI: 10.1103/PhysRevD.58.124031. arXiv: gr-qc/9706057.

[363] Norman Gürlebeck. "No-hair theorem for Black Holes in Astrophysical Environments". In: *Phys. Rev. Lett.* 114.15 (2015), p. 151102. DOI: 10.1103/PhysRevLett.114.151102. arXiv: 1503.03240 [gr-qc].

[364] Eric Poisson. "Compact body in a tidal environment: New types of relativistic Love numbers, and a post-Newtonian operational definition for tidally induced multipole moments". In: *Phys. Rev. D* 103.6 (2021), p. 064023. DOI: 10.1103/PhysRevD.103.064023. arXiv: 2012.10184 [gr-qc].

[365] Massimiliano Maria Riva et al. "Vanishing of nonlinear tidal Love numbers of Schwarzschild black holes". In: *Phys. Lett. B* 854 (2024), p. 138710. DOI: 10.1016/j.physletb.2024.138710. arXiv: 2312.05065 [gr-qc].

[366] Hua Fang and Geoffrey Lovelace. "Tidal coupling of a Schwarzschild black hole and circularly orbiting moon". In: *Phys. Rev. D* 72 (2005), p. 124016. DOI: 10.1103/PhysRevD.72.124016. arXiv: gr-qc/0505156.

[367] Thibault Damour and Alessandro Nagar. "Relativistic tidal properties of neutron stars". In: *Phys. Rev. D* 80 (2009), p. 084035. DOI: 10.1103/PhysRevD.80.084035. arXiv: 0906.0096 [gr-qc].

[368] Panagiotis Charalambous, Sergei Dubovsky, and Mikhail M. Ivanov. "On the vanishing of Love numbers for Kerr black holes". In: *Journal of High Energy Physics* 2021.5 (May 2021). ISSN: 1029-8479. DOI: 10.1007/jhep05(2021)038. URL: http://dx.doi.org/10.1007/JHEP05(2021)038.

[369] Maria J. Rodriguez et al. "Love numbers for rotating black holes in higher dimensions". In: *Phys. Rev. D* 108.8 (2023), p. 084011. DOI: 10.1103/PhysRevD.108.084011. arXiv: 2304.03743 [hep-th].

[370] Sreejith Nair, Sumanta Chakraborty, and Sudipta Sarkar. "Asymptotically de Sitter black holes have nonzero tidal Love numbers". In: *Phys. Rev. D* 109.6 (2024), p. 064025. DOI: 10.1103/PhysRevD.109.064025. arXiv: 2401.06467 [gr-qc].

[371] Takuya Katagiri, Tact Ikeda, and Vitor Cardoso. "Parametrized Love numbers of nonrotating black holes". In: *Phys. Rev. D* 109.4 (2024), p. 044067. DOI: 10.1103/PhysRevD.109.044067. arXiv: 2310.19705 [gr-qc].

[372] Takuya Katagiri, Hiroyuki Nakano, and Kazuyuki Omukai. "Stability of relativistic tidal response against small potential modification". In: *Phys. Rev. D* 108.8 (2023), p. 084049. DOI: 10.1103/PhysRevD.108.084049. arXiv: 2304.04551 [gr-qc].

[373] Rafael A. Porto. "The Tune of Love and the Nature(ness) of Spacetime". In: *Fortsch. Phys.* 64.10 (2016), pp. 723–729. DOI: 10.1002/prop.201600064. arXiv: 1606.08895 [gr-qc].

[374] Jibril Ben Achour et al. "Hidden symmetry of the static response of black holes: applications to Love numbers". In: *JHEP* 07 (2022), p. 112. DOI: 10.1007/JHEP07(2022)112. arXiv: 2202.12828 [gr-qc].

[375] Panagiotis Charalambous, Sergei Dubovsky, and Mikhail M. Ivanov. "On the vanishing of Love numbers for Kerr black holes". In: *Journal of High Energy Physics* 2021.5, 38 (May 2021), p. 38. DOI: 10.1007/JHEP05(2021)038. arXiv: 2102.08917 [hep-th].

[376] Panagiotis Charalambous, Sergei Dubovsky, and Mikhail M. Ivanov. "Love symmetry". In: *JHEP* 10 (2022), p. 175. DOI: 10.1007/JHEP10(2022)175. arXiv: 2209.02091 [hep-th].

[377] Mudit Rai and Luca Santoni. "Ladder symmetries and Love numbers of Reissner-Nordström black holes". In: *JHEP* 07 (2024), p. 098. DOI: 10.1007/JHEP07(2024)098. arXiv: 2404.06544 [gr-qc].

[378] Samuel E Gralla. "On the ambiguity in relativistic tidal deformability". In: *Classical and Quantum Gravity* 35.8 (Mar. 2018), p. 085002. ISSN: 1361-6382. DOI: 10.1088/1361-6382/aab186. URL: http://dx.doi.org/10.1088/1361-6382/aab186.

[379] Alexander M. Polyakov. "Quantum Geometry of Bosonic Strings". In: *Phys. Lett. B* 103 (1981). Ed. by I. M. Khalatnikov and V. P. Mineev, pp. 207–210. DOI: 10.1016/0370-2693(81)90743-7.

[380] James Edward Pringle. "Accretion Discs in Astrophysics". In: *Annual Review of Astronomy and Astrophysics* 19 (1981), pp. 137–160. URL: https://api.semanticscholar.org/CorpusID:123606936.

[381] N. I. Shakura and R. A. Sunyaev. "Black Holes in Binary Systems: Observational Appearances". In: *Symposium - International Astronomical Union* 55 (1973), 155–164. DOI: 10.1017/S007418090010035X.

[382] Stephen William Hawking. "Particle creation by black holes". In: *Communications in Mathematical Physics* 43 (1975), pp. 199–220. URL: https://api.semanticscholar.org/CorpusID:55539246.

[383] Don N. Page. "Particle emission rates from a black hole: Massless particles from an uncharged, nonrotating hole". In: *Phys. Rev. D* 13 (2 1976), pp. 198–206. DOI: 10.1103/PhysRevD.13.198. URL: https://link.aps.org/doi/10.1103/PhysRevD.13.198.

[384] Richard Brito, Vitor Cardoso, and Paolo Pani. *Superradiance: New Frontiers in Black Hole Physics*. Springer International Publishing, 2020. ISBN: 9783030466220. DOI: 10.1007/978-3-030-46622-0. URL: http://dx.doi.org/10.1007/978-3-030-46622-0.

[385] Carlos A.R. Herdeiro, Eugen Radu, and Nuno M. Santos. "A bound on energy extraction (and hairiness) from superradiance". In: *Physics Letters B* 824 (2022), p. 136835. ISSN: 0370-2693. DOI: https://doi.org/10.1016/j.physletb.2021.136835. URL: https://www.sciencedirect.com/science/article/pii/S0370269321007759.

[386] R. Penrose and R. M. Floyd. "Extraction of Rotational Energy from a Black Hole". In: *Nature Physical Science* 229.6 (Feb. 1971), pp. 177–179. DOI: 10.1038/physci229177a0.

[387] James M. Bardeen, Brandon D. Carter, and Stephen William Hawking. "The four laws of black hole mechanics". In: *Communications in Mathematical Physics* 31 (1973), pp. 161–170. URL: https://api.semanticscholar.org/CorpusID:54690354.

[388] Jacob D. Bekenstein. "Black Holes and Entropy". In: *Phys. Rev. D* 7 (8 1973), pp. 2333–2346. DOI: 10.1103/PhysRevD.7.2333. URL: https://link.aps.org/doi/10.1103/PhysRevD.7.2333.

[389] J. A. de Freitas Pacheco and J. E. Horvath. "Generalized second law and phantom cosmology: Accreting black holes". In: *Class. Quant. Grav.* 24 (2007), pp. 5427–5434. DOI: 10.1088/0264-9381/24/22/007. arXiv: 0709.1240 [gr-qc].

[390] J. A. S. Lima et al. "Phantom Accretion by Black Holes and the Generalized Second Law of Thermodynamics". In: *Astropart. Phys.* 33 (2010), pp. 292–295. DOI: 10.1016/j.astropartphys.2010.02.008. arXiv: 0808.0860 [gr-qc].

[391] Jaime Redondo-Yuste, David Pereñiguez, and Vitor Cardoso. "Ringdown of a dynamical spacetime". In: *Phys. Rev. D* 109 (4 2024), p. 044048. DOI: 10.1103/PhysRevD.109.044048. URL: https://link.aps.org/doi/10.1103/PhysRevD.109.044048.

[392] Hengrui Zhu et al. "Imprints of Changing Mass and Spin on Black Hole Ringdown". In: *arXiv e-prints*, arXiv:2404.12424 (Apr. 2024), arXiv:2404.12424. DOI: 10.48550/arXiv.2404.12424. arXiv: 2404.12424 [gr-qc].

[393] Kashif Alvi. "Energy and angular momentum flow into a black hole in a binary". In: *Physical Review D* 64.10 (Oct. 2001). ISSN: 1089-4918. DOI: 10.1103/physrevd.64.104020. URL: http://dx.doi.org/10.1103/PhysRevD.64.104020.

[394] Katerina Chatziioannou, Eric Poisson, and Nicolás Yunes. "Tidal heating and torquing of a Kerr black hole to next-to-leading order in the tidal coupling". In: *Physical Review D* 87.4 (Feb. 2013). ISSN: 1550-2368. DOI: 10.1103/physrevd.87.044022. URL: http://dx.doi.org/10.1103/PhysRevD.87.044022.

[395] Soichiro Isoyama and Hiroyuki Nakano. "Post-Newtonian templates for binary black-hole inspirals: the effect of the horizon fluxes and the secular change in the black-hole masses and spins". In: *Class. Quant. Grav.* 35.2 (2018), p. 024001. DOI: 10.1088/1361-6382/aa96c5. arXiv: 1705.03869 [gr-qc].

[396] Sayak Datta et al. "Tidal heating as a discriminator for horizons in extreme mass ratio inspirals". In: 101.4, 044004 (Feb. 2020), p. 044004. DOI: 10.1103/PhysRevD.101.044004. arXiv: 1910.07841 [gr-qc].

[397] M. V. S. Saketh et al. "Modeling horizon absorption in spinning binary black holes using effective worldline theory". In: *Phys. Rev. D* 107.8 (2023), p. 084006. DOI: 10.1103/PhysRevD.107.084006. arXiv: 2212.13095 [gr-qc].

[398] Alexandre Le Tiec, Marc Casals, and Edgardo Franzin. "Tidal Love numbers of Kerr black holes". In: *Phys. Rev. D* 103 (8 2021), p. 084021. DOI: 10.1103/PhysRevD.103.084021. URL: https://link.aps.org/doi/10.1103/PhysRevD.103.084021.

[399] P. C. Vaidya. "The gravitational field of a radiating star". In: *Proc. Indian Acad. Sci. A* 33.5 (1951), p. 264. DOI: 10.1007/BF03173260.

[400] Eric Poisson. *A Relativist's Toolkit: The Mathematics of Black-Hole Mechanics*. Cambridge University Press, 2004. DOI: 10.1017/CBO9780511606601.

[401] William B. Bonnor and P. C. Vaidya. "Spherically symmetric radiation of charge in Einstein-Maxwell theory". In: *General Relativity and Gravitation* 1 (1970), pp. 127–130. URL: https://api.semanticscholar.org/CorpusID:122643316.

[402] M. Murenbeeld and J. R. Trollope. "Slowly Rotating Radiating Sphere and a Kerr-Vaidya Metric". In: *Phys. Rev. D* 1 (12 1970), pp. 3220–3223. DOI: 10.1103/PhysRevD.1.3220. URL: https://link.aps.org/doi/10.1103/PhysRevD.1.3220.

[403] M Carmeli and M Kaye. "Gravitational field of a radiating rotating body". In: *Annals of Physics* 103.1 (1977), pp. 97–120. ISSN: 0003-4916. DOI: https://doi.org/10.1016/0003-4916(77)90263-9. URL: https://www.sciencedirect.com/science/article/pii/0003491677902639.

[404] Manasse R. Mbonye and Ronald L. Mallett. In: *Foundations of Physics* 30.5 (2000), 747–774. ISSN: 0015-9018. DOI: 10.1023/a:1003789027892. URL: http://dx.doi.org/10.1023/A:1003789027892.

[405] Brien C. Nolan and Thomas J. Waters. "Even perturbations of the self-similar Vaidya space-time". In: *Physical Review D* 71.10 (May 2005). ISSN: 1550-2368. DOI: 10.1103/physrevd.71.104030. URL: http://dx.doi.org/10.1103/PhysRevD.71.104030.

[406] Brien C. Nolan. "Odd-parity perturbations of self-similar Vaidya spacetime". In: *Class. Quant. Grav.* 24 (2007), pp. 177–200. DOI: 10.1088/0264-9381/24/1/010. arXiv: gr-qc/0608040.

[407] Cheng-Gang Shao et al. "Quasinormal modes in time-dependent black hole background". In: *Phys. Rev. D* 71 (2005), p. 044003. DOI: 10.1103/PhysRevD.71.044003. arXiv: gr-qc/0410025.

[408] Elcio Abdalla, Cecilia B. M. H. Chirenti, and Alberto Saa. "Quasinormal modes for the Vaidya metric". In: *Phys. Rev. D* 74 (2006), p. 084029. DOI: 10.1103/PhysRevD.74.084029. arXiv: gr-qc/0609036.

[409] Cecilia Chirenti and Alberto Saa. "Quasinormal modes for the charged Vaidya metric". In: *J. Phys. Conf. Ser.* 314 (2011). Ed. by Victor Aldaya, Carlos Barcelo, and Jose Luis Jaramillo, p. 012086. DOI: 10.1088/1742-6596/314/1/012086. arXiv: 1012.5110 [gr-qc].

[410] Cecilia Chirenti and Alberto Saa. "Nonstationary regime for quasinormal modes of the charged Vaidya metric". In: *Phys. Rev. D* 84 (2011), p. 064006. DOI: 10.1103/PhysRevD.84.064006. arXiv: 1105.1681 [gr-qc].

[411] Kai Lin, Yang-Yi Sun, and Hongsheng Zhang. "Quasinormal Modes for Dynamical Black Holes". In: *Phys. Rev. D* 103.8 (2021), p. 084015. DOI: 10.1103/PhysRevD.103.084015. arXiv: 2104.06631 [gr-qc].

[412] Alex B Nielsen. "The spatial relation between the event horizon and trapping horizon". In: *Classical and Quantum Gravity* 27.24 (Nov. 2010), p. 245016. ISSN: 1361-6382. DOI: 10.1088/0264-9381/27/24/245016. URL: http://dx.doi.org/10.1088/0264-9381/27/24/245016.

[413] Alex B. Nielsen. "Revisiting Vaidya Horizons". In: *Galaxies* 2.1 (Feb. 2014), pp. 62–71. DOI: 10.3390/galaxies2010062.

[414] Valerio Faraoni, Edgard Gunzig, and Pasquale Nardone. "Conformal transformations in classical gravitational theories and in cosmology". In: *Fund. Cosmic Phys.* 20 (1999), p. 121. arXiv: gr-qc/9811047.

[415] Vitor Cardoso et al. "Geodesic stability, Lyapunov exponents and quasinormal modes". In: *Phys. Rev. D* 79.6 (2009), p. 064016. DOI: 10.1103/PhysRevD.79.064016. arXiv: 0812.1806 [hep-th].

[416] Jay Solanki and Volker Perlick. "Photon sphere and shadow of a time-dependent black hole described by a Vaidya metric". In: *Phys. Rev. D* 105.6 (2022), p. 064056. DOI: 10.1103/PhysRevD.105.064056. arXiv: 2201.03274 [gr-qc].

[417] R.A. Konoplya and Z. Stuchlík. "Are eikonal quasinormal modes linked to the unstable circular null geodesics?" In: *Physics Letters B* 771 (Aug. 2017), 597–602. ISSN: 0370-2693. DOI: 10.1016/j.physletb.2017.06.015. URL: http://dx.doi.org/10.1016/j.physletb.2017.06.015.

[418] Akash K. Mishra, Sumanta Chakraborty, and Sudipta Sarkar. "Understanding photon sphere and black hole shadow in dynamically evolving spacetimes". In: *Phys. Rev. D* 99.10 (2019), p. 104080. DOI: 10.1103/PhysRevD.99.104080. arXiv: 1903.06376 [gr-qc].

[419] Yong Song. "The evolutions of the innermost stable circular orbits in dynamical spacetimes". In: *Eur. Phys. J. C* 81.10 (2021), p. 875. DOI: 10.1140/epjc/s10052-021-09623-6. arXiv: 2108.00696 [gr-qc].

[420] Che-Yu Chen, Hsu-Wen Chiang, and Jie-Shiun Tsao. "Eikonal quasinormal modes and photon orbits of deformed Schwarzschild black holes". In: *Phys. Rev. D* 106.4 (2022), p. 044068. DOI: 10.1103/PhysRevD.106.044068. arXiv: 2205.02433 [gr-qc].

[421] Yasutaka Koga et al. "Dynamical photon sphere and time evolving shadow around black holes with temporal accretion". In: *Phys. Rev. D* 105.10 (2022), p. 104040. DOI: 10.1103/PhysRevD.105.104040. arXiv: 2202.00201 [gr-qc].

[422] Yaghoub Heydarzade and Vitalii Vertogradov. *Dynamical Photon Spheres in Charged Black Holes and Naked Singularities*. 2024. arXiv: 2311.08930 [gr-qc]. URL: https://arxiv.org/abs/2311.08930.

[423] R. A. Konoplya and A. Zhidenko. "Nonoscillatory gravitational quasinormal modes and telling tails for Schwarzschild–de Sitter black holes". In: *Phys. Rev. D* 106 (12 2022), p. 124004. DOI: 10.1103/PhysRevD.106.124004. URL: https://link.aps.org/doi/10.1103/PhysRevD.106.124004.

[424] Shijun Yoshida and Toshifumi Futamase. "Numerical analysis of quasinormal modes in nearly extremal Schwarzschild-de Sitter space-times". In: *Phys. Rev. D* 69 (2004), p. 064025. DOI: 10.1103/PhysRevD.69.064025. arXiv: gr-qc/0308077.

[425] A. Zhidenko. "Quasinormal modes of Schwarzschild de Sitter black holes". In: *Class. Quant. Grav.* 21 (2004), pp. 273–280. DOI: 10.1088/0264-9381/21/1/019. arXiv: gr-qc/0307012.

[426] J.B. Seaborn. *Hypergeometric Functions and Their Applications*. Texts in Applied Mathematics. Springer New York, 2013. ISBN: 9781475754438. URL: https://books.google.it/books?id=HJXkBwAAQBAJ.

[427] Z.X. Wang and D.R. Guo. *Special Functions*. World Scientific Publishing Company, 1989. ISBN: 9789814507530. URL: https://books.google.it/books?id=c44GCwAAQBAJ.

[428] Walter D. Goldberger and Ira Z. Rothstein. "An Effective field theory of gravity for extended objects". In: *Phys. Rev. D* 73 (2006), p. 104029. DOI: 10.1103/PhysRevD.73.104029. arXiv: hep-th/0409156.

[429] Ira Z. Rothstein. "Progress in effective field theory approach to the binary inspiral problem". In: *Gen. Rel. Grav.* 46 (2014), p. 1726. DOI: 10.1007/s10714-014-1726-y.

[430] Michèle Levi. "Effective Field Theories of Post-Newtonian Gravity: A comprehensive review". In: *Rept. Prog. Phys.* 83.7 (2020), p. 075901. DOI: 10.1088/1361-6633/ab12bc. arXiv: 1807.01699 [hep-th].

[431] Walter D. Goldberger. "Effective field theories of gravity and compact binary dynamics: A Snowmass 2021 whitepaper". In: *Snowmass 2021*. June 2022. arXiv: 2206.14249 [hep-th].

[432] Kostas D. Kokkotas and Bernd G. Schmidt. "Quasinormal modes of stars and black holes". In: *Living Rev. Rel.* 2 (1999), p. 2. DOI: 10.12942/lrr-1999-2. arXiv: gr-qc/9909058.

[433] Emanuele Berti, Vitor Cardoso, and Andrei O. Starinets. "Quasinormal modes of black holes and black branes". In: *Class. Quant. Grav.* 26 (2009), p. 163001. DOI: 10.1088/0264-9381/26/16/163001. arXiv: 0905.2975 [gr-qc].

[434] Nicola Franchini and Sebastian H. Völkel. "Testing General Relativity with Black Hole Quasi-Normal Modes". In: (May 2023). arXiv: 2305.01696 [gr-qc].

[435] R. Abbott et al. "Tests of general relativity with binary black holes from the second LIGO-Virgo gravitational-wave transient catalog". In: *Phys. Rev. D* 103.12 (2021), p. 122002. DOI: 10.1103/PhysRevD.103.122002. arXiv: 2010.14529 [gr-qc].

[436] R. Abbott et al. "Tests of General Relativity with GWTC-3". In: (Dec. 2021). arXiv: 2112.06861 [gr-qc].

[437] Gregorio Carullo, Walter Del Pozzo, and John Veitch. "Observational Black Hole Spectroscopy: A time-domain multimode analysis of GW150914". In: *Phys. Rev. D* 99.12 (2019). [Erratum: Phys.Rev.D 100, 089903 (2019)], p. 123029. DOI: 10.1103/PhysRevD.99.123029. arXiv: 1902.07527 [gr-qc].

[438] Roberto Cotesta et al. "Analysis of Ringdown Overtones in GW150914". In: *Phys. Rev. Lett.* 129.11 (2022), p. 111102. DOI: 10.1103/PhysRevLett.129.111102. arXiv: 2201.00822 [gr-qc].

[439] Eliot Finch and Christopher J. Moore. "Searching for a ringdown overtone in GW150914". In: *Phys. Rev. D* 106.4 (2022), p. 043005. DOI: 10.1103/PhysRevD.106.043005. arXiv: 2205.07809 [gr-qc].

[440] Gregorio Carullo et al. "Reply to Comment on "Analysis of Ringdown Overtones in GW150914"". In: *Phys. Rev. Lett.* 131 (2023), p. 169002. DOI: 10.1103/PhysRevLett.131.169002. arXiv: 2310.20625 [gr-qc].

[441] Marco Crisostomi et al. "Neural posterior estimation with guaranteed exact coverage: The ringdown of GW150914". In: *Phys. Rev. D* 108.4 (2023), p. 044029. DOI: 10.1103/PhysRevD.108.044029. arXiv: 2305.18528 [gr-qc].

[442] Costantino Pacilio, Swetha Bhagwat, and Roberto Cotesta. "Simulation-based inference of black hole ringdowns in the time domain". In: (Apr. 2024). arXiv: 2404.11373 [gr-qc].

[443] Vasco Gennari, Gregorio Carullo, and Walter Del Pozzo. "Searching for ringdown higher modes with a numerical relativity-informed post-merger model". In: *Eur. Phys. J. C* 84.3 (2024), p. 233. DOI: 10.1140/epjc/s10052-024-12550-x. arXiv: 2312.12515 [gr-qc].

[444] Andrea Maselli et al. "Parametrized ringdown spin expansion coefficients: a data-analysis framework for black-hole spectroscopy with multiple events". In: *Phys. Rev. D* 101.2 (2020), p. 024043. DOI: 10.1103/PhysRevD.101.024043. arXiv: 1910.12893 [gr-qc].

[445] Gregorio Carullo. "Enhancing modified gravity detection from gravitational-wave observations using the parametrized ringdown spin expansion coeffcients formalism". In: *Phys. Rev. D* 103.12 (2021), p. 124043. DOI: 10.1103/PhysRevD.103.124043. arXiv: 2102.05939 [gr-qc].

[446] Andrea Maselli et al. "Black hole spectroscopy beyond Kerr: Agnostic and theory-based tests with next-generation interferometers". In: *Phys. Rev. D* 109.6 (2024), p. 064060. DOI: 10.1103/PhysRevD.109.064060. arXiv: 2311.14803 [gr-qc].

[447] Gregorio Carullo et al. "Constraints on Kerr-Newman black holes from merger-ringdown gravitational-wave observations". In: *Phys. Rev. D* 105.6 (2022), p. 062009. DOI: 10.1103/PhysRevD.105.062009. arXiv: 2109.13961 [gr-qc].

[448] Paolo Pani and Vitor Cardoso. "Are black holes in alternative theories serious astrophysical candidates? The Case for Einstein-Dilaton-Gauss-Bonnet black holes". In: *Phys. Rev. D* 79 (2009), p. 084031. DOI: 10.1103/PhysRevD.79.084031. arXiv: 0902.1569 [gr-qc].

[449] Nicolas Yunes and Frans Pretorius. "Dynamical Chern-Simons Modified Gravity. I. Spinning Black Holes in the Slow-Rotation Approximation". In: *Phys. Rev. D* 79 (2009), p. 084043. DOI: 10.1103/PhysRevD.79.084043. arXiv: 0902.4669 [gr-qc].

[450] Paolo Pani et al. "Slowly rotating black holes in alternative theories of gravity". In: *Phys. Rev. D* 84 (2011), p. 087501. DOI: 10.1103/PhysRevD.84.087501. arXiv: 1109.3996 [gr-qc].

[451] Andrea Maselli et al. "Rotating black holes in Einstein-Dilaton-Gauss-Bonnet gravity with finite coupling". In: *Phys. Rev. D* 92.8 (2015), p. 083014. DOI: 10.1103/PhysRevD.92.083014. arXiv: 1507.00680 [gr-qc].

[452] Paolo Pani. "Advanced Methods in Black-Hole Perturbation Theory". In: *Int. J. Mod. Phys. A* 28 (2013). Ed. by V. Cardoso et al., p. 1340018. DOI: 10.1142/S0217751X13400186. arXiv: 1305.6759 [gr-qc].

[453] Nicola Franchini. "Slow rotation black hole perturbation theory". In: *Phys. Rev. D* 108.4 (2023), p. 044079. DOI: 10.1103/PhysRevD.108.044079. arXiv: 2305.19313 [gr-qc].

[454] Pablo A. Cano et al. "Gravitational ringing of rotating black holes in higher-derivative gravity". In: *Phys. Rev. D* 105.2 (2022), p. 024064. DOI: 10.1103/PhysRevD.105.024064. arXiv: 2110.11378 [gr-qc].

[455] Lorenzo Pierini and Leonardo Gualtieri. "Quasi-normal modes of rotating black holes in Einstein-dilaton Gauss-Bonnet gravity: the first order in rotation". In: *Phys. Rev. D* 103 (2021), p. 124017. DOI: 10.1103/PhysRevD.103.124017. arXiv: 2103.09870 [gr-qc].

[456] Lorenzo Pierini and Leonardo Gualtieri. "Quasinormal modes of rotating black holes in Einstein-dilaton Gauss-Bonnet gravity: The second order in rotation". In: *Phys. Rev. D* 106.10 (2022), p. 104009. DOI: 10.1103/PhysRevD.106.104009. arXiv: 2207.11267 [gr-qc].

[457] Pratik Wagle, Nicolas Yunes, and Hector O. Silva. "Quasinormal modes of slowly-rotating black holes in dynamical Chern-Simons gravity". In: *Phys. Rev. D* 105.12 (2022), p. 124003. DOI: 10.1103/PhysRevD.105.124003. arXiv: 2103.09913 [gr-qc].

[458] Manu Srivastava, Yanbei Chen, and S. Shankaranarayanan. "Analytical computation of quasinormal modes of slowly rotating black holes in dynamical Chern-Simons gravity". In: *Phys. Rev. D* 104.6 (2021), p. 064034. DOI: 10.1103/PhysRevD.104.064034. arXiv: 2106.06209 [gr-qc].

[459] Asad Hussain and Aaron Zimmerman. "Approach to computing spectral shifts for black holes beyond Kerr". In: *Phys. Rev. D* 106.10 (2022), p. 104018. DOI: 10.1103/PhysRevD.106.104018. arXiv: 2206.10653 [gr-qc].

[460] Vitor Cardoso et al. "Parametrized black hole quasinormal ringdown: Decoupled equations for nonrotating black holes". In: *Phys. Rev. D* 99.10 (2019), p. 104077. DOI: 10.1103/PhysRevD.99.104077. arXiv: 1901.01265 [gr-qc].

[461] Ryan McManus et al. "Parametrized black hole quasinormal ringdown. II. Coupled equations and quadratic corrections for nonrotating black holes". In: *Phys. Rev. D* 100.4 (2019), p. 044061. DOI: 10.1103/PhysRevD.100.044061. arXiv: 1906.05155 [gr-qc].

[462] Sebastian H. Völkel, Nicola Franchini, and Enrico Barausse. "Theory-agnostic reconstruction of potential and couplings from quasinormal modes". In: *Phys. Rev. D* 105.8 (2022), p. 084046. DOI: 10.1103/PhysRevD.105.084046. arXiv: 2202.08655 [gr-qc].

[463] Shin'ichi Hirano et al. "Parametrized black hole quasinormal ringdown formalism for higher overtones". In: *Phys. Rev. D* 110.2 (2024), p. 024015. DOI: 10.1103/PhysRevD.110.024015. arXiv: 2404.09672 [gr-qc].

[464] Sebastian H. Völkel et al. "Constraining modifications of black hole perturbation potentials near the light ring with quasinormal modes". In: *Phys. Rev. D* 106.12 (2022), p. 124036. DOI: 10.1103/PhysRevD.106.124036. arXiv: 2209.10564 [gr-qc].

[465] Nicola Franchini and Sebastian H. Völkel. "Parametrized quasinormal mode framework for non-Schwarzschild metrics". In: *Phys. Rev. D* 107.12 (2023), p. 124063. DOI: 10.1103/PhysRevD.107.124063. arXiv: 2210.14020 [gr-qc].

[466] Rajes Ghosh et al. "Quasinormal modes of nonseparable perturbation equations: The scalar non-Kerr case". In: *Phys. Rev. D* 108.2 (2023), p. 024038. DOI: 10.1103/PhysRevD.108.024038. arXiv: 2303.00088 [gr-qc].

[467] Masashi Kimura. "Note on the parametrized black hole quasinormal ringdown formalism". In: *Phys. Rev. D* 101.6 (2020), p. 064031. DOI: 10.1103/PhysRevD.101.064031. arXiv: 2001.09613 [gr-qc].

[468] Pablo A. Cano et al. *Higher-derivative corrections to the Kerr quasinormal mode spectrum*. Sept. 2024. arXiv: 2409.04517 [gr-qc].

[469] github. *parametrized_qnm_framework*. 2024. URL: https://github.com/sebastianvoelkel/parametrized_qnm_framework.

[470] Emanuele Berti, Vitor Cardoso, and Clifford M. Will. "On gravitational-wave spectroscopy of massive black holes with the space interferometer LISA". In: *Phys. Rev. D* 73 (2006), p. 064030. DOI: 10.1103/PhysRevD.73.064030. arXiv: gr-qc/0512160.

[471] J. M. Bardeen and W. H. Press. "Radiation fields in the schwarzschild background". In: *J. Math. Phys.* 14 (1973), pp. 7–19. DOI: 10.1063/1.1666175.

[472] Oscar J. C. Dias et al. "Eigenvalue repulsions in the quasinormal spectra of the Kerr-Newman black hole". In: *Phys. Rev. D* 105.8 (2022), p. 084044. DOI: 10.1103/PhysRevD.105.084044. arXiv: 2109.13949 [gr-qc].

[473] S. Chandrasekhar. "The Mathematical Theory of Black Holes". In: *Fundam. Theor. Phys.* 9 (1984). Ed. by B. Bertotti, F. de Felice, and A. Pascolini, pp. 5–26. DOI: 10.1007/978-94-009-6469-3_2.

[474] Alan L. Dudley and J. D. Finley. "Separation of Wave Equations for Perturbations of General Type-D Space-Times". In: *Phys. Rev. Lett.* 38 (1977), pp. 1505–1508. DOI: 10.1103/PhysRevLett.38.1505.

[475] Alan L. Dudley and J. D. Finley III. "Covariant Perturbed Wave Equations in Arbitrary Type D Backgrounds". In: *J. Math. Phys.* 20 (1979), p. 311. DOI: 10.1063/1.524064.

[476] Emanuele Berti and Kostas D. Kokkotas. "Quasinormal modes of Kerr-Newman black holes: Coupling of electromagnetic and gravitational perturbations". In: *Phys. Rev. D* 71 (2005), p. 124008. DOI: 10.1103/PhysRevD.71.124008. arXiv: gr-qc/0502065.

[477] Aaron Zimmerman et al. "Quasinormal Modes Beyond Kerr". In: *Astrophys. Space Sci. Proc.* 40 (2015). Ed. by Carlos F. Sopuerta, pp. 217–223. DOI: 10.1007/978-3-319-10488-1_19. arXiv: 1406.4206 [gr-qc].

[478] Pratik Wagle et al. "Perturbations of spinning black holes in dynamical Chern-Simons gravity: Slow rotation equations". In: *Phys. Rev. D* 109.10 (2024), p. 104029. DOI: 10.1103/PhysRevD.109.104029. arXiv: 2311.07706 [gr-qc].

[479] Jose Luis Blázquez-Salcedo et al. "Quasinormal modes of Kerr black holes using a spectral decomposition of the metric perturbations". In: *Phys. Rev. D* 109.6 (2024), p. 064028. DOI: 10.1103/PhysRevD.109.064028. arXiv: 2312.10754 [gr-qc].

[480] Adrian Ka-Wai Chung and Nicolas Yunes. *Ringing out General Relativity: Quasi-normal mode frequencies for black holes of any spin in modified gravity*. May 2024. arXiv: 2405.12280 [gr-qc].

[481] Adrian Ka-Wai Chung and Nicolas Yunes. *Quasi-normal mode frequencies and gravitational perturbations of black holes with any subextremal spin in modified gravity through METRICS: the scalar-Gauss-Bonnet gravity case*. June 2024. arXiv: 2406.11986 [gr-qc].

[482] Bryce S. DeWitt and Robert W. Brehme. "Radiation damping in a gravitational field". In: *Annals Phys.* 9 (1960), pp. 220–259. DOI: 10.1016/0003-4916(60)90030-0.

[483] Swetha Bhagwat et al. "On choosing the start time of binary black hole ringdowns". In: *Phys. Rev. D* 97.10 (2018), p. 104065. DOI: 10.1103/PhysRevD.97.104065. arXiv: 1711.00926 [gr-qc].

[484] Lionel London, Deirdre Shoemaker, and James Healy. "Modeling ringdown: Beyond the fundamental quasinormal modes". In: *Physical Review D* 90.12 (2014). DOI: 10.1103/physrevd.90.124032. URL: https://doi.org/10.1103%2Fphysrevd.90.124032.

[485] Macarena Lagos and Lam Hui. "Generation and propagation of nonlinear quasinormal modes of a Schwarzschild black hole". In: *Phys. Rev. D* 107 (4 2023), p. 044040. DOI: 10.1103/PhysRevD.107.044040. URL: https://link.aps.org/doi/10.1103/PhysRevD.107.044040.

[486] Hengrui Zhu et al. "Nonlinear Effects In Black Hole Ringdown From Scattering Experiments I: spin and initial data dependence of quadratic mode coupling". In: (Jan. 2024). arXiv: 2401.00805 [gr-qc].

[487] Sizheng Ma and Huan Yang. "Excitation of quadratic quasinormal modes for Kerr black holes". In: *Phys. Rev. D* 109.10 (2024), p. 104070. DOI: 10.1103/PhysRevD.109.104070. arXiv: 2401.15516 [gr-qc].

[488] Neev Khera, Sizheng Ma, and Huan Yang. "Quadratic Mode Couplings in Rotating Black Holes and Their Detectability". In: (Oct. 2024). arXiv: 2410.14529 [gr-qc].

[489] Stanislav Babak et al. "Fundamental physics and cosmology with LISA". In: *Class. Quant. Grav.* 28 (2011). Ed. by Donald Marolf and Daniel Sudarsky, p. 114001. DOI: 10.1088/0264-9381/28/11/114001. arXiv: 1011.2062 [gr-qc].

[490] Alberto Sesana. "Black Hole Science With the Laser Interferometer Space Antenna". In: *Front. Astron. Space Sci.* 8 (2021), p. 601646. DOI: 10.3389/fspas.2021.601646. arXiv: 2105.11518 [astro-ph.CO].

[491] K. G. Arun et al. "New horizons for fundamental physics with LISA". In: *Living Rev. Rel.* 25.1 (2022), p. 4. DOI: 10.1007/s41114-022-00036-9. arXiv: 2205.01597 [gr-qc].

[492] Monica Colpi et al. "LISA Definition Study Report". In: (Feb. 2024). arXiv: 2402.07571 [astro-ph.CO].

[493] Yi-Ming Hu. "Gravitational Wave Astrophysics with TianQin: A brief progress review". In: Sept. 2024. arXiv: 2409.19664 [gr-qc].

[494] Antoine Klein et al. "Science with the space-based interferometer eLISA: Supermassive black hole binaries". In: *Phys. Rev. D* 93.2 (2016), p. 024003. DOI: 10.1103/PhysRevD.93.024003. arXiv: 1511.05581 [gr-qc].

[495] Matteo Bonetti et al. "Post-Newtonian evolution of massive black hole triplets in galactic nuclei – IV. Implications for LISA". In: *Mon. Not. Roy. Astron. Soc.* 486.3 (2019), pp. 4044–4060. DOI: 10.1093/mnras/stz903. arXiv: 1812.01011 [astro-ph.GA].

[496] Enrico Barausse et al. "Massive Black Hole Merger Rates: The Effect of Kiloparsec Separation Wandering and Supernova Feedback". In: *Astrophys. J.* 904.1 (2020), p. 16. DOI: 10.3847/1538-4357/abba7f. arXiv: 2006.03065 [astro-ph.GA].

[497] Pratika Dayal et al. "The hierarchical assembly of galaxies and black holes in the first billion years: predictions for the era of gravitational wave astronomy". In: *Mon. Not. R. Astron. Soc.* 486.2 (June 2019), pp. 2336–2350. DOI: 10.1093/mnras/stz897. arXiv: 1810.11033 [astro-ph.GA].

[498] Enrico Barausse et al. "Implications of the pulsar timing array detections for massive black hole mergers in the LISA band". In: *Phys. Rev. D* 108.10 (2023), p. 103034. DOI: 10.1103/PhysRevD.108.103034. arXiv: 2307.12245 [astro-ph.GA].

[499] David Izquierdo-Villalba et al. "Connecting low-redshift LISA massive black hole mergers to the nHz stochastic gravitational wave background". In: *Astron. Astrophys.* 686 (2024), A183. DOI: 10.1051/0004-6361/202449293. arXiv: 2401.10983 [astro-ph.GA].

[500] Emanuele Berti et al. "Spectroscopy of Kerr black holes with Earth- and space-based interferometers". In: *Phys. Rev. Lett.* 117.10 (2016), p. 101102. DOI: 10.1103/PhysRevLett.117.101102. arXiv: 1605.09286 [gr-qc].

[501] Enrico Barausse, Vitor Cardoso, and Paolo Pani. "Can environmental effects spoil precision gravitational-wave astrophysics?" In: *Phys. Rev. D* 89.10 (2014), p. 104059. DOI: 10.1103/PhysRevD.89.104059. arXiv: 1404.7149 [gr-qc].

[502] Nicolas Yunes and Frans Pretorius. "Fundamental Theoretical Bias in Gravitational Wave Astrophysics and the Parameterized Post-Einsteinian Framework". In: *Phys. Rev. D* 80 (2009), p. 122003. DOI: 10.1103/PhysRevD.80.122003. arXiv: 0909.3328 [gr-qc].

[503] Curt Cutler and Michele Vallisneri. "LISA detections of massive black hole inspirals: Parameter extraction errors due to inaccurate template waveforms". In: *Phys. Rev. D* 76 (2007), p. 104018. DOI: 10.1103/PhysRevD.76.104018. arXiv: 0707.2982 [gr-qc].

[504] Michele Vallisneri. "Testing general relativity with gravitational waves: a reality check". In: *Phys. Rev. D* 86 (2012), p. 082001. DOI: 10.1103/PhysRevD.86.082001. arXiv: 1207.4759 [gr-qc].

[505] Laura Sampson, Neil Cornish, and Nicolás Yunes. "Mismodeling in gravitational-wave astronomy: The trouble with templates". In: *Phys. Rev. D* 89.6 (2014), p. 064037. DOI: 10.1103/PhysRevD.89.064037. arXiv: 1311.4898 [gr-qc].

[506] Marc Favata. "Systematic parameter errors in inspiraling neutron star binaries". In: *Phys. Rev. Lett.* 112 (2014), p. 101101. DOI: 10.1103/PhysRevLett.112.101101. arXiv: 1310.8288 [gr-qc].

[507] Pankaj Saini, Marc Favata, and K. G. Arun. "Systematic bias on parametrized tests of general relativity due to neglect of orbital eccentricity". In: *Phys. Rev. D* 106.8 (2022), p. 084031. DOI: 10.1103/PhysRevD.106.084031. arXiv: 2203.04634 [gr-qc].

[508] Jocelyn S. Read. "Waveform uncertainty quantification and interpretation for gravitational-wave astronomy". In: *Class. Quant. Grav.* 40.13 (2023), p. 135002. DOI: 10.1088/1361-6382/acd29b. arXiv: 2301.06630 [gr-qc].

[509] Caroline B. Owen et al. "Waveform accuracy and systematic uncertainties in current gravitational wave observations". In: *Phys. Rev. D* 108.4 (2023), p. 044018. DOI: 10.1103/PhysRevD.108.044018. arXiv: 2301.11941 [gr-qc].

[510] Chantal Pitte et al. "Detectability of higher harmonics with LISA". In: *Phys. Rev. D* 108.4 (2023), p. 044053. DOI: 10.1103/PhysRevD.108.044053. arXiv: 2304.03142 [gr-qc].

[511] Shubham Kejriwal, Lorenzo Speri, and Alvin J. K. Chua. "Impact of correlations on the modeling and inference of beyond vacuum–general relativistic effects in extreme-mass-ratio inspirals". In: *Phys. Rev. D* 110.8 (2024), p. 084060. DOI: 10.1103/PhysRevD.110.084060. arXiv: 2312.13028 [gr-qc].

[512] Anuradha Gupta et al. "Possible causes of false general relativity violations in gravitational wave observations". In: (May 2024). DOI: 10.21468/SciPostPhysCommRep.5. arXiv: 2405.02197 [gr-qc].

[513] Rohit S. Chandramouli et al. "Systematic biases due to waveform mismodeling in parametrized post-Einsteinian tests of general relativity: The impact of neglecting spin precession and higher modes". In: *Phys. Rev. D* 111.4 (2025), p. 044026. DOI: 10.1103/PhysRevD.111.044026. arXiv: 2410.06254 [gr-qc].

[514] Mudit Garg et al. "Systematics in tests of general relativity using LISA massive black hole binaries". In: (Oct. 2024). DOI: 10.1093/mnras/stae2605. arXiv: 2410.02910 [astro-ph.GA].

[515] Sophia Yi et al. "Systematic biases from the exclusion of higher harmonics in parameter estimation on LISA binaries". In: (Feb. 2025). arXiv: 2502.12237 [gr-qc].

[516] Olaf Dreyer et al. "Black hole spectroscopy: Testing general relativity through gravitational wave observations". In: *Class. Quant. Grav.* 21 (2004), pp. 787–804. DOI: 10.1088/0264-9381/21/4/003. arXiv: gr-qc/0309007.

[517] Emanuele Berti, Vitor Cardoso, and Clifford M. Will. "Gravitational-wave spectroscopy of massive black holes with the space interferometer LISA". In: *Physical Review D* 73.6 (2006). ISSN: 1550-2368. DOI: 10.1103/physrevd.73.064030. URL: http://dx.doi.org/10.1103/PhysRevD.73.064030.

[518] Fernando Echeverria. "Gravitational-wave measurements of the mass and angular momentum of a black hole". In: *Phys. Rev. D* 40 (10 1989), pp. 3194–3203. DOI: 10.1103/PhysRevD.40.3194. URL: https://link.aps.org/doi/10.1103/PhysRevD.40.3194.

[519] Emanuele Berti et al. "Extreme Gravity Tests with Gravitational Waves from Compact Binary Coalescences: (II) Ringdown". In: *Gen. Rel. Grav.* 50.5 (2018), p. 49. DOI: 10.1007/s10714-018-2372-6. arXiv: 1801.03587 [gr-qc].

[520] Alexandre Toubiana et al. "Measuring source properties and quasinormal mode frequencies of heavy massive black-hole binaries with LISA". In: *Phys. Rev. D* 109.10 (2024), p. 104019. DOI: 10.1103/PhysRevD.109.104019. arXiv: 2307.15086 [gr-qc].

[521] Lee Lindblom, Benjamin J. Owen, and Duncan A. Brown. "Model Waveform Accuracy Standards for Gravitational Wave Data Analysis". In: *Phys. Rev. D* 78 (2008), p. 124020. DOI: 10.1103/PhysRevD.78.124020. arXiv: 0809.3844 [gr-qc].

[522] R. A. Fisher. "On the Mathematical Foundations of Theoretical Statistics". In: *Phil. Trans. Roy. Soc. Lond. A* 222 (1922), pp. 309–368. DOI: 10.1098/rsta.1922.0009.

[523] Emanuele Berti et al. "Inspiral, merger and ringdown of unequal mass black hole binaries: A Multipolar analysis". In: *Phys. Rev. D* 76 (2007), p. 064034. DOI: 10.1103/PhysRevD.76.064034. arXiv: gr-qc/0703053.

[524] Emanuele Berti et al. "Matched-filtering and parameter estimation of ringdown waveforms". In: *Phys. Rev. D* 76 (2007), p. 104044. DOI: 10.1103/PhysRevD.76.104044. arXiv: 0707.1202 [gr-qc].

[525] Neil J. Cornish and Louis J. Rubbo. "The LISA response function". In: *Phys. Rev. D* 67 (2003). [Erratum: Phys.Rev.D 67, 029905 (2003)], p. 022001. DOI: 10.1103/PhysRevD.67.029905. arXiv: gr-qc/0209011.

[526] Sylvain Marsat and John G. Baker. "Fourier-domain modulations and delays of gravitational-wave signals". In: (June 2018). arXiv: 1806.10734 [gr-qc].

[527] Curt Cutler. "Angular resolution of the LISA gravitational wave detector". In: *Phys. Rev. D* 57 (1998), pp. 7089–7102. DOI: 10.1103/PhysRevD.57.7089. arXiv: gr-qc/9703068.

[528] Michele Maggiore. *Gravitational Waves. Vol. 1: Theory and Experiments*. Oxford University Press, 2007. ISBN: 978-0-19-171766-6, 978-0-19-852074-0. DOI: 10.1093/acprof:oso/9780198570745.001.0001.

[529] Richard H. Price. "Nonspherical Perturbations of Relativistic Gravitational Collapse. I. Scalar and Gravitational Perturbations". In: *Phys. Rev. D* 5 (10 1972), pp. 2419–2438. DOI: 10.1103/PhysRevD.5.2419. URL: https://link.aps.org/doi/10.1103/PhysRevD.5.2419.

[530] Mark Ho-Yeuk Cheung et al. "Extracting linear and nonlinear quasinormal modes from black hole merger simulations". In: *Phys. Rev. D* 109.4 (2024). [Erratum: Phys.Rev.D 110, 049902 (2024)], p. 044069. DOI: 10.1103/PhysRevD.109.044069. arXiv: 2310.04489 [gr-qc].

[531] Hengrui Zhu et al. "Challenges in quasinormal mode extraction: Perspectives from numerical solutions to the Teukolsky equation". In: *Phys. Rev. D* 109.4 (2024), p. 044010. DOI: 10.1103/PhysRevD.109.044010. arXiv: 2309.13204 [gr-qc].

[532] S. Babak et al. "A Template bank to search for gravitational waves from inspiralling compact binaries. I. Physical models". In: *Class. Quant. Grav.* 23 (2006), pp. 5477–5504. DOI: 10.1088/0264-9381/23/18/002. arXiv: gr-qc/0604037.

[533] D. J. A. McKechan, C. Robinson, and B. S. Sathyaprakash. "A tapering window for time-domain templates and simulated signals in the detection of gravitational waves from coalescing compact binaries". In: *Class. Quant. Grav.* 27 (2010). Ed. by Zsuzsa Marka and Szabolcs Marka, p. 084020. DOI: 10.1088/0264-9381/27/8/084020. arXiv: 1003.2939 [gr-qc].

[534] Costantino Pacilio et al. "Flexible mapping of ringdown amplitudes for nonprecessing binary black holes". In: *Physical Review D* 110.10 (Nov. 2024). ISSN: 2470-0029. DOI: 10.1103/physrevd.110.103037. URL: http://dx.doi.org/10.1103/PhysRevD.110.103037.

[535] Keefe Mitman et al. "Probing the ringdown perturbation in binary black hole coalescences with an improved quasi-normal mode extraction algorithm". In: (Mar. 2025). arXiv: 2503.09678 [gr-qc].

[536] Hiroyuki Nakano and Kunihito Ioka. "Second Order Quasi-Normal Mode of the Schwarzschild Black Hole". In: *Phys. Rev. D* 76 (2007), p. 084007. DOI: 10.1103/PhysRevD.76.084007. arXiv: 0708.0450 [gr-qc].

[537] Enrico Barausse, Viktoriya Morozova, and Luciano Rezzolla. "On the mass radiated by coalescing black-hole binaries". In: *Astrophys. J.* 758 (2012). [Erratum: Astrophys.J. 786, 76 (2014)], p. 63. DOI: 10.1088/0004-637X/758/1/63. arXiv: 1206.3803 [gr-qc].

[538] Fabian Hofmann, Enrico Barausse, and Luciano Rezzolla. "The final spin from binary black holes in quasi-circular orbits". In: *Astrophys. J. Lett.* 825.2 (2016), p. L19. DOI: 10.3847/2041-8205/825/2/L19. arXiv: 1605.01938 [gr-qc].

[539] Curt Cutler and Eanna E. Flanagan. "Gravitational waves from merging compact binaries: How accurately can one extract the binary's parameters from the inspiral wave form?" In: *Phys. Rev. D* 49 (1994), pp. 2658–2697. DOI: 10.1103/PhysRevD.49.2658. arXiv: gr-qc/9402014.

[540] Michele Vallisneri. "Use and abuse of the Fisher information matrix in the assessment of gravitational-wave parameter-estimation prospects". In: *Phys. Rev. D* 77 (2008), p. 042001. DOI: 10.1103/PhysRevD.77.042001. arXiv: gr-qc/0703086.

[541] Samaya Nissanke et al. "Exploring Short Gamma-ray Bursts as Gravitational-wave Standard Sirens". In: 725.1 (Dec. 2010), pp. 496–514. DOI: 10.1088/0004-637X/725/1/496. arXiv: 0904.1017 [astro-ph.CO].

[542] Michele Vallisneri. "Beyond Fisher: exact sampling distributions of the maximum-likelihood estimator in gravitational-wave parameter estimation". In: *Phys. Rev. Lett.* 107 (2011), p. 191104. DOI: 10.1103/PhysRevLett.107.191104. arXiv: 1108.1158 [gr-qc].

[543] Katerina Chatziioannou et al. "Constructing Gravitational Waves from Generic Spin-Precessing Compact Binary Inspirals". In: *Phys. Rev. D* 95.10 (2017), p. 104004. DOI: 10.1103/PhysRevD.95.104004. arXiv: 1703.03967 [gr-qc].

[544] Michael Pürrer and Carl-Johan Haster. "Gravitational waveform accuracy requirements for future ground-based detectors". In: *Phys. Rev. Res.* 2.2 (2020), p. 023151. DOI: 10.1103/PhysRevResearch.2.023151. arXiv: 1912.10055 [gr-qc].

[545] Alexandre Toubiana and Jonathan R. Gair. "Indistinguishability criterion and estimating the presence of biases". In: (Jan. 2024). arXiv: 2401.06845 [gr-qc].

[546] Blake Moore et al. "Towards a Fourier domain waveform for non-spinning binaries with arbitrary eccentricity". In: *Class. Quant. Grav.* 35.23 (2018), p. 235006. DOI: 10.1088/1361-6382/aaea00. arXiv: 1807.07163 [gr-qc].

[547] Veome Kapil et al. "Systematic bias from waveform modeling for binary black hole populations in next-generation gravitational wave detectors". In: *Phys. Rev. D* 109.10 (2024), p. 104043. DOI: 10.1103/PhysRevD.109.104043. arXiv: 2404.00090 [gr-qc].

[548] Lorena Magaña Zertuche et al. "High precision ringdown modeling: Multimode fits and BMS frames". In: *Phys. Rev. D* 105.10 (2022), p. 104015. DOI: 10.1103/PhysRevD.105.104015. arXiv: 2110.15922 [gr-qc].

[549] Lorena Magaña Zertuche et al. "High-Precision Ringdown Surrogate Model for Non-Precessing Binary Black Holes". In: (Aug. 2024). arXiv: 2408.05300 [gr-qc].

[550] J. Aasi et al. "Advanced LIGO". In: *Class. Quant. Grav.* 32 (2015), p. 074001. DOI: 10.1088/0264-9381/32/7/074001. arXiv: 1411.4547 [gr-qc].

[551] Pau Amaro Seoane et al. "Astrophysics with the Laser Interferometer Space Antenna". In: *Living Rev. Rel.* 26.1 (2023), p. 2. DOI: 10.1007/s41114-022-00041-y. arXiv: 2203.06016 [gr-qc].

[552] Lodovico Capuano, Luca Santoni, and Enrico Barausse. "Black hole hairs in scalar-tensor gravity and the lack thereof". In: *Physical Review D* 108.6 (Sept. 2023). ISSN: 2470-0029. DOI: 10.1103/physrevd.108.064058. URL: http://dx.doi.org/10.1103/PhysRevD.108.064058.

[553] Astrid Eichhorn et al. "Breaking black-hole uniqueness at supermassive scales". In: (Dec. 2023). arXiv: 2312.11430 [gr-qc].

[554] Clemente Smarra, Lodovico Capuano, and Adrien Kuntz. *Probing supermassive black hole scalarization with Pulsar Timing Arrays*. 2025. arXiv: 2505.20402 [gr-qc]. URL: https://arxiv.org/abs/2505.20402.

[555] Gabriele Franciolini et al. "Effective Field Theory of Black Hole Quasinormal Modes in Scalar-Tensor Theories". In: *JHEP* 02 (2019), p. 127. DOI: 10.1007/JHEP02(2019)127. arXiv: 1810.07706 [hep-th].

[556] Lam Hui et al. "Effective Field Theory for the perturbations of a slowly rotating black hole". In: *JHEP* 12 (2021), p. 183. DOI: 10.1007/JHEP12(2021)183. arXiv: 2111.02072 [hep-th].

[557] Brandon Carter. "Killing Horizons and Orthogonally Transitive Groups in Space-Time". In: *Journal of Mathematical Physics* 10.1 (1969), pp. 70–81. DOI: 10.1063/1.1664763. eprint: https://doi.org/10.1063/1.1664763. URL: https://doi.org/10.1063/1.1664763.

[558] Elcio Abdalla, Cecilia B.M.H Chirenti, and Alberto Saa. "Quasinormal mode characterization of evaporating mini black holes". In: *Journal of High Energy Physics* 2007.10 (Oct. 2007), 086–086. ISSN: 1029-8479. DOI: 10.1088/1126-6708/2007/10/086. URL: http://dx.doi.org/10.1088/1126-6708/2007/10/086.

[559] Hans Peter Nollert. "Quasinormal modes of Schwarzschild black holes: The determination of quasinormal frequencies with very large imaginary parts". In: *Phys. Rev. D* 47 (1993), pp. 5253–5258. DOI: 10.1103/PhysRevD.47.5253.

[560] Michael Boyle et al. "The SXS Collaboration catalog of binary black hole simulations". In: *Class. Quant. Grav.* 36.19 (2019), p. 195006. DOI: 10.1088/1361-6382/ab34e2. arXiv: 1904.04831 [gr-qc].

[561] Emanuele Berti and Antoine Klein. "Mixing of spherical and spheroidal modes in perturbed Kerr black holes". In: *Phys. Rev. D* 90 (6 2014), p. 064012. DOI: 10.1103/PhysRevD.90.064012. URL: https://link.aps.org/doi/10.1103/PhysRevD.90.064012.

[562] L London and E Fauchon-Jones. "On modeling for Kerr black holes: basis learning, QNM frequencies, and spherical-spheroidal mixing coefficients". In: *Classical and Quantum Gravity* 36.23 (Nov. 2019), p. 235015. ISSN: 1361-6382. DOI: 10.1088/1361-6382/ab2f11. URL: http://dx.doi.org/10.1088/1361-6382/ab2f11.

[563] Jordan Moxon et al. *The SpECTRE Cauchy-characteristic evolution system for rapid, precise waveform extraction*. 2021. arXiv: 2110.08635 [gr-qc]. URL: https://arxiv.org/abs/2110.08635.

[564] Keefe Mitman et al. "Fixing the BMS frame of numerical relativity waveforms with BMS charges". In: *Phys. Rev. D* 106.8 (2022), p. 084029. DOI: 10.1103/PhysRevD.106.084029. arXiv: 2208.04356 [gr-qc].

[565] Sascha Husa et al. "Frequency-domain gravitational waves from nonprecessing black-hole binaries. I. New numerical waveforms and anatomy of the signal". In: *Phys. Rev. D* 93.4 (2016), p. 044006. DOI: 10.1103/PhysRevD.93.044006. arXiv: 1508.07250 [gr-qc].

[566] Sebastian Khan et al. "Frequency-domain gravitational waves from nonprecessing black-hole binaries. II. A phenomenological model for the advanced detector era". In: *Phys. Rev. D* 93.4 (2016), p. 044007. DOI: 10.1103/PhysRevD.93.044007. arXiv: 1508.07253 [gr-qc].

[567] Ajit Kumar Mehta et al. "Tests of general relativity with gravitational-wave observations using a flexible theory-independent method". In: *Phys. Rev. D* 107.4 (2023), p. 044020. DOI: 10.1103/PhysRevD.107.044020. arXiv: 2203.13937 [gr-qc].

[568] Chantal Pitte et al. "Exploring tests of the no-hair theorem with LISA". In: *Phys. Rev. D* 110 (10 2024), p. 104003. DOI: 10.1103/PhysRevD.110.104003. URL: https://link.aps.org/doi/10.1103/PhysRevD.110.104003.